Christopher C. White
Jon Martin
J. Thomas Chapin *Editors*

Service Life Prediction of Exterior Plastics

Vision for the Future

Springer

Service Life Prediction of Exterior Plastics

Christopher C. White • Jon Martin
J. Thomas Chapin
Editors

Service Life Prediction of Exterior Plastics

Vision for the Future

Springer

Editors
Christopher C. White
Polymeric Materials Group
National Institute of Standards
    and Technology
Gaithersburg, MD, USA

Jon Martin
Montgomery Village, MD, USA

J. Thomas Chapin
Underwriters Laboratories Inc.
Northbrook, IL, USA

Preface

Risk permeates every aspect of product commercialization. How risk is assessed, therefore, is critical to ability and rapidity of an industry to innovate. This volume updates progress in delineating advances in the state of the art in service life prediction for polymeric materials exposed outdoors. Accurate in-service performance estimates would greatly reduce risk in introducing a product into the marketplace. By increasing the reliability of the predictions for polymeric materials, the pace of innovation in industries that rely on these materials will also increase.

The mission of the 5th International Symposium on Service Life Prediction, which was held in Monterey California on March 3–8, 2013, was to provide an international forum for presenting and discussing the latest scientific and technical advances leading to more reliable and quantitative predictions for the weathering performance of polymeric materials. This meeting had three concurrent, underlying themes: a symposium on service life prediction for all polymer containing systems, a workshop on changes to the Underwriters Laboratories' (UL) UL 746 standard testing requirements, and a National Science Foundation workshop on Composite Durability. The objectives of each theme were identical and involved the following:

- To critically examine the methods and methodology used to assess current service life prediction.
- To present advances in laboratory, field exposures, and modeling approaches leading to more quantitative results that are both repeatable and reproducible.
- To discuss strategies for implementing these advances
- To identify outstanding issues related to implementation of these advances.

Ninety-five distinguished scientists attended the symposium including 21 scientists from 11 countries and 50 technical presentations. Each day was divided into a morning session devoted to service life prediction and an afternoon session involving a discussion of UL 746. Sessions near the end of the week were focused on the NSF composite durability workshop.

The opening talks of the workshop were focused on an overview of the current state of the art in service life prediction. A number of statistical models were presented including work on silicone hard coats and reflective outdoor coatings.

This was followed by the results of a number of case studies of exposure on a variety of materials including wood-plastic composites, polymer sport field coverings, and subcomponent systems common to photovoltaic panels. Degradation of commodity thermoplastic and thermoplastic systems was also presented.

A vigorous discussion followed a series of talks on the limitations of service life predictions models, tools, procedures, and methods. This discussion focused on ensuring that the increase in any factor does not change the mechanism of degradation. As an example, increasing the temperature beyond a phase change in the polymer, such as the glass transition temperature, could change the dominant mechanism of degradation for the polymer material.

The NSF composite workshop included presentations on molecular modeling of the materials from molecular dynamics models to constitutive models of behavior. Also included were a series of discussions on the thermo-mechanical effects on polymer composites.

Excellent papers were presented in all areas of service life prediction including advances in modeling, field and laboratory exposures, and characterization techniques.

A common concern from discussions following the presentations involved the treatment of water in models and experiments. Water, when it is included in the models, is characterized by the relative humidity and not the activity of water within the material. Water is also present as rain, ice, and steam within these materials. A focus on including a more detailed and accurate description of water will be a focus of future research.

Throughout the conference, a dedicated group of researchers labored to improve the methods, tools, and techniques underlying Underwriters Laboratory methods. These methods, specifically the UL 746 standard test methods, are instrumental in assuring the safety of commercial products used in everyday life. The goal of the UL 746 sessions was to increase this safety level while decreasing the time needed to obtain a UL 746 safety certification. The hard work of these researchers is summarized in the first paper presented in this volume.

The editors thank the Monterey organizing committee as well as the authors and participants for making the 5th International Symposium a success. The organizing committee, cochaired by Tom Chapin (UL), Anastasia Muliana (Texas A&M), Valeria La Saponara (University of California Davis), and Chris White (NIST) included:

Pravin Gandhi, Underwriters Laboratories Inc.
George Fechtmann, Underwriters Laboratories Inc.
Noe Navarro, Underwriters Laboratories Inc.
Joannie Chin, National Institute of Standards and Technology
Xiaohong GU, National Institute of Standards and Technology
Grace Hsuan, National Science Foundation
Matt Celina, Sandia National Laboratory
Mike Kempe, National Renewal Energy Laboratory
Mark Nicols, Ford Motor Company
Berry Douglas, Boeing Company
Alex Bradley, DuPont

Leonardo Lopez, Dow Chemical
James Pickett, General Electric
Jeff Quill, Q-Lab
Kurt Wood, Arkema
Sheila Ray, Nuclear Regulatory Commission
Steve Duren, Adhesives and Sealant Council
Bor Yann Liaw, University of Hawaii
Thomas Reichert, Fraunhofer ICT
Andreas Wolf, Dow Corning
Michael Kohl, Fraunhofer
Tsuyoshi Shioda, Mitsui Chemical
Anastasia Muliana, Texas A&M University
Valeria La Saponara University of California Davis

Gaithersburg, MD, USA   Christopher C. White
Montgomery Village, MD, USA   Jon Martin
Northbrook, IL, USA   J. Thomas Chapin

Contents

Contributors

Peter Beavis Atomic Weapons Establishment (AWE), Aldermaston, Reading, UK

David M. Burns 3M Company, St. Paul, MN, USA

Tim Cartwright Atomic Weapons Establishment (AWE) Aldermaston, Reading, UK

Jennifer David, Ph.D. Momentive Performance Materials Inc., Wilton, CT, USA

Julie Etheridge Atomic Weapons Establishment (AWE), Aldermaston, Reading, UK

Joel Forman Exponent, Inc., Natick, MA, USA

Aaron Forster Engineering Laboratory, National Institute of Standards and Technology, Gaithersburg, MD, USA

Sean P. Fowler Q-Lab Corporation, Cleveland, OH, USA

Patrick Gaume Engineering Laboratory, National Institute of Standards and Technology, Gaithersburg, MD, USA

Anja Geburtig BAM Federal Institute for Materials Research and Testing, Berlin, Germany

Travis Q. Gregar 3M Company, St. Paul, MN, USA

Henry K. Hardcastle Atlas, Ametek Measurement and Calibration Technologies, Chicago, IL, USA

Robert Hayes, Ph.D. Momentive Performance Materials Inc., Wilton, CT, USA

Donald Hunston Engineering Laboratory, National Institute of Standards and Technology, Gaithersburg, MD, USA

H. Issard AREVA TN International, Saint Quentin en Yvelines, France

Masayuki Ito Advanced Research Institute for Science and Engineering, Waseda University, Kodaira, Tokyo, Japan

Niaz Khan Atomic Weapons Establishment (AWE), Aldermaston, Reading, UK

Søren Kiil Department of Chemical and Biochemical Engineering, Technical University of Denmark, DTU, Kongens Lyngby, Denmark

Michael Koehl Fraunhofer ISE, Freiburg, Germany

Anil Kumar Atomic Weapons Establishment (AWE), Aldermaston, Reading, UK

Amy Langhorst Engineering Laboratory, National Institute of Standards and Technology, Gaithersburg, MD, USA

Gerhard Manier Weiterstadt, Germany

Paul Morrell Atomic Weapons Establishment (AWE), Aldermaston, Reading, UK

Axel Müller HTCO, Freiburg, Germany

Noé P. Navarro UL LLC, San José, CA, USA

F. Nizeyimana AREVA TN International, Saint Quentin en Yvelines, France

Mogon Patel Atomic Weapons Establishment (AWE), Aldermaston, Reading, UK

James E. Pickett GE Global Research, Niskayuna, NY, USA

Laura Pilon Atomic Weapons Establishment (AWE), Aldermaston, Reading, UK

Jeffrey P. Quill Q-Lab Corporation, Cleveland, OH, USA

Thomas Reichert Fraunhofer ICT, Pfinztal, Germany

Artur Schönlein ATLAS MTT, Linsengericht-Altenhasslau, Germany

Deborah Stanley Engineering Laboratory, National Institute of Standards and Technology, Gaithersburg, MD, USA

Kar Tean Tan Engineering Laboratory, National Institute of Standards and Technology, Gaithersburg, MD, USA

Department of Materials Science and Engineering, University of Maryland, College Park, MD, USA

Peter Trubiroha Berlin, Germany

Teodora Vatahska HTCO, Freiburg, Germany

Volker Wachtendorf BAM Federal Institute for Materials Research and Testing, Berlin, Germany

Gregory Von White II Sandia National Laboratories, Albuquerque, NM, USA

Christopher White Engineering Laboratory, National Institute of Standards and Technology, Gaithersburg, MD, USA

Kenneth M. White 3M Company, St. Paul, MN, USA

Kevin White Exponent, Inc., Natick, MA, USA

Kurt A. Wood Arkema, Inc., King of Prussia, PA, USA

Matthias Zäh Clariant, Gersthofen, Germany

Chapter 1
Predicting Elevated Temperature Ratings of Polymeric Materials

Noé P. Navarro

Abstract Product development cycles have become shorter with time, with companies standing to gain significantly by making their products available to the marketplace faster than what was typical to expect in the past. Even with this speed, producers need to comply with all quality and safety requirements, and consumers expect no less on these attributes. To this end, product developers and manufacturers have to work closely with their design teams to understand the customer's demands and to meet the product's performance, quality, and safety requirements. Specifically with safety, manufacturers have to understand end-use requirements as well as design a product that is expected to comply with all aspects of third-party safety certification. Faster cannot be synonymous with a loss in safety. Thus, speed in getting new products without loss of safety is a basic expectation of the marketplace and of society at large.

Keywords Performance • Aging • Thermal • Material • Compound • Formulation • Safety • Polymer • Heat • Degradation • Arrhenius • Ingredient • Additive • Modeling • Retention

Introduction

Product development cycles have become shorter with time, with companies standing to gain significantly by making their products available to the marketplace faster than what was typical to expect in the past. Even with this speed, producers need to comply with all quality and safety requirements, and consumers expect no less on these attributes. To this end, product developers and manufacturers have to work closely with their design teams to understand the customer's demands and to meet the product's performance, quality, and safety requirements. Specifically with safety, manufacturers have to understand end-use requirements as well as design a product that is expected to comply with all aspects of third-party safety certification. Faster cannot be synonymous with a loss in safety. Thus, speed in getting new

N.P. Navarro (✉)
UL LLC, 455E Trimble Road, San José, CA 95131, USA
e-mail: Noe.P.Navarro@ul.com

products without loss of safety is a basic expectation of the marketplace and of society at large.

Manufacturers are working closely with their design teams and the customer's design teams, using all available data to predict the expected performance of the product in the end-use application. In parallel, or subsequent to screening of design, the manufacturer must also seek third-party safety certification by organizations such as UL with recognized safety certification value. However, safety certification processes and the manufacturer's research activities for ensuring safety in the end-use application often diverge due to fundamental differences in responsibilities of the independent certification body and the originator of the technology. The safety certification process relies on a set of standard requirements that is, and especially so in the case of polymeric materials, intended for the end-use application. The certification testing is general in scope and performance based, relying on property characteristics to be considered further up the product chain. Yet, the design of a plastic part is very specific to the end-use application and its relative function in the overall product. Thus, predicting safety in an end-use product application starts with the research activities conducted by the plastic manufacturer to meet the overall customer demands for performance, quality, and safety. This research most often starts with a comparison of performance to existing plastic parts that have been used in similar applications with similar plastic compounds. The number of tests conducted on a plastic part at the manufacturer's research facilities to validate customer requirements is typically more than what is required in the plastic compound's UL safety certification process. But this detailed manufacturer's compositional information has enormous practical value for making a faster safety certification decision with no loss of safety. There is an opportunity for industry and safety certification bodies such as UL to work together and for the manufacturer to share research information with the safety certification body, to reduce time to market without sacrificing safety.

It is well known that since the advent of polymeric materials based upon crosslinked, phenolic-based resins, the expected performance has been based on past experience with this particular class of polymeric materials. The reason why thermoset materials are considered acceptable in switches at a 150 °C rated temperature is because it has been known to perform acceptably in applications at this level. That is, expected performance is based on past experience. The challenge with this experiential approach is that a fundamental understanding of the science behind performance is constantly advancing. In the 1960s, when advanced thermoplastic materials became available for widespread use, the opportunity to consider models for service life prediction that would be faster than traditional experience in the field was explored with the Arrhenius activation energy model. This was a progressive approach to evaluate polymeric materials with a model that would generate elevated temperature ratings faster; examples of use of this approach are IEC 60216-1 [1] and UL 746B [2]. To quote IEC 60216, "the listing of the thermal capabilities… based on service experience, was found to be impractical, owing to the rapid development of novel polymer and insulation technologies and the long time necessary to acquire appropriate service experience." Since then no other methods

have gained as wide an acceptance to model expected performance. There may be an opportunity to look at methods and techniques for fundamental polymer characterization to determine polymer characteristics in a very short time, such as dynamic mechanical analysis (DMA), thermogravimetric analysis (TGA), differential scanning calorimetry (DSC), and thermomechanical analysis (TMA), and to correlate this information to long-term thermal performance. Thus, while the adoption of Arrhenius activation energy equations to thermal aging was a major step forward in the 1960s, there may be an opportunity to look at analytical techniques to replace, or at least reduce, heat aging time.

The challenges with industry sharing product research and compositional information with certification bodies are many. For one, there is a fear of loss of confidentiality for the specific manufacturer, and the danger that the information disclosed may make its way to the competition. Another challenge is being able to communicate complex polymer science principles very specific to proprietary formulas—the manufacturer is likely to be much more adept at the technology they are intimately familiar with, and it can be difficult for the certification body personnel to thoroughly understand the technology when information is shared in a general basis to ensure intellectual property protection. Yet another challenge is a lack of standardization on the use of test data not specifically referenced in the standard that is being used to evaluate compliance.

If communicating specific information about a polymeric material to be able to make a prediction of its performance is a challenge, choosing the most effective model to make that prediction can be tough as well due to the complexity in the different chemistries. Polymeric materials are complex in nature, and there is more than one class of polymeric materials commercially available depending on the characteristics examined, for example, thermoset vs. thermoplastic compounds, crystalline vs. amorphous morphology, etc. Each is designed differently and each may perform differently as a result of temperature transitions and responses that complicate a uniform approach to using polymer characterization for the prediction of heat aging durability of all polymeric compounds. Viscoelastic behavior and time dependence play another important role in polymer behavior. The changes over time can be chemical or physical modes of degradation. One polymeric material can exhibit weight loss as a proxy for degradation, while another may not. A material may cross-link, or cure, and thus improve its thermo-oxidative resistance as it ages. Thus, a "one size fits all" approach to a polymeric material's service life prediction may not be possible. In fact, the abovementioned issues contribute also to some of the issues with the use of Arrhenius models today, but over time, practitioners of heat aging have devised some rules to reduce their impact. Practitioners of the Arrhenius activation energy approach caution against "excessive acceleration," i.e., one must stay within the realm of mechanisms that apply to the aging we are trying to predict with the accelerated higher-temperature heat aging tests [3]. Excessively high temperatures may invalidate the Arrhenius assumption of studying the same mechanism. Caution is required to ensure there is no loss of safety as we work on reducing time to market, as we look at analytical techniques to reduce heat aging.

Involvement of industry, certification bodies, scientific experts, and academia is crucial to discuss the path forward. The criteria of relative performance can never be abandoned during this transition where we study the unknown with a known reference with a rating, as it mitigates risk and ties back to observed service performance. Caution may very well mean an approach where we look at the magnitude of change in product design and then design a mix of analytical tools and heat aging, which is appropriate to the change. Small variations in polymeric materials may very well be the place to start exploring the use of analytical predictors of heat age performance.

While we pursue innovative solutions to shortening product safety evaluation times, we should also pursue the assessment of existing data on products and evaluate trends to determine if it is possible to rationalize shorter evaluation cycles for even larger variations.

In this paper, we will look at the status of current UL practices for elevated temperature ratings, look at opportunities offered for polymeric variations, and then look at the data mining approach to predict ratings.

Present Processes and Models to Predict Elevated Temperature Ratings

In this section, we summarize the interaction between producer and UL, in getting elevated temperature ratings established on a given product.

Certification processes for the producer start after "formulation or composition freeze"; in other words, to a large extent, the producer has already evaluated a number of variations or new material compositions for suitability in an application and decided on commercializing a specific mixture of identified ingredients with a precise concentration range and purity. The manufacturing process is also optimized to produce the finished product with defined properties. The producer then lists the new product grade (reflecting the composition of matter) with UL; this step includes the evaluation of flame ratings at a minimum, but may include evaluation of other short-term properties as covered by UL 746A [4] and UL 94 [5]. The producer then establishes a project with UL for getting elevated temperature ratings assigned.

When defining a project for elevated ratings, UL approaches "all polymeric materials deemed equivalent" as a first step in the evaluation process. There are some specific exceptions related to an evaluation, for example, the method for evaluating failure for polypropylene and the method by which different generic types have a different default relative thermal index (RTI) assigned, with the default for all plastics being 50 °C unless such a generic RTI has been established in UL 746B [2] for the polymeric type. For example, most polyphenylene sulfide (PPS)-based compounds can be assigned a generic RTI of 130 °C through suitable analytical identification without the need of temperature aging. This generic method is simple and extremely fast when considering the length of time typically associated with temperature aging, but the drawback is that sometimes the generic rating may not

reflect the typically accepted used temperature. For example, even though polyether ether ketone (PEEK) may have an expected used temperature of 220 °C, the generic rating is significantly lower at 130 °C. Yet, to be able to assign a temperature rating of 220 °C to PEEK, the evaluation is treated the same as any other polymer, when defining an elevated temperature test program, and it doesn't consider specifically the chemical, kinetic, and performance properties of PEEK.

In such an evaluation, the principle of relative performance is used. To take the simplest case of evaluating one new product grade, it is subjected to heat aging along with a control polymeric compound with recognized elevated temperature rating and on which UL has done a complete four-temperature evaluation in the past. One of the principles behind such side-by-side evaluation is to overcome any issues with oven design and performance affecting heat aging. Sample-to-sample and lot-to-lot variations must be considered in the elevated temperature investigation. The former may be evaluated in the standard deviations of the individual tests. The latter, however, is not as easy to predict.

The selection of control materials, unfortunately, also plays a large role in determining the elevated temperature rating of the candidate. Control materials may exhibit certain elevated temperature aging behavior, but may differ in composition; one may degrade in 10,000 h at its rated temperature rating, while another may degrade at 90,000 h.

Treating every material as equivalent for evaluation according to UL 746B [2] means that chemical formulation information is not considered for the evaluation of temperature ratings and assessment of elevated end-use temperatures. As an example of this point, if a producer has an unfilled polymer product with RTI ratings, and needs to get ratings for a new product which is the same polymer plus 30 % glass fiber, the fact that glass fiber would be infinitely superior in heat aging does not stop the full heat aging evaluation of the 30 % glass fiber-filled product or potentially the glass-filled product getting a lower temperature index assignment based on noise and technique limitations. Minor effects, such as glass fiber sizing (surface coatings) or impurities, may affect high-temperature performance.

While the heat aging evaluation may take 1–2 years, there is an option to obtain provisional ratings assigned prior to the completion of the evaluation. However, these rules may be too conservative, as they necessitate control and candidate failure at one or more temperatures; thus getting provisional ratings can easily take 6 months or longer.

With the standard program, per UL 746B [2], the control and candidate are heat aged at four temperatures in a full elevated temperature rating program. Usually a loss of 50 % of starting property value (F50) is taken to indicate the end of life of the material at that specific temperature. Thus, in the ideal world, for both candidate and control, for a given property such as tensile strength, we end up with four values of life at four different temperatures. Then, the Arrhenius model is employed to determine lifelines. From the lifelines, a correlation time is determined based on the assigned elevated temperature rating of the control. The temperature at which the correlation time is identified in the lifeline of the candidate material is then assigned to be its elevated relative temperature index (Fig. 1.1). The same process is followed

for toughness and electrical properties, to assign three temperature indices: mechanical strength, mechanical with impact, and electrical.

The control material selected may or may not belong to the producer of the candidate. That is, it may or may not have a similar composition. But it is expected to have an adequate heat aging field service history to be considered an adequate control material for use as the basis for the comparison.

To compute the 50 % property retention value, a material is heat aged to several time intervals, and although five specimens may be tested at each time interval, only
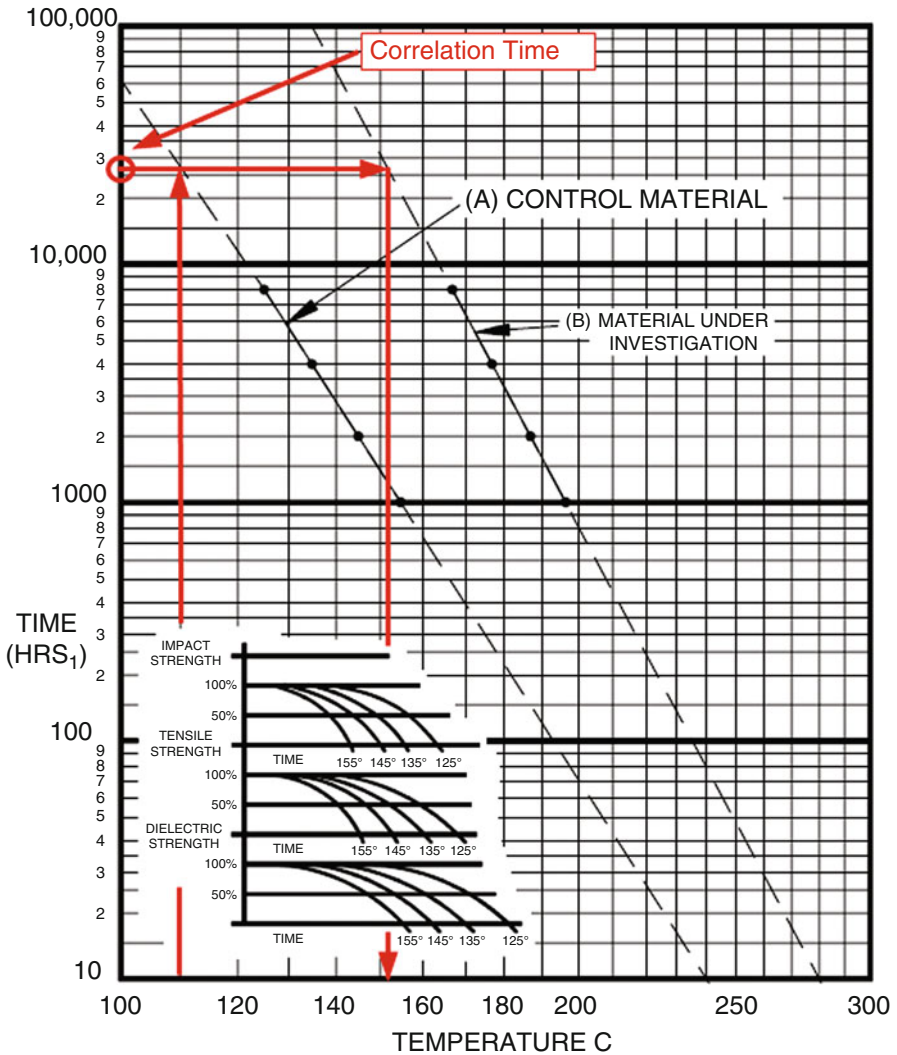
Fig. 1.1 Illustration of the determination of correlation time. UL 746B [2], 4th Edition
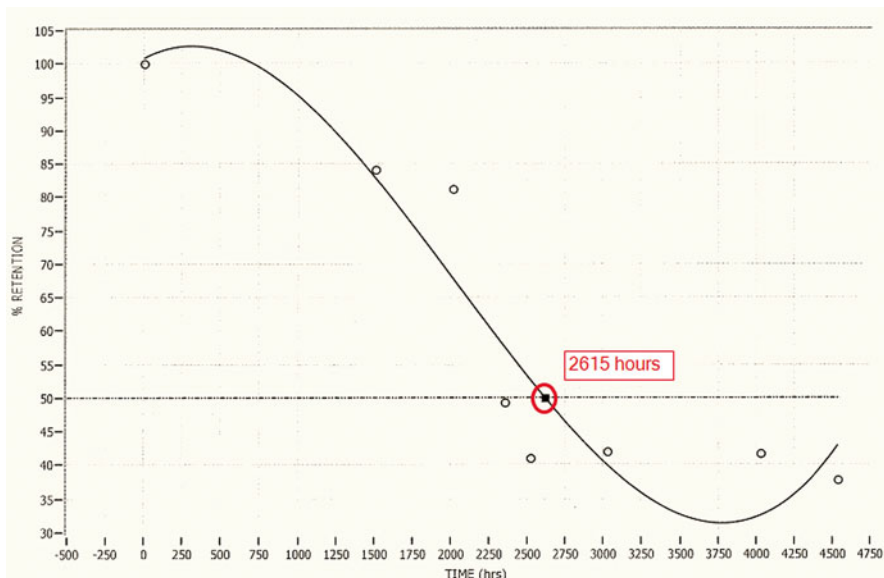
Fig. 1.2 Determination of end of life, in hours, at a given temperature and 50 % retention of initial tested property values

the average relative retention based on the percentage of the degradation of the initial property at each time interval is used to compute the 50 % end of lifetime value (Fig. 1.2). This value is computed by fitting up to a third-order polynomial regression equation, using R-square values as one of the parameters of regression model suitability. However, the standard allows for consideration of practical options for using the appropriate regression model.

The control and candidate must last at least 500 h at the highest temperature used and at least 5,000 h at the lowest temperature used. Sometimes, this causes a delay, in that an additional exposure temperature (or two) may be needed if the criteria are not met. For this reason, most producers tend to suggest reduced temperatures, which tend to prolong the program. It is also noted that in some thermally stable systems, such as fluoropolymers, highly heat stabilized systems, or amorphous polymers such as polysulfones and polycarbonates that are limited in accelerated heat aging by the glass transition temperature, failure is not reached in this time frame, and this results in longer time frames for the evaluation. For example, one may wait up to 20,000 h (2.3 years) and still not reach the degradation levels to define end of life in order to determine an elevated RTI.

In such cases, there is an opportunity to do proof testing at time intervals, such as 15,000 h or 20,000 h, to bring such programs to a close. For example, if property retention is greater than 60 % after 10,000 h, and candidate and control are tracking similarly, the program could resort to using a very conservative slope on an Arrhenius lifeline or by assigning the same ratings to control and candidate based on the similarity of test results.

In addition to the four-temperature or four-point program referred above, the UL 746B [2] standard allows for conducting two-point and one-point programs, which do limit the potential upside of getting higher elevated RTI ratings by offering reduction in heat aging. These programs typically are used for what is called a "related material" evaluation, which results in the same ratings for the candidate as the control.

As the discussion continues on the need for faster ways to determine and assign temperature indices, there may be opportunities to improve the existing methodology further. For example, the following may be considered:

– Using individual retention test results in the end of life regression analysis rather than the average values
– Defining end of life other than 50 % property retention
– Drafting a method for forcing closure of programs at 10,000 h of aging
– Faster assignment of provisional ratings based on a robust review of available data

Predicting Elevated Temperature Ratings Based on Producer's Available Data and Limited Heat Aging and Analytical Equivalency Validation at UL

In this section, we discuss the engagement of the producer with UL before finalizing the composition ("recipe freeze") or of producer supplying relevant developmental data or defining a shorter UL side-by-side comparative heat aging equivalency program in cases of minor polymer variations, i.e., small changes in composition.

The typical product development process for a producer (manufacturer) begins with the goals for marketing a specific set of materials which fit and meet market needs (Fig. 1.3). These goals are communicated to R&D to start activities for developing and understanding the viability of the developed materials in the marketplace. R&D conducts lab and production-scale trials and testing before developing a formulation that reaches the specification phase. After the product reaches the specification phase, meaning that it is tested and ready for production, it reaches the "recipe freeze" phase. From the company's perspective, at this point the material is ready for mass production and for sale. However, if the product is intended to be used in applications that need compliance with third-party safety marks, "recipe freeze" is the beginning of the process of safety certification. This can be a relatively rapid process for applications where flammability and short-term properties are the only compliance concern or a very long and unpredictable process if an elevated temperature rating is necessary.

This product development process suggests that there is substantial formulation and testing information generated by the producer by the time the process reaches the selection of the final composition or "recipe freeze." At this point the producer feels confident in the product that has been developed, and the safety certification is viewed as a formality that has to be fulfilled to enable the product to be fully market-
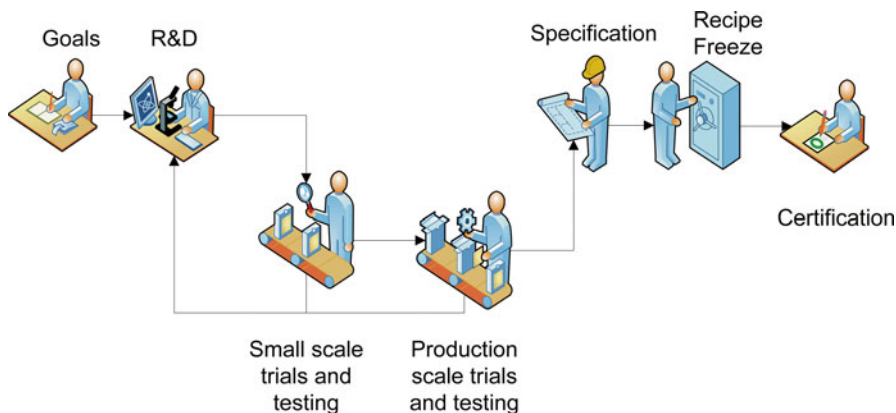
Fig. 1.3 Typical plastic compound formulation development process

able. R&D believes that if the data produced to develop and test the product to performance attributes and to reach the "recipe freeze" phase were taken into consideration by the certification organization, it would make it easier to determine compliance, especially when an elevated temperature rating is necessary.

If the plastic compound producer is willing to divulge research and development (R&D) data and field testing information generated in the product development process to get to "recipe freeze," it might be possible for the safety certification organization to determine whether the material meets expected levels of performance at elevated temperatures. Based on the level of information available, the certification organization can make certification requirement decisions that can help in providing ratings. If the information framework can be broadly standardized across the industry, then the certification organization can issue a formal Certification Requirement Decision (CRD) that can be consistently applied on each individual scenario.

It must be recognized that the information that is divulged by the producer cannot be standardized, as each development path is unique based on the unique science and developmental process of the producer. For example, if one is simply substituting a polyester material with another "similar" polyester material, and both materials are produced by the same manufacturer who has intimate knowledge of the differences between the two materials, then presentation of this information along with confirmation by the certification body by analytical means that "the polyesters are equivalent" would add to the affirmation by the producer and lead to the candidate getting equivalent temperature index ratings with limited confirmatory heat aging equivalency. In another case, the producer may be developing a more heat-stable material for robustness and reliability, but from a rating point, the elevated temperature rating for the control is good enough for the marketplace; thus, the producer may be able to supply analytical and their own heat age data to again convince the certification body to do a more limited evaluation. In yet another case, previous heat aging data could be referred to avoid heat aging completely and

get ratings based on research of prior data. Thus, only a framework could be standardized to facilitate this information sharing to speed time to market.

Once a level of standardization is known, or expected to exist, a proposal to develop or revise a standard can be submitted to the Standard Technical Panel (STP). In the case of elevated temperature ratings per UL 746B [2], the standard development process is under the control of the UL Plastics STP. A proposal can be submitted to this panel together with a CRD. Once a CRD is published, the elements of the standard proposal can be applied for evaluating products that result in published certification.

To summarize the discussion pertaining to the use of producer's information to speed up assignment of elevated temperature indices, there are two distinct steps to get equivalent temperature indices for new candidate products compared to controls with established ratings: (1) a sharing of analytical data between UL and producer as well as UL running additional standard or a tailored set of analyses to confirm producer's affirmation and (2) a sharing of heat aging data between UL and producer as well as UL running a limited side-by-side heat aging equivalency program to validate heat aging performance. A conformance decision by UL is needed on both steps, and knowledge about the end-use application can be helpful in reaching such a decision.

An area that can benefit from information sharing is related to polymer compound ingredient changes, more commonly referred to as "polymer variations." This is where a brand new compound formulation is not necessarily being designed, but rather an existing formulation is being modified to meet specific end-use requirements. The information provided to the certification organization can be used to validate performance in accordance with practices acceptable in industry. For example, a practice that has been found acceptable is a confirmation of performance between the "candidate" formulation (the one undergoing ingredient changes) and the "control" formulation (the one already approved) at a prescribed elevated temperature for 2,000 h. It is possible therefore to design a test program to evaluate compound ingredient changes with this program with the following elements:

– Specimens are aged at 2,000 h at an elevated temperature. The specimens are tested at 0 and 2,000 h to compute percent retention at 2,000 h.
– The elevated temperature is selected based on the material composition and selected properties, paying special attention to transition temperatures of the material and making sure that aging temperatures are chosen to avoid influence from the transition temperatures on the test results.
– The elevated temperature is selected based on the ability to provide a reasonable, recognizable, or measurable level of degradation at 2,000 h.
– The comparison between the *candidate* and the *control* is done through a robust statistical analysis (p-level of 0.05) where the variation in the heat age data is taken into consideration to define whether the two are equivalent or not.
– Primary properties are chosen to be tested.

After the aging is conducted, the following analysis can be conducted:

– An analysis of variation that confirms with at least 95 % probability that the performance of the *candidate* compound formulation is comparable to the *control*
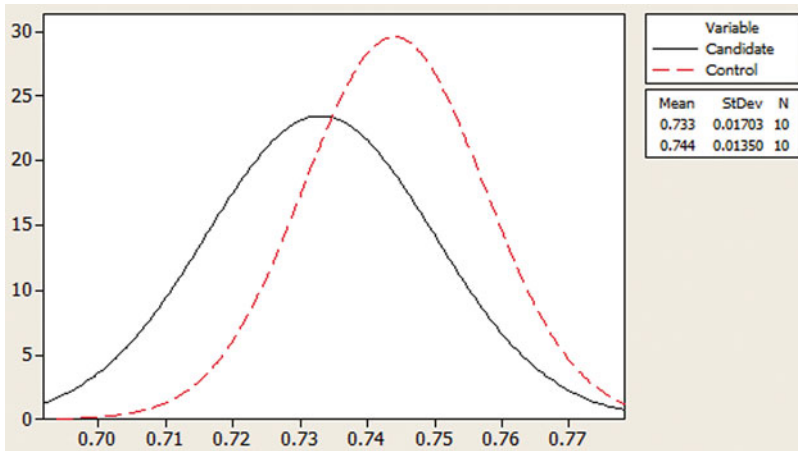
Fig. 1.4 p-value=0.127, materials statistically not different: acceptable
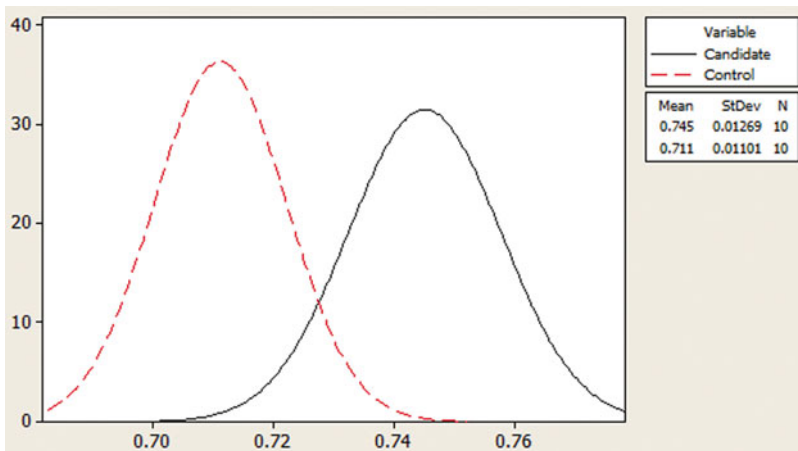
Fig. 1.5 p-value=0.000, materials are statistically different, but candidate outperforming control: acceptable

formulation. This would mean that the statistical p-value of the comparison would have to be greater than 0.05 (Fig. 1.4).

– If the performance of the candidate, based on the results of the chosen properties, is consistently greater than the performance of the control, the statistical p-value can be considered acceptable at values lower than 0.05, since this would mean that the candidate material can be expected to meet the requirements with the same confidence as the control material (Fig. 1.5). That is, the performance is different, but the candidate is outperforming the control.
– If the performance of the candidate is consistently lower than the performance of the control, the statistical p-value must be adhered to, since any value lower than 0.05 would suggest that the probability that the candidate and control materials are
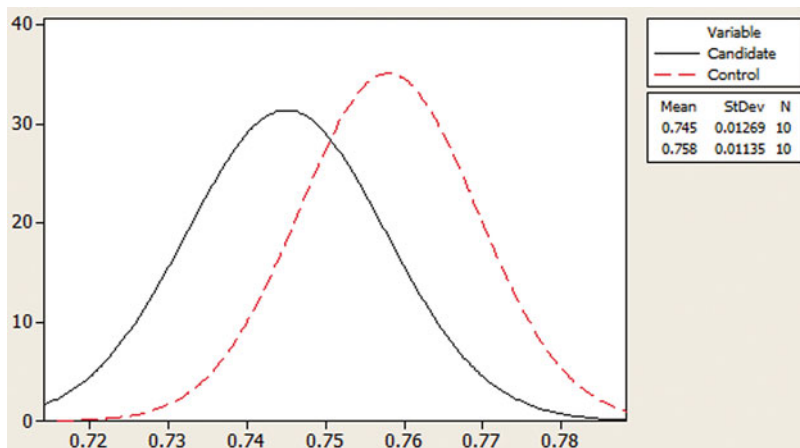
Fig. 1.6 p-value=0.027, materials are statistically different, and candidate underperforming control: not acceptable

different is greater than 95 %, and the performance is expected to consistently be lower than the control material (Fig. 1.6).

Since the expectation is that the performance of the candidate formulation will be the same as the performance of the control formulation, the elevated temperature ratings to be assigned to the formulation undergoing ingredient changes can only be the same. Ratings higher than those of the control material would have to be evaluated through the requirements of UL 746B [2] for the determination of elevated temperature relative thermal indices.

When this "2,000 h" program does not yield desirable results, meaning that the performance of the formulation of the candidate is confirmed to be lower than the control's at 2,000 h, then the Arrhenius activation energy model can be used to estimate long-term elevated temperature performance. Already in UL Standard of Safety 746B [2], there are methods described to evaluate plastic compounds to estimate long-term elevated temperature performance, as also described in the prior section of this paper. These methods are referenced in IEEE documents 1 [6], 98 [7], and 101 [8] and in IEC standards (60216-1 through 60216-6) that are similar in nature. But since these methods rely on a determination of end of life of the plastic compound at 50 % retention of initial property values, the data generated in the "2,000-h" program cannot be used, and the compound manufacturer is left with no option but to wait for enough data to be generated through a 4-point program, 2-point program, or 1-point program to be able to certify the compound formulation with elevated temperature ratings. This is the reason why it is critical for the compound manufacturer to have generated enough data through R&D, small-scale and production-scale trials, and testing to feel confident that the ingredient changes in the formulation do not result in a lower level of performance. This work helps in reducing the likelihood that

the candidate material will result in different and lower performance at 2,000 h resulting in having to restart a program that will typically take more time.

Before concluding this section, it is emphasized that the use of polymer analytical characterization methods can provide substantial new data and insight into material behavior and help develop faster heat aging studies with no loss in safety. These tools such as DSC, PDSC, DMA, and TGA conducted in both oxidizing and inert environments can help in characterizing and comparing materials even before they are exposed to high-temperature environments for extended periods of time.

Improving the Current Elevated Temperature Assignment Model

As mentioned previously, the existing elevated temperature assignment methodology could be further improved by:

– Using individual retention test results in the end of life regression analysis rather than the average values
– Defining end of life other than 50 % retention (as appropriate)
– Drafting a method for forcing closure of programs at 10,000 h of aging
– Assigning provisional ratings faster based on a robust review of available data

Regardless of whether the single temperature 2,000-h heat aging program is used or the full four-point traditional UL 746B [2] program, it is imperative that a better statistical analysis be conducted on the data to analyze material performance. But, to design a test program with a robust statistical method, it requires a thoughtful understanding of the material property to be tested and the variation in test results when the plastic compound is tested for a given property. For example, it is well understood in the plastics industry that test properties to determine material toughness, such as impact strength test methods like Charpy or Izod, sometimes produce test results that are not very consistent. Because the typical sample size suggested by most standards is five specimens per set, it is sometimes difficult to determine the sample variation. And if this sample variation is not properly taken into consideration, it can result in a lack of fit to a regression curve necessary for determination of end of property life. Thus, one potential improvement would be for sample size to reflect the variation in the property test results for the specific material. Either the test property needs to be selected so that variation is reduced or the sample size needs to be selected large enough so that the variation is appropriately taken into consideration in the analysis.

In terms of defining end of life with 50 % retention, it is challenging to evaluate polymeric compounds for performance at elevated temperatures using the Arrhenius activation energy model when the individual behavior of different compound classes and formulations does not necessarily fit the model. The Arrhenius model may work very well when the compound exhibits first-order kinetics (Feller, 147). However, plastic compound formulations are complex chemical mixtures of multiple

Fig. 1.7 The polyethylene (PE) and polytetrafluoroethylene (PTFE) chemical structures

components designed to serve specific purposes and in some cases designed specifically to prevent the very reason the Arrhenius model works, gradual thermal oxidation. Reaching 50 % property degradation is sometimes difficult in a reasonable time, going as long as 15,000 h or longer before an aging experiment has to be stopped due to no data at the 50 % retention point. And although Arrhenius assumes that an increase in temperature will result in faster degradation times, this is not always physically possible. In the case of polytetrafluoroethylene, increasing the temperature any higher than 320 °C causes the polymer to melt resulting in an experiment that no longer yields useful results by choosing ever higher temperatures to accelerate thermo-oxidative degradation resulting in a decrease in aging time. However, for polyethylene it is possible to cause thermo-oxidative degradation at temperatures much lower than the melting temperature. The explanation for the differences in thermal stability is directly associated with the chemical structure of these polymers (Fig. 1.7); the C–H bonds in PE are susceptible to thermal oxidation, while PTFE hinders chain scission through perfluorination by eliminating vulnerable C–H bonds.

These two different polymer structures serve as the simplest example of how the Arrhenius activation energy model works well for polyethylene, but the degradation mechanism of PTFE is more complex. Fortunately for the plastics industry (but not so for those making predictions on temperature performance), polymeric compounds are a mixture of different components that are included to achieve the requirements of the end user. If the end user asks for a material that is highly stable at higher than typical temperatures, the compounder will attempt to add ingredients that can stabilize the formulation in the presence of oxygen and heat. There is a wide variety of strategies to achieve thermal stability in the industry, and the purpose is to protect the polymer chains from dangerous oxidizing radicals. Therefore, by trying to prevent oxidation, the most common predictive model that primarily relies on oxidation taking place may no longer be applicable. Thus, other models or methodologies would be welcomed to provide a reliable high-temperature profile of the compound in question.

The relation between thickness and assigned elevated ratings could be reexamined to determine the effect of surface oxidation and how it may shield oxidative attack deeper in the tested specimens. Researchers have discovered that some materials exhibit surface oxidation that inhibits further degradation of the interior material. For these classes of materials, a way to rationalize and reduce heat aging at different

thicknesses would also be a benefit. But for that matter, thinner samples present their own challenges in testing and characterization.

And though it is difficult to fit the lack of property degradation data to the Arrhenius model, the opportunity is there to draft a standard method that would provide for completing aging programs shortly after 5,000 h if significant degradation is not observed. One method that has been proposed is the use of a standard slope using an assumed end point at 10,000 h of aging and an extrapolation to a 20,000-h lifetime prediction.

Finally, knowing the basic chemical, kinetic, thermal, and viscoelastic properties of a material relative to a known and already rated material, it may be possible to assign similar ratings on a provisional basis for safety certification if the data provides confidence that the materials are to be considered to have similar profiles on all reviewed and generated data. The 2,000-h temperature validation would secure the ratings if the retention levels between the candidate and the control are found to be statistically similar.

Future Opportunities on Predicting Elevated Temperature Ratings

Since the 1960s, UL has accumulated a substantial volume of heat aging data based upon thousands of investigations on an enormous range of polymeric materials. There exists an opportunity to analyze or mine this data to discover trends and reduce uncertainty in elevated temperature assignments and thus to reduce the necessary burden of proof.

This data-mining model is based on existing information already available for similar compound formulations. This model can work well with compound manufacturers that have already conducted plenty of material evaluations to predict high-temperature polymer compound performance. For example, if one of these manufacturers has already evaluated 30 different formulations of a polyamide and they are all rated with elevated temperature ratings, it may be possible to get a "cloud" of ratings with all the different degradation profiles for each one of the formulations. If a new formulation is designed within the same polymer class and with similar ingredients as those in the "cloud," it may be possible to make inferences about the performance of the new formulation.

As shown in Fig. 1.8, the questions about the ratings of a particular formulation are not impossible to answer when additional information is available about similar known formulations for the same polymer class. If similar ingredients are used, it can be reasonably expected to see similar polymer performance. With this expectation it may be possible to assign a rating on a provisional basis and to conduct a set of material property tests to validate and confirm the similarity in material performance of the new formulation.
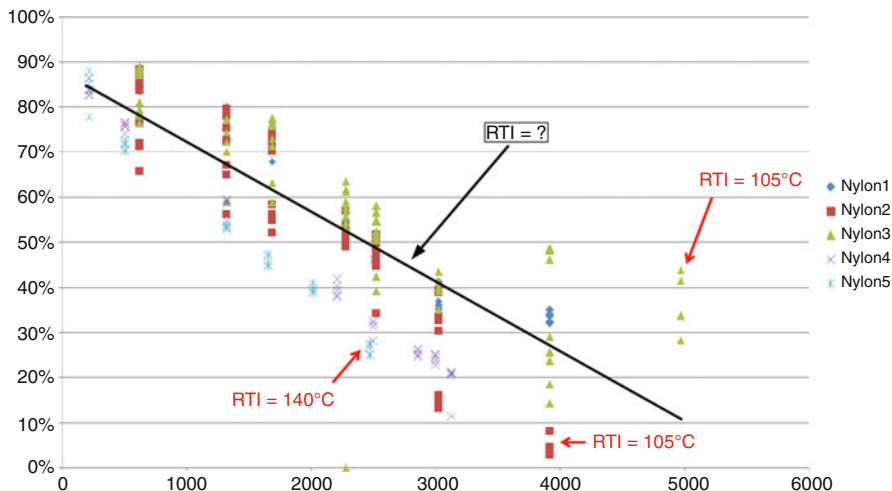
Fig. 1.8 Relative temperature index (RTI) cloud of known formulations and prediction of RTI on new formulation using similar compound ingredients in the "cloud" of several nylon formulations

This "cloud" modeling can begin with the individual manufacturers and can grow into larger sets of data that can analyze performance across manufacturers for all polymer classes. The data mining for this type of relational database can be daunting, but the benefits in predicting long-term high-temperature performance of similar compound formulations can be immeasurable. This would allow for a very quick prediction in performance based on similarity of ingredients in the formulation serving the purpose of meeting a customer need fast and without loss of safety. Based on this "cloud" analysis, the probability is high that the temperature rating will be similar to existing formulations and a fast confirmation based on existing test methods can help confirm the performance. A 2,000-h confirmatory test can serve to confirm similar performance in a much swifter manner than existing long-term aging methods using the Arrhenius activation energy model.

Once the cloud concept has been experimented with and established, a further step in the future would be to extrapolate out of the cloud, to assign better materials even higher ratings than the cloud covers.

Another model is already provided by an existing UL standard but needs further analysis and refinement. In UL Standard 746A [4], Table 9.1 has a generic list of ingredients that can be used in a polymeric compound formulation within acceptable concentrations. The table includes concentrations that are possible to include in formulations without the need to conduct additional testing in the compound. Consequently, it also includes information about concentrations that require testing to determine the similarity or the lack of similarity in the compound formulation. When the concentration levels are beyond the indicated values, sometimes the testing will include long-term elevated temperature aging.

Additive	Addition	Deletion	Replacement [6]	Change in Level
	(absolute %)	(absolute %)	(absolute %)	(normalized %)
UV stabilizer	≤0.3%, See A >0.3 but ≤5%, See AD >0.5%, See BDE Thermal aging!	≤0.5%, See A >0.5%, See BE No Thermal aging!	≤0.15%, See A >0.15% but ≤0.25%, See AD >0.25%, See BDE	Increase ≤30%, See A Increase >30%, See BDE Decrease ≤30%, See AE Decrease >30%, See BDE

Fig. 1.9 Illustration of the contradiction in adding and deleting a UV stabilizer

Table 9.1 in UL 746A [4] needs clarification on the way it describes testing for ingredients that need to be added or deleted vs. ingredients that need to be replaced or where the concentration level is changed using the same ingredient. The table appears to be more stringent on replacements and changes in level that it might be for the absolute addition and deletion of ingredients. For example, in the case of an antioxidant, it is possible to remove up to 0.5 % concentration without requiring a long-term elevated temperature aging, but a change in level of 30 % normalized content would require long-term aging even if the change in concentration is less than 0.5 % absolute. The same happens with replacement of ingredients and equally for the rest of the generic ingredients listed in the table.

Table 9.1 needs refinement to address certain ingredients that may have a different effect than originally considered when the table was developed. The perfect example of needed refinements in the table is the UV stabilizer ingredient (Fig. 1.9). In this case adding a UV stabilizer requires thermal aging, but deleting it does not. The assumption for not requiring thermal aging to delete a UV stabilizer is possibly due to the fact that UV stabilizers are added independently to prevent UV light radicals from attacking the polymer chain. Since it is not added to prevent thermal oxidation, deleting it is not expected to affect thermal oxidation. But if this logic follows its conclusion, then adding a UV stabilizer should not require thermal aging as is proposed in the table, since a UV stabilizer would be expected to enhance the oxidative properties of the compound or at least not have an effect at all. Thus, to refine the table it might be required to propose a modification to remove the requirement for running long-term thermal aging when UV stabilizer is added to the compound. Other ingredients on the table may need to be reviewed with the same level of scrutiny to make sure their changes lead logically to the appropriate investigation.

Conclusions

It is appropriate to emphasize that the shorter development cycles challenge the existing methods to develop temperature indices and relative temperature indices for polymeric materials. Compounders and material suppliers work hard to develop a product that meets their customer's expectations for products that meet performance, quality, and safety requirements. And thus, the current process, although

respected for its fundamental science, is considered to take too long to deliver products with the safety certification required in the marketplace. By looking at novel ways of analyzing material's thermal and viscoelastic properties, it must be possible to work together with product suppliers to review their own research and development data and validating new material performance based on the similarity with known and already evaluated materials.

This is the first step. Other steps that need to be taken that would more fundamentally change the way polymeric materials are evaluated are by mining the retention data for already heat-aged materials and associating it with their formulations on an aggregated plot of multiple lifelines, the RTI cloud. This cloud could create RTI boundaries where the lowest rating would be possible to be assigned to a polymeric material within the cloud with only a few analytical tests run to confirm the basic chemistry of the compound. The highest rating would require a validation through oven aging, but even those aging temperatures and times would be easily predicted by the formulation's position within the cloud.

Although this would be a major step, minor steps can be taken as discussed in this paper. Future steps can be defined as this UL 746B [2] LTTA Forum continues discussions on what is possible to accomplish through science, in order to continue to chip away at cycle times to meet market demands while making sure that requirements are met without loss of safety.

References

1. IEC 60216–1 (2013) Electrical insulating materials - thermal endurance properties - Part 1: ageing procedures and evaluation of test results, 6 edn
2. UL 746B (2013) Polymeric materials - long term property evaluations, 4th edn
3. Feller RL (1994) Accelerated aging – photochemical and thermal aspects, p. 97
4. UL 746A (2013) Polymeric materials - short term property evaluations, 6th edn
5. UL 94 (2013) Test for flammability of plastic materials for parts in devices and appliances, 6th edn
6. IEEE 1 – Recommended practice - General principles for temperature limits in the rating of electrical equipment and for the evaluation of electrical insulation
7. IEEE 98 – Standard for the preparation of test procedures for the thermal evaluation of solid electrical insulating materials
8. IEEE 101 – Guide for the statistical analysis of thermal life test data

Chapter 2
Laboratory-Based Predictions of Weathering in Outdoor Environments over the Entire Degradation Pathway

Kenneth M. White, David M. Burns, and Travis Q. Gregar

Abstract A useful estimate of outdoor service life for a material or product based on laboratory weathering experiments requires a careful assessment of the degradation pathways that result from exposure. Furthermore, converting real-world conditions into parameters that serve as inputs to models based on the accelerated weathering stresses of radiation, heat, and moisture is not trivial. In an effort to study these relationships, a model material was weathered under accelerated conditions in the laboratory, from which mathematical formulas were derived to describe the resultant photodegradation rate as a function of irradiance and temperature. Calculations for a specific geographical location yielded degradation as a function of time that exhibited excellent agreement with actual outdoor weathering results over the entire degradation period. Variations on the method of calculation proved the mathematical model to be robust. Investigation of chemical degradation in the model material revealed the possibility of more than one reaction pathway. Such behavior is readily apparent in other polymer systems we have studied, wherein the exposure conditions employed can lead to a lack of synchronization of changes in the material or can produce significantly different degradation pathways, both of which affect lifetime estimates.

Keywords Service-life prediction • Real-world validation • Degradation pathways • Degradation-rate model • Accelerated life testing • Cumulative damage model

Introduction

The objective of a service-life prediction (SLP) protocol is to provide the tools for estimating the functional life of a product without having to wait to measure time to failure in time-consuming, natural weathering tests. SLP can also be employed to

K.M. White (✉) • D.M. Burns • T.Q. Gregar
3M Company, 3M Center 235-BB-44, St. Paul, MN 55144-1000, USA
e-mail: kmwhite@mmm.com

assess how service life varies when a product is used in different climates or environments. Ideally, the output of an SLP study would be a formula describing the degradation of product function over the course of its lifetime:

$$P(t) = P(0) + \int_0^t \frac{dP}{d\tau} d\tau \tag{2.1}$$

Here, P is a property that changes over time due to weathering exposure until it reaches a point determined to be indicative of product failure. The rate of this degradation process, $dP/d\tau$, depends on the stresses to which the product is exposed. Generally, the SLP protocol limits these stresses to radiation, heat, and water—those of primary importance in the outdoor environment. The degradation rate also depends on the chemical and physical reactions involved and their associated kinetics, keeping in mind that they may not be zero order. This "degradation-rate" approach is different from accelerated life testing, which instead determines the effect of environmental stresses on time-to-failure data. In so doing, it focuses on the end state of the material. Not only does the degradation-rate method shown here provide time-to-failure estimates; it tracks degradation in the material along the entire pathway to failure.

The value of any SLP approach lies in its ability to predict real-world results. For example, it should be able to provide an estimate of time to failure for a given outdoor location with some degree of accuracy. It should demonstrate that both the manner of degradation and the associated pathway toward failure are identical in the laboratory and outdoor weathering exposures. Finally, it should be able to do this using readily available climate data from multiple global locations as inputs to the stress-dependent formula, such as the degradation-rate model given by Eq. (2.1).

A number of studies have been conducted to investigate how well SLP accomplishes these goals for selected polymer-based materials [1–4]. From these, reasonable estimates of lifetime were obtained as compared to actual values of time to failure observed for outdoor exposures. Some of the predictions covered the entire degradation pathway, for which changes in material properties generally followed a trend similar to that measured during outdoor weathering. The SLP methods employed varied somewhat from study to study and all used measured climate data to test their models.

In order for SLP to continue to gain credibility as a viable tool for gauging the durability of a polymeric material, a careful examination of its capability should be conducted. By performing the investigation with a model material whose degradation attributes are well behaved and generally understood, the SLP protocol itself can be tested. The objectives of the study include:

1. To develop a laboratory-based weathering degradation model and examine it as applied to a real material in a real environment
2. To determine if the model is consistent with the actual degradation rate observed for the material as well as the chemistry and physics responsible for degradation in the material

3. To validate the result predicted by the model over the entire degradation pathway by comparing it with results from a real-world exposure
4. To examine the many approximations made throughout the entire SLP process and assess how robust—and ultimately, how useful—the model will be

One of the advantages offered by this study is the ability to examine the sensitivity of the SLP estimate to climate data. In order to use the SLP model, one must have access to a dataset that includes values for solar irradiance, ambient temperature, and some measure of exposure to water. Since each SLP estimate is particular to a given location in the world, these values generally come from climatic models that are based on multi-year averages. Because weather data will vary from year to year, an assessment of how well these averages represent the weather in any given year is of interest. This study compares SLP results obtained using average climate data with results obtained using weather data measured during the actual outdoor exposure.

A significant challenge encountered in the utilization of the SLP methodology is the need to convert climate data into a form that can be used by the model. For example, solar irradiance for a given outdoor location is typically reported for the wavelength range 290–3,000 nm, but the SLP model is typically based on an irradiance that is experimentally controlled at 340 nm. There are multiple ways to perform the necessary transformations, which could lead to differences in the resulting lifetime estimates. The robustness of the SLP model with regard to these transformations is examined in this study in an effort to assess the level of variability that may result due to the particular transformation selected.

There is also more than one way to apply an SLP model in order to generate a lifetime estimate. Some studies have employed a cumulative damage model in which, akin to the method of Miner's Rule [5], the "fraction of life lost" during each time interval in the exposure is determined and the fractions are summed over all intervals until the point in time at which service life runs out. Others have modeled as a continuous function of time the degradation of a property that relates to the failure mode. This latter method, which has been discussed in the literature in detail [6], served as the basis in this study for determining the complete degradation curve resulting from exposure. The lifetime estimate that it produced is compared herein to a corresponding estimate obtained using the cumulative damage model.

Experiment

The model material that was weathered in this study was a fluorescent yellow poly(vinyl chloride) (PVC) film containing the dye C. I. Solvent Yellow 98, additives typically found in plasticized vinyl, and a hydroxybenzophenone UV absorber. The glass transition temperature (T_g) of the film was below −20 °C, as determined by differential scanning calorimetry. Its transparency, which was retained during weathering, made it possible to conduct a highly quantitative study. The dye fades

Fig. 2.1 Degradation of
absorbance for Solvent
Yellow 98 in polycarbonate
(PC) and poly(vinylchloride)
(PVC) films exposed in
ASTM G155 Cycle 1
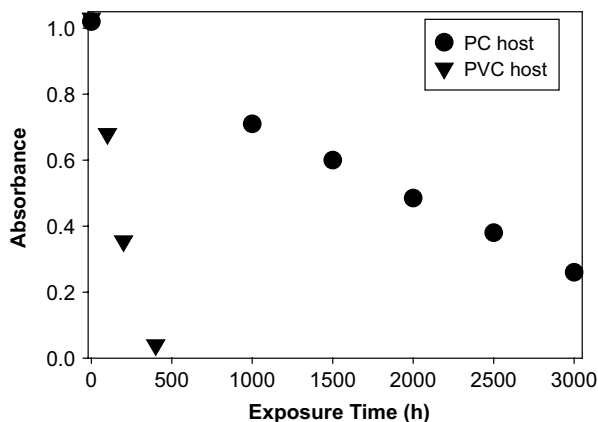
under exposure to light, and the resulting decrease in dye concentration was
monitored via visible absorption spectroscopy.

Although the degradation of interest pertains to dye molecules, the polymer
host has a very significant effect on the rate of degradation of this colorant. Its
lifetime in polycarbonate far exceeds that in vinyl (see Fig. 2.1)[1], thus affecting the
applications for which it can be used in products. Guest-host interactions such as
this are not unusual. The type of guest colorant can also affect the durability of a
polymer host. Regardless, the choice of this model material meets the requirement
of an easily interpretable failure mode that can be used to test the attributes of the
SLP method.

Individual 250-μm film specimens were cut to just over 25 mm×25 mm in size
and mounted between aluminum plates having 25 mm×25 mm windows. Prior to
cutting the specimens, the film was annealed at 70 °C for 24 h so that the weathering
exposure itself would not induce any shrinkage that could cause a change in absor-
bance and confound the results. For the outdoor weathering (Arizona45S), the alu-
minum plates containing the specimens were affixed to larger holders (2 specimens
per holder) and mounted unbacked at 45° tilt, facing south at the DSET Laboratories
test site near New River, Arizona. The exposure was conducted according to ASTM
G7-05[2] under direct sunlight from July 23 to October 21, 2008. One holder was
removed from exposure every 5 days up to a total of 30 days and every 10 days
thereafter up to a total of 90 days. For the duration of the test, solar irradiance and
temperature data were collected at 1-min intervals. The irradiance data included
total solar (full spectrum) and TUVR (295–385 nm) measurements made at a 45°
tilt. The temperature data comprised black panel and white panel measurements—
also at 45° tilt—as well as ambient temperatures.

---

[1] Exposure conducted according to Cycle 1 in ASTM G155-05a Standard Practice for operating
xenon arc light apparatus for exposure of nonmetallic materials

[2] ASTM G7-05 Standard Practice for atmospheric environmental exposure testing of nonmetallic
materials

The accelerated laboratory weathering was performed in Atlas Ci5000 Weather-Ometers®, each with a xenon arc light source surrounded by a quartz inner filter and a 3M proprietary outer filter [7] to approximate daylight. The weathering cycle consisted of an 8-h segment with light only, followed by a 4-h dark segment, a portion of which included water spray. The experiments employed four different levels of irradiance (0.3, 0.5, 0.75, and 1.0 W/m²/nm at 340 nm) with white panel temperature (WPT) held at 70 °C and five different levels of temperature (50, 55, 60, 65, and 70 °C) with irradiance held at 0.75 W/m²/nm. The exposures were temporarily interrupted at regular intervals in order to measure the progress of the specimen degradation. In a separate set of experiments, the effect of exposure to multiple levels of water was also examined. The impact of increasing time of wetness from 4 up to 50 % of total cycle time was found to be sufficiently small that it could be ignored.

Degradation due to weathering was followed by measuring the absorbance of the dyed film as a function of time of exposure. Spectra were measured using a Shimadzu UV-2550 spectrophotometer (UV-2401 for some replicates) set at 1-nm bandpass and equipped with a holder assembly that ensured repeatable positioning of a specimen each time it was measured. A file specimen that was kept in the dark at room temperature was also measured at each interval. Its spectra revealed that the repeatability of the absorption measurement was very near to the photometric repeatability specified for the spectrophotometer (±0.001 absorbance units).

For each spectrum, the peak absorbance at 455 nm was determined. This value was corrected for losses in the spectrophotometer due to reflection at both film surfaces by subtracting the absorbance reading obtained at 800 nm, where no dye absorption was detected. The observed losses were in agreement with reflectivity values predicted from the refractive index of PVC. The peak absorbance was also corrected by subtracting the residual absorbance that persisted at 455 nm after the film had been completely bleached. This method of correcting for residual absorbance gave the same result as scaling the initial absorption band to fit each subsequent one and determining the fraction lost as a function of time. No evidence for weathering-induced yellowing of the PVC host itself was observed.

Results and Discussion

A major premise of SLP, as with any accelerated weathering protocol, is that the degradation pathway resulting when environmental conditions are employed to accelerate the degradation to failure in the laboratory must be identical to the pathway observed for the natural exposure. To verify this condition, absorption spectra for the fluorescent vinyl films measured as a function of weathering exposure are displayed in Fig. 2.2. One can readily see that changes to the spectra followed the same pathway for both the laboratory and outdoor exposures shown. Similar results were observed for the remaining laboratory weathering cycles, thus satisfying the requirement.
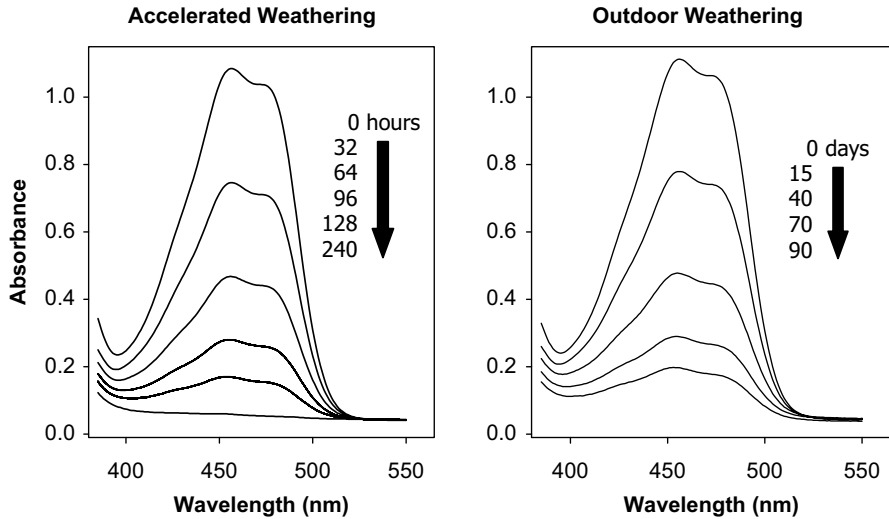
Accelerated Weathering

Outdoor Weathering

Fig. 2.2 Degradation of absorbance in the fluorescent yellow vinyl films resulting from exposures in the laboratory (I=1.0 W/m²/nm at 340 nm, WPT=70 °C) and outdoors (Arizona45S). These spectra were not corrected for reflection losses

Deriving the SLP Model

In a previous study [8], a model based on a first-order rate equation was derived to account for the effect of irradiance on the degradation rate of dye concentration in the fluorescent vinyl film. This model was subsequently modified to account for the impact of temperature by including an Arrhenius factor:

$$-\frac{\mathrm{d}D(z,t)}{\mathrm{d}t} = \frac{\sigma^* I(z,t)}{k_2 \sigma^* I(z,t) + k_3} e^{-K\left(\frac{1}{T+273.15} - \frac{1}{343.15}\right)} D(z,t) \tag{2.2}$$

where D is the local concentration of the dye and I is the local irradiance, both of which depend on depth in the film (z) and exposure time (t). The absorption cross section is given by σ^*. The Arrhenius factor is shown explicitly with fitting parameter K equal to E_a/R, where E_a is the Arrhenius activation energy and R is the gas constant. The effect of temperature T (in °C) is relative to 343.15 K (70 °C), which is used as the reference temperature since the exposures as a function of irradiance all operated at this WPT. Parameters k_2 and k_3 are constants that come from the derivation of the model [8]. Equation (2.2) can express the decrease in absorbance of the fluorescent vinyl films with weathering exposure because dye concentration was determined to be directly proportional to absorbance, in accordance with Beer's Law.

In order to determine the values for K, k_2, and k_3 in the SLP model, the absorbance data obtained as a function of exposure time for all eight laboratory weathering
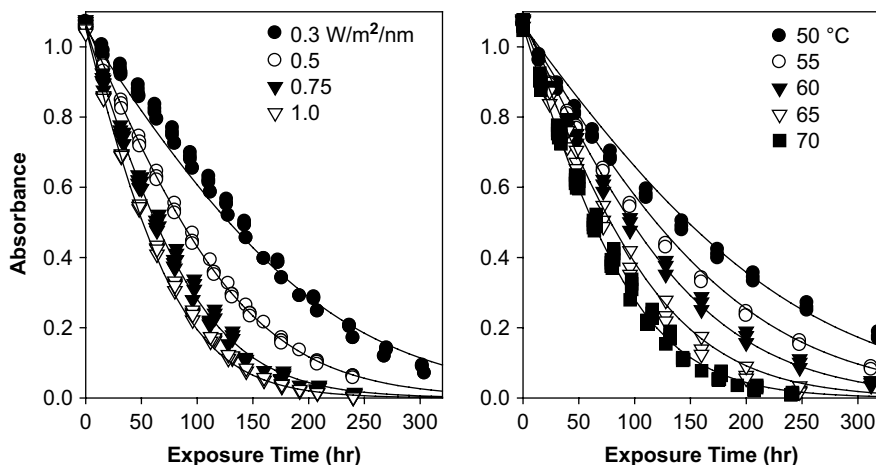
Fig. 2.3 Degradation of peak absorbance in the film specimens as a function of the indicated exposure conditions. The curves represent a simultaneous fit to all of the data using Eq. (2.2)

conditions were fit simultaneously using a simplex algorithm [9] applied to an iterative numerical method described previously [10]. For the experimental absorbance data, exposure time was defined as time during which the light in the weathering chamber was on, since the model predicts no degradation when $I = 0$. The fit, represented by the solid curves displayed in Fig. 2.3, yielded K = 4,710 K, $k_2 = 21.0$ s^{-1}, and $k_3 = 53.6$ s^{-2}. Absorbance data for all 33 film specimens included in the study are also plotted in the figure, indicating how well the model accounts for the experimental results.

Individual fits to the absorbance data were also performed for each film specimen according to the conditions under which it was weathered. Defining a pseudo-rate constant, k_{eff}, as the pre-factor of D on the right-hand side of Eq. (2.2), a value of k_{eff} was then determined for each specimen. These values are graphed in Fig. 2.4, showing both the dependence as a function of irradiance and as a function of temperature. The solid curves in the plots were calculated using the aforementioned parameters obtained from the fit of all of the experimental absorbance data. Thus, the curve in the plot of irradiance dependence is also influenced by results from the temperature-dependent experiments, and vice versa. The linear response in the temperature plot signifies Arrhenius-like behavior in the temperature range shown. The lack of linearity in the irradiance plot is indicative of reciprocity failure. The dependence on irradiance given by the model in Eq. (2.2) is different from the commonly used power law. It has been shown [8] to be consistent with photophysics of degradation from the triplet state, previously observed in other dyes of a similar class [11]. An outcome of this expression is that unlike the power law, it exhibits linear dependence at low levels of irradiance, which would be expected in a photochemical reaction.
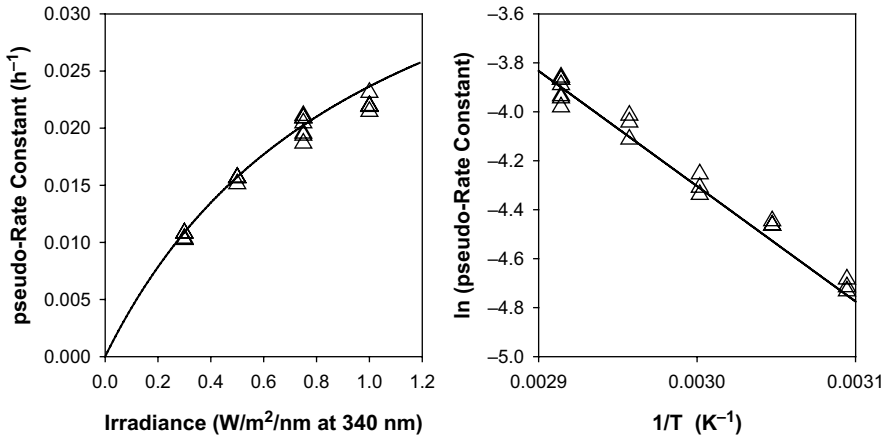
Fig. 2.4 Rate of degradation of absorbance determined for the individual film specimens plotted according to their exposure conditions. The curves were calculated using the parameters obtained by simultaneously fitting all of the absorbance data with Eq. (2.2)

Calculating the SLP Estimate

In order to utilize the derived model to predict degradation of absorbance in the fluorescent vinyl film due to outdoor exposure in Arizona, climate data for the appropriate time period needs to be transformed into a set of parameters that the model can use. With regard to the irradiance parameter, solar irradiance from the outdoor exposure must be represented by an appropriate value for the xenon arc irradiance at 340 nm in the laboratory exposure. Both total solar irradiance (290–3,000 nm) and ultraviolet solar irradiance (295–385 nm, commonly referred to as TUVR) data from the outdoor site were measured during the Arizona45S exposure. However, the graph in Fig. 2.5 shows why a conversion is difficult. The plots of the ratio of total solar irradiance to TUVR measured as a function of time of the day near New River, AZ, for a south-facing, 45° specimen tilt on July 28, 2008, and October 21, 2008, reveal that the fraction of TUVR (and thus, 340-nm radiation) in the total solar irradiance varies significantly with the time of the day and the day of the year. In midsummer, the solar radiation reaching the specimen around dawn and dusk is largely due to light scattering, which favors short wavelength (UV) radiation. Thus, the ratio drops off at the beginning and end of the day. In contrast, during the fall, the solar radiation striking the specimen around dawn and dusk is primarily from direct sunlight, which is deficient in UV radiation that has been scattered out of the light path from the low-lying sun. This causes the ratio to rise sharply. During the middle of the day, when irradiance has its greatest effect on photodegradation, the ratio is fairly constant.

Since TUVR data from the outdoor exposure site were available, it was decided to convert the TUVR to actinic irradiance and then use the measured spectral power
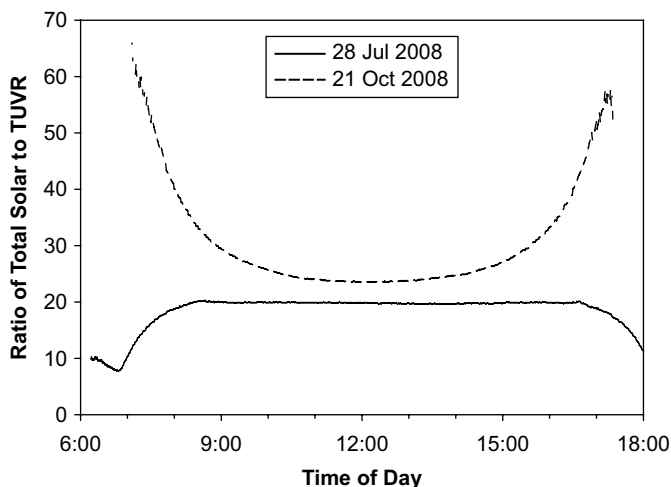
Fig. 2.5 Effect of time of the day and day of the year on the amount of UV radiation present in the total solar irradiance measured at New River, Arizona

Table 2.1 Calculated ratio of irradiance at 400–520 nm to TUVR (295–385 nm) for a specimen near New River, Arizona, facing south, tilted at 45°

Date	Time (approx.)	400–520 nm/TUVR
July 24, 2008	12:30PM	4.1
July 24, 2008	5:50PM	4.0
Sep 6, 2008	12:30PM	4.3
Sep 6, 2008	5:20PM	5.1
Oct 21, 2008	12:00PM	4.8
Oct 21, 2008	4:50PM	7.0

distribution of the xenon arc source to further convert to irradiance at 340 nm for input to the model. It was assumed that the actinic radiation was limited to the 400–520 nm range, since the dye absorbs very strongly in this region compared to the UV, and inclusion of UV absorbers in the film minimized the level of UV radiation reaching the dye anyway. Factors to convert TUVR to actinic irradiance were determined using SMARTS 2.9.5 [12, 13]. The SMARTS calculations provided spectral solar irradiance at a specified zenith and azimuth of the sun for a given specimen orientation and geographical location. The results corresponding to the sun's position near peak solar height and prior to sunset for various days during the Arizona45S exposure are displayed in Table 2.1. The ratios of irradiance at 400–520 nm to TUVR for peak sun were similar throughout the exposure. Closer to sunset the ratios varied to a greater extent, especially in the latter half of the exposure, but under these circumstances, the solar irradiance was significantly lower and had less impact on degradation. Ultimately, a value of 4.1 was selected and adjusted using the spectrum of the xenon arc source to yield a conversion factor set at 0.0154. Irradiance values at 340 nm were determined for the SLP model of the Arizona45S exposure by multiplying measured TUVR data by this constant factor.
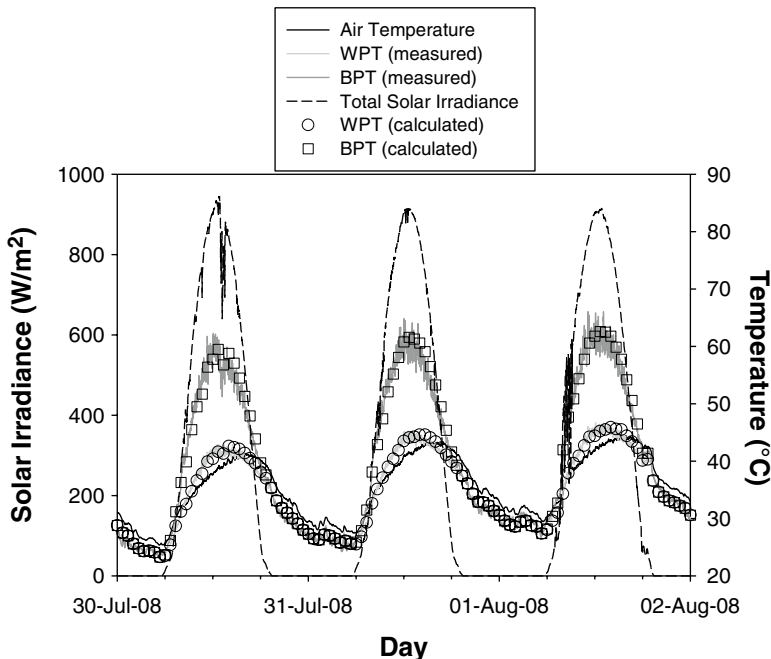
Fig. 2.6 Climate data measured at the exposure site near New River, Arizona. The individual points for WPT and BPT were calculated based on the measured air temperature (in K) and solar irradiance (in W/m²), using the following values for the parameters in Eq. (2.4): $h=35$ W/m²/K, $\alpha=1\times10^{-8}$ W/m²/K⁴, $\beta=1\times10^{-7}$ W/m²/K⁴, $a=0.95$ (BPT), and $a=0.22$ (WPT)

Correlating a temperature that is available from climate data with the WPT parameter that was used to fit the laboratory degradation data by means of the SLP model also poses a number of challenges. Typically, climate data include only ambient (air) temperatures. These must somehow be converted to the WPTs used to control the laboratory weathering devices. Even then, one must consider whether such a conversion would translate to equivalent film specimen temperatures for both the outdoor and laboratory exposures. If the resulting film specimen temperatures are different, the correlation between outdoor air temperature and WPT in a laboratory weathering chamber may not be sufficient to provide a useful SLP estimate.

The relationship between air temperature and a specimen temperature in an outdoor exposure has often been expressed as

$$T_{\text{specimen}} = T_{\text{air}} + \frac{a}{h}I \tag{2.3}$$

where a is the absorptivity for solar radiation by the specimen, h is the combined convection and radiation heat transfer coefficient of the specimen, and I is the total solar irradiance. There is a problem with this expression, however, as demonstrated by the data graphed in Fig. 2.6. If the white panel in the outdoor exposure of Fig. 2.6

is taken to be a specimen, one can readily see from Eq. (2.3) that there is no constant *a/h* factor that could convert the air temperature to the WPT for all points in time. This is because the WPT is sometimes *below* the air temperature, which Eq. (2.3) cannot predict. In fact, Eq. (2.3) was derived as a fictitious "sol-air temperature" for use in determining the effect of solar radiation on heat transfer through buildings [14].

By explicitly accounting for the effect of radiative heat transfer between the specimen and the sky [15], another expression was derived:

$$T_{\text{specimen}} = T_{\text{air}} + \frac{aI - \alpha T_{\text{air}}^4}{h + \beta T_{\text{air}}^3} \tag{2.4}$$

where α and β are parameters that depend on the emissivity of the specimen and its environment. Taking values for air temperature and total solar irradiance plotted in Fig. 2.6, the corresponding WPT can be modeled by Eq. (2.4) using reasonable values for the other parameters. The results depicted in the figure indicate that a good fit can be attained not only for a white panel, but also for a black panel. Nevertheless, for the SLP analysis in this study, it was not necessary to make use of Eq. (2.4). Since white panel (45° tilt, south-facing) temperature data were measured during the Arizona45S exposure, they were used directly in the SLP model for the temperature parameter.

Comparing the SLP Estimate to the Arizona45S Exposure

The SLP model determined via laboratory weathering experiments was employed to predict the degradation of peak absorbance for the fluorescent vinyl film weathered in the Arizona45S exposure from July 23 to October 21, 2008. The resulting prediction, calculated at 1-min intervals, is plotted in Fig. 2.7. The zigzag appearance in the curve comes from the fact that the SLP model predicts no degradation at
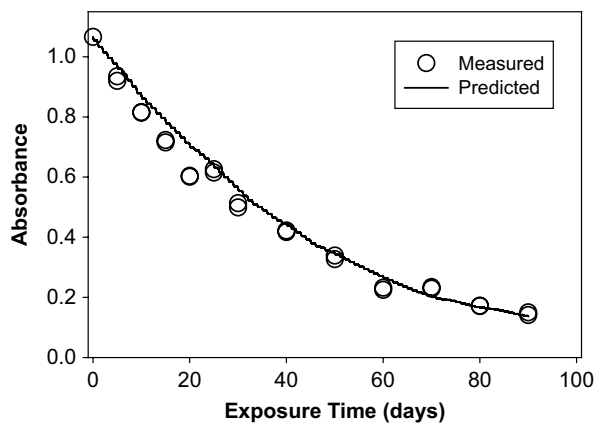

Fig. 2.7 Degradation of peak absorbance in the film specimens predicted by the SLP model for the outdoor exposure near New River, Arizona, from July 23 to Oct 21, 2008. The prediction was based on climate data measured at the site during the exposure. The degradation observed experimentally is shown for comparison

night. The absorbance measured from the fluorescent vinyl film specimens weathered outdoors according to Arizona45S during this same time period is also plotted in the figure. The SLP estimate exhibits excellent agreement with the measured degradation, confirming the validity of the SLP methodology when applied to this material, which degrades relatively quickly due to stresses from solar radiation and heat.

Full exploitation of the SLP model demands the ability to make lifetime estimates for specimens in other orientations and geographic locations. Obviously, measured climate data will usually not be available to make such lifetime estimates. Instead, calculated climate data using models based on averages over many years must be used. One such model, METEONORM, provides hourly data for total solar irradiance and air temperature in numerous locations around the world [16]. Since TUVR and WPT data are not provided, conversions for total solar irradiance and air temperature to the laboratory weathering device parameters of irradiance at 340 nm and WPT, respectively, must be derived.

A SMARTS calculation of solar irradiance around noon near New River, Arizona, for a south-facing specimen at 45° tilt showed that the ratios of 340-nm irradiance to the irradiance from 400 to 520 nm on July 24, September 6, and October 21 were similar to each other (within ±10 %) and to the ratio measured from a xenon arc source used in an SLP weathering device. This means that for a given irradiance at 340 nm, the irradiance for 400–520 nm would be nearly the same in both the Arizona outdoor and laboratory SLP exposures. Therefore, results from the SMARTS calculation were used to assign a value of 0.18 to convert total solar irradiance from METEONORM (in MJ/m^2 for a 1-h interval) to irradiance at 340 nm (in W/m^2/nm) for the SLP model. The true value of this conversion factor actually varies substantially, depending on the day of the year and time of the day. The effect of variability was minimized by selecting a value representative of noontime conditions, when the effect of solar irradiance on the degradation would be greatest.

In spite of the limitations of Eq. (2.3) pointed out previously, it is the simplest expression available to convert air temperature for use in the SLP model. By setting the factor *a/h* equal to 2, the effects of air temperature (°C) and total solar irradiance (in MJ/m^2 for a 1-h interval) from METEONORM were combined to estimate WPT ($T_{specimen}$ in Eq. (2.3)) for the environmental conditions during the Arizona45S exposure. These calculated outdoor WPTs were used for the WPTs utilized by the SLP model, again making the assumption that this would constitute equal film temperatures in the outdoor and laboratory exposures.

With a means to convert the irradiance and temperature data from METEONORM in hand, values corresponding to Phoenix, Arizona (35 mi/56 km south of New River), for the period July 23 through October 21 were determined and put into the SLP model to generate an estimate for the degradation of peak absorbance in the fluorescent vinyl film exposed under Arizona45S conditions. The predicted absorbance, calculated at 1-h intervals, is plotted in Fig. 2.8 along with the prediction obtained previously using actual climate data measured at the New River site during

Fig. 2.8 A comparison of degradation in the film specimens predicted by the SLP model based on measured and modeled climate data
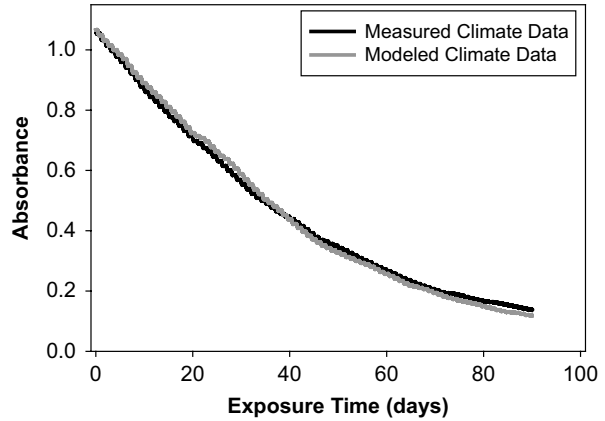
the period of the exposure. The agreement between the two curves is very good, considering the assumptions and approximations that were made to derive the irradiance and temperature data used for inputs to the SLP model.

Comparing the SLP Estimate to Estimates from Alternative Models

Derivation of the SLP model in this study was accomplished via a simultaneous fit of the complete set of absorbance degradation data from the film specimens in all eight SLP exposure conditions. For comparison, we analyzed the experimental data with the cumulative damage model used in accelerated life testing. In this case, lifetime was estimated based on the end state of the degraded material instead of accounting for the entire degradation pathway. Time to failure (t_F) was determined for each of the 33 film specimens exposed in the SLP weathering cycles by interpolating to the point in time at which peak absorbance reached a value of 0.2, an arbitrarily defined failure. All of the t_F values were simultaneously fit with the Accelerated Life Testing module in Minitab® software [17] using the expression

$$\ln t_F = \beta_0 + \beta_1 \ln I + \beta_2 \frac{1}{T} + \sigma \epsilon \tag{2.5}$$

Table 2.2 A comparison of t_F estimates for failure in fluorescent vinyl film when peak absorbance falls to a value of 0.2. The values were derived from multiple SLP models using two different sources of climate data

SLP model	Climate data	Time to failure (days)
Degradation rate (Eq. 2.2)	Measured	71
Degradation rate (Eq. 2.2)	Modeled	69
Accelerated life test (Eq. 2.5) (sum over fraction of life lost until failure)	Modeled	70
Accelerated life test (Eq. 2.5) (calculated using values for I_{eff} and T_{eff})	Measured	72 ± 7
Outdoor result	Actual	~75

where I is irradiance, T is temperature, and the last term accounts for statistical variability. For the fit, values for I and T corresponded to the irradiance and WPT set points, respectively. The coefficients obtained from the fit ($\beta_0 = -9.26$, $\beta_1 = -0.690$, $\beta_2 = 4{,}760$) are an indication of the relative effect of these stresses on the degradation.

Using Eq. (2.5), the fraction of life lost could be calculated for a given outdoor exposure interval and the fractions summed over the course of the exposure until failure was reached. As in the previous analysis, I and T were derived from modeled climate data. This yielded the time to failure, displayed in Table 2.2. It is compared with values for t_F determined from each of the degradation curves shown in Fig. 2.8. Following a previously described formalism for deriving constant effective temperature [18], a value for T_{eff} was determined for the accelerated life test model using measured climate data. The formalism was extended to also derive an analog for constant effective irradiance, I_{eff}. These inputs were then used in Eq. (2.5) to calculate t_F. Because constant parameters were used, the calculation enabled an estimation of the error (95 % confidence interval) as well. This is a measure of how well the model fit the experimental data. It does not take into account variability in the climate itself. Even so, based on the value calculated for the error, all of the estimates from the several SLP analyses are in agreement with the experimental outdoor result, as seen in Table 2.2.

Robustness of the SLP Model

A key attribute of any predictive model is its robustness. The SLP model can be deemed robust when its output—the lifetime estimate—is not overly sensitive to variations in the model parameters or in the values of the inputs. This attribute can be examined in three ways. First, the SLP estimate plotted in Fig. 2.7 did extremely well in predicting the degradation of absorbance in the fluorescent vinyl film even with the approximations and assumptions made to derive the inputs to the model from measured climate data. Conversion of solar irradiance data to irradiance at

340 nm made use of a constant factor even though its variability over the course of a day and at different times of the year is significant. The assumption that film specimen temperatures in an outdoor exposure and in a laboratory weathering device are nearly equal if their corresponding WPTs are equal is another possible source of error. The risks of such approximations and the need to exercise caution when employing them have been emphasized [2]. Nevertheless, this study has shown that the SLP model can be successful even when assumptions like these are made.

Second, a comparison of the degradation curves in Fig. 2.8 demonstrates that variability in the inputs to the SLP model did not have a significant effect on the resulting lifetime estimates. Not only did the climate data used to generate these curves come from different sources (measured vs. modeled data); the mathematical expressions used to convert the data into useful inputs to the model were also different. A third approach expressed the inputs as effective temperature and irradiance values that were taken to be constant throughout the duration of the SLP analysis. Despite this, essentially the same result was obtained for all sets of climate data.

Finally, the multiple SLP models examined in this work all yielded essentially the same lifetime estimate. The principal model put forth in this study, based on Eqs. (2.1) and (2.2), analyzed the entire absorbance degradation curve of the fluorescent vinyl film. In contrast, analysis via the accelerated life test model [Eq. (2.5)] targeted a single point—the value of t_F at which the absorbance of the film reached 0.2. The fact that these two approaches led to the same result is a consequence of the theoretical prediction that the inverse relationship between rate constant and failure time will hold [19] provided that:

1. The degradation rate depends on the concentration of a species involved in a microscopic reaction, and
2. That reaction is the single reaction primarily responsible for progress toward failure

The existence of this relationship offers the advantage of universality, in that the accelerated life test model can be applied in cases where derivation of a mathematical expression for the degradation of the property of the material under investigation is not straightforward.

Elucidating the Degradation Pathway

The foregoing requirements that determine the applicability of the accelerated life test model to SLP estimation demand an understanding of the degradation pathways involved. Several supplementary experiments were conducted in order to elucidate the pathway(s) corresponding to loss of 455-nm absorbance in the fluorescent yellow vinyl film that served as the model material in this study. In addition to those

already reported [8], these experiments included exposing samples in the weathering chamber continuously, with dark segments of 0, 16, or 20 h every 24-h period, and exposing samples in sealed vials enriched in oxygen. The results led to several observations:

1. Light was required to initiate and perpetuate degradation [8].
2. There was an apparent induction period at low irradiance [8].
3. Intermittent exposures or addition of oxygen slowed degradation. These conditions also produced increased absorption near 400 nm.
4. After exposure, degradation continued in the dark at a slower rate that was highly dependent on temperature.
5. Lower initial dye concentration reduced the degradation rate [8].
6. Addition of radical scavengers slowed degradation [20].

Interpretation of these observations, in conjunction with degradation mechanisms reported for dyes of a similar class [11, 21], generated a number of hypotheses for the manner by which the degradation proceeds:

1. The fluorescent yellow dye degrades via a bimolecular reaction involving semi-reduced radicals formed from the triplet state.
2. Aerobic conditions deactivate the reactive species, yielding H_2O_2.
3. Oxidation of the dye may compete with the primary degradation pathway.

When deprivation of oxygen under accelerated conditions was investigated as a possible cause of reciprocity failure in the irradiance response, it was discovered instead that oxygen actually slowed the degradation. This can lead to a secondary reaction in the dark, involving oxidation of the dye by peroxide that yields a new absorption band near 400 nm [22]. This secondary reaction seemed to play a minor role, as evidenced by the agreement between the accelerated laboratory exposures and the outdoor experiments. However, if the outdoor exposures had initiated in months with lower irradiance and cooler temperatures, one wonders how well the model may have worked, given the possibility of competing degradation reactions.

An example of a polymer film for which understanding the degradation pathways is critical to predicting lifetime was found for poly(ethylene terephthalate) (PET). The issue here pertained to multiple failure modes that did not necessarily relate to a single degradation reaction. PET films weathered in the laboratory according to a high-irradiance version of ASTM G154 Cycle 1[3] exhibited the same increase in absorbance at 330 nm as specimens exposed outdoors in Florida (5° tilt, open, south-facing). The overlay obtained using an appropriate shift factor can be seen in Fig. 2.9. However, the same shift factor did not produce similar agreement for degradation of the haze induced in the film. This lack of synchronization between changes in absorbance and haze suggested that the laboratory weathering test

---

[3]ASTM G154-06 Standard Practice for operating fluorescent light apparatus for UV exposure of nonmetallic materials
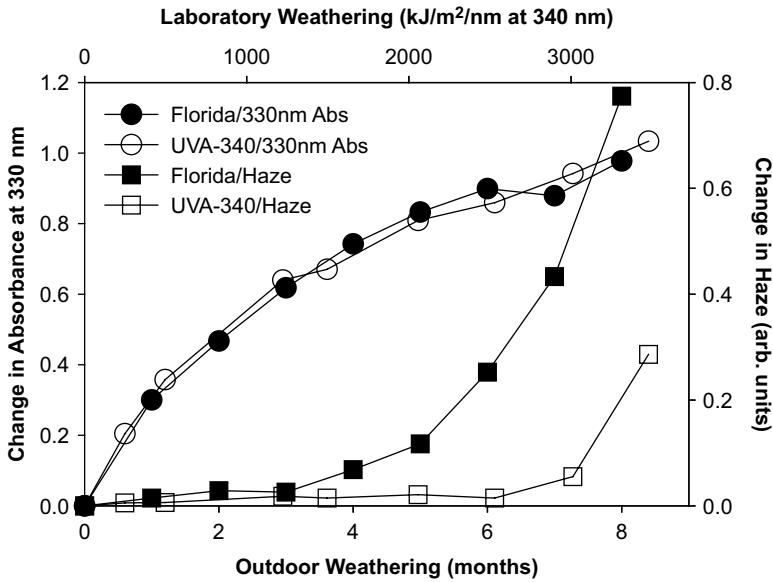
Fig. 2.9 Comparison of the increase in absorbance at 330 nm and haze measured as the average offset in the absorbance spectrum at 580–600 nm for PET films weathered in Florida at 5° tilt and in the laboratory according to ASTM G154 Cycle 1 (UVA-340) at high irradiance. The horizontal axes were scaled relative to each other to give the best overlay for change in absorbance at 330 nm

method did not adequately produce the same degradation in PET as that observed due to outdoor weathering in Florida. After trials with laboratory weathering exposures that included increased cycling of wet/dry periods, it was found that by including a sufficiently long exposure to water and utilizing a xenon arc light source with a full solar spectrum, degradation causing changes in absorbance, haze, and gloss is brought into synchronization (see Fig. 2.10).

Nevertheless, all is not solved. Microscopic observation of the surfaces of the weathered PET films revealed changes in chemistry and micro-cracking due to weathering that were not identical in both the laboratory test method and outdoor exposure. In particular, the FTIR spectrum of the surface of the PET sample exposed in Florida revealed generation of chemical species that were not reproduced via the laboratory test. Even orientation of a sample can affect synchronization of failure modes by altering the relative amounts of solar irradiance and water to which the specimen may be exposed.

Fig. 2.10 Synchronization
of multiple failure modes in
PET films achieved for both
the outdoor Florida and
accelerated xenon arc
weathering exposures
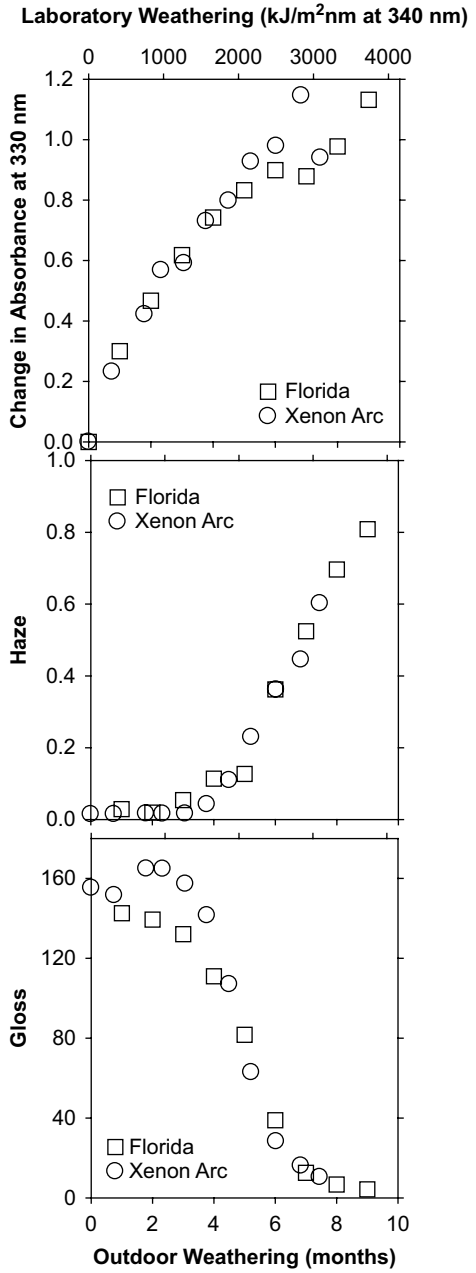
Conclusion

This comparative study has definitively demonstrated an SLP test protocol that can provide a lifetime estimate in excellent agreement with the observed lifetime of a material that degrades in the out-of-doors due to color fade arising primarily from solar radiation and heat. Furthermore, the prediction was shown to be valid for the entire degradation curve of the material and not limited to a single time-to-failure estimate. Seeing that the fluorescent vinyl film that was studied suffered loss of absorbance over a period of only a few months, it is understandable that additional validation studies are needed for more durable materials having other failure modes. Furthermore, the degradation of the fluorescent dye basically followed first-order kinetics. Degradation of other aspects of appearance, mechanical behavior, and physical properties of other polymeric and inorganic materials may not be so easily described and could pose challenges when trying to model change occurring throughout the period of the outdoor exposure.

A significant finding is that the SLP model was determined to be fairly robust. The validity of the model was first affirmed by obtaining input values from climate data measured during the actual exposure period. However, when inputs were derived from modeled climate data for the same time period, the resulting estimate was essentially the same. The utility of SLP estimates has been questioned, given the fact that climatic conditions vary so much from year to year. In this case, using modeled climate data based on 20- and 30-year averages proved to still give a viable prediction of lifetime. Further evidence of robustness was found in the relative insensitivity of the SLP model to the method for conversion of climate data into irradiance and temperature inputs and whether the analysis applied to the full set of degradation data or to time-to-failure values only.

This study has spawned a number of discoveries that will also be useful when analyzing and interpreting SLP data. Extraction of irradiance values at 340 nm from total solar irradiance data should include an evaluation of the impact of time of the day and day of year. Investigating the role of radiative heat transfer in the temperature of a specimen may lead to better modeling, not just for input temperatures for SLP estimates but also for determining temperature distributions in products whose designs may limit allowable temperatures. The degradation mechanism is also very important. If multiple pathways occur or if degradation is not directly dependent on the concentration of a single species, the SLP model may not be suitable for estimating lifetime without appropriate modifications.

The success of this comparison between the SLP estimate and the observed degradation in an outdoor exposure was for a material in which only stresses due to solar radiation and heat were significant. It is well known that water can have a great impact on the degradation and failure of many other materials. Significant progress has been made for some materials in accounting for the effect of relative humidity on time to failure [23]. However, modeling the impact of dew and rainfall poses a challenge, including how to measure them. There is much need for improving the theoretical, experimental, and empirical aspects of the weathering stress that water affords in order to include it in SLP models.

References

1. Fischer RM, Ketola WD (2005) In: Martin JW, Ryntz RA, Dickie RA (eds) Service life prediction: challenging the status quo. Federation of Societies for Coatings Technology, Blue Bell, PA, p 79
2. Hardcastle HK (2004) ANTEC 2004 plastics: annual technical conference, vol 3, Special Areas. Society of Plastics Engineers, Chicago, IL, p 4077
3. Jorgensen G, Bingham C, King D, Lewandowski A, Netter J, Terwilliger K, Adamsons K (2002) In: Martin JW, Bauer DR (eds) Service life prediction: methodology and metrologies, ACS symposium series 805. American Chemical Society, Washington, DC, p 100
4. Gu X, Stanley D, Byrd WE, Dickens B, Vaca-Trigo I, Meeker WQ, Nguyen T, Chin JW, Martin JW (2009) In: Martin JW, Ryntz RA, Chin J, Dickie RA (eds) Service life prediction of polymeric materials: global perspectives. Springer, New York, p 3
5. Miner MA (1945) J Appl Mech 12:A159
6. Meeker WQ, Escobar LA, Chan V (2002) In: Martin JW, Bauer DR (eds) Service life prediction: methodology and metrologies, ACS symposium series 805. American Chemical Society, Washington, DC, p 396
7. Fischer RM, Guth BD, Ketola WD, Riley JW US Patent 6,859,309
8. White KM, Fischer RM, Ketola WD (2009) In: Martin JW, Ryntz RA, Chin J, Dickie RA (eds) Service life prediction of polymeric material: global perspectives. Springer, New York, p 71
9. Nedler JA, Mead R (1965) Comput J 7:308
10. Pickett JE, Moore JE (1993) Polym Degrad Stab 42:231
11. Leaver IH (1980) In: Allen NS, McKellar JF (eds) Photochemistry of dyed and pigmented polymers. Applied Science, London, p 161
12. Gueymard C (2001) Sol Energy 71:325
13. Gueymard C (1995) SMARTS, A simple model of the atmospheric radiative transfer of sunshine: algorithms and performance assessment, Professional paper FSEC-PF-270-95. Florida Solar Energy Center, Cocoa, FL
14. Threlkeld JL (1970) Thermal environmental engineering, 2nd edn. Prentice-Hall, Englewood Cliffs, NJ
15. Dean SW, Reiser DB (1995) In: Kirk WW, Lawson HH (eds) Atmospheric corrosion, ASTM STP 1239. American Society for Testing and Materials, Philadelphia, PA, p 3
16. METEONORM (2007) v. 6.0, available from Meteotest, Bern, Switzerland
17. Minitab® v. 16, available from Minitab Inc., State College, PA, USA (2010). Use of the accelerated life testing model is explained therein. In: Nelson W (ed) (1990) Accelerated testing: statistical models, test plans, and data analyses. Wiley, New York
18. Pickett JE, Sargent JR (2009) Polym Degrad Stab 94:189
19. Klinger DJ (1992) Microelectron Reliab 32:987
20. White KM, Pavelka LA, Lightle VL, Coderre JC US Patent 6,110,566
21. Imamura M, Koizumi M (1956) Bull Chem Soc Jpn 29:899
22. Kadhim AM, Mak K-H, Peters AT (1982) J Soc Dyers Colour 98:56
23. Pickett JE, Coyle DJ (2013) Polym Degrad Stab 98:1311

Chapter 3
Hydrolysis Kinetics and Lifetime Prediction for Polycarbonate and Polyesters in Solar Energy Applications

James E. Pickett

Abstract The hydrolysis kinetics of polyesters and BPA polycarbonate appear to be second order in water, that is, second order in relative humidity (RH). This finding, combined with activation energies for hydrolysis, was used in a service life prediction model for a photovoltaic (PV) module front sheet application. The modeling process involves: (1) finding finely time-parsed climatic data for a benchmark location, (2) calculating module temperature and RH from the climatic data, and (3) applying the kinetics to determine the amount of degradation that occurs in 1 year relative to accelerated laboratory conditions, 85 °C and 85 % RH in this case. Acceleration factors under laboratory conditions are very high, especially for poly(ethylene terephthalate) (PET), leading to predicted lifetimes of several centuries if hydrolysis is the only degradation mode. The model was tested for sensitivity to assumptions and experimental uncertainties, and hydrolysis can be considered unimportant in this solar energy application. Concerns about PET suitability on the basis of its relatively short embrittlement times in the 85 °C/85 % RH damp heat test are unfounded.

Keywords Service life prediction • Activation energy • Hydrolysis • Kinetics • PET • Polycarbonate • Solar

Introduction

As part of the US Department of Energy Solar America Initiative in 2008–2009, we were interested in lightweight, flexible PV modules that would have a polymer film as the front sheet. The film would have to transmit as much light as possible in the range of 380–1,200 nm, protect the module from moisture and physical damage, and withstand full sunlight and temperatures as high as 90 °C for at least 20 years.

J.E. Pickett (✉)
GE Global Research, 1 Research Circle, Niskayuna, NY 12309, USA
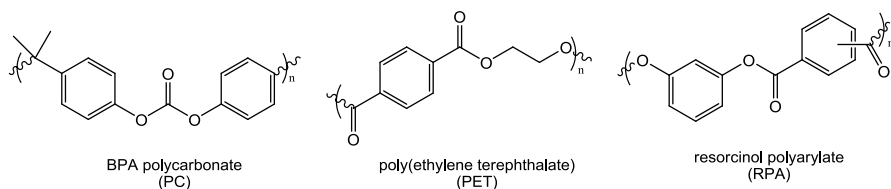e-mail: dr.james.pickett@gmail.com

Fig. 3.1 Structures of the candidate polymers

Only a handful of polymers seemed viable candidates: fluorocarbons such as poly(tetrafluoroethylene) (PTFE), polyesters such as poly(ethylene terephthalate) (PET), aromatic polycarbonates (PC), and polyarylates such as resorcinol polyarylate (RPA). Poly(methyl methacrylate) (PMMA) would be an attractive candidate, but its heat distortion temperature is less than the maximum service temperature. PTFE was already established as a PV front sheet material in flexible amorphous silicon modules. We observed that in flat roof applications, these modules sometimes developed corrosion spots due to cuts and punctures through the thin, soft PTFE. We desired a lower cost and mechanically more robust front film.
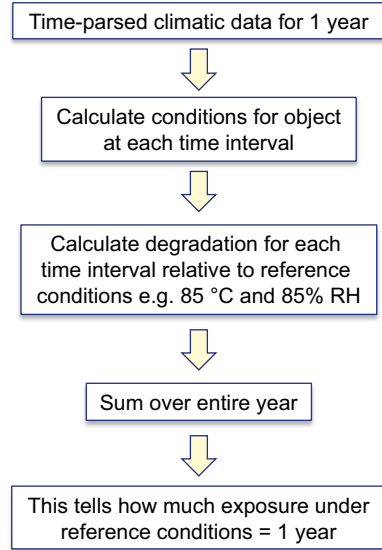
Structures of the candidate polymers are shown in Fig. 3.1. All three are condensation polymers and are subject to hydrolysis. Qualification standards for PV[1] generally require at least 1,000 h of testing under conditions of 85 °C and 85 % relative humidity (RH), but this does not answer the question of actual lifetime. Designing resistance to sunlight is a separate issue and is not the subject of this report. RPA is a self-protecting polymer and is expected to have adequate weatherability if thick enough [1], and we sought a coating or co-extruded solution for PC [2] and PET.

There is no single best, accepted method for service life prediction. One complication is that the environmental conditions during use are variable from hour to hour during the day and throughout the year. How can these ever-varying conditions be related to a simple set of laboratory test conditions? We took the approach outlined in Fig. 3.2. The idea is to relate the degradation at every short time interval during a year in use to a set of reference conditions that can be used for testing in the laboratory. By adding up all the intervals, one can find the hours under the reference conditions that should produce the same amount of degradation as in 1 year of use. This is the correlation factor for those test conditions. We will choose the test conditions of 85 °C and 85 % RH as the reference for the purpose of this exercise, but any conditions not so extreme as to change the mechanism of degradation can be used.

We must have several types of information to carry out this process successfully. Ideally, one would like finely parsed data for the relevant environmental variables taken on the actual article under a variety of reasonable use conditions for several years. Such data rarely exist, and the prediction often must be made for the article before it is even designed, much less in a test field for a year or more. Therefore, we rely on models to calculate the conditions in the article using time-parsed climatic data as inputs. These models can vary in quality but are fairly straightforward as

---

[1] For example, IEC 61215 (crystalline silicon), IEC 61646 (thin film), IEC 61730 (all modules, safety), and Underwriters Laboratories UL1703.

Fig. 3.2 Outline of a service
life prediction process

Time-parsed climatic data for 1 year

⇩

Calculate conditions for object
at each time interval

⇩

Calculate degradation for each
time interval relative to reference
conditions e.g. 85 °C and 85% RH

⇩

Sum over entire year

⇩

This tells how much exposure under
reference conditions = 1 year

long as we keep in mind the assumptions behind them. Better models can always be used as they are created. Once the conditions are calculated, the kinetic parameters of the degradation reaction(s) are used to determine the amount of degradation relative to the reference conditions at each time interval. This requires knowing the rate equation and the activation energy for degradation, sometimes a difficult and time-consuming task. But once the kinetics are known, the degradation increments are easily summed to give the correlation between the reference conditions and the use conditions, that is, the amount of time in the accelerated test that gives the same amount of degradation as a year in the field.

This method essentially is the same as one very recently described by Kempe and Wohlgemuth [3], in which the authors used model equations to calculate the temperature and moisture content of solar modules using time-parsed climatic data and then used kinetic parameters to calculate the average effective temperature and RH. These values can be used to calculate the amount of degradation in a given amount of time or to derive a correlation to reference conditions. Kempe and Wohlgemuth used more sophisticated temperature and moisture models than we used in this work, but we will see that our conclusions are quite similar.

The Lifetime Model

Time-Parsed Climatic Data

Outdoor environmental conditions vary greatly over the course of a day and from day to day and season to season during the year. Any single year can be more or less harsh than average, but we can assume that an article such as a PV module will

encounter approximately average exposure if it is to be used for 10 or 20 years or more [4]. Manufacturers generally design products to perform adequately in a reasonable worst case environment if failure does not cause injury or property damage. In the case of PV modules used in North America, a reasonable worst case for hydrolytic damage is a subtropical environment such as Miami, FL. A reasonable worst case for a hot, sunny environment is Phoenix, AZ, and it is no coincidence that these are the locations of many commercial outdoor exposure facilities. Complete climatic data have been collected at many of these sites every few minutes for many years. We will use 1 year of such a data set to determine the importance of the time interval, but these data files generally are not freely available to the public.

Excellent sets of data acquired at 1 h intervals are available from the National Renewable Energy Laboratory (NREL) website [5]. The data are compiled as a "Typical Meteorological Year" (TMY) by assembling selected "average" months into an "average" year for a defined span of years. The most recent is TMY3 that covers the years 1991–2005 for 1,020 locations throughout the United States and its territories. Some stations average over as many as 30 years. A user's manual [6] gives a full description of the kinds of data and how they are selected. The datasets can be downloaded as comma-separated values (CSV) text files that are directly readable by spreadsheet applications such as Microsoft Excel™. A portion of the Miami dataset is shown in Fig. 3.3. The headings for many of the columns are cryptic,

722020	MIAMI INTL AP FL		−5	25.817	−80.3	11		
Date (MM/DD/ YYYY)	Time (HH:MM)	ETR (W/m^2)	ETRN (W/m^2)	GHI (W/m^2)	GHI source	GHI uncert (%)	DNI (W/m^2)	…44 more columns irradiance temperature RH, dew point atmos -pheric pressure wind speed and direction cloud cover, visibility precipitation
1/1/1995	1:00	0	0	0	1	0	0	
1/1/1995	2:00	0	0	0	1	0	0	
1/1/1995	3:00	0	0	0	1	0	0	
1/1/1995	4:00	0	0	0	1	0	0	
1/1/1995	5:00	0	0	0	1	0	0	
1/1/1995	6:00	0	0	0	1	0	0	
1/1/1995	7:00	0	0	0	1	0	0	
1/1/1995	8:00	98	1191	39	1	10	262	
1/1/1995	9:00	369	1415	218	1	10	694	
1/1/1995	10:00	606	1415	394	1	10	768	
1/1/1995	11:00	785	1415	540	1	10	747	
1/1/1995	12:00	896	1415	411	1	10	230	
1/1/1995	13:00	928	1415	503	1	10	324	
1/1/1995	14:00	882	1415	514	1	10	517	
1/1/1995	15:00	759	1415	396	1	10	107	
1/1/1995	16:00	568	1415	313	1	10	117	
1/1/1995	17:00	323	1415	116	1	10	152	
1/1/1995	18:00	61	955	16	1	10	22	
1/1/1995	19:00	0	0	0	1	0	0	
1/1/1995	20:00	0	0	0	1	0	0	
1/1/1995	21:00	0	0	0	1	0	0	
1/1/1995	22:00	0	0	0	1	0	0	
1/1/1995	23:00	0	0	0	1	0	0	
1/1/1995	24:00:00	0	0	0	1	0	0	

… 8736 more rows: selected typical months to make an average year

Fig. 3.3 Excerpt from the Miami TMY3 dataset [5]

so it is necessary to refer to the user's manual to select the relevant columns. We used data for global horizontal irradiance (column 5), dry bulb temperature (column 32), and RH (column 38) in this work. More sophisticated models might use wind direction and speed (columns 44 and 47), total sky cover (column 26), and atmospheric pressure (column 41).

Temperature Model

The article temperature must be known in order to calculate its degradation rate. Solar modules generally are nearly black, so they get hot in the sun. We were interested in applications in which the module might be attached directly to a roof, so the back can be considered to be well insulated. Several temperature models have been described in the literature at various levels of complexity [7–12]. These models generally require empirical constants that we did not have. Instead, we adapted a simple equation that was derived from a dataset of the surface temperature of a black polycarbonate roof panel attached to a closed minivan in Arizona over the course of a year [13]. This is shown as Eq. (3.1) where T_{mod} is the module surface temperature, T_{amb} is the ambient dry bulb temperature, and I is the global horizontal irradiance in W/m^2. As it turns out, the selection of the model is not critical in the case of hydrolysis reactions, as will be shown in the Sensitivity section.

$$T_{\text{mod}} = T_{\text{amb}} - 3.843 \times 10^{-6} I^2 + 0.521 I - 3.25 \tag{3.1}$$

Humidity Model

An important variable in polymer hydrolysis is the amount of water (more properly, the activity of water) dissolved within the polymer. Since water vapor is a condensable gas, the concentration of water dissolved in the polymer, $C_{\text{w, solid}}$, at some temperature, T, is given by Eq. (3.2) where $S_{\text{w, solid}}$ is the solubility of water in the solid at T, p_{w} is the partial pressure of water vapor, and p_{sat} is the saturation vapor pressure of water at T. The ratio $p_{\text{w}}/p_{\text{sat}}$ is the definition of RH, so the appropriate metric is RH, not the just the vapor pressure of water[2]:

$$C_{\text{w, solid}} = S_{\text{w, solid}} \frac{p_{\text{w}}}{p_{\text{sat}}} = S_{\text{w, solid}} RH \tag{3.2}$$

Consider a PV module in a tropical location on a hot, humid summer day with no breeze. The module might reach a temperature as high as 85 °C while the ambient RH is 85 %. However, the conditions within the module are not 85 °C and 85 % RH

---

[2] Thanks to Dr. Dennis Coyle, GE Global Research, for this analysis.

or at least not for very long. The important RH is that of the boundary layer at the surface of the hot module, and in the hot air, the RH is much lower because the saturation vapor pressure must be calculated for the module temperature, not the ambient air temperature, as shown in Eq. (3.3) where the subscript amb denotes ambient conditions and the subscript mod indicates module conditions. The saturation water vapor pressure at temperature T is given by the Magnus Equation or one of its variants [14] shown in Eq. (3.4) where T is in °C and p is in hPa. Thus, multiplying the result from Eq. (3.4) at ambient temperature by the ambient RH gives the vapor pressure of water. Dividing this by the result from Eq. (3.4) at the module temperature gives the RH that the module sees. Therefore, while the module can be 85 °C and the ambient RH 85 %, the module actually is equilibrated at <10 % RH at 85 °C. We assume that the equilibration time for the thin (<300 μm) films is fast enough that the calculated RH at any particular time is a close enough approximation to the RH at which the film is equilibrated when averaged throughout the cycles of the year.

$$RH_{mod} = \frac{p_{H_2O}}{p_{sat,T_{mod}}} = \frac{RH_{amb} \times p_{sat,T_{amb}}}{p_{sat,T_{mod}}} \tag{3.3}$$

$$p_{sat,T} = \exp\left(6.4154 + \frac{17.62T}{243.12 + T}\right) \tag{3.4}$$

The results of the model calculations for a hot, humid day in Miami (July 4, 1990, from the TMY3 dataset) are shown in Fig. 3.4 for temperature and Fig. 3.5 for RH. As the irradiance increases, the module temperature increases, as expected. The water vapor pressure actually remains within a fairly narrow range during the
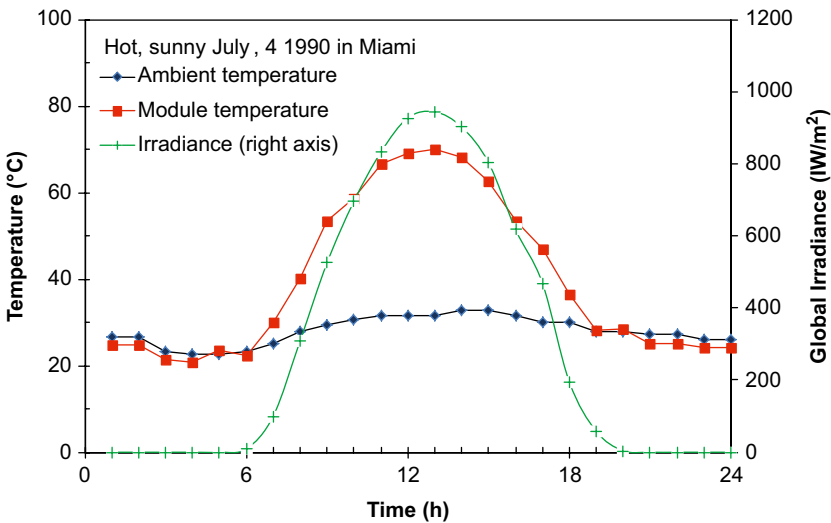

Fig. 3.4 Ambient dry bulb temperature, irradiance, and calculated (Eq. 3.1) solar module temperatures from Miami TMY3 dataset for July 4, 1990
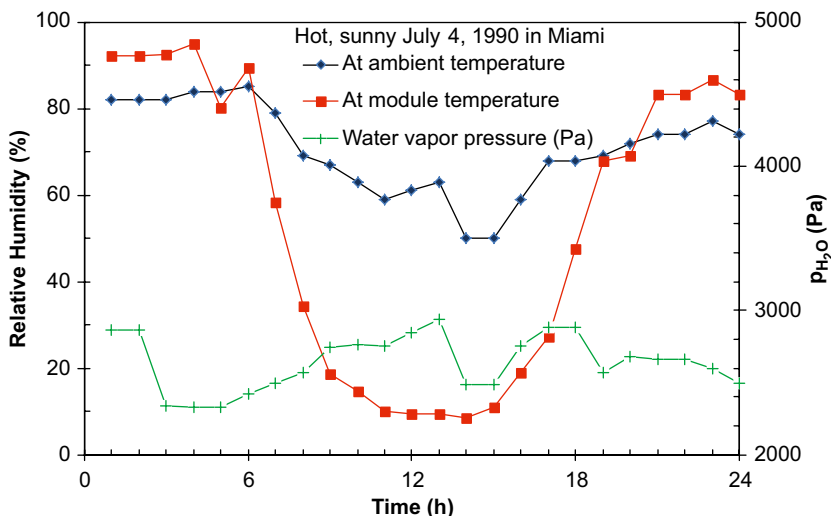
Fig. 3.5 Ambient relative humidity, water vapor pressure, and calculated RH at solar module temperature from Miami TMY3 dataset for July 4, 1990

day, but the RH decreases as the ambient temperature increases and decreases to ~10 % RH at the module temperature during the middle of the day. A spreadsheet can be filled with these types of calculations using ambient climatic data as inputs and getting article temperature and RH as outputs. Again, more sophisticated models for calculating temperature and moisture content of the article can be used if they are available.

Hydrolysis Kinetics

Our detailed analysis of the hydrolysis kinetics for PC, PET, and RPA under humidity aging conditions has been published elsewhere [15]. The key rate equation is shown as Eq. (3.5) in which the inverse of the failure time t_{fail} is proportional to a rate constant k and the *RH* raised to the nth power. The value of n is the number of molecules of water involved in the rate-determining hydrolysis step. Intuitively, there seems to be no reason why n should be anything but 1, but we found the data to be much more consistent with $n = 2$. Other workers have found that the hydrolysis of PC at 100 °C was nonlinear with [*RH*] [16], although the fit was better with $n = 3$ in our analysis of their data. Other work on PET [17] also found the hydrolysis not to be linear in [*RH*] and agreed very well with $n = 2$ in our analysis. None of the previous work has an explanation for the nonlinear effect of [*RH*] on the hydrolysis rate.

$$\frac{1}{t_{fail}} \propto k\left[RH\right]^{n} \qquad (3.5)$$

Table 3.1 Kinetic parameters for Eqs. (3.6) and (3.7)

Polymer	E_a		$\ln(A)$
	(kcal/mol)	(kJ/mol)	
PC	21.9 ± 2.3	92 ± 9.6	24.9 ± 3.2
PET	30.9 ± 1.6	129 ± 6.7	39.3 ± 2.2
RPA	24.3 ± 2.9	102 ± 12.1	30.0 ± 4.0

Ranges show the 95 % confidence interval [15]

The small molecule literature has some precedent for hydrolysis reactions under pH neutral conditions to be second order in water [18–21]. The hydrolysis mechanism requires some catalytic species either to polarize the carbonyl group or to aid in moving a proton from one oxygen to another. In the absence of added catalyst, as would be the case for a clean polymer, another molecule of water serves this purpose. We can think of condensation polymer hydrolysis as a water-catalyzed hydrolysis. Since two molecules of water are required in the rate-determining step (one as the reactant and one as the catalyst), the kinetics are second order in water. The water concentration in the polymer is proportional to the RH, so the kinetics are second order in RH.

The hydrolysis appears to obey Arrhenius kinetics in the temperature range of 95–65 °C, so the rate constant can be replaced by the usual exponential term as shown in Eq. (3.6) or rearranged as Eq. (3.7). All of the various proportionality constants are gathered together in A. Failure in our work is defined as the time (days) required to cause a brittle break when a film 5–12 mils thick (125–300 μm) is bent across a ¼-in. (6.4 mm) diameter rod. The values for the kinetic parameters assuming $n = 2$ are shown in Table 3.1 [15]. The quality of the fit showing calculated and experimental values is shown in Fig. 3.6. An important observation is that the activation energy for PET is considerably higher than for PC, meaning that PET is much more sensitive to temperature differences than PC or RPA.

$$\frac{1}{t_{\text{fail}}} = A \exp\left(-E_a / RT\right)\left[RH\right]^n \tag{3.6}$$

$$t_{\text{fail}} = \frac{\exp\left(E_a / RT\right)}{A\left[RH\right]^n} \tag{3.7}$$

Implementation of the Model

With the kinetic parameters known, it is now possible to calculate the degradation in each parsed time interval relative to some reference condition. This leads to a correlation factor between laboratory test conditions and the modeled conditions. Alternatively, one could calculate the absolute amount of degradation in that interval leading to a prediction of the number of years before failure. The advantage of the
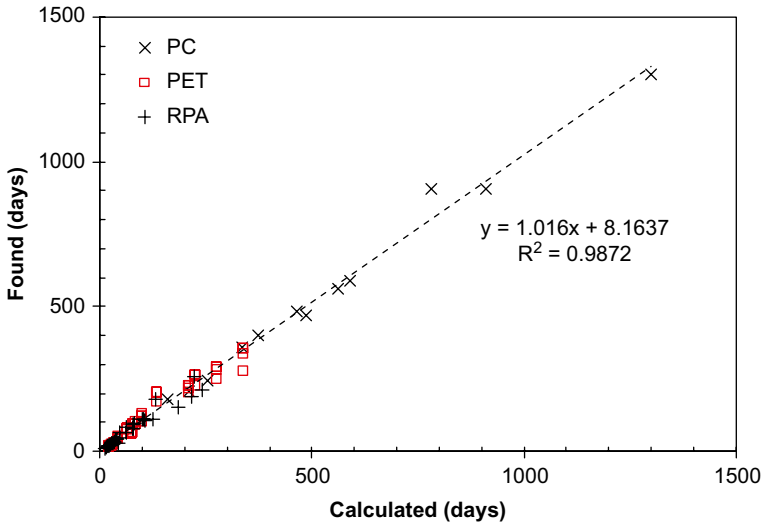
Fig. 3.6 Found vs. calculated values for polymer embrittlement using the parameters in Table 3.1 and Eq. (3.7) with $n = 2$ [15]

former approach is that it is understandable to a decision maker that this process establishes a correlation for a particular class of materials, that a particular material of that class lasts X days under test conditions and should therefore last Y years in the field. The straight lifetime calculation assumes that the kinetic parameters have been determined for the particular material, not a class of materials. While this is likely to be a more accurate approach, it is difficult to do all the experiments necessary to generate the kinetic parameters for all the grades and variations of each candidate material. It is much more likely that a correlation will be established by exhaustively testing a few materials under multiple conditions, and afterward, similar materials will be tested under only one or two conditions and predictions made by using the same correlation. Another advantage to the correlation factor method is that it does not require the value for *A* in Eq. (3.6) or (3.7) because it cancels out when dividing the rate at use conditions by the rate under the reference conditions. This can reduce some of the error. We will use the correlation factor approach in this exercise.

The rate is calculated for each parsed time interval using Eq. (3.6) and is divided by the rate under the reference conditions, which will be the same for each interval. The relative rates are summed for the year and multiplied by the time interval. In this case, the time interval is 1 h, so the sum gives the number of hours under the reference conditions that causes degradation equal to 1 year under the calculated field conditions.

Figure 3.7 shows the rates relative to 85 °C and 85 % RH reference conditions for PC on a hot, humid summer day assuming the kinetics are first or second order in RH. During the day, the higher temperature dramatically increases the hydrolysis rate if the kinetics are first order in RH as shown by the squares. In contrast, the
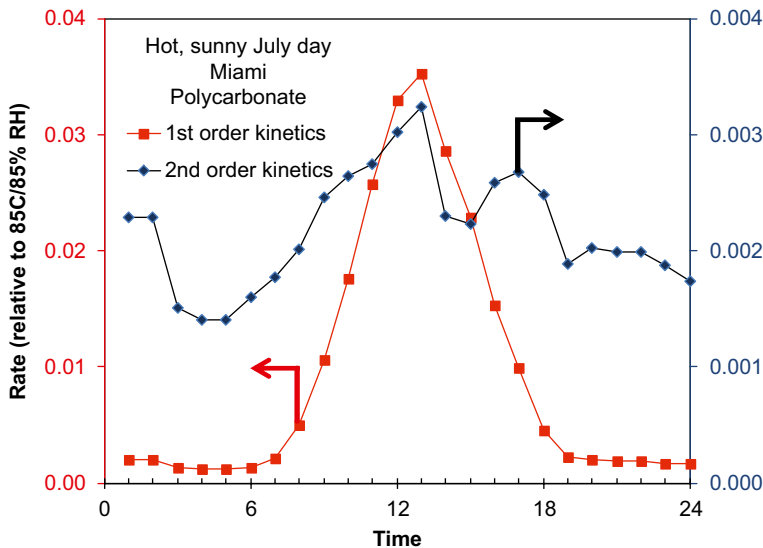
Fig. 3.7 Rates of hydrolysis for PC relative to 85 °C and 85 % RH for July 4, 1990, in Miami using parameters in Table 3.1 assuming first-order kinetics (*squares, left axis*) and second-order kinetics (*diamonds, right axis*)

relative rates are much lower for second-order kinetics (diamonds, right axis) and show much less variation during the day as the effects of higher temperature and lower RH nearly cancel out. Note how hydrolysis at night contributes a much greater portion to the overall daily degradation under second-order kinetics compared with first order.

Figure 3.8 shows the relative hydrolysis rates for PET. One sees that the rates are lower for PET than for PC, and though the rates for a reaction second order in RH are only about a tenth that for first order, the second-order rate has the same shaped curve. PET has a much higher activation energy, so the effect of temperature is stronger for PET than for PC and does not so perfectly cancel out the effect of lower RH during the sunny part of the day.

The model's results for the three polymers assuming kinetics second order in RH [$n = 2$ in Eq. (3.6)] are shown in Table 3.2. When the relative rates for all the parsed time intervals are summed, one finds that for PC only 14 h of 85 °C and 85 % RH aging are required to make the same amount of degradation as 1 year on a solar module in Miami. For PET, only 2.3 h are required. Thus, the standard damp heat testing conditions accelerate hydrolysis by factors of 600–3,800 depending on the material being tested. Our samples of PC and PET underwent brittle failure after 483 and 98 days, respectively, of 85 °C/85 % RH testing, which corresponds to 840 and 1,000 years under use conditions. No one is supposing that these polymers will indeed last that long, but one can conclude that hydrolysis is not likely to be an issue. Kempe and Wohlgemuth [3] came to similar conclusions for PET, calculating a hydrolysis lifetime of 500–1,000 years depending on how the PV module was mounted.
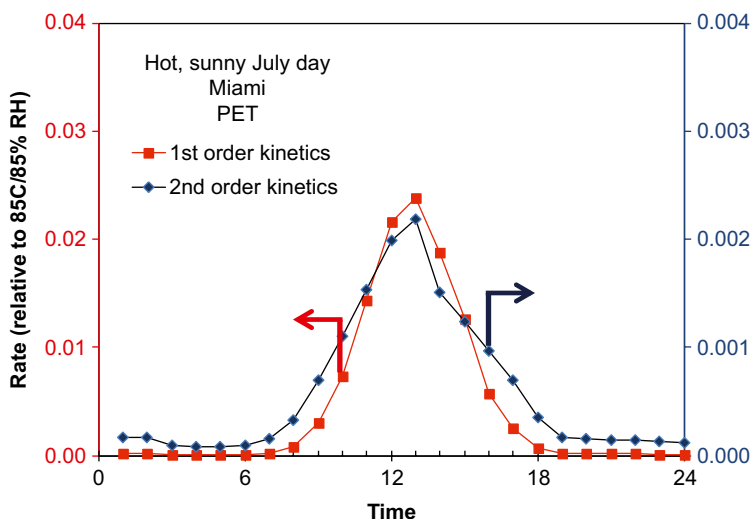
Fig. 3.8 Rates of hydrolysis for PET relative to 85 °C and 85 % RH for July 4, 1990, in Miami using parameters in Table 3.1 assuming first-order kinetics (*squares, left axis*) and second-order kinetics (*diamonds, right axis*)

Table 3.2 Model results for kinetics second order in RH ($n=2$)

	PC	PET	RPA
E_a (kcal/mol)	21.9	30.9	24.3
Hours 85 °C/85 % RH per year Miami	13.8	2.3	8.1
85 °C/85 % RH life (days)[a]	483	98	77
85 °C/85 % RH life (hours)	11,592	2,352	1,848
Calculated Miami life (years)	837	1,023	230

[a]From Pickett and Coyle [15]

Sensitivity Analysis

The key parameter of activation energy has a 5–10 % error range with 95 % confidence limits. The greatest risk comes from overestimating the size of E_a, because that will cause one to expect greater acceleration under the hot accelerated aging conditions. In addition, the finding of kinetics second order in RH is a novel one and should be considered uncertain pending independent confirmation. The effects of reducing the E_a by 10 % and/or assuming first-order kinetics are shown in Table 3.3. Either change makes dramatic differences in the calculated lifetime. The change in E_a reduces the calculated lifetime by roughly a factor of two, while the change in kinetic order for RH makes a three- to fivefold reduction depending on E_a. When the effects are combined, the safety margins narrow considerably with only a factor of two remaining for RPA, although PC and PET are probably still acceptable.

Table 3.3 Calculated
lifetimes (years) in Miami
using the E_a of Table 3.1 or
10 % lower values and
assuming kinetics first or
second order in RH

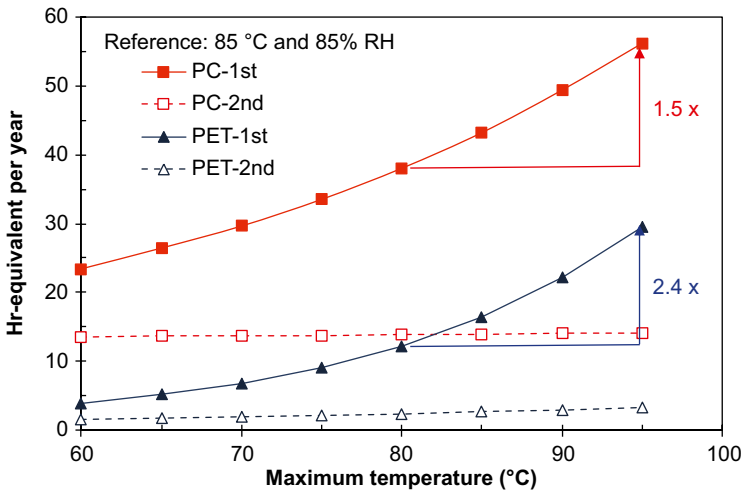| E_a	n	PC	PET	RPA
Nominal	1	306	195	69
−10 %	1	214	138	48
Nominal	2	837	1,023	230
−10 %	2	493	595	132

Fig. 3.9 Hours at 85 °C and 85 % RH needed to cause the same degradation as 1 year in Miami as a function of maximum solar module temperature for PC and PET assuming kinetics 1st order (*solid*) or 2nd order (*open*) in RH

Another source of error can come from the calculated temperature of the solar module. A very simple model was used that relies only on irradiance, ambient temperature, and an assumed maximum temperature. In this case, we assumed that the maximum temperature would be 80 °C in Miami. The results obtained from adjusting the model to reach other maximum temperatures are shown in Fig. 3.9. Surprisingly, the effect of the temperature model is very small if the kinetics are second order in RH. In the case of a low E_a hydrolysis, as for PC, there is no effect at all. With a high E_a hydrolysis, as for PET, the correlation changes by 40 % if the maximum temperature were 95 °C instead of 80 °C. The differences are much greater if the hydrolysis kinetics are assumed to be first order in RH: 50 % for PC and 140 % for PET with the same temperature change. Thus, the accuracy of the temperature model is not critical in the case of second-order kinetics but is quite important if the kinetics were first order in RH.

Slightly more sophisticated models use wind speed as an additional parameter and fit empirical constants for particular module designs. Kempe and Wohlgemuth [3] used the model of King et al. [7], which is shown as Eq. (3.8) where I is the irradiance (W/m²) and W is the wind speed (m/s). Several parameter sets are offered in King's paper. The insulated-back glass/polymer module is closest to our situation

Table 3.4 Hours at 85 °C and 85 % RH equivalent to 1 year aging in Miami using different models for the module temperature

Model	PC $n=1$	PC $n=2$	PET $n=1$	PET $n=2$	T_{avg}	T_{max}
This work 80 °C max	38	14	12	2	31	80
This work 95 °C max	56	14	30	3	34	95
King [7]	43	14	16	3	34	84
TamizhMani [8]	22	13	4	2	27	59
$w_3 = 0.076$	35	14	9	2	34	68

and has $a = -2.81$, $b = -0.0455$. Another model is by TamizhMani et al. [8], which is shown as Eq. (3.9) with constants $w_1 = 0.943$, $w_2 = 0.028$, $w_3 = -1.528$, and $c = 4.3$ for an "average" module. The authors did not have an insulated-back module in their study, so we used the model both with the average parameters and also with the wind coefficient at half value for an insulated back: $w_3 = -0.076$.

$$T_{mod} = I \times \exp(a + bW) + T_{amb} \tag{3.8}$$

$$T_{mod} = w_1 T_{amb} + w_2 I + w_3 W + c \tag{3.9}$$

Table 3.4 shows the hours at 85 °C and 85 % RH that correspond to 1 year of degradation in Miami for PC and PET with various assumptions for kinetic order and temperature model. As before, we see that kinetics second order in RH are not very sensitive to the temperature model. The King model agreed well with our assumption of 80 °C maximum temperature and gave similar correlation factors as our temperature model. The TamizhMani model gave lower average and maximum temperatures, which is not surprising since it assumed cooling on both sides. The temperatures came more in line when the wind parameter was halved to −0.076. We could further adjust the parameters by increasing w_2 parameter (a "blacker" module), and the correlations agreed with the other models when T_{max} reached the 80 °C range. We conclude that the effects of the wind average out over the course of the year and fitting module temperature with ambient temperature and irradiance alone is good enough for these calculations, even if the hydrolysis were first order in RH.

Time Parsing Interval

Another key question is how finely parsed the climatic data must be. The TMY3 dataset is parsed in 60 min intervals, which might seem too coarse. Michael Kempe of NREL in Golden, Colorado, provided us with a dataset for Miami, 2002, with the climatic data parsed in 10 min intervals. We used our model on this dataset using points at various intervals without averaging. The results in Table 3.5 surprisingly show that the parsing interval makes <1 % difference in the range of 10–120 min.

Table 3.5 Hours at 85 °C and 85 % RH equivalent to 1 year aging in Miami using a 2002 dataset parsed at various intervals for PC and PET assuming kinetics 1st or 2nd order in RH

Polymer	E_a (kcal/mol)	n	2002 dataset parsing (min)					TMY3
			10	20	30	60	120	1 h
PC	21.9	1	48.2	48.2	48.0	47.9	47.9	37.9
PC	21.9	2	15.3	15.3	15.3	15.3	15.4	13.8
PET	30.9	1	19.9	20.0	19.8	19.7	19.7	12.1
PET	30.9	2	3.1	3.1	3.1	3.1	3.1	2.3

The absolute values for the correlation to 85 °C and 85 % RH aging are slightly different than the results using the TMY3 dataset (the average module RH was higher in the 2002 dataset), but the lack of sensitivity to the parsing interval is striking.

Perspective on Service Life Prediction

Since the conference from which this volume derives was subtitled "Vision for the Future," we will offer our perspective on service life prediction and how it should evolve moving forward. Articles fail because some physical or chemical changes have accumulated that compromise the article's ability to withstand the stresses normally encountered during use or have caused unacceptable loss of esthetics or performance. The changes happen at some rate that depends on the environmental stresses on the article—heat, moisture, sunlight, mechanical loading and cycling, etc. The trick is to understand how these stresses affect the article, singly and in combination, in a reasonable amount of time.

Successful service life prediction requires three sets of information: conditions in the end-use environment, degradation rates or failure times in some accelerated environment, and the kinetic laws that relate the two. The quality of the prediction depends on the quality of all three sets of information, so none can be neglected. Most importantly, since knowing all three generally requires the skills of more than one discipline, the future of service life prediction depends on a synthesis of science and engineering. Science is needed to understand the kinetics and to sort out which environmental stresses are likely to be important and which can safely be ignored, especially when chemical changes are important. Engineering is needed to create the models for how the article responds to environmental stresses and to determine how much degradation in properties can be tolerated before failure. The worlds of mechanical and electrical engineering, material science, and chemistry have tended to revolve separately around the service life problem, but greater progress is made when they collaborate.

Engineers want and need standard tests and properties. Tensile strength and modulus tests are meaningful independent of material—steel, glass, or plastic,

it's all the same. But this is not the case for tests of degradation. Steel, glass, and plastic are all going to degrade differently under damp heat, and to make matters worse, polyethylene, polyesters, and polycarbonates will all be different. Engineering crosses the line into chemistry as soon as chemical bonds are made or broken, and the nuances of chemical reactions and kinetics cannot be ignored.

The Problem of the One-Point Test

A particularly difficult problem arises when quick-and-dirty qualification tests are used to predict lifetimes. The test using 85 °C/85 % RH damp heat for 1,000 h is a good example. Lore has it that this was originally used to test the hermeticity of electronic devices. Perhaps there were data suggesting that devices that passed the test lasted a good long time in the field, but it is unlikely that there was any real correlation between the test and service life. The test would find designs that were poorly sealed or used materials that degraded quickly under these conditions. Tests like this often take on a life of their own, especially if they are the first of their kind. Engineers looking for humidity tests extended it widely and certainly into applications where its predictive value was limited.

So, let's say that a qualification standard calls for a certain amount of property retention after 1,000 h of damp heat. This gives precisely one piece of information: the amount of degradation at 1,000 h or perhaps just a pass/fail. That's not even a rate; it's just one data point in time. What can you do with one data point? This was considered by Dixon at Westinghouse for thermal degradation of electrical insulation [22]. One can make an Arrhenius graph, plot the point, and assume an average activation energy as the slope to draw a line. Dixon shows a frequency distribution for activation energies ranging from 7 to 50 kcal/mol for nearly 70 materials. (Interestingly, some material names like "silicone" appeared more once with vastly different values since all silicones are not created equal.) By finding that 95 % of materials had $E_a \leq 9$ kcal/mol, he could make a conservative estimate by using that value for the Arrhenius plot. A chemist shudders at such an analysis, but it is all that can be done with one data point.

The present case is shown as an Arrhenius plot in Fig. 3.10. The accelerated testing is performed at relatively high temperatures where PET fails much sooner than PC. However, the extrapolated lines cross because they have different slopes, that is, different activation energies. At the effective use temperature of ~25 °C[3], the PET might actually last longer than PC, but both have an order magnitude longer lifetime than required for a 25 years life if the Arrhenius extrapolation is to be believed. This outcome cannot be predicted from the test data at the single condition of 85 °C and 85 % RH for a set amount of time. Note that the problem is not one of the

---

[3] Calculated using the module temperature and RH and kinetics 2nd order in RH from the Miami TMY3 dataset and the method for effective temperature described in [13].
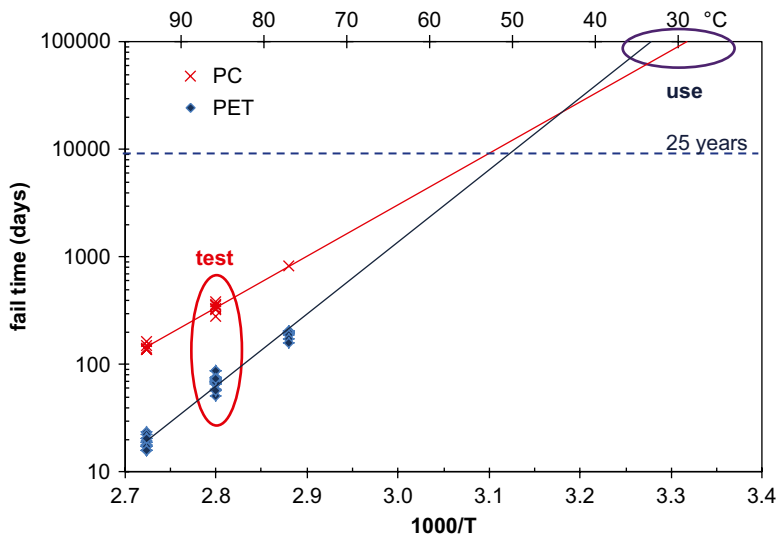
Fig. 3.10 Extrapolated Arrhenius plot for PC and PET hydrolysis normalized to 100 % RH assuming kinetics second order in RH. Failure times need to be divided by $[RH]^2$ to find the fail time at a particular RH

correlation of the test to the "real world," but the correlation of the test *conditions* to real-world *conditions* for a *particular material*. The correlation depends on the actual duty cycle and the degradation kinetics of the material as well as the lifetime under test conditions.

A problem arises from the words we use. There is in fact no such thing as an "Accelerated Life Test" much less a "Highly Accelerated Life Test." There are only accelerated and highly accelerated *degradation* tests. It may be instructive to consider how other physical property testing data are used. Physical properties such as tensile strength of a material are used as parameters in engineering models to predict performance in a finished object. A tensile test of steel cannot be used to predict the length of a bridge span that can be built from that steel without many other parameters and a good model. Similarly, degradation data under one set of conditions cannot be used to predict how long something will last without many other parameters and a good model. There cannot be a single test for how long something will last any more than there can be a single test for bridge length. The test data feed the model that generates a prediction. Different models must be constructed for different materials, exposure conditions, and applications just as different models must be constructed for different types of bridges. Service life prediction arises from using the appropriate model to get from the accelerated degradation data to the use conditions. The future of service life prediction lies not so much in defining the tests as in understanding the need for good definition of use conditions and the chemical and physical models for degradation.

Conclusions

Successful service life prediction models require good, time-parsed information about use conditions, knowledge of how environmental variables affect the rate of degradation, and good rate data under at least one set of accelerated conditions. There are various ways this information can be sliced and put into different models or approaches, but all the pieces must be present in some form. In the three-step approach, one can establish the kinetics for a material and use those kinetics to calculate service life from accelerated test data for a particular formulation using that material. The approach is not without risk since one cannot know when a formulation change is drastic enough to change the kinetics, but it may be the best that can be done with limited time and resources.

The hydrolysis of polycarbonate and PET under humidity aging conditions appears to be second order in RH—a water-catalyzed hydrolysis reaction taking place under pH neutral conditions. The activation energies for PC and PET are different, ~22 kcal/mol (92 kJ/mol) for PC and ~31 kcal/mol (129 kJ/mol) for PET. RPA is intermediate at 24 kcal/mol (102 kJ/mol). The large difference in E_a between PET and PC means that their Arrhenius plots cross so that the brittle failure times are PC > PET at high temperatures, PC = PET at ~42 °C, and PET > PC at lower temperatures. Accelerated testing usually takes place at high temperature to the disadvantage of PET, while actual use conditions are in the low temperature regime where PET may be equivalent to or better than PC. In all cases, including RPA, the hydrolysis lifetimes are likely to be more than adequate for solar energy applications such as front and back sheets for PV modules.

The second-order kinetics cause some surprising conclusions. In general, RH decreases as the temperature increases and vice versa. When the E_a is low as for PC, the fact that the RH term is squared approximately cancels the effect of temperature. When the E_a is high as for PET, the temperature effect still dominates but not as much. As a result, the lifetime prediction is not very sensitive toward the accuracy of the temperature model. The results were also not very sensitive toward the time interval used in parsing the climatic data for both PC and PET; 10 min and 2 h parsing surprisingly gave nearly the same results.

References

1. Pickett JE, Sybert PD, Carter RL, Gibson DA, Rice ST (2007) Weathering characteristics of resorcinol arylate copolymers. Polym Prepr 48(1):643–644
2. Zhou J, Pickett JE, Chakravarti S US Patent application US 20120248497

3. Kempe MD, Wohlgemuth JH (2013) Evaluation of temperature and humidity on PV module component degradation. In: 39th IEEE photovoltaic specialists conference, Tampa, FL, 16–21 June 2013 (also NREL PV module reliability workshop, Golden CO, 26–27 Feb 2013)

4. Pickett JE, Gardner MM (2005) Reproducibility of Florida weathering data. Polym Degrad Stab 90:418–430

5. http://rredc.nrel.gov/solar/old_data/nsrdb/1991-2005/tmy3/

6. Wilcox S, Marion W (2008) Users manual for TMY3 data sets. Technical report NREL/TP-581-43156, Revised May 2008. http://www.nrel.gov/docs/fy08osti/43156.pdf

7. King DL, Boyson WE, Kratochvil JA Photovoltaic array performance model. SAND2004-3535, Sandia National Laboratories. http://prod.sandia.gov/techlib/access-control.cgi/2004/043535.pdf

8. TamizhMani G, Ji L, Tang Y, Petacci L, Osterwald C Photovoltaic module thermal/wind performance: long-term monitoring and model development for energy rating. NREL/CD-520-33586, p 936. http://www.nrel.gov/docs/fy03osti/35645.pdf

9. Skoplaki E, Boudouvis AG, Palyvos JA (2008) A simple correlation for the operating temperature of photovoltaic modules of arbitrary mounting. Sol Energy Mater Sol Cells 92:1393–1402

10. Davis MW, Fanney AH, Dougherty BP (2001) Prediction of building integrated photovoltaic cell temperatures. Trans ASME 123:200–210

11. Bijl P, Heikkilä A, Syrjälä S, Aarva A, Poikonen A (2011) Modeling of sample surface temperature in an outdoor weathering test. Polym Test 30:485–492

12. Koehl M, Heck M, Wiesmeier S, Wirth J (2011) Modeling of the nominal operating cell temperature based on outdoor weathering. Sol Energy Mater Sol Cells 95:1638–1646

13. Pickett JE, Sargent JR (2009) Sample temperatures during outdoor and laboratory weathering exposures. Polym Degrad Stab 94:189–195

14. Alduchov OA, Eskridge E (1996) Improved Magnus form approximation of saturation vapor pressure. J Appl Meteorol 35:601–609

15. Pickett JE, Coyle DJ (2013) Hydrolysis kinetics of condensation polymers under humidity aging conditions. Polym Degrad Stab 98:1311–1320

16. Golovoy A, Zinbo M (1989) Water sorption and hydrolytic stability of polycarbonates. Polym Eng Sci 29:1733–1737

17. McMahon W, Birdsall HA, Johnson GR, Camilli CT (1959) Degradation studies of polyethylene terephthalate. J Chem Eng Data 4:57–79

18. Jencks WP, Carriuolo J (1961) General base catalysis of ester hydrolysis. J Am Chem Soc 83:1743–1750

19. Euranto EK, Cleve NJ (1963) Kinetics of the neutral hydrolysis of chloromethyl chloroacetate. Acta Chem Scand 17:1584–1594

20. Hsieh Y-H, Weinberg N, Wolfe S (2009) The neutral hydrolysis of methyl acetate—Part 1. Kinetic experiments. Can J Chem 87:539–543

21. Shi Z, Hsieh Y-H, Weinberg N, Wolfe S (2009) The neutral hydrolysis of methyl acetate—Part 2. Is there a tetrahedral intermediate? Can J Chem 87:544–555

22. Dixon RR (1980) Thermal aging predictions from an Arrhenius plot with only one data point. IEEE Trans Electr Insul EI-15(4):331–334

Chapter 4
A Kinetic Model for Predicting Polymeric Neutron Shieldings Lifetime

F. Nizeyimana and H. Issard

Abstract Polymers are widely used in radioactive material transport/storage casks. Their neutron shielding ability relies mostly on their concentrations in hydrogen atoms which slow down neutrons. However, in-service high temperatures are responsible for H abstraction decreasing polymers shielding capability. Therefore, their long-term properties must be accurately predicted. In this regard, a multi-year R&D program has been set up to elucidate oxidation mechanisms of neutron shielding materials and develop a nonempirical lifetime prediction methodology. This paper deals with accelerated aging tests and modeling of a vinylester based neutron shielding product, commercially known as *TN Vyal B*™. Samples are exposed to various temperatures up to 160 °C and O_2 partial pressure and analyzed using various experimental techniques. Basically, thin free films are fully oxidized while thick samples show the diffusion-limited oxidation (DLO): a superficial layer is oxidized whereas the core is not affected. Therefore, to investigate the long-term properties, it is obvious that DLO phenomenon must be taken into account by coupling both oxidation kinetic and oxygen diffusion. In our case, there is a good agreement between simulated weight losses and oxidation thicknesses. Based on degradation assessment and design temperature of dry storage casks, *TN Vyal B*™ excellent resistance can be confirmed.

F. Nizeyimana (✉) • H. Issard
AREVA TN International, 1, rue des hérons, Montigny Le Bretonneux,
78 054 Saint Quentin en Yvelines, France
e-mail: fidele.nizeyimana@areva.com

Introduction

Polymeric resins are widely used thanks to their versatility. In aeronautic applications, they are chosen to replace metallic components for mass and cost reduction. In automobile industry, they are nowadays present in numerous cars components as well as paints. Other important applications for polymers are offshore industry (boats shells), civil engineering (concretes, electrical cables insulators…), to name a few.

In our case, the polymer resin based composite is used as a neutron shielding in radioactive material transport/storage casks. Over service life of the casks, initial properties of neutron shielding may fall due to thermal oxidation and neutron radiation. To our knowledge, degradation of shielding polymers via neutron radiation is insignificant. However, oxidation effects can be dramatic and irreversible, especially for the very long-term service. Thermal oxidation reactions are associated with crosslinking, chain scission, hydrogen atoms abstraction, leading to oxidation products buildup. These products are generally concentrated in a thin superficial layer.

Long-term properties are commonly assessed using an Arrhenius model. However, controversies related to the use of these models have been reported [1, 2]. Gillen et al. [1] examined risks taken by considering the same activation energy (Ea) for a great range of temperatures (even a narrow change in Ea affects extrapolated predictions). Their work also shows another important mechanism that leads to a non-Arrhenius behavior, involving diffusion-limited oxidation (DLO).

Recently, to simulate oxidation aging more confidently, new methodologies have been derived [3–6]. In this paper, the time–temperature behavior will be clarified using results obtained by optical microscopy and Micro-ATR analysis. Furthermore, from Arrhenius limitations stated above, TN International has adopted a new and accurate model for predicting its neutron shielding polymeric materials. The model is derived from a mechanistic scheme [7] coupled with Fick 2nd law, $\frac{\partial [O_2]}{\partial t} = D \frac{\partial^2 [O_2]}{\partial z^2}$. The same approach has been previously developed and applied to epoxies [3, 5, 6], bismaleimides [4], to name a few. The aim of this paper is to demonstrate the robustness of this nonempirical model on a vinylester resin based neutron shield, *TN Vyal B*™.

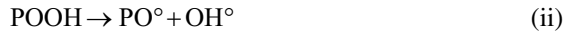## Theoretical Calculations and Modeling

Our kinetic model methodology is based on a kinetic mechanism and O_2 diffusion permeation parameters.
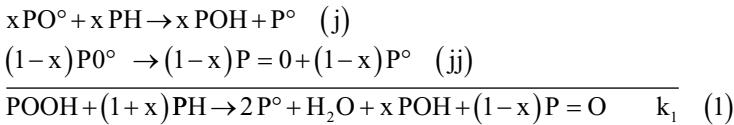
(a) *Schematic mechanism*

This mechanism is derived from scheme proposed by British scientists Bolland and Gee [7]. It is possible to divide the scheme in three steps: initiation, propagation, and termination. Without getting into further details, the derivative scheme is

described below. To our knowledge, unfortunately, no other nuclear actor has implemented this methodology, even though, the neutron shielding materials are required to last decades in service.

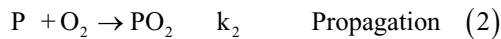During the first step, ***initiation***, hydroperoxides (POOH) are decomposed free radicals (PO°, OH°, PO°, P°):

$$POOH \rightarrow PO° + OH° \qquad (ii)$$

$$PO° + PH \rightarrow POOH + P° \qquad (iii)$$

$$OH° + PH \rightarrow H_2O + P° \qquad (iv)$$

Radicals can reorganize with β-scission in either carbonylated (P=O) or alcoholic (POH) products:

$$
\begin{array}{l}
x\,PO° + x\,PH \rightarrow x\,POH + P° \quad (j) \\
(1-x)\,P0° \rightarrow (1-x)\,P = 0 + (1-x)\,P° \quad (jj) \\
\hline
POOH + (1+x)\,PH \rightarrow 2\,P° + H_2O + x\,POH + (1-x)\,P = O \qquad k_1 \quad (1)
\end{array}
$$

It is worth noting that a few of the products P=O and POH are volatile and together with water, they are responsible for oxidation-induced mass loss. They are denoted by "V" in initiation reaction:

$$POOH + 2\,PH \rightarrow 2\,P° + H_2O + {}^-V \qquad k_1 \qquad \text{Initiation} \quad (1)$$

The ***propagation*** step follows with two reactions taking place; the first reaction consists in combination of O_2 and P° radicals yielding a new radical $PO_2°$. While the latter react with polymer to produce hydroperoxides and P° radicals. Propagation reactions are given below:

$$P + O_2 \rightarrow PO_2 \qquad k_2 \qquad \text{Propagation} \quad (2)$$

$$PO_2 + PH \rightarrow POOH + P \qquad k_3 \qquad \text{Propagation} \quad (3)$$

Besides, free radicals could react with each other, yielding stable (inactive) species. This process is known as ***termination***:

$$P + P \rightarrow \text{inactive products} \qquad k_4 \qquad \text{Termination} \quad (4)$$

$$P + PO_2 \rightarrow \text{inactive products} \qquad k_5 \qquad \text{Termination} \quad (5)$$

$$PO_2 + PO_2 \rightarrow \text{inactive products} + O_2 \quad k_6 \qquad \text{Termination} \quad (6)$$
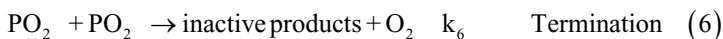
From the chemical scheme detailed above, a system of differential equations can be set to describe all species concentrations over aging time.

$$\frac{d[P^\circ]}{dt} = 2k_1[POOH] - k_2[O_2][P^\circ] + k_3[PH][PO_2{}^\circ] - 2k_4[P^\circ]^2 - k_5[P^\circ][PO_2{}^\circ] \quad \text{(I)}$$

$$\frac{d[PO_2{}^\circ]}{dt} = k_2[O_2][P^\circ] - k_3[PH][PO_2{}^\circ] - k_5[P^\circ][PO_2{}^\circ] - 2k_6[PO_2{}^\circ] \quad \text{(II)}$$

$$\frac{d[POOH]}{dt} = -k_1[POOH] + k_3[PH][PO_2{}^\circ] \quad \text{(III)}$$

$$\frac{d[PH]}{dt} = -k_3[PH][PO_2{}^\circ] - 2k_1[POOH] \quad \text{(IV)}$$

$$\frac{d[O_2]}{dt} = -k_2O2[P^\circ] + k_6[PO_2{}^\circ]^2 + D\frac{\partial^2[O_2]}{\partial z^2} \quad \text{(V)}$$

It should be emphasized that the final equation (Eq. V) is composed of two terms. The first, $-k_2O_2[P^\circ] + k_6[PO_2{}^\circ]^2$, corresponds to O_2 consumption and the second to Fick's 2nd law, $\frac{\partial[O_2]}{\partial t} = D\frac{\partial^2[O_2]}{\partial z^2}$, where D is O_2 diffusion and $[O_2]$ represents O_2 concentration in depth x.

$[O_2]$ values shift from equilibrium concentration (C_s) on samples surface to nil in the core. C_s is given by Henry's law: $C_s = S_{O_2} \times p_{O_2}$, where S is O_2 solubility in the polymer and p the O_2 partial pressure. Parameters D and S are obtained experimentally by permeation tests. They are given in Table 4.1.

The set of differential equations written above were solved numerical by the finite difference method of Runge–Kutta (Ode23tb of Matlab). Basically, a polymer sample is discretized into N knots equally spaced with a distance Δx:
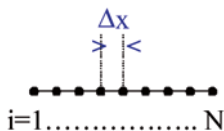
(Lines $i=1$ and $i=N$ correspond to both surfaces of the sample).

$$Initial\ conditions(t=0), i=1,\ldots,N; [P^\circ]=0; [PO_2{}^\circ]=0; [PH]=[PH]_0;$$
$$[POOH]=[POOH]_0$$

Table 4.1 Oxygen parameters used in our model

T (°C)	120	140	160
D 10^{-12} (m²s)	3.9	4.9	6.0
C_s (atmospheric pressure)	3.5×10^{-4} mol/l		
C_s (2×10^5 Pa)	3.5×10^{-3} mol/l		

For each time $t > 0$; $i = 1,..., N$, the system of differential equations can be rewritten as follow:

$$\frac{d[P°]}{dt}i = 2k_1[POOH]_i - k_2 C_i[P°]_i + k_3[PH]_i[PO_2°]_i - 2k_4[P°]_i^2 - k_5[P°]_i[PO_2°]_i$$

$$\frac{d[PO_2°]}{dt}i = k_2 C_i[P°]_i - k_3[PH]_i[PO_2°]_i - k_5[P°]_i[PO_2°]_i - 2k_6[PO_2°]_i^2$$

$$\frac{d[POOH]}{dt}i = -k_1[POOH]_i + k_3[PH]_i[PO_2°]_i$$

$$\frac{d[PH]}{dt}i = -k_3[PH]_i[PO_2°]_i - 2k_1[POOH]_i$$

The weight variation is calculated taking into account the reaction I (initiation) that leads to water yield, volatile products, as well as O_2 grafting on polymer chains during oxidation process:

$$\frac{1}{m_0}\frac{dm}{dt} = \underbrace{\frac{32}{\rho_0}R(C)}_{\substack{\text{mass uptake due } O_2 \\ \text{uptake}}} - \underbrace{\frac{18}{\rho_0}\frac{d[H_2O]}{dt} - \frac{M_V}{\rho_0}\frac{d[V]}{dt}}_{\substack{\text{mass loss : water and} \\ \text{oxidation products}}}$$

$$R(C) = k_2 C[P°] - k_6[PO_2°]^2$$

Experimental

Material

The material is a TN International patented polymer composite, *TN Vyal B™*, here after referred to as a vinylester composite.

Its polymer matrix, vinylester resin, can be affected by long-term exposure in severe conditions. Prior to aging tests, matrix films (30 μm < thickness < 45 μm) and composite thick samples (0.5 mm < thickness < 2 mm) were cured at 80 °C for 12 h and post-cured at 160 °C for 2–4 h. Following this process, the material's cure is enhanced and unreacted free species are eliminated.

Measurements

Samples were exposed between 120 and 160 °C in pure oxygen at partial pressure of 2×10^5 Pa and atmospheric pressure. Then, various chemical, physical, and mechanical characterizations were performed on the industrial neutron shielding

(vinylester composite). To confirm or go further into understanding of observed phenomena, specific and limited analyses were done on the vinylester matrix free films.

(a) Gravimetric analysis

Gravimetric analysis was carried out periodically over aging time using a balance with a relative accuracy of 10^{-4}. Weight changes were calculated as follows:

$$\frac{m}{m_0}(\%) = \frac{m_t - m_0}{m_0} \times 100 \quad \text{with } m_0, m_t \text{ corresponding to initial weight and weight at aging time } t, \text{ respectively.}$$

(b) Infrared Spectroscopy

Two methods of IR measurements were carried out. First of all, IR spectra were collected in the region 4,000–400 cm^{-1} directly on matrix free films (30–40 μm of thickness). The FTIR machine used was a Brucker IFS 28 Spectrometer. Spectra were recorded in a transmission mode with an average of 32 scans. To determine species concentration, C (expressed in mol/l), Beer–Lambert law was applied:

$$C = \frac{A}{\varepsilon l} \quad \text{where } A \text{ is absorbance and } \varepsilon \text{ and molar absorptivity and sample s thickness respectively.}$$

The second method was Micro-ATR Spectroscopy where a Spotlight 300 apparatus coupled with Spectrum 100 FTIR Spectrometer is used. With this technique, IR spectra are recorded in the entire oxidized layer. Two of the peaks which presented noticeable changes were particularly monitored:

– 1,727 cm^{-1} which seemed to increase in absorbance during aging
– 1,145 cm^{-1} which only appeared after samples exposure

Then, the obtained profiles were compared to the prediction.

(c) Dynamic mechanical analysis (DMA)

This method provides a comprehensive understanding of material's internal molecular mobility, over aging time as well as structural changes. Plus, glass temperature (Tg) changes over aging time gives an interesting information on residual crosslinking or even post-cure taking place due to aging processes.

Measurements were conducted on 2 mm thick samples using a NETZCH DMA 242 instrument in a tensile mode. Measurements conditions are listed below:

Temperature scans between 30 and 200 °C
Heating rate of 5 °C/min
Frequency of 1 Hz

As there's no standard of determining Tg, its values can be monitored as an offset of storage modulus, E', or on maxima of loss modulus E'' and loss tangent, tanδ. In our case, Tg data were collected on E′.

Results and Discussion

Identification of Structural Changes

Measurements on free films were carried out to assess changes in the vinylester matrix network over time. Figure 4.1 displays the comparison between IR spectra of a film at t_0 and after its exposure to 160 °C under 2×10^5 Pa for 645 h.

The main spectra modifications are given below:

- Slight decrease of C–H at 2,935 cm^{-1} due to H abstraction during oxidation process
- Significant increase in intensity of 1,725 cm^{-1} peak due to "new" carbonyl groups (C=O) build up
- Broadening of 1,244 cm^{-1} peak (aromatic C–O) suggesting complex molecular rearrangements
- The peak corresponding to C–O methacrylate at 1,180 cm^{-1} shifts to lower wave-length number (1,170 cm^{-1})

As shown in Fig. 4.2a, carbonyl groups (C=O) buildup increases steadily until over 650 h, then stabilizes with aging time. In addition, evolution of the new peak that appeared at 1,170 cm^{-1} after exposure is presented in Fig. 4.2b. It was quantified by rationing its absorbance with the internal reference at 1,494 cm^{-1} (related to stable aromatic C=C bonds). Its evolution displays a sharp increase after only 50 h followed by a slight and progressive increase up to around 400 h. All of this IR results suggest that oxidation is time-dependent process. They also reveal that C–H oxidation depends on its position in the polymer chain. Hence, C–H in α-position to
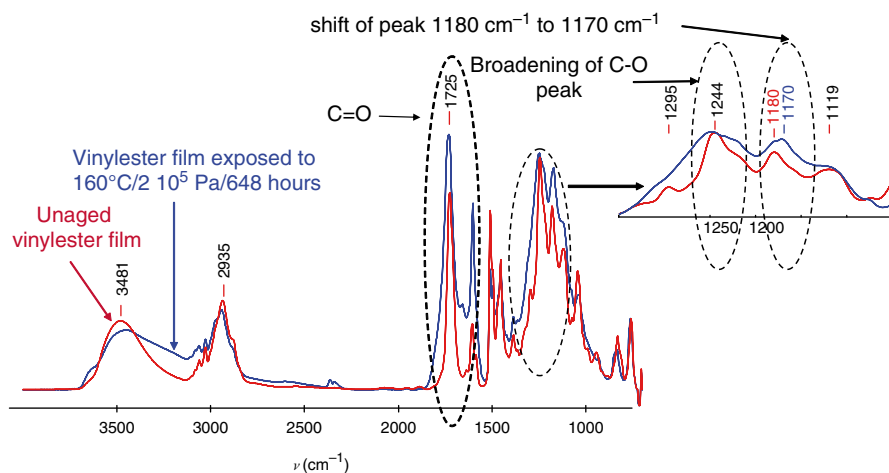
Fig. 4.1 FTIR spectra of a vinylester free film: (**a**) before aging; (**b**) after exposure to 160 °C under 2×10^5 Pa of O_2 for 648 h
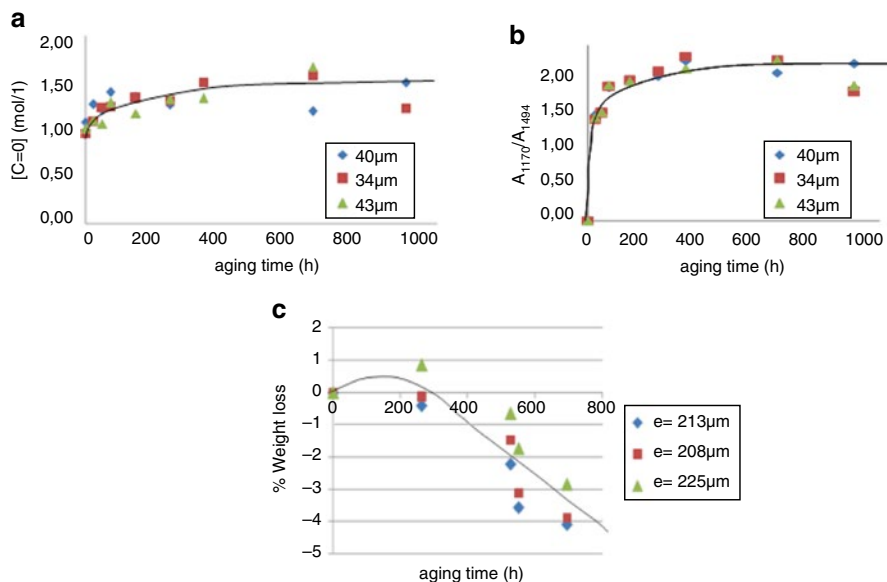
Fig. 4.2 Evidence of free films degradation: (**a**) carbonyl groups (C=O) buildup; (**b**) increase of the peak at 1,170 cm⁻¹; (**c**) variation of films weight

oxygen ($-CH_2-O-$) or tertiary ($-CH_2-CH-CH_3$) are oxidized quite rapidly, and, consequently, concentration oxidation products also increase rapidly. That is what is observed during the first hours of aging. Finally, relative stability observed after 650 h does not mean that oxidation has stopped. In fact, one could be aware that, at this stage, there is a competition between oxidation and evaporation of a part of volatile oxidation products.

By gravimetric analysis showed in Fig. 4.2c, two steps are observed. The slight mass uptake observed until 200 h indicate the grafting of oxygen atoms on polymer chains during the second reaction of propagation. It is worth mentioning that this step wasn't observed for composite samples, probably due to early predominance of evaporation (weight loss) over mass uptake. The sharp weight loss at higher duration indicates once again the evaporation of volatile oxidation products stated above.

In addition of FTIR and gravimetric analysis, structural changes were also evaluated with DMA analysis performed on vinylester composite exposed to different temperatures and O_2 partial pressure. The results are shown in Fig. 4.3.

Quite interestingly, the evolution of *Tg* seems to follow a "master curve" whatever the aging conditions. *Tg* quick increase is seen before 100 h where it reaches roughly 150 °C. Then, *Tg* increases progressively to an "indefinite" value or *Tg∞* of 170 °C. This result is a good indication of a post-cure related to recombination of radicals generated by oxidation. Meanwhile, over 1,200 h, *Tg* seems to decrease slightly. Even if this decrease is less significant, an important question can be raised here: are there any chain scission reactions that may lead to a drop of crosslinking density at higher exposure durations?
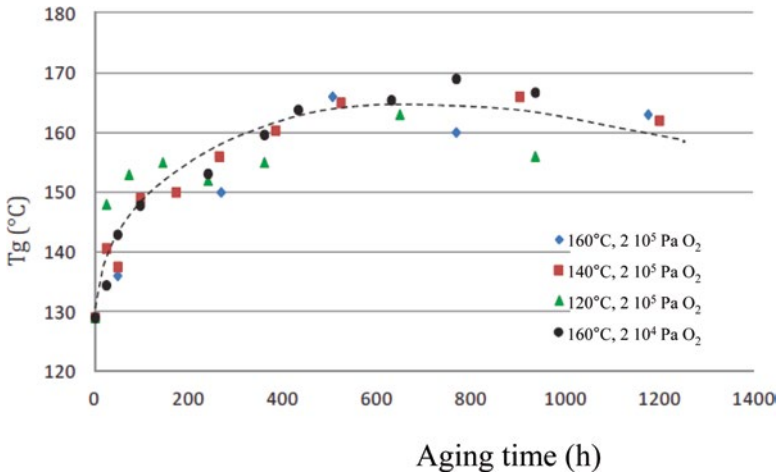
Fig. 4.3 The change in *Tg* of vinylester composite during its exposure to different temperatures and O_2 pressure
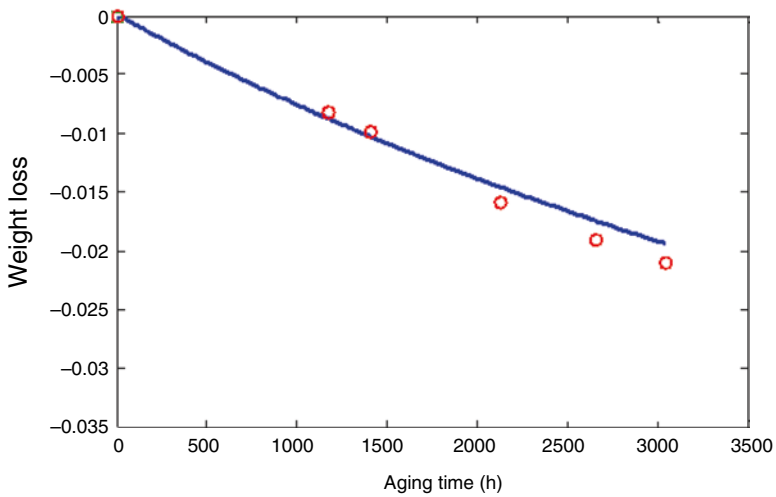

Fig. 4.4 Weight loss curve obtained for vinylester composite at 140 °C under 2×10^5 Pa of O_2: experimental (**o**), model (—)

Weight Loss Modeling

The kinetic model was used to predict oxidation-induced weight loss for samples exposed to different temperatures and oxygen pressure. For instance, in Fig. 4.4, a quite acceptable agreement is shown for composite samples exposed to 140 °C and 2×10^5 Pa of O_2.
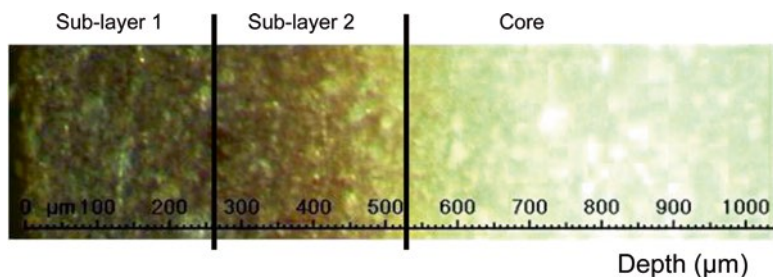
Fig. 4.5 Optical photography of a composite sample (thickness = 2 mm) exposed to 160 °C/2×10⁵ Pa of O₂ for 1,200 h

Oxidation Layers Profiling

As mentioned earlier, only superficial layer is affected by samples exposure to oxidative environment. This phenomenon is qualitatively shown in Fig. 4.5 for samples aged at 160 °C/2×10⁵ Pa of O₂. Degradation is symmetrical relative to the center; therefore, only half the sample is shown.

By optical microscopy, color heterogeneities or gradient in sample thickness are easily observed confirming the existence of diffusion-controlled oxidation. First of all, from the sample's edge, a layer of roughly 250 μm is browned (sub-layer 1) followed by a yellowing of around 250 μm (sub-layer 2) while the core of the sample has kept its original color. Therefore, based on this experimental technique, overall oxidation layer can be estimated to extend to a depth of 500 μm.

On the other hand, using μATR, oxidation layers were also successfully determined by measuring the concentration of oxidation products for all studied aging conditions. They were compared to profile prediction.

Figure 4.6 displays a three-dimensional (3D) presentation of degradation using our model. As expected, oxidation products buildup showed an exponential evolution with the higher concentration on sample's edge decreasing continually to the core.

Overall, the higher the aging temperature, the greater was the oxidation layer thickness. For instance, in Fig. 4.7, oxidized layer profiles of samples aged separately for around 1,200 h at 160 °C 2×10⁵ Pa of O₂ and atmospheric pressure are presented. As can be seen, for the same aging temperature, oxidized thickness is roughly doubled when the pressure is increased from atmospheric pressure to 2×10⁵ Pa. Finally and most interestingly, it is clear that there's a relative good agreement between simulated and experimental profiles obtained by μATR.
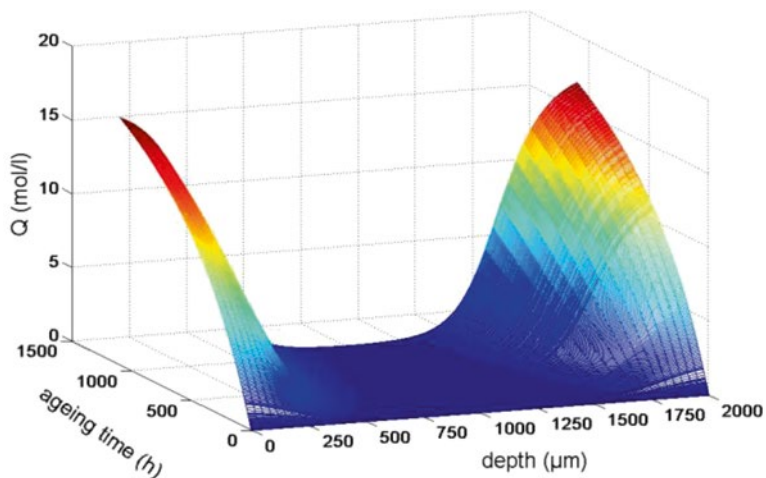
Fig. 4.6 3D presentation of predicted OL profile of TN Vyal B™ exposed at 160 °C/2×10^5 Pa O$_2$ for 1,200 h
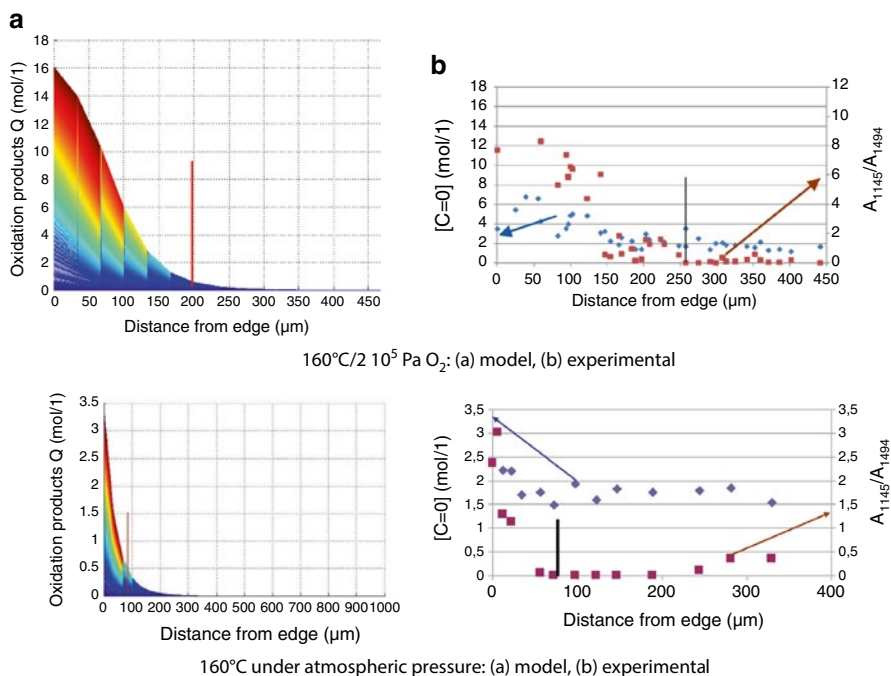

Fig. 4.7 Example of simulated and experimental oxidized layer thickness for composite samples exposed to 160 °C/2×10^5 Pa O$_2$ and atmospheric pressure for 1,200 h. 160 °C/2×10^5 Pa O$_2$: (**a**) model, (**b**) experimental. 160 °C under atmospheric pressure: (**a**) model, (**b**) experimental

Conclusion

The material studied is a TN International vinylester based neutron shielding product, commercially known as *TN Vyal B*™. The focus of our study was to investigate the material's thermal degradation mechanism using accelerated aging tests and to validate a nonempirical model for predicting long-term in-service properties. Conclusions are the following:

- Aging leads to superficial oxidative layer buildup suggesting a DLO effect. IR measurements show a slight decrease of C–H groups (hydrogen abstraction) followed by an increase in carbonyl groups in the oxidized layer
- Exposure of free films to high temperatures and oxygen caused early mass uptake (due to O_2 grafting on polymer chain) followed by a dramatic drop of mass (due to volatile oxidation products). For composite, however, mass uptake is very rapid and difficult to be monitored
- In the initial exposure time, *Tg* increases due to post-cure. At longer exposures, *Tg* starts to decrease due to some polymer chain scission
- A good correlation of experimental and simulated data is obtained on weight changes as well as oxidation profiles
- The new approach allows a great understanding of our neutron shielding long-term performance

References

1. Gillen KT, Celina M, Clough R, Wise J (1997) Extrapolation of accelerated aging data – Arrhenius or Erroneous? Trends Polym Sci 5(8):250–257
2. Celina M, Gillen KT, Assink RA (2005) Accelerated aging and lifetime prediction: review of non Arrhenius behavior due to two competing processes. Polym Degrad Stab 90:395–404
3. Colin X, Marais C, Verdu J (2001) A new method for predicting the thermal oxidation of thermoset matrices: application to an amine crosslinked epoxy. Polym Test 20:795–803
4. Colin X, Marais C, Verdu J (2002) Kinetic modelling and simulation of gravimetric curves: application to the oxidation of bismaleimide and epoxy resins. Polym Degrad Stab 78:545–553
5. Bellenger V, Decelle J, Huet N (2005) Ageing of a carbon epoxy composite for aeronautic application. Compos Part B 36(3):189–194
6. Bellenger V, Verdu J (1985) Oxidative skeleton breaking in epoxy-amine networks. J Appl Polym Sci 30:363–374
7. Bolland JL, Gee G (1946) Kinetic studies in the chemistry of rubber and related materials. Trans Faraday Soc 42:236–243

Chapter 5
How Can We Effectively Use Accelerated Methods to Predict the Decorative Properties of PVDF-Based Coatings?: A Practical Approach

Kurt A. Wood

Abstract Poly(vinylidene fluoride) (PVDF) resins are the dominant component of some of the most weatherable commercially available decorative coatings. These coatings can have color retention and chalk resistance service lifetimes of decades. We have recently outlined a quantitative service life prediction model for the decorative properties of coatings of this type (Wood K (2009) A quantitative model for the prediction of gloss retention, color change, and chalking for poly(vinylidene fluoride)/acrylic blends. In: Proceedings of 4th European weathering symposium, Budapest, Hungary, Sept 2009). The model is based on the "contraction" theory of gloss loss and chalking, coupled with simple assumptions about the photochemical kinetics of two-resin hybrid systems where one resin (PVDF) is much more weatherable than the other (in this case, an acrylic). Because different mechanisms account for gloss loss, color change, and chalking, the relative rates of change for each of these properties can be different, in accordance with experimental observations. We outline a methodology that uses insights from the model, empirical data from accelerated tests, and long-term weathering test data from solvent-based baked PVDF coatings, to predict the service life of new waterborne no-bake PVDF coatings.

Introduction

The outstanding outdoor weatherability of paints and coatings based on poly (vinylidene fluoride) (PVDF) resins is well demonstrated by 40 years of commercial use on premier architectural structures [1]. The coatings meet some of the most

K.A. Wood (✉)
Arkema, Inc., King of Prussia, PA 19406, USA
e-mail: kurt.wood@arkema.com

demanding manufacturer performance standards, such as AAMA 2605 for "superior" spray coatings on aluminum.[1] Traditional PVDF paints are applied as solvent (nonaqueous) dispersions [2–4], to generate, after baking, a hybrid binder [5] structure with 70–80 wt% PVDF and 20–30 wt% of a miscible acrylic resin (e.g., a methyl methacrylate-ethyl acrylate copolymer). Color is generally provided by highly color-stable inorganic pigments. The PVDF polymer is highly inert and is completely resistant to UVA and UVB radiation [6]. In this context, for highly weatherable paints, it is the acrylic polymer which must be considered the "weak link" of the binder—even though the acrylics which are used are themselves highly weatherable.

Given the inherent durability of the raw materials used in these paints, and the long service life desired for the final coating product, the need for practical and accurate ways to predict the service life of PVDF-based coatings is acute. This is particularly the case as many new raw materials, including new water-based hybrid resin products combining these resins in aqueous dispersion form [7], have recently become commercially available. The new water-based PVDF hybrid resin technology represents an important technical advance, because it allows the application of durable PVDF-based coatings under field-applied and low-temperature bake OEM conditions, without the emission of high levels of volatile organic compounds (VOCs).

Fortunately, for coatings based on blends of PVDF and acrylic resins, there are two factors that make the quest for quantitative service life prediction tractable. First, a very large number of formulations based on PVDF-acrylic solvent dispersion formulations have been on exposure around the world for decades, in addition to undergoing various accelerated tests. For these reference formulations, there is a good understanding of the real-world service life, and they can be used as meaningful long service life controls when testing new formulations. They can also be used to understand the limits of using particular accelerated methods to predict outdoor performance for PVDF-based coatings. Second, since the weathering resistance of the acrylic resin component is significantly worse than the resistance of the PVDF component, formulations based on pure acrylic resins can be considered to be a second kind of control. We have argued previously [8] that using these two reference points, a simple quantitative model can be used to calculate *relative* rates of change for important key properties, for blends of PVDF and acrylic resins vs. the case for a (faster changing) pure acrylic formulation—considering the PVDF component as mainly an inert bystander.

This paper outlines how this quantitative weathering model can be used, first to better understand the linkages between natural and accelerated testing and, second, to predict outdoor gloss and color retention, as well as chalk resistance, for waterborne coatings based on new PVDF-acrylic hybrid latex materials. A general methodology for this approach is depicted in Fig. 5.1.

---

[1] AAMA is the American Architectural Manufacturers Association, www.aamanet.org.

Methodology for Service Life Prediction

Established products   *Newer products*

Accelerated

Outdoor

• *The predictions rely on a general model for weathering of PVDF-acrylic blends*
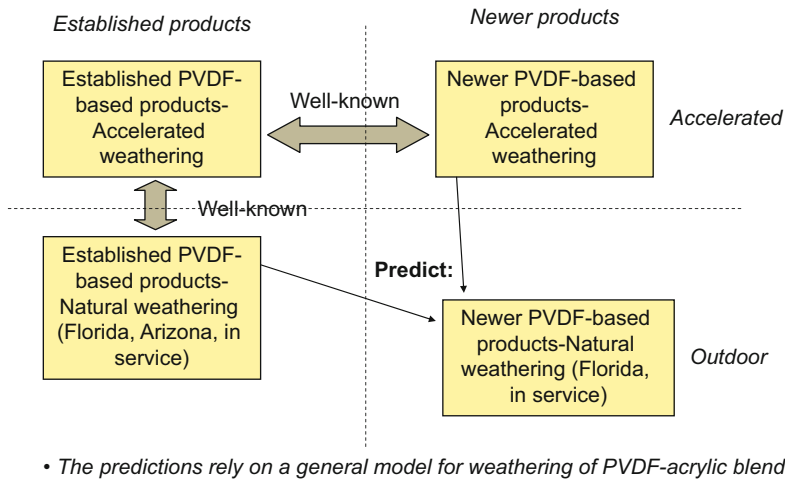
Fig. 5.1 Proposed methodology for predicting the service life of newer PVDF products. A general weathering model is used to understand the limitations of the linkages between accelerated and outdoor exposure testing and between different PVDF-based coating platforms, as well as to predict the outdoor performance of newer products

Physical and Chemical Models for Chalk Resistance and Gloss and Color Retention

In many worldwide standards for coating weatherability, including the AAMA standards for architectural coatings, chalk resistance and gloss and color retention are key performance metrics. A conceptual model for chalk resistance and gloss retention was advanced by Colling and Dunderdale [9] in a major 1981 review paper. They pointed out that even if the pigment in a paint only has a protective (UV light blocking) function, the evolution of gloss loss and chalking will be substantially different depending on whether the coating binder degrades primarily at the air-coating interface ("erosion") or throughout the bulk as far as light is able to penetrate ("contraction") (Fig. 5.2). From a chemical kinetics standpoint, this means that the bulk binder may undergo photodegradation at some particular rate, but there might also be an enhancement of the rate at, or very near, the top surface of the coating. Since pigments, and particularly the most important pigment in coatings, TiO_2, can also have some photocatalytic surface activity, this could be a third mechanism contributing to the photodegradation rate. Colling and Dunderdale presented considerable evidence for the contraction mechanism being dominant in paint systems where low photoactivity grades of TiO_2 were used.[2]

---

[2] In several studies, we have also found considerable evidence for a contraction mechanism in PVDF-based thermoplastic coatings; see [10].

Fig. 5.2 Contraction and
erosion models for paint
degradation, as proposed by
Colling and Dunderdale [9]
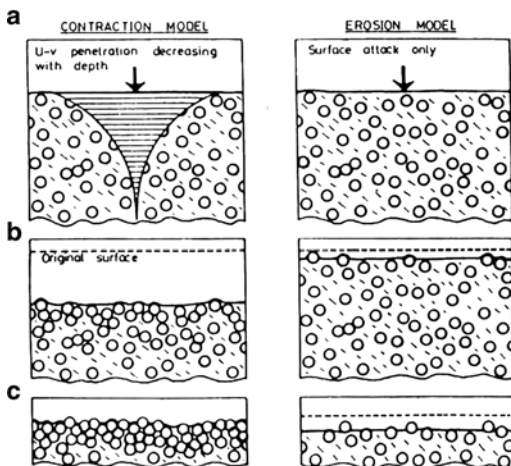
Colling and Dunderdale showed that the contraction model was far more compelling than the erosion model in explaining certain weatherability trends for alkyd paints made with rutile titanium dioxide. Many of these trends are similar to those observed for many PVDF-acrylic blend paints:

- Mass loss often precedes gloss loss. There is an observed retention of gloss, or even a modest increase in gloss, during the initial period of weathering and prior to the onset of chalking.
- There is an observed increased in surface PVC (pigment volume concentration) during the early stages of weathering and prior to the onset of chalking.
- Gloss loss (surface roughening) may lag behind the increase in surface PVC, but it always precedes chalking.
- Gloss retention rates depend strongly on the quality of the distribution of the pigment within the coating.

According to the contraction model, chalking occurs when the surface PVC reaches the CPVC (critical PVC)—i.e., when surface pigments are no longer encapsulated. For systems containing dark-colored pigments, chalking is associated with significant color changes. Color changes prior to the onset of chalking can be attributed to effects related to near-surface PVC changes (i.e., to pigment spacing changes which alter the scattering properties of the pigments), as well as to whatever chemical changes are occurring with the pigment itself.

The contraction model is a physical model linking gloss loss and chalking in particular to near-surface mass loss in the coating. In fact, the loss of surface acrylic has been documented for PVDF-acrylic blend coatings, both exposed in the outdoors [10, 11] and in accelerated weathering cabinets [12]. The loss of acrylic mass through photochemical degradation processes would be expected in any case for these primarily thermoplastic resins, as the photooxidative pathways of many acrylic resins are known to include chain scission and "unzipping" reactions, which lead to
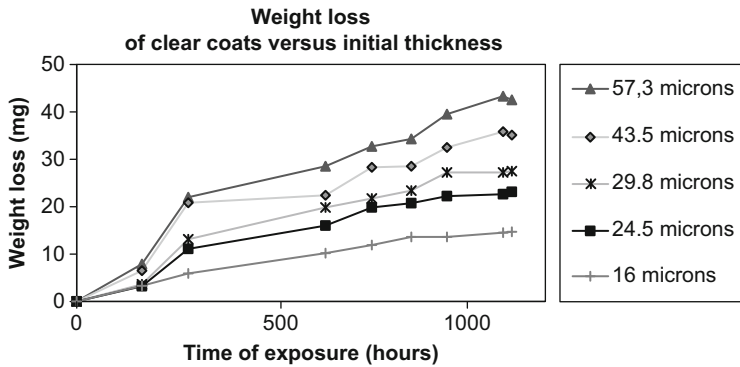
Fig. 5.3 Weight loss of an acrylic clear coat on top of a black PVDF primer, as a function of coating thickness

mass loss through the volatilization of the reaction by-products [13–15]. In studies of pure acrylics and PVDF-acrylic blends in UV fluorescent cabinets, mass loss rates typically exhibit two stages, prior to any late-stage behavior associated with coating failure (Fig. 5.3) [16]. There is an initial transient period—typically the first 200–300 h when UVB (313 nm) bulbs are used—which often exhibits relatively high rates of mass loss. High rates of mass loss may simply be due to incomplete physical drying of the coating but may also reflect the loss of a more photolabile fraction in the coating (this might include the lowest molecular weight species, residual surfactants in waterborne coatings, other additives, etc.). For clear coats, where mass loss is greater (and more easily measured) due to the lack of pigment shielding effects, this may involve the loss of several percent of the coating mass. After this initial transient and perhaps induction period, clear coats typically exhibit a long period, which may last several thousand hours, of steady-state mass loss, usually at a slower mass loss rate. This steady-state mass loss rate indicates first-order kinetics, i.e., that there is a nearly constant concentration of a rate-limiting component which is undergoing photochemical reactions, leading relatively rapidly to mass loss. For thermoplastic clear coats, there is often little change in the coating gloss or haze during this period, consistent with a uniform homogenous contraction of the coating.

Of course, a constant mass loss rate cannot be maintained indefinitely, and so at some point—which may be at 3,000–4,000 h for a weatherable acrylic latex clear coat in a UVB fluorescent chamber—other macroscopic indications of coating degradation generally occur, such as film whitening or cracking. These same macroscopic events are often used as decorative service life end point markers. Consequently, if slow, steady-state mass loss is the primary mode of weathering for a particular coating, the decorative service lifetime should be directly affected by that mass loss rate. Of course, to make a quantitative linkage between the mass loss rate and the changes in the macroscopic decorative properties, a detailed *physical* model which relates the macroscopic properties to the evolution of the coating

mass distribution is needed. The contraction model of Colling and Dunderdale is a natural starting point for such a physical model, since it specifically focuses on mass loss effects.

Two-Resin Model: Predictions for PVDF-Acrylic Coatings with Inert Pigments

If first-order mass loss kinetics are determinative in this way for the service life of coatings based on a particular thermoplastic resin, it should be possible to make quantitative predictions for the *relative* performance of coatings based on *blends* of this resin (in this case, an acrylic) with a much more photochemically inert second resin. In particular, if the two main binder components are PVDF and acrylic resins, then due to the chemical inertness of the PVDF resin, the rate of mass loss may be posited to be proportional in first order to the concentration of the acrylic component in the binder. In other words, as long as the mixing of the two-resin components occurs at a fine enough scale, the degradation rate will be proportional to the amount of acrylic in the system. One major advantage of estimating relative rates in this way—and consequently the relative service life compared to that of a less durable reference system—is that it is not necessary to know the photochemical details of the mass loss mechanism for the reference system. These photochemical kinetic mechanisms may be very complex for real-life commercial materials such as waterborne acrylics [17].

Figure 5.4 shows schematically what would be expected from these models, for the case of PVDF-acrylic paints made with inert pigments, such as the mixed metal oxide pigments commonly used in many commercial architectural paints. These paints typically show minimal color fade and little or no chalking even after decades of outdoor exposure—even if they have lost gloss after several decades.

The contraction model predicts, consistent with chemical analyses, that the coating surface regions will lose acrylic over time and become enriched in the more photochemically inert PVDF component. As the near-surface acrylic content diminishes, the rate of further degradation of the coating slows dramatically, and it reaches a point of near stasis once the acrylic at the surface is substantially gone. By this point in time, gloss loss will have occurred, with gloss loss happening over a time scale which is roughly inversely proportional to the initial acrylic content, according to the photooxidative cycle model. However, if the ratio of PVDF to pigment is high enough, so that the surface PVC stays below the critical PVC even after the loss of all the surface acrylic, the coating will resist chalking essentially indefinitely. The minimum quantity of PVDF needed for this is straightforward to calculate, as long as the critical PVC is known or can be conservatively estimated. Likewise, since large color changes in coatings normally result either from the chemical degradation of the pigment or from chalking, the net color change will be small even after very long periods of time, as long as stable inorganic pigments were used. This phenomenon is well documented for many PVDF coatings around the world,
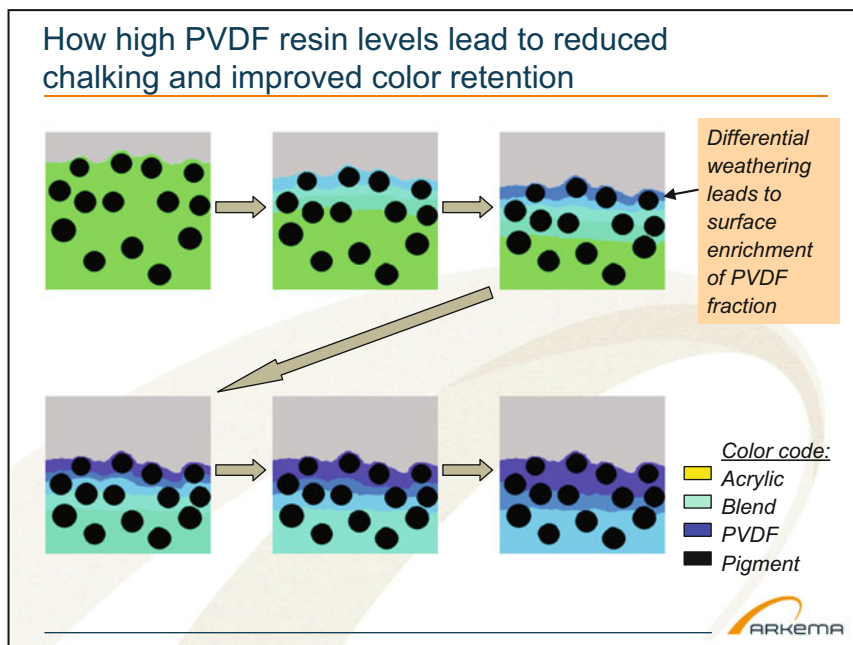
Fig. 5.4 Schematic for compositional changes in PVDF-acrylic blends, as a result of weathering

which were formulated with 70–80 % PVDF in line with commercial license requirements.[3]

It should be noted that this ability to resist chalking and color fade is due partly to the thermoplastic nature of the PVDF resin, which permits film integrity to be maintained even while contraction processes are occurring.[4] Thermosetting fluoropolymer systems, which rely on a cross-linked network to achieve pigment encapsulation, may still be subject to chalking at long times through a different failure mechanism.

Our previous paper [8] explores some other implications of the model, for instance, the prediction that the rates for gloss loss related processes, and color fade rates for *organic* pigments, should be roughly proportional to the total fraction of

---

[3] The historical license requirement for KYNAR 500® PVDF specifies a minimum content of 70 wt% KYNAR 500 PVDF on total binder and a minimum of 40 wt% on total coating solids. If the critical PVC is about 50 % and the density for PVDF, acrylic, and metal oxide pigment are about 1.78, 1.18, and 4.5, respectively, it may be calculated that a typical license composition with 60:40 binder:pigment mass ratio will easily meet the critical PVC requirement, the PVC being about 19 % with the acrylic included and 27 % if a weathered surface region with only pigment and PVDF is considered.

[4] The glass transition temperatures for PVDF homopolymers and copolymers are in the -40 °C to -30 °C range, permitting considerable mobility of the polymer chains at normal service life temperatures.
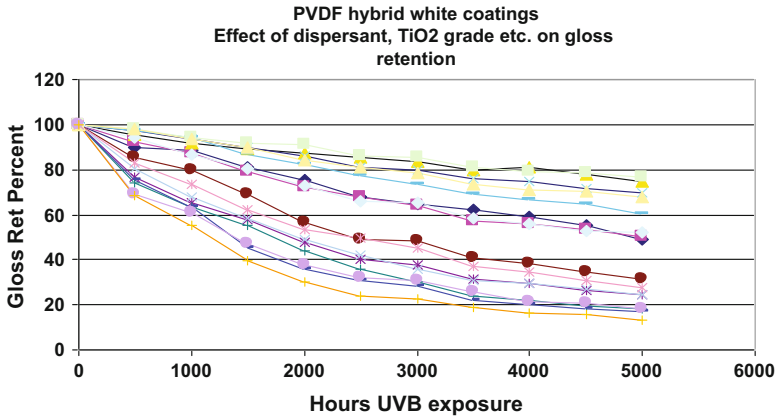
PVDF hybrid white coatings
Effect of dispersant, TiO2 grade etc. on gloss
retention

Fig. 5.5 Percent $60°$ gloss retention for white PVDF hybrid coatings with varying TiO_2 grade, dispersant, etc., as a function of UVB (313 nm) fluorescent cabinet exposure
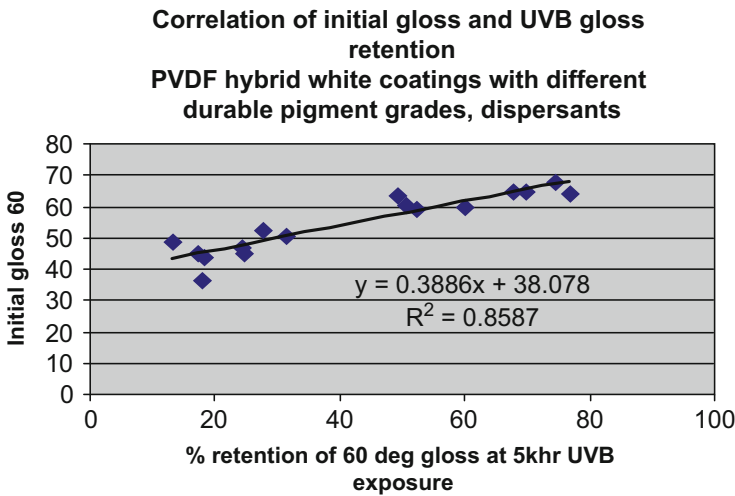
Correlation of initial gloss and UVB gloss
retention
PVDF hybrid white coatings with different
durable pigment grades, dispersants

$$y = 0.3886x + 38.078$$
$$R^2 = 0.8587$$

Fig. 5.6 Correlation of initial gloss, and percent gloss retention after 5,000 h UVB (313 nm) fluorescent cabinet exposure, for the white PVDF hybrid DOE series

acrylic in the binder. The net impact of TiO_2 is particularly complex, as both protective effects (UV blocking) and photocatalytic contributions can be important. As a result, the quality of the pigment dispersion in the dry paint film turns out to have a large effect on some properties such as gloss retention. Figures 5.5 and 5.6 summarize the results we obtained in one study of white PVDF hybrid coatings, which demonstrate this effect dramatically. Sixteen different coatings were prepared in a 2^4 Design-of-Experiment layout, where the four variables were durable TiO_2 grade, dispersant grade, air-dry vs. force-bake, and annealing conditions prior to exposure.

Initial gloss levels for the coatings varied between 36 and 68, reflecting differences in the quality of the TiO_2 dispersion in the dry coating film [18]. Florida exposure testing of this series is still ongoing; however, UVB fluorescent cabinet testing shows dramatic differences in the percent gloss retention of the different coatings (Fig. 5.5). When the percent gloss retention at 5,000 h UVB exposure is compared with the initial gloss for each coating, a strong statistical correlation can be observed (Fig. 5.6).

Some Practical Considerations About Accelerated Weathering Test Options for Architectural Coatings

For premium architectural coatings, the AAMA finishes standards (see Footnote 1) are commonly used as a reference and in many cases as a specification. The weathering requirements of the top-end "superior performance" standards (AAMA 2605 for aluminum, AAMA 615 for vinyl, AAMA 625 for composites) rely heavily on South Florida exposure testing results at 45° south-facing. The superior standards require >50 % gloss retention at 60°, plus a ΔE (Hunter Lab) <5 color retention, for washed panels after 10 years South Florida exposure, as well as chalk and erosion resistance. Recognizing the general lack of correlation between accelerated and Florida weathering results for architectural coatings [19], the use of accelerated weathering methods is not allowed as a substitute for Florida testing in the superior specifications—with the exception of the AAMA 625 composite standard, which does allow 2900MJ UV of ASTM G90 Fresnel testing to be used as an alternative to 10 years of Florida exposure (cutting the exposure time required by about a factor of four).

The requirement of 10 years of Florida testing may seem like an insurmountable obstacle to the introduction of new raw materials for coatings, given that coating companies may be offering dozens to literally hundreds or thousands of different coating formulations, each of them based typically on a dozen or more raw materials. However, beyond some degree of flexibility which is built into the AAMA system,[5] in practice other factors besides standards usually weigh heavily on the choices that end users make about which coating system to use, especially factors such as branding, warranties, and other marketing tools. In such an environment, the manufacturers of coatings are often making decisions about whether or not to begin using new raw materials, based on their assessments of long-term warranty and brand-related risks. For high-end architectural coatings, besides ensuring coating adhesion, the ability of the coating to maintain color and avoid chalking is usually one of the highest concerns.

From this perspective, for coating manufacturers, accelerated weathering data can be an invaluable complement to outdoor weathering data in helping to establish

---

[5] Two examples are allowing the use of color ranges (without a change in pigment or coating resin) in AAMA 2605 and allowing provisional listing on the AAMA Verified Components List while weathering testing is pending.

realistic expectations for decorative property (gloss and color) retention, even when high degrees of correlation cannot always be expected across resin platforms or pigment classes. Three main accelerated weathering options are available to the coating producers and their suppliers. Fresnel solar concentrators (ASTM-G90) use mirrors to provide a direct concentration of solar UV radiation but have the disadvantages of inadequate water saturation of the coating, vs. Florida exposure [20], and of being difficult to use with heat-sensitive substrates such as PVC siding. Xenon arc weathering cabinets (ASTM G155), with appropriate filters, can provide a very close spectral match to sunlight across both the UV and visible regions of the spectrum, but the exposure cycles most commonly used with these cabinets also do not match water saturation levels that are seen in many outdoor environments. The third option, UV fluorescent cabinets (ASTM G154), commonly uses longer water condensation cycles—and so more accurately reproduces Florida exposure in this one respect. However, of the three accelerated methods, UV fluorescent cabinets do the worst job of simulating the solar light spectrum, not only in the visible region but also in the UVB region, particularly if the more aggressive UVB (313 nm) bulbs are used. The UVB (313 nm) bulbs have significant UV intensity down to about 270 nm wavelength, meaning more energetic photons than are experienced in outdoor field exposures.

Despite the limitations of UVB-313 fluorescent cabinet testing, in our work with PVDF-based coatings over the past several decades, we have chosen to use UVB-313 fluorescent testing as our primary accelerated method to complement outdoor testing in Florida and elsewhere. There are two principal practical reasons for this: one is that UV fluorescent cabinet testing is significantly less expensive than the other accelerated methods, so that many more coatings can be tested for screening purpose. The other (related to the choice of UVB bulbs) is that because of the high weatherability of PVDF coatings, less aggressive accelerated methods generally take impractically long times—literally years in many cases—to show signs of degradation.

Through our in-house weathering testing program, extensive UVB-313 and 20+ year Florida data is available for literally hundreds and, in some cases, thousands of panels, based on several different PVDF coating product platforms: baked PVDF homopolymer solvent (nonaqueous) dispersion coatings, baked PVDF homopolymer waterborne coatings, and baked and air-dry PVDF copolymer solution coatings. More than 10 years of Florida and UVB-313 data are also now available for air-dry, and low-temperature bake, PVDF-acrylic hybrid waterborne coatings based on PVDF copolymers. These data yield a considerable understanding of the limits of correlation between the two exposure test environments for PVDF-based coatings, which compensates for the disadvantages of the accelerated method. Some relevant observations, for *PVDF*-based coatings containing durable inorganic pigments, include:

- For similar formulations (same % PVDF in binder, same pigment at same loading level), long-term color shifts are usually comparable across PVDF product platforms, for both Florida south 45° and UVB-313 exposures.
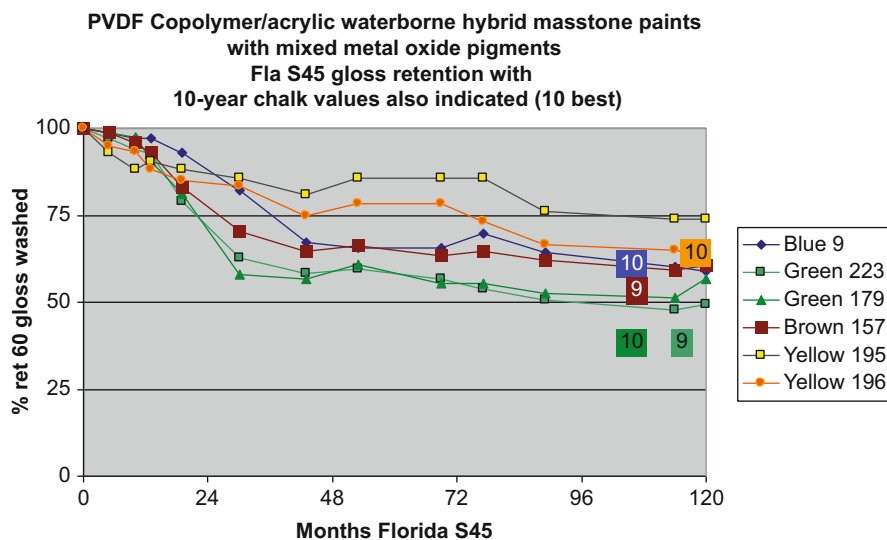
Fig. 5.7 Florida gloss retention for waterborne masstone paints based on copolymer PVDF-acrylic (70:30 by weight) hybrids. Initial pigment volume concentrations in these coatings were about 20 %. The lack of chalking after 10 years exposure and the pattern of initial gloss loss, followed by a gloss "plateau" region, are consistent with what would be predicted by a 2-resin contraction model

- Film erosion and chalking from UVB-313 exposure is minimal in nearly all cases (similar to Florida), as long as the coating's initial film formation and resin blend morphology were adequate (i.e., a PVDF continuous phase was present).
- For similar formulations (same % PVDF in binder, same pigment at same loading level), rates of gloss loss are generally somewhat faster for PVDF copolymer-based coatings, compared to PVDF homopolymer-based coatings. This is seen both in Florida and in UVB-313 testing. Gloss loss patterns for PVDF copolymer coatings often show a "plateau" or leveling-off behavior along the lines of what would be expected for a Fig. 5.4-type film contraction process (cf. Fig. 5.7). The fact that homopolymer PVDF coatings tend to show less initial gloss loss is thought to be related to PVDF crystallinity effects.
- UVB-313 testing does *NOT* work well to predict the relative ranking of TiO_2 grades for Florida gloss retention.

Based on this substantial body of empirical data, there is strong evidence that the physical piece of the 2-resin weathering model—i.e., contraction leading to chalking when/if surface binder degradation leads to the CPVC being exceeded—is generally applicable to both the accelerated and the natural weathering of PVDF-acrylic coatings, across the range of natural and accelerated exposure conditions of interest. At the same time, the gloss and TiO_2 ranking observations suggest, not surprisingly, that the chemical piece of the model, where the details of the photochemical kinetics dominate, is more sensitive to various details of the exposure

conditions, as well as to morphological elements like crystallinity which could affect molecular diffusion rates.

The applicability of the physical piece of the 2-resin model provides some theoretical justification for use of UVB-313 fluorescent testing in the particular limited context of predicting chalking and associated color fade for PVDF-based systems. Under the UVB-313 test conditions, the "unnatural" UVB wavelengths below about 290 nm would be expected to rapidly drive the degradation of the acrylic component, as deep as those wavelengths can penetrate into the coating. We can exploit this behavior in at least two ways. In clear coats, we can directly probe the resin blend morphology [11] in the final coating film, including measurements of mass loss. For pigmented systems, we can use UVB exposure to rapidly drive the coating surface to a state somewhat approximating where it will be in Florida after many years. The rate at which it gets to that final quasi-static condition is less important than the actual state that it evolves to (i.e., is it stable in gloss, and non-chalking, like typical high-PVDF content systems at long time? Or is the coating chalking and eroding?).

A Specific Approach for Predicting the Performance of New Waterborne PVDF Hybrid Coatings

Based on these considerations, we can outline a specific approach to validate new PVDF-based resin products and coatings made from them:

- Verify that the coating film resin blend morphology is similar to the morphology of established products with a long outdoor exposure track record. (We have used a variety of analytical techniques to do this, in addition to UVB weight loss studies with clear coats.)
- Formulate coatings using proven raw materials which are also used with the established products (e.g., specific pigment grades)
- Use UVB fluorescent exposure as a primary method for screening formulations for weatherability (with a special focus on color fade and chalking), since the UVB attack on the acrylic component will mimic what happens outdoors at long times.
- Monitor parallel outdoor exposures to look primarily for unanticipated new failure modes.
- Outdoor exposures should also verify that expectations of similar weathering for similar formulations are correct.

Using this approach, we developed a specific 70:30 PVDF-acrylic hybrid latex product that we predicted would have weathering performance in low-temperature (50 °C) bake paints very close to that of commercial high-temperature baked solvent-borne PVDF systems formulated at a similar 70:30 resin weight ratio. We now have more than 10 years of Florida exposure data for coatings made with the PVDF-acrylic hybrid latex technology. As was predicted, these coatings show
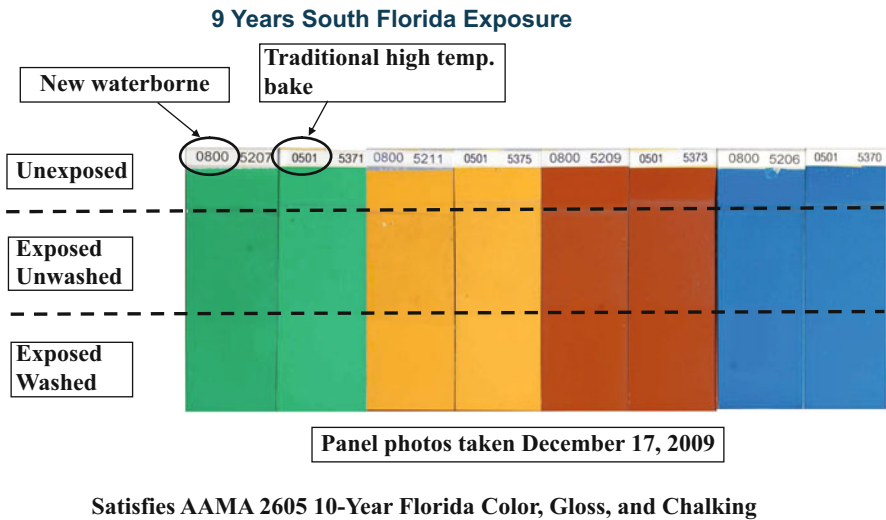
Comparison of new and old PVDF platforms

Fig. 5.8 Comparison of 70 % PVDF hybrid (*left*) and baked PVDF solvent coatings, formulated with durable inorganic pigments, after 9 years Florida exposure

color fade (Fig. 5.8) and chalk resistance (Fig. 5.7) performance which is very similar to the benchmark traditional solvent-borne baked PVDF coatings. Florida gloss retention values for the waterborne coatings are also generally sufficient to pass the 10-year requirements of the AAMA specifications (Fig. 5.7). These earliest waterborne PVDF hybrid systems can now be used as a second benchmark or reference, against which to evaluate newer PVDF hybrid materials.

Concluding Remarks

By using a 2-resin weathering model based on the contraction theory of Colling and Dunderdale, we can make sense of a large body of empirical data for the gloss and color retention performance, and chalk resistance, of PVDF-based coatings exposed both in Florida and in accelerated test cabinets. The physical insights of the model are particularly valuable for understanding the risks of chalking and associated color changes, which are among the most important performance concerns for developers of new coatings. The contraction model also helps explain where UVB fluorescent cabinet testing correlates with outdoor exposure for PVDF-based systems—and where it does not. Based on these insights, we were able to successfully match the performance of solvent PVDF finishes with new waterborne PVDF hybrid latex materials.

To more accurately predict rates of outdoor *gloss* loss in PVDF-based systems, and some other decorative properties like color fade of organic pigments, more attention to the details of the relevant photochemical kinetics would be needed. In our group, we are considering two possible lines of attack in this area. One option is a new proposed test cycle for xenon arc cabinets [21] that incorporates a much longer time of wetness. Another is to run multiple fluorescent cabinets in parallel under different conditions of light, temperature, and humidity to gain mechanistic insights about the most relevant factors affecting weathering kinetics.

References

1. KYNAR 500® (1965) PVDF for coatings has been in continuous commercial production since it was introduced by the Pennsalt Company
2. Humphrey S, Drujon X (1996) Polymeric materials encyclopedia, vol 11. CRC Press, Boca Raton, p 8591
3. Iezzi RA (1997) Fluoropolymer coatings for architectural applications. In: Modern fluoropolymers. Wiley, New York, p 14
4. Hatcher H, Tocher A (2002) The role of high performance inorganic pigments in surface coatings. Paint Coat Indus 18:46
5. Gaboury SR, Wood KA (2002) Tailoring coating properties through control of PVDF copolymer phase behavior. Surf Coat Intl Part B Coat Trans 85(B4):243
6. Philippart J-L, Siampiringue N, Strassel A, Lemaire (1989) Photochemical inertness of poly (vinylidene fluoride) at short and at long wavelengths. J Makromol Chem 190:413
7. Gupta R, Wood K (2007) Novel fluoropolymer-based emulsion technology: striving for "green" coatings", paint and coatings industry, July 2007, pp 70–80; also published. In: Proceedings of the waterborne and higher solids conference, advances in intelligent coating design, New Orleans, LA, Feb 2007
8. Wood K (2009) A quantitative model for the prediction of gloss retention, color change, and chalking for poly(vinylidene fluoride)/acrylic blends. In: Proceedings of 4th European weathering symposium, Budapest, Hungary, Sept 2009
9. Colling JH, Dunderdale J (1981) The durability of paint films containing titanium dioxide-contraction, erosion, and clear layers theories. Prog Org Coat 9:47–84
10. Faucheu J, Wood KA, Sung L-P, Martin JW (2006) Relating gloss loss to topographical features of a PVDF coating. JCT Res 3(1):29–39
11. Wood K (2007) Surface and bulk effects on the weatherabilty of premium exterior architectural paints. In: Proceedings of 9th Nűrnberg congress, Nűrnberg, Germany, 7–9 May 2007
12. Gu X, Michaels CA, Nguyen D, Jean YC, Martin JW, Nguyen T (2006) Surface and interfacial properties of PVDF/acrylic copolymer blends before and after UV exposure. Appl Surf Sci 252(14):5168–5181
13. Allen NS, Regan CJ, Dunk WAE, McIntyre R, Johnson B (1997) Aspects of the thermal, photodegradation and photostabilisation of water-borne fluorinated-acrylic coating systems. Polym Degrad Stab 58:149–157
14. Chiantore O, Trossarelli L, Lazzari M (2000) Photooxidative degradation of acrylic and methacrylic polymers. Polymer 41:1657–1668
15. Chiantore O, Lazzari M (2001) Photo-oxidative stability of paraloid acrylic protective polymers. Polymer 42:17–27
16. Wood KA, De Robien S (2009) A quantitative model for weathering-induced mass loss in thermoplastic paints. In: Martin JW, Ryntz R (eds) Service life prediction of polymeric materials: global perspectives. Springer, New York, pp 457–474. ISBN 978-0-387-84875-4

17. Barker P (2013) Modelling, mechanisms and markets: how knowing the fundamentals helps new product development. In: Proceedings of European coatings congress, Nuremberg, Germany, 18–19 Mar 2013
18. Diebold M (2009) Effect of TiO_2 pigment on gloss retention: a two-component approach. JCT Coat Tech, 6, pp 32–39
19. Cocuzzi DA, Pilcher GR (2013) Ten-year exterior durability test results compared to various accelerated weathering devices: joint study between ASTM international and national coil coaters association. Prog Org Coat 76(6):979–984
20. Misovski T, Nichols ME, Hardcastle HK (2009) The influence of water on the weathering of automotive paint systems. In: Martin JW, Ryntz RA, Chin J, Dickie RA (eds) Service life prediction of polymeric materials: global perspectives. Springer, New York, pp 295–308. ISBN 978-0-387-84875-4
21. ASTM D7869-13; Quill J (2013) New proposed ASTM test method for accelerated weathering of automotive and aerospace coatings. In: Proceedings of European coatings congress, Nuremberg, Germany, 18–19 Mar 2013

Chapter 6
Accelerated Testing: Understanding Experimental Design and Error Propagation

Kevin White and Joel Forman

Introduction

One of the most challenging tasks for the designer of a durable product is developing an understanding of the long-term performance of the product in the context of normal aging and degradation. Typically, the intended lifetime of the product is years to decades, making empirical determinations of performance degradation over that time span impractical. The ability to make reliable estimations of product performance over long periods of time based on measurements made over a relatively short time period becomes an important need for the designer.

A survey of the available literature shows that accelerated testing is utilized in various forms across an increasingly diverse array of industries. These methodologies often involve the application of heat to the test sample during some stressing condition to increase the rate at which the degradation mode of interest occurs. In most instances, these types of tests are effective at highlighting specific weakness(es) in a design or material, but reliable lifetime prediction is necessarily more complicated because the response to heat, stress, or both is nonlinear as a function of time.

One methodology for addressing nonlinear degradation in heat-accelerated testing, especially for systems where sample performance degradation is the result of a chemical process, involves the application of Arrhenius theory. The theory, developed by Svante Arrhenius, a Swedish physicist and Nobel Prize winner, has its origin in chemical kinetics and relates the rate of a chemical reaction to the driving force required for the chemical reaction to initiate and the temperature at which the reaction is occurring. If the degradation of some relevant performance metric can be reliably linked to a chemical reaction, Arrhenius theory may be used to predict the change in that performance metric with respect to time and/or temperature.

K. White (✉) • J. Forman
Exponent, Inc., 9 Strathmore Road, Natick, MA 01760, USA
e-mail: kwhite@exponent.com

The use of Arrhenius theory in the context of accelerated performance degradation prediction requires that two assumptions can be reliably made:

1. The change in a performance metric of interest (ΔMetric) is dominated by a single chemical change in the system.
2. The rate of that single chemical change in the system is accurately described by zeroth- (0th) or first-order reaction rate kinetics.

If these assumptions are made, the change in ΔMetric as a function of temperature can be described by the Arrhenius equation:

$$\Delta \mathrm{Metric} = Ae^{-E_a/RT}$$

The quantity A is called the frequency factor; it is a dimensionless quantity that describes the probability that a change in ΔMetric will occur. The activation energy, E_a, is the energy required to initiate change in ΔMetric, while the value R is the universal gas constant and T is the temperature in degrees Kelvin.

By taking the natural log of Equation 1, the Arrhenius equation can be reduced to its linear form:

$$\ln \Delta \mathrm{Metric} = \left(-\frac{E_a}{R} \right)\left(\frac{1}{T} \right) + \ln A$$

The quantity E_a is an intrinsic property of the degradation reaction causing a change in ΔMetric and is assumed to be independent of temperature. Therefore, by plotting the natural log of ΔMetric vs. $1/T$, one is able to obtain a solution for this value. The activation energy for the degradation reaction, E_a, is equal to the product of the negative slope of the plotted line and the universal gas constant ($-m(R)$). The value of A, for any given temperature, is the y-intercept of the line resulting from the plot of ln CF vs. $1/T$.

While this relatively simple and accurate relationship bears the name of Arrhenius, it was the work of fellow Nobel Prize winner Jacobus van't Hoff, a Dutch physical and organic chemist, that gave physical justification for the theory and the mathematical relationship that we use today. During his work with the theories of Arrhenius, van't Hoff made an important observation: for simple reactions, the reaction rate doubles with an approximate 10 °C increase in temperature [1]. This observation can be mathematically applied to the Arrhenius equation to give a relationship that describes change in the system as a function of temperature and time:

$$\Delta \mathrm{Metric} = A \exp\left(\frac{-E_a}{RT} \right)\left(\frac{t}{t^1} \right)^{\frac{1}{2}}$$

In this expression of the Arrhenius equation, t^1 is the time between the initial and final measurements defining the ΔMetric value used to obtain solutions for E_a and A. The variable t is the time at which the calculated value of ΔMetric is valid.

Therefore, a plot of ΔMetric vs. *t* yields a curve that predicts the time-dependent change profile of the metric of interest at any chosen T.[1]

While this approach to estimating long-term performance is relatively straight-forward, adequate description of the associated measurement error and its propagation through all of the calculations is complex. In practice one could repeat the experiment several times to quantify its variability, but this would be potentially costly and time consuming. This paper describes a statistical treatment to place confidence bounds on Arrhenius-based performance degradation predictions by way of a hypothetical example.

Hypothetical Experimental Example

In this example we separate 120 samples into 4 groups of 30 samples and place the sample groups into ovens set to four different temperatures: 20, 35, 50, and 65 °C. The sample groups will be "aged" in these ovens during the experiment. A baseline measurement of *Metric* is made for each sample before aging. The samples are aged at the four different temperatures until a measureable change in *Metric* has occurred at all of the temperatures (typically a period of weeks to months). At the end of this time period, they are removed and *Metric* is measured a second time to establish values for ΔMetric. The result of these changes is shown in the histograms in Fig. 6.1. Figure 6.2 shows this data plotted with ln(ΔMetric) as the independent axis and (1/T) as the dependent axis. The line on this plot is the least-squares fit to this data. Values for E_a and A are obtained from the slope and *y*-intercept of the line.

With the knowledge of E_a and A for the degradation mode of interest, one can make predictions as to how the samples will age at various temperatures. This is shown in Fig. 6.3, where we note that prediction temperatures need not be the same as experimental temperatures. This procedure is a standard way for making these aging predictions; however, it does not provide confidence bounds on the predictions. This is important, because there can be quite a bit of variability in how samples age, as can be seen in Figs. 6.1 and 6.2. In fact, if this experiment was repeated on a different set of samples from the same manufacturer, it would result in different values for E_a and A which would result in different aging predictions.

To quantify this phenomena, one can repeat the aging experiment multiple times and observe the results. Unfortunately, this would be both time and cost intensive and would give limited insight into the effects of sample aging variability. As an alternative, one can perform a Monte Carlo simulation [2] to generate a large number of

---

[1] It is important to note that the square root function of the time-based Arrhenius equation (the acceleration factor) derives from the twofold increase in rate for every 10   °C observed by van't Hoff. It is only appropriate for reactions with an activation energy of approximately 70 kJ/mol or less. Reactions with a higher activation energy require independent calculation of the acceleration factor.
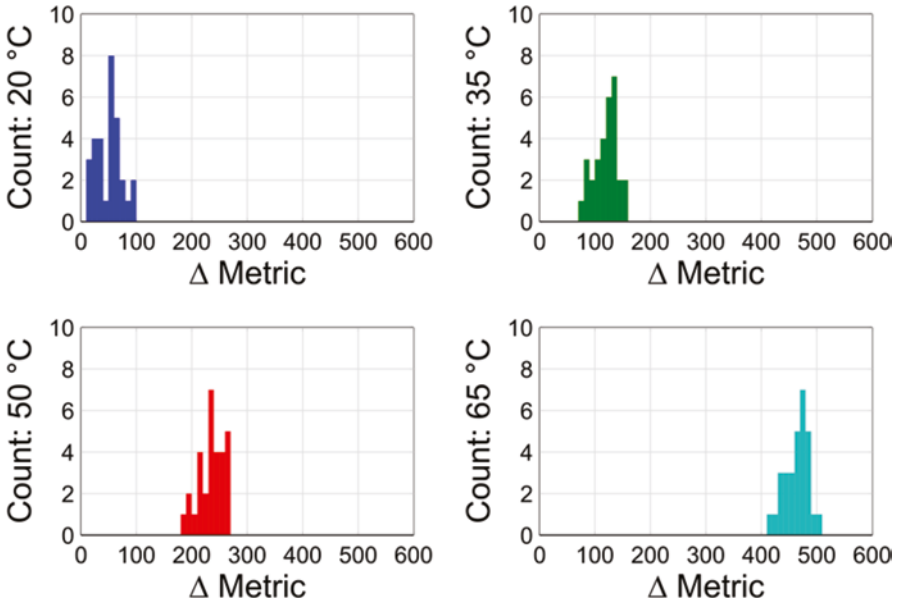
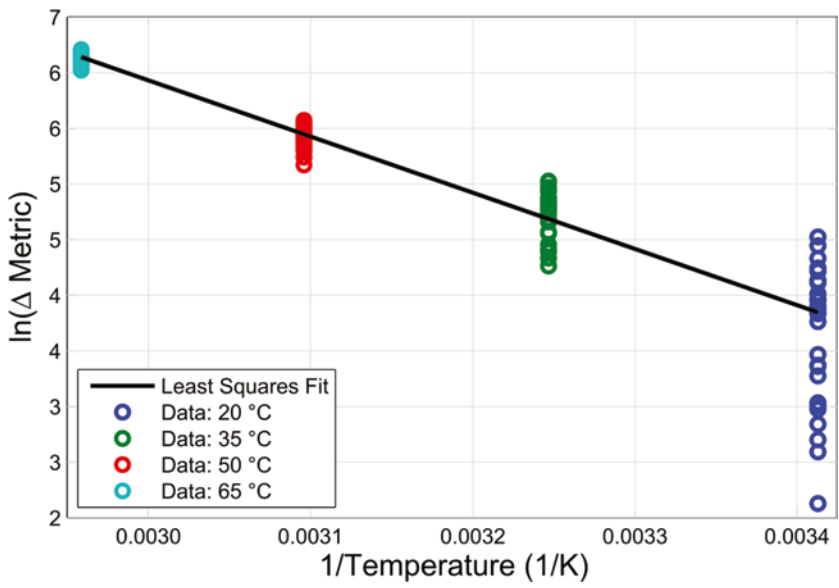Fig. 6.1 Histograms of ΔMetric from the simulated experiment

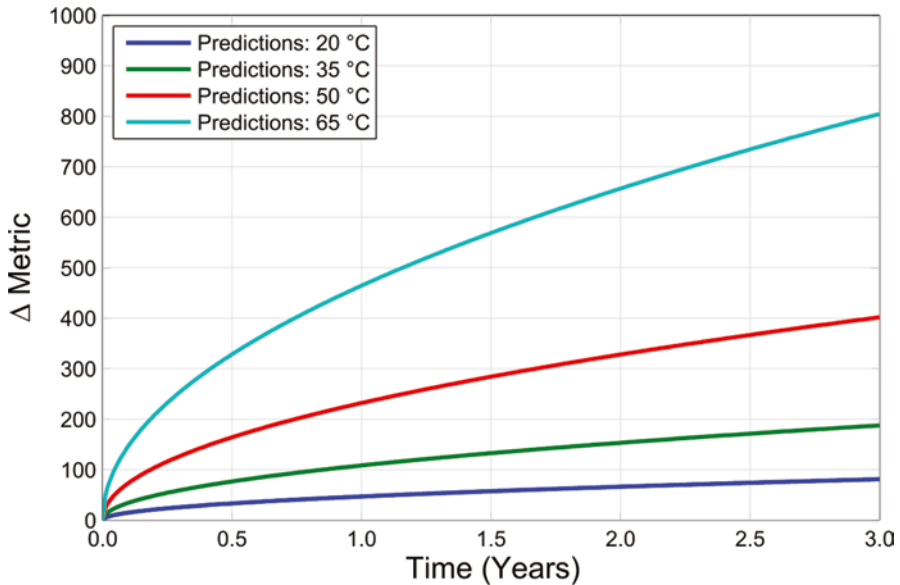Fig. 6.2 Data from the simulated experiment on an Arrhenius plot

Fig. 6.3 Aging predictions at various temperatures from Arrhenius correlation

experiment realizations[2] that are statistically similar to the collected data. To create statistically similar experiments, we use the method of "bootstrapping" [3] as it does not require us to make assumptions about the underlying statistical distribution of the data.

The Monte Carlo/Bootstrapping Statistical Treatment

The statistical treatment proceeds in three major steps: the generation of predictions from statistical realizations, the sorting of these predictions, and the percentile selection of the sorted predictions based on the desired confidence bounds. Each statistical realization is generated in the same manner. Specifically, we use bootstrapping to produce a random sampling of each sample temperature group's data. We choose bootstrapping specifically because it avoids the need to make assumptions on the underlying statistical distributions associated with the experiment.

We start with the measured ΔMetric for each sample at a given temperature and then perform uniform random sampling with replacement of this data to generate another set with the same number of samples. This process is repeated for each

---

[2]A "realization" is a single simulated experiment of the Monte Carlo approach representing a unique, statically similar representation of the actual data set.
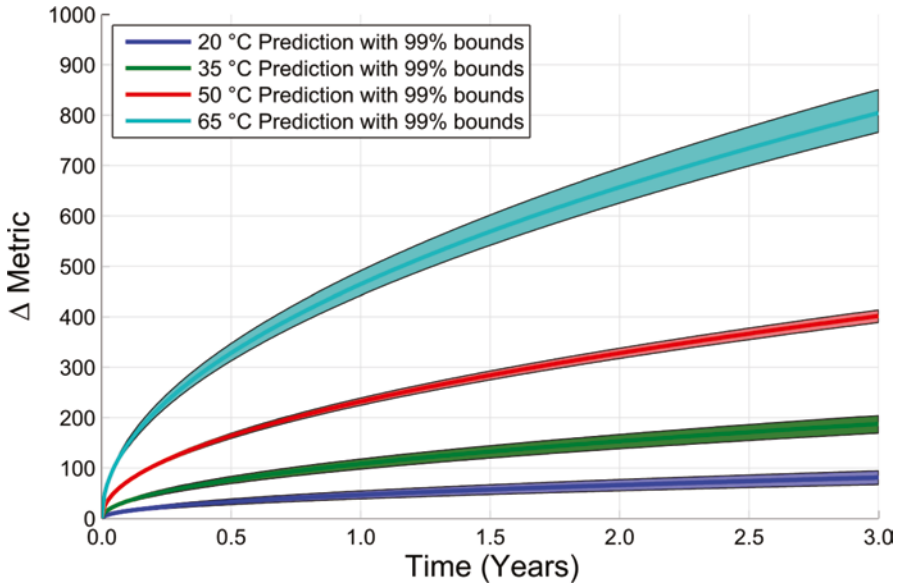
Fig. 6.4 Aging predictions and 99 % confidence bounds of the mean at various temperatures

temperature group of samples. The resulting data set is statistically similar to the data collected from the experiment but incorporates the sample aging variations.

Since this processed data is mathematically similar to the collected experimental data, it can be processed in an identical manner. As an example, we can fit values of E_a and A for the realization and then use these to make predictions at our temperatures of interest. The predictions are saved for later use and the values of E_a and A can optionally be saved for later analysis. This process is repeated to generate an appropriately large number of realizations so that the confidence bounds are consistent. In practice one can select a large number and then repeat the overall process several times to insure that this number is adequately large. If computation time is an issue, then more formal methods for deciding the appropriate number of realizations can be used.

Each realization has a prediction stored for each temperature. For each temperature, we have ΔMetric at each time step. These are sorted by numerical value and then the percentiles are used to establish the confidence bound. If one is using a confidence bound of $X\%$, then one selects the *(100 − X)/2* and *(100 + X)/2* percentiles as the upper and lower bounds. This establishes a region within which $X\%$ of the realization predictions fall within. This can be performed at each temperature of interest to compute a proper error bound.

Figure 6.4 shows the result of this procedure when used with the previous example. The shaded regions show the 99 % confidence bound of the mean, which is very informative for understanding the effects of sample to sample variability on aging. The highlights of this are summarized in Table 6.1 where we show the experiment and

Table 6.1 Aging predictions and 99 % confidence bounds of the mean at various temperatures

Temperature (ºC)		1 year	2 years	3 years
20	Lower bound	38.8	54.8	67.1
20	Experiment	46.8	66.1	81.0
20	Upper bound	54.4	77.0	94.3
35	Lower bound	97.7	138.2	169.3
35	Experiment	108.3	153.1	187.5
35	Upper bound	117.8	166.5	204.0
50	Lower bound	224.6	317.6	388.9
50	Experiment	232.0	328.0	401.8
50	Upper bound	238.8	337.8	413.7
65	Lower bound	442.2	625.4	765.9
65	Experiment	464.4	656.8	804.4
65	Upper bound	491.2	694.6	850.8

its confidence bounds at various times and temperatures. This information is very useful for product designers hoping to understand how sample aging during storage will affect device performance. In particular, it allows them to make decisions regarding what percentage of samples are expected to perform appropriately under different aging conditions.

Conclusion

This statistical treatment has a few key advantages. First, it provides a mathemati - cally appropriate way to place confidence bounds on Arrhenius-based aging experi- ments. Second, it does this without requiring additional experimental data. By using bootstrapping, it also avoids the need for a priori knowledge regarding how sample variability will affect aging. However, if one would like to incorporate this a priori knowledge (perhaps from previous experience with aging-specific samples), then one could fit the experimental data to an appropriate parametric distribution and use this derived distribution to generate realizations rather than bootstrapping. A major motivation of this method is that it avoids taking additional experimental data. However, if one was in a situation where this was not an issue, this method could be used as an additional supplement for understanding variability. We believe that this method is an invaluable tool for understanding the variability associated with Arrhenius aging predictions.

References

1. Connors K (1990) Chemical kinetics: the study of reaction rates in solution. VCH, New York
2. Ross SM (2007) Introduction to probability models, 9th edn. Elsevier, Amsterdam
3. Davison AC, Hinkley AC (1997) Bootstrap methods and their application. Cambridge University Press, Cambridge, MA
4. Celina M, Gillen KT, Assink RA (2005) Polym Degrad Stab 90(3):395–404
5. Waterman KC, Adami RC (2005) Int J Pharm 293(1–2):101–125
6. Liaw BY, Roth EP, Jungst RG, Nagasubramanian G, Case HL, Doughty DH (2003) J Power Sour 119–121:874–886

Chapter 7
The Effect of Non-radiation Factors on the Weathering of Silicone Hardcoats

Jennifer David and Robert Hayes

Abstract In the course of many years of developing thermally cured hardcoat systems at Momentive Performance Materials Inc. (MPM), it has been observed that model predictions of time to failure for coatings subjected to cycled temperature, humidity, and radiation are not always accurate. Particularly in systems where cracking failures occur sooner than adhesion failures, these models seem to break down. This paper reviews the results from ongoing experiments at MPM that attempt to decouple the radiation factor from the typical weathering exposure conditions of a hardcoat system on a polycarbonate substrate. The goal is to identify a "best case" or "entitlement" lifetime for a coating that has not experienced any photodegradation. Additionally, these experiments provide direction as to which factors are most critical in driving cracking failure in hardcoat systems. Discovery of the driving forces for crack propagation in these systems should enable a new model to be derived that would be a better predictor of real-world failure.

Introduction

In the course of many years of developing thermally cured hardcoat systems at Momentive Performance Materials Inc. (MPM), it has been observed that model predictions of time to failure for coatings subjected to cycled temperature, humidity, and radiation are not always accurate. Particularly in systems where cracking failures occur sooner than adhesion failures, these models seem to break down. This paper reviews the results from ongoing experiments at MPM that attempt to decouple the radiation factor from the typical weathering exposure conditions of a hardcoat system on a polycarbonate substrate. The goal is to identify a "best case" or "entitlement" lifetime for a coating that has not experienced any photodegradation.

J. David, Ph.D. (✉) • R. Hayes, Ph.D.
Momentive Performance Materials Inc., Waterford, NY, USA
e-mail: Jennifer.David@momentive.com

Additionally, these experiments provide direction as to which factors are most critical in driving cracking failure in hardcoat systems. Discovery of the driving forces for crack propagation in these systems should enable a new model to be derived that would be a better predictor of real-world failure.

Overview of the Hardcoat System

The subject of this paper is a commercially available MPM hardcoat system, consisting of a topcoat and a primer layer. This type of system is generally applied over a polycarbonate substrate to serve as a protective barrier. The primer material is an acrylate-based thermoplastic, and the topcoat is a silicone resin that is cured to high cross-link density through the application of heat. Both the primer and the topcoat are applied by dip or flow coating from solvent solutions to achieve target dry-film builds. Typical dry-film builds for the topcoat range from 3 to 10 μm while the range for the primer is between 1 and 4 μm. The presence of solvent in both the topcoat and the primer promotes an intermixing of the applied layer with the polymer layer immediately below. Thus, between the primer and the polycarbonate, an interpenetrating layer is formed that contains both the primer and the polycarbonate. This layer is typically 1–2 μm in thickness. Similarly, an interpenetrating layer is formed at the interface of the siloxane resin topcoat and the primer, with a dimension of approximately 0.3 μm.

In the typical coating process, the primer is applied to the substrate and is left at ambient conditions for 20 min to flash off the solvent carrier. After this, the primer polymer is "set" by heating at 125 °C for 20–30 min. Next, the topcoat is applied and subjected to the same wait time at ambient to flash off the solvent. The topcoat then is cured by heating for 45–60 min at 125 °C.

The siloxane topcoat is best described as a highly cross-linked resin formed by the condensation of multifunctional silane monomers. It contains colloidal silica nanoparticles that can range in diameter from 5 to 50 nm. These nanoparticles have functional groups that participate in the condensation reactions during the thermal cure process of the siloxane, such that the colloidal silica becomes covalently bound to the resin. Figure 7.1 shows an interpretation of the chemical structure of the cross-linked resin bound to colloidal silica. A typical micrograph of the cured topcoat is also shown, illustrating the uniform dispersion of the colloidal silica filler that is observed in these systems. In addition to the colloidal silica, the topcoat also contains UV absorbers, which can be present in the cured coating at levels up to 10 % by weight. The primer also contains UV absorbers, which can be present up to 25 % by weight in the dried film.

Hardcoat systems of the type described in this paper can enable plastics to be used in applications for which they would otherwise be unsuitable, due to sensitivity of the plastic to UV degradation, chemical agents, or abrasion. The largest current market for these types of systems is automotive forward lighting applications, as protective coatings for clear polycarbonate headlamps. Other automotive applications include coatings for black polycarbonate side pillars and tinted
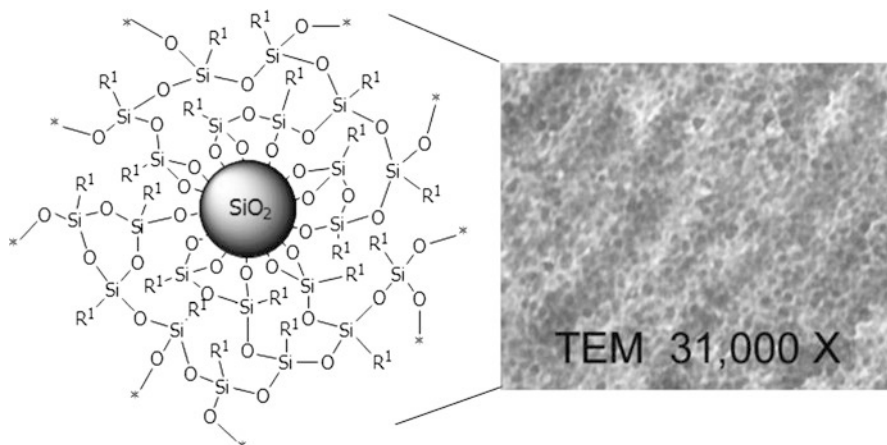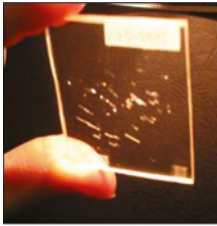
Fig. 7.1 A representation of a cross-linked siloxane matrix filled with colloidal silica (*left*) and a micrograph from an actual coating (*right*). The micrograph shows the good dispersion of the silica nanoparticles that is typically observed throughout the siloxane topcoat (Note: Test results. Actual results may vary)
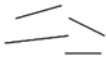
polycarbonate sunroofs. A large untapped market for hardcoats is automotive glazing, where the use of polycarbonate is desired to enable glass replacement in rear, side, and front windows, providing fuel savings and design flexibility. In these applications, coatings that can exceed 10 years of service life in the most extreme environments are desired.

Optical clarity is a key performance criterion; to properly function in the application, the coating must be transparent. Anything that compromises this capability (delamination, scratches, cracks, haze, or discoloration) will limit the usable life of the part that is coated. Adhesion failures of the coating cause rapid degradation of the polycarbonate substrate and can compromise both the mechanical and optical properties of the substrate part. For many years, adhesion was the biggest issue that limited the usable lifetimes of these coatings in the application space. A great deal of work has been done, spanning many years, to understand the factors contributing to the loss of adhesion and resulted in the discovery that UV damage at the interface between the primer and the polycarbonate layers was the key issue causing failure [1]. Optimization of the UV absorbers in the topcoat and primer layers has significantly extended the coating lifetimes before adhesion failure occurs. Currently, the most objectionable failure mode, the failure mode that limits the use of these coatings in automotive glazing, is cracking.

Figure 7.2 shows an example of a cracked thermal hardcoat on a clear polycarbonate substrate. During the development and evaluation of a new hardcoat in the laboratory, the type and severity of cracking of the coating is monitored by a visual inspection process as the coating undergoes weathering. There are three types of cracking that are typically observed: directional, network, and mudcrack, with the representative morphologies shown in Fig. 7.2. Generally a coating is considered to be "failed" when the cracking is just visible to the trained observer. In practice, the

Cracking is measured by a semi-quantitative rating system:

Type:	Directional	Network	Mudcrack

Severity: 1(incipient), 2 (just visible), 3 (extensive)

Fig. 7.2 The semiquantitative protocol used to analyze cracking in hardcoat systems. Samples are examined visually and the type and severity of cracks is assessed. A coating is rated as "failed" when it reaches a cracking severity of "1.5" on this scale. At this point, cracks are just becoming visible to a trained observer

failure point for cracking is estimated as the exposure point that is halfway between the last crack severity rating of "0" and the first crack severity rating of "3," at an effective severity rating of "1.5."

Given the lengthy nature of many of these weathering experiments, a convention is used within MPM in order to draw preliminary conclusions from cracking data as the weathering experiment progresses, without waiting for all of the samples to reach a crack rating of "3." Equations 7.1, 7.2, and 7.3 show the calculations used to report cracking time to failure in each of the three possible scenarios. If at the last read point the sample has reached a crack severity rating (y) of "3," then the cracking time to failure can be calculated directly as the exposure time (x) to reach a "1.5" rating, as shown in Eq. (7.1). (Note that this is a generalized equation and the same result can be obtained by calculating the average exposure time of the first "3" rating and the last "0" rating.) If at the last read point the sample has only reached a crack severity rating of "2" or "1," the exposure time to failure is estimated as shown in Eqs. (7.2) and (7.3), respectively.

$$y = 1.5 = \left(\frac{3}{\left| \left(\begin{array}{c} \text{Exposure} \\ \text{at last "0"} \\ \text{rating point} \end{array} \right) - \left(\begin{array}{c} \text{Exposure} \\ \text{at first "3"} \\ \text{rating point} \end{array} \right) \right|} \right) \bullet \left(x - \left(\begin{array}{c} \text{Exposure} \\ \text{at last "0"} \\ \text{rating point} \end{array} \right) \right) \qquad (7.1)$$

$$y = 1.5 = \left(\frac{2}{\left| \left(\begin{array}{c} \text{Exposure} \\ \text{at last "0"} \\ \text{rating point} \end{array} \right) - \left(\begin{array}{c} \text{Exposure} \\ \text{at last "2"} \\ \text{rating point} \end{array} \right) \right|} \right) \bullet \left(x - \left(\begin{array}{c} \text{Exposure} \\ \text{at last "0"} \\ \text{rating point} \end{array} \right) \right) \qquad (7.2)$$

$$y = 1.5 = \left(\cfrac{1}{\left| \begin{pmatrix} \text{Exposure} \\ \text{at last "0"} \\ \text{rating point} \end{pmatrix} - \begin{pmatrix} \text{Exposure} \\ \text{at last "1"} \\ \text{rating point} \end{pmatrix} \right|} \right) \bullet \left(x - \begin{pmatrix} \text{Exposure} \\ \text{at last "0"} \\ \text{rating point} \end{pmatrix} \right) \quad (7.3)$$

Adhesion failures described in this paper are determined visually by a standard crosshatch tape test, as described in ASTM D-3359. In this method, coatings are evaluated on a semiquantitative scale ranging from 5B to 0B. The 5B rating is considered to be 0 % adhesion loss. The time to fail for adhesion is estimated as the exposure point that is halfway between the final pass adhesion rating and the first fail adhesion rating. A rating of 4B corresponds to the beginning of coating loss at the intersections of the crosshatch cut marks to a level of 5 % maximum coating loss. Any rating worse than 4B is considered a failure.

For both failure modes of cracking and adhesion, when weathering studies are conducted in the laboratory, exposure is reported in kilojoules per square meter at a specified wavelength. When weathering studies are conducted in the field, exposure is reported in years.

Weathering Protocol and Prediction Methodology

To determine the expected lifetime of hardcoats in the real world, several strategies are employed. These involve accelerated laboratory weathering to mimic natural conditions as well as actual outdoor field testing. The accelerated weathering studies are done in commercially available chambers that expose the test coupons to cycles of radiation, temperature, and water spray. The exposure protocol used in the studies discussed in this paper is a modified version of ASTM G 155 Cycle 1, referred to here as "GMOD." The modification involves an increase in the radiation intensity from 0.35 to 0.75 W/m² nm (at 340 nm). Borosilicate glass is used for both the inner and outer filters of the source lamp to best mimic the spectral distribution of Florida sunlight [2]. Radiation from a xenon arc lamp is applied continuously for both segments of each cycle. The first segment is 102 min long in which the temperature of the chamber is controlled such that the black panel temperature sensor within the chamber is held at 65 °C. In the second 18 min segment, the chamber temperature is uncontrolled and a continuous water spray of average ambient temperature is applied to the front, coated side of the test panels. The water used for the spray is prefiltered to achieve a conductivity below 5 μS/cm. In a typical experiment, the test panels are removed from the chamber after every 1,000 kJ/m² of exposure and checked for adhesion, cracking, haze, and color changes. Results may also be correlated with real-time exposure in Florida or Arizona.

MPM's lifetime predictions for adhesion failure in hardcoats rely on equivalencies that were derived at MPM from real-world exposure testing coordinated with accelerated weathering experiments. For coatings on black polycarbonate substrates, 2,300 kJ/m^2 of radiation in the weathering chamber at GMOD conditions was found to correlate to 1 year of real-world exposure in Florida at an exposure angle of 45° to the horizontal. For coatings on clear polycarbonate substrates, a radiation exposure of 2,800 kJ/m^2 was found to best correlate to the same 1 year Florida exposure conditions. The lower dosage required for adhesion failure on black polycarbonate substrates is anticipated due to the fact that radiative exposure will result in temperature differences, depending on the color of the exposed specimen. Exposed to the same radiation dose, a coating on a black polycarbonate substrate will experience a higher temperature than the same coating on a clear polycarbonate substrate. This is because the black substrate absorbs more energy than the clear substrate, reaching a higher temperature. The higher temperature drives a higher rate of degradation of the UV absorbers in the coating, leading to a shorter adhesion time to failure.

It is important to note that at MPM predictions of cracking times to failure are calculated differently from predictions of adhesion times to failure. For cracking, one cycle in the GMOD experiment is equated to 1 day in the real world. The rationale is that the change in temperature experienced by the black panel in a GMOD cycle, of about 20 °C (36 °F), is more consistent with a diurnal cycle than with small fluctuations in temperature that might occur many times throughout the course of a day.

Other researchers have developed and published models that predict real-world adhesion times to failure for coatings [1, 3]. For hardcoat systems, these models are based on failures by loss of adhesion at the interface between the primer and the polycarbonate layers. As the UV absorbers present in the silicone resin topcoat and the primer layers degrade, the UV transmission to the polycarbonate increases. At a certain point, degradation of the polycarbonate begins and delamination occurs at the interface with the primer. The Pickett model used by MPM, and described in [1], predicts the adhesion time to failure by considering the degradation rate of the UV absorber, the dose required to cause failure in the system when no UV absorber is present, and the initial transmission of the coating. Absorbance of radiation by the UV absorbers in the coating is a function of the UV absorber concentration (C), the molar absorptivity of the UV absorber (ε), as well as the coating thickness or path length (l). As shown in Fig. 7.3, as these parameters increase, the model predicts that adhesion time to failure should also increase, since less radiation reaches the sensitive polycarbonate-primer interface. Figure 7.3 additionally shows the model predictions for three different degradation rate constants (K) of the UV absorber. At any absorbance value (determined by C, ε, and l), a smaller K value shifts the failure curve to longer times.
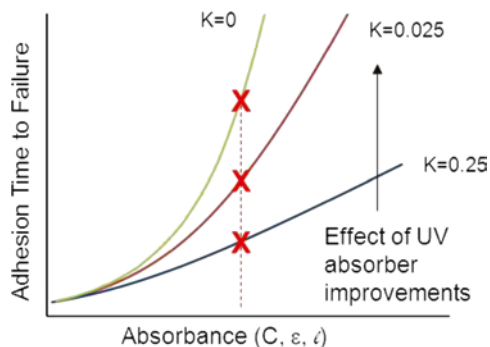
Fig. 7.3 Predictions for coating adhesion failure times as derived from the Pickett model of [1]. Absorbance of the UV absorber molecules in a coating depends on their concentration (*C*), molar absorptivity (*ε*), and path length (*l*). As any of these increase, the adhesion time to failure of the coating increases. A lower UV absorber degradation rate constant (*K*) also results in a longer adhesion time to failure

Time to Failure Predictions for a Typical Coating Subjected to GMOD Conditions

Experimental

A series of panel substrates coated with a commercial MPM coating system were prepared using standard flow coating procedures and cured according to the standard protocols outlined above. To better study the effect of primer and topcoat thickness on cracking and adhesion failures, panels were prepared with film thicknesses that spanned a broader range than typical (4.2–11.4 µm for the topcoat and 0.7–6.2 µm for the primer). Coatings were prepared on both black and clear injection-molded polycarbonate substrates. Lexan® 143R-701 pellets were used to make the black substrate panels, and Lexan® LS2-111 pellets were used to make the clear substrate panels. The pellets were purchased from SABIC Innovative Plastics and molded into panels of 4″ × 6″ at an injection molding company.

To reduce the molded-in stresses that are known to be present for injection-molded panels, an annealing process was used on the panels prior to application of the primer and topcoat. To anneal, the panels were clipped at one end, hung in a forced air oven, and heated at 130 °C for more than four hours. They were then cooled slowly to room temperature over the course of more than four hours. Samples of size 1.75″×2.5″ were cut from the central region of the coated panels using a band saw. By taking samples from the center of the plaques, the most uniform thicknesses across the samples could be obtained. The samples were tested for thicknesses of primer and topcoat. They were then placed into the weathering chamber and the GMOD protocol was initiated.

For this study, an Atlas Ci4000 Xenon Weather-Ometer® was used. The samples were removed for testing after each 1,000 kJ/m² of dosage and were then returned to the chamber for further exposure. The MPM correlations of 2,300 kJ/m² (black) and 2,800 kJ/m² (clear) were used to convert the measured adhesion time to failure in kilojoules per square meter to predicted real-world time to failure in years, as described in the previous section. Cracking time to failure predictions were made using the number of thermal cycles the sample experienced before failure, also as described in the previous section.

Results and Analysis

Figure 7.4 shows the Pickett adhesion failure model from the literature (lines) as overlaid on the two adhesion failure datasets, clear and black, from this GMOD experiment. The literature model does predict the correct adhesion failure trends for these coatings on black and clear substrates when subjected to GMOD conditions in the accelerated weathering chamber. The clear dataset shows the best fit with the model, whereas the black dataset shows substantially more deviation at higher primer thicknesses. The deviation from the model fit most likely suggests the beginning of a mixed failure mode, where the adhesion failure becomes influenced by an alternate mode of failure occurring in the coating system [4].
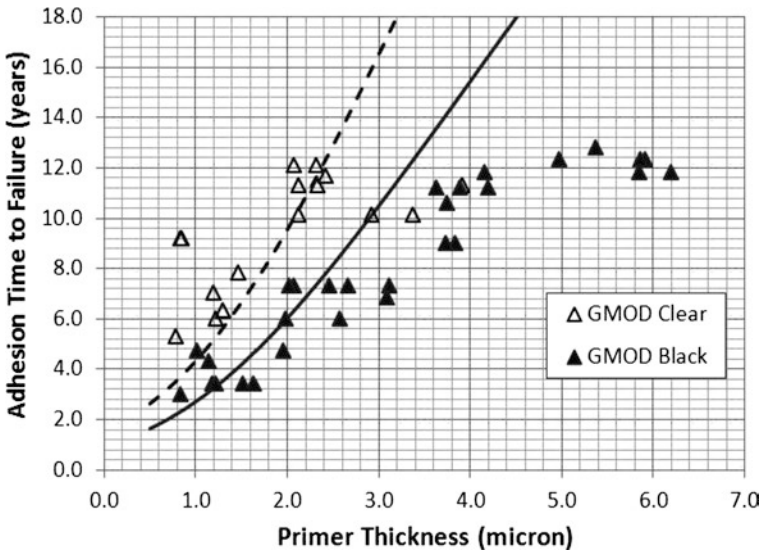
Fig. 7.4 Comparison of GMOD adhesion failure data (*symbols*) with the Pickett model predictions (*lines*) of [1] for this system. The clear GMOD sample failure data shows a better fit with the model predictions compared with that of the black GMOD samples (Note: Test results. Actual results may vary)
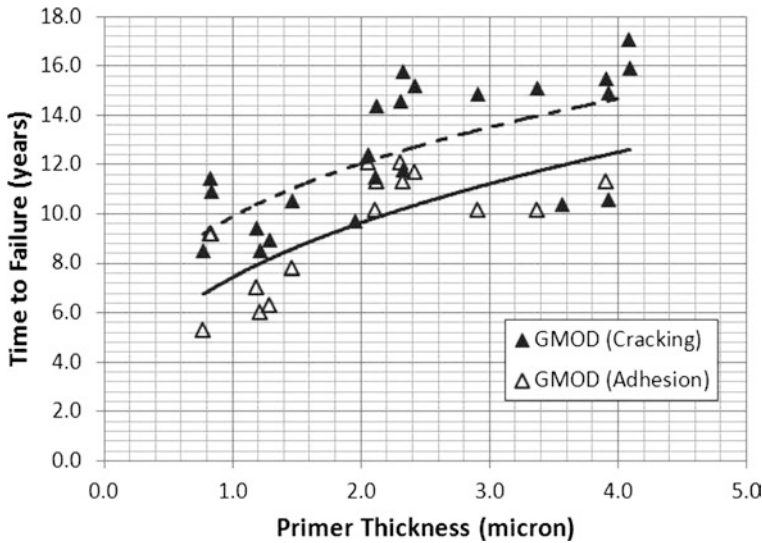
Fig. 7.5 Comparison of GMOD failure modes for coatings on clear substrates. Cracking (*solid symbols*) is a later failure mode compared with adhesion (*open symbols*). In this graph, the *lines* are drawn to guide the eye and do not represent fit equations to the data (Note: Test results. Actual results may vary)

For the same clear and black GMOD sample sets shown in Fig. 7.4, cracking failures were also measured as a function of weathering chamber exposure. An overlay of the two failure modes of adhesion and cracking for these samples is shown in Fig. 7.5 for the clear set and Fig. 7.6 for the black set. As can be seen in the graph of Fig. 7.5, the earlier first mode of failure for clear samples is generally adhesion and cracking appears to be a later failure mode. This is true particularly at lower primer thicknesses as there appears to be more scatter in the data at higher primer thicknesses. In contrast, as shown in Fig. 7.6, failures by cracking occur sooner for the black samples than failures by adhesion for all but the very lowest primer thickness samples. Additionally, Fig. 7.6 shows that the cracking failure data for the black samples has a negative trend with primer thickness, which is opposite to the trend observed in the adhesion failure data of these same samples. It is reasonable to expect then that the adhesion time to failure data may show greater deviation from the model prediction lines in the black dataset, as shown in Fig. 7.4. For black samples the alternate failure mode of cracking is likely to have a larger influence on the system failure as primer thickness increases.

As shown in Fig. 7.4 and illustrated further by the analysis of this experiment, the time to failure model used here, built from adhesion data, is not always able to predict the actual adhesion failure times, particularly in cases where the failure occurs by an alternate mode such as cracking. In those cases, failure often occurs sooner than would have been predicted. Additionally, as improvements have been made to the UV absorber technology over the years, pushing the adhesion time to failure
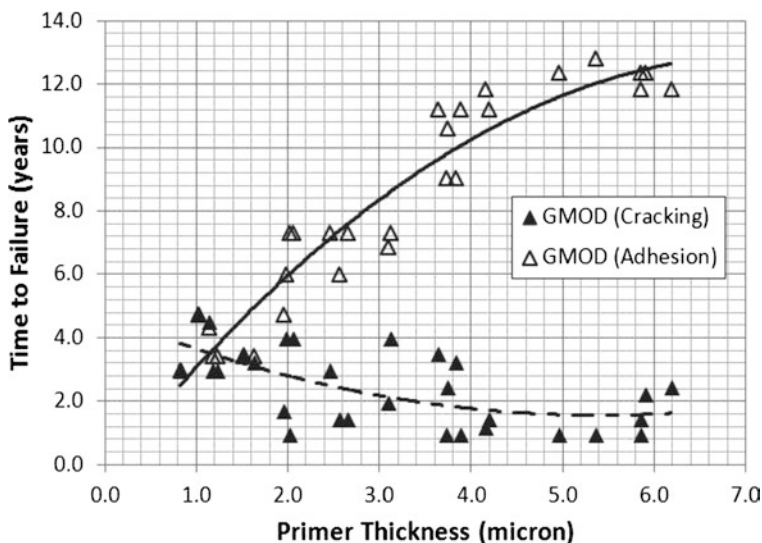
Fig. 7.6 Comparison of GMOD failure modes for coatings on black substrates. In contrast to the clear sample GMOD failure data of Fig. 7.5, here cracking (*solid symbols*) is a much earlier failure mode than adhesion (*open symbols*). Additionally, the two failure modes show opposite trends with primer thickness. In this graph, the *lines* are drawn to guide the eye and do not represent fit equations to the data (Note: Test results. Actual results may vary)

longer and longer, the lack of a model to predict failure by cracking has become more problematic. There is a clear need for a new model function that can be used to predict time to failure by cracking.

Entitlement Study of Non-radiative Factors

Experimental

A study was devised to isolate the factors that are most important in causing cracking failure in hardcoat systems. This experiment was designed to mimic GMOD conditions of temperature and humidity in the absence of radiation. By eliminating radiation, a key source of chemical degradation and one of the primary factors in adhesion failure was removed from the system. This study was therefore conceived as a model experiment to determine the "best case" or "entitlement" performance of a coated system with respect to adhesion and cracking, for a theoretical case in which UV absorber performance has been optimized to the point where no photo-degradation can occur.

Retained samples from the GMOD study described in the previous section were used in this entitlement study to ensure that a direct comparison of the two

experiments could be made. These retained samples had been coated and cured as a part of the same population of samples tested by GMOD, as described above, but had been stored at ambient laboratory conditions and had never been exposed in the weatherometer. Both clear and black sample retains were used in the entitlement study.

The chamber used for the entitlement experiment was an ESPEC SCP-220 environmental chamber. The best match of the temperature and humidity profile of a GMOD experiment was achieved with a two-step cycle in the ESPEC. The first step consisted of a 100 min hold at 65 °C and 14 % relative humidity, and the second step consisted of a 20 min hold at 45 °C and 95 % relative humidity. It is important to note that no water spray was applied in the entitlement experiment. Other researchers have shown that the presence of liquid water can be a critical factor in coating failure [5]. Though condensate was observed within the ESPEC chamber during the cycles, the presence of liquid water on the surface of the parts was not a controlled factor the way that it was in the GMOD experiment. The remainder of this section describes the approach used to select the temperature and relative humidity settings for the two cycles used in the entitlement study. The intent of the entitlement experiment was to mimic as closely as possible the conditions that a black part would experience in the GMOD experiment.

The temperature in a weatherometer is controlled using the temperature reading from a black painted metallic panel mounted within the chamber. This temperature reading is recorded by the weatherometer and is known as the black panel temperature. The black panel temperature profile measured in a typical GMOD cycle is significantly different than the ambient chamber temperature profile, as can be measured by temperature recorder placed within the chamber. In this work, a standalone datalogger from Omega® (OM-EL-USB-2-LCD) was used for this purpose. These temperature differences are illustrated in Fig. 7.7. The temperature profile of the entitlement study was designed to mimic the black panel temperature profile as
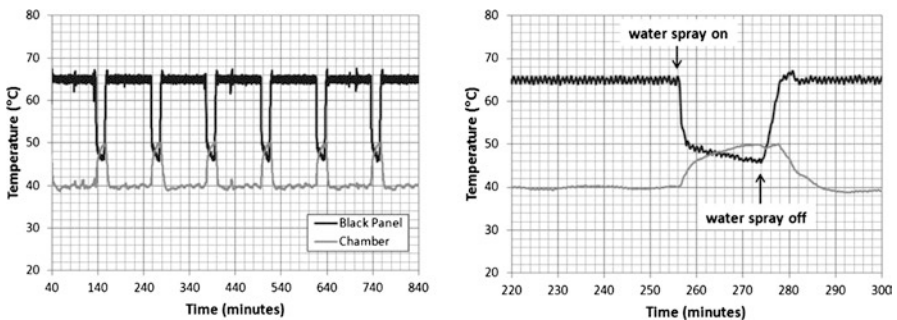
Fig. 7.7 Temperature conditions measured in a GMOD experiment in the Atlas weatherometer. The temperature of the black painted metallic panel inside the weatherometer (the black panel temperature) is considerably different than the ambient chamber temperature profile as measured by a stand-alone datalogger mounted within the weatherometer. The graph on the *right* shows the details for a single cycle (Note: Test results. Actual results may vary)
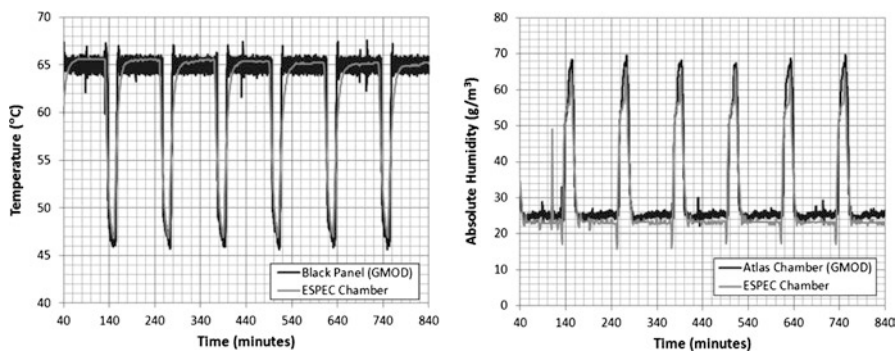
Fig. 7.8 Equivalence of the temperature and humidity profiles for the GMOD and entitlement experiments. The temperature comparison (*left*) shows that the ambient chamber temperature in the ESPEC throughout the cycles of the entitlement experiment matches closely with that of the black panel temperature as measured in the GMOD experiment. The ambient water vapor density (absolute humidity) within the two chambers (*right*) also matches closely for the two studies (Note: Test results. Actual results may vary)

recorded by the weatherometer during a typical GMOD cycle. The use of the metal black panel temperature for the entitlement study is likely an underestimation of the true heat history of a nonmetallic black sample exposed to GMOD conditions, since a nonmetallic black substrate has poorer heat transfer. However, this approach seemed to be a good first approximation in the absence of direct temperature measurements of the actual black samples tested in GMOD conditions.

Figure 7.8 shows the equivalence of temperature cycles used in the entitlement study in the ESPEC chamber as overlaid with those of cycles in a typical GMOD test. The GMOD temperature profile shown in Fig. 7.8 is the black panel temperature. The temperature reading in the ESPEC chamber was recorded with a temperature and humidity recorder placed within the chamber. As can be seen, there is good overlap of the temperature profile for the two experiments; all samples (black and clear) in the ESPEC chamber experience the same temperature profile as the metallic black panel in the GMOD experiment.

Figure 7.8 also shows a comparison of the humidity measured in a GMOD experiment with the entitlement experiment run in the ESPEC. Specifically, the absolute humidity profiles are compared in this graph. Absolute humidity is the mass of water vapor present in a unit volume of air at a given temperature. Absolute humidity was selected as the appropriate parameter to match when designing the entitlement study. As was illustrated in Fig. 7.7, in a typical GMOD cycle, the black panel temperature and the ambient chamber temperature are quite different. Therefore, the relative humidity at the surface of the black panel in a GMOD experiment is different than the ambient relative humidity recorded in the GMOD chamber by a stand-alone datalogger. By controlling the absolute humidity in the ESPEC chamber to mimic that of the GMOD chamber, the water density of the two chambers should be equivalent. By simultaneously controlling the temperature of the

ESPEC chamber to be the same as the black panel temperature in the GMOD chamber, the relative humidity at the surface of all of the parts (black and clear) in the ESPEC chamber should mimic the relative humidity at the surface of the black panel in a GMOD experiment. There is good agreement between the temperature and absolute humidity curves in Fig. 7.8. Therefore, all samples (black and clear) in the ESPEC chamber experience the same relative humidity at their surfaces as the metallic black panel in the GMOD experiment.

In a typical GMOD experiment, as in real-world exposure, when coatings on black and clear substrates are exposed to the same conditions, they experience different stresses; when exposed to the same radiation dose at the same ambient temperature, a black substrate will reach a higher temperature than a clear substrate. The entitlement experiment eliminated this temperature difference between the clear and black samples since the ESPEC heated the samples by convection. In the entitlement experiment, all of the clear and black samples should have experienced the same temperature and humidity stresses. Accordingly, it was expected that there would be no difference in adhesion or cracking times to failure in the entitlement experiment between the black and the clear samples.

Results and Analysis

The entitlement experiment was initiated in May 2011 and is ongoing as of the writing of this paper. To determine the effective real-world exposure in years for the entitlement study, the decision was made to equate one temperature and humidity cycle in the entitlement study with 1 day of real-world exposure, the same approach as is used at MPM for cracking time to failure analysis in a GMOD experiment. As discussed for the GMOD experiment, the temperature and relative humidity ranges used in this entitlement study for a given cycle (20 °C and 81 %, respectively) are large variations and are more consistent with a diurnal cycle than small fluctuations up and down throughout a day. Using this assumed relationship (one cycle in the entitlement study as equivalent to 1 day of real-world exposure), the entitlement data presented are the results at a point corresponding to approximately 10 years of real-world exposure. Although both adhesion and cracking failures are being monitored for the samples in the entitlement study, the only failures observed until this point have been due to cracking.

The same visual inspection method of analysis of cracking used in the GMOD experiment has been used for this entitlement experiment. The entitlement experiment has not yet completed and only a portion of the samples had reached a cracking severity rating of "3" at the time of this writing. For these samples the true cracking time to failure could be calculated according to Eq. (7.1). For the rest of the samples, cracking times to failure were estimated using the crack severity rating at the last read point recorded (either "2" or "1") and Eqs. (7.2) and (7.3). Table 7.1 provides the details of the percentages of black and clear samples that had reached the various severity ratings at the time of the analysis reported here. As shown in the

Table 7.1 Summary of cracking status for samples in the entitlement experiment at the time of the analysis reported here

Crack severity rating at last read point	Samples at each severity rating (%)		Confidence weighting factor	Weighted maturity (%)	
	Black	Clear		Black	Clear
3	72	9	1	72	9
2	24	73	0.5	12	36
1	4	18	0.25	1	5
0	0	0	0	0	0
Total	100	100		85	50

table, the majority of the black samples (72 %) had reached a crack severity rating of "3," whereas the majority of the clear samples (73 %) had only achieved a crack severity rating of "2."

At MPM, a maturity calculation is typically provided alongside ongoing weathering results. This calculation weights the percentages of samples at each severity rating. A weighting factor of 1 is used for the percentage of samples that have achieved a crack severity rating of "3." Weighting factors of 0.5 and 0.25 are used for the percentages of samples that have achieved crack severity ratings of "2" and "1," respectively. The maturity calculation is used to provide a relative confidence ranking of the overall dataset results. As shown in Table 7.1, the maturity calculation yields a value of 85 % for the black samples of the entitlement experiment and 50 % for the clear samples.

The data from the entitlement experiment is plotted in Fig. 7.9. The truncation of both datasets at about 10 years is clearly visible, particularly for the clear dataset, for which the majority of the samples had still not reached a crack severity rating of "3." There are three points in this graph, two in the clear dataset and one in the black dataset, for which the cracking time to failure is shown as exceeding 10 years. These points are the cracking time to failure estimations for the three samples that had only reached a crack severity of "1" as of the last read date. Since cracking time to failure is determined at a severity rating of "1.5," these points resulted in predicted exposure times beyond that of the last read.

Although only limited conclusions can be drawn from the clear dataset, due to the relatively low maturity, analysis of the earliest time to failure data is instructive. Preliminary results in Table 7.1 and Fig. 7.9 do show that the clear samples are succumbing to cracking failures at longer times than the black samples. For example, the earliest time to failure for the clear samples occurs at about 8.5 years. At this point more than half of the black samples have already failed. Since the radiative contribution to sample heating was eliminated in the entitlement experiment, this result was quite surprising. As discussed above, radiation is known to raise temperature to a higher value in a black sample compared with a clear sample, but the use
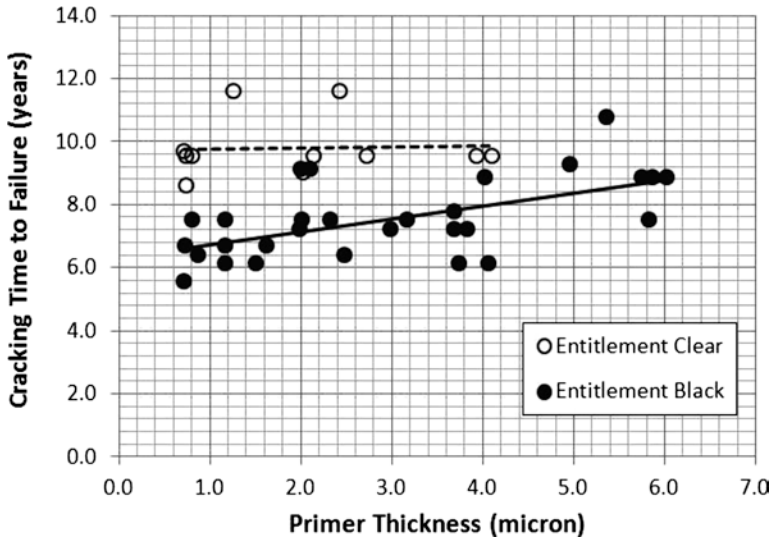
Fig. 7.9 Black and clear datasets from the entitlement experiment. The earliest failure for the clear dataset (at about 8.5 years) occurs after the majority of the black samples have already failed. In this graph, the *lines* are drawn to guide the eye and do not represent fit equations to the data (Note: Test results. Actual results may vary)

of a temperature and humidity chamber and the exclusion of radiative heating should have eliminated this factor. The environments of both the black and the clear samples in the entitlement experiment should be equivalent.

One possibility explored was whether the black and the clear substrates have different coefficient of thermal expansion (α_T) values. Equation (7.4) is well known in the coating literature [6]. It describes the thermal stress (σ_T) seen by a coating in terms of the Young's modulus of the coating (E) and the difference in thermal expansion coefficient ($\Delta\alpha_T$) between the coating and the substrate for a temperature cycle ΔT. In the case here, where the Poisson ratio (ν) of the coating is expected to be small, the equation can be used in its simplified format, as shown. If the black substrate's thermal expansion value was higher than that of the clear, it could be part of the explanation for the higher cracking rates observed in the coatings on the black substrates compared to the coatings on the clear substrates over an equivalent temperature range. According to Eq. (7.4), in this scenario, the stress experienced by the coating on the black sample over same temperature range for each cycle of the experiment would be larger than that experienced by the coating on the clear sample.

$$\sigma_T = \left(E / 1 - v^2 \right) \cdot \Delta\alpha_T \cdot \Delta T$$

$$\left(\text{at small } v \right) \quad \sigma_T \cong E \cdot \Delta\alpha_T \cdot \Delta T \tag{7.4}$$

The expansion coefficients for uncoated annealed panels of both black and clear polycarbonate were measured using a TA Instruments Q400 thermomechanical analyzer fitted with an expansion probe and tested in dynamic mode over a temperature range of 30–200 °C at ramp rate of 5 °C/min. The expansion coefficients were taken from the linear section of the curve, before the softening of the polycarbonate began, generally over the range of 40–140 °C. The initial measurement of the panels suggested that there could be up to a 25 % difference between the substrates: the black substrate α_T measurement was 8.6×10^{-5}/°C by this method, compared to the clear substrate α_T measurement of 6.9×10^{-5}/°C. Repeat testing was done with a new black and clear panel from the same uncoated and annealed set and tested at three locations on each panel to obtain data on the variability expected in this test on these panels. This follow-up testing found that the black annealed panels had an expansion coefficient of $7.9 \pm 0.9 \times 10^{-5}$/°C whereas the clear annealed panels had an expansion coefficient of $7.7 \pm 1.6 \times 10^{-5}$/°C. The original measurements are within the ranges of the repeat measurements, but this new data suggests there is no measurable difference in the expansion coefficients of the two samples when the sample variability is taken into account. As such, the difference in cracking lifetimes cannot be explained by a difference in expansion coefficient of the two substrates.

A second observation of note in the data of Fig. 7.9 is that the trend of cracking time to failure for the black samples increases as a function of primer thickness. Since the experiment was set up as a designed experiment with factors of primer thickness, topcoat thickness, and color, it was possible to investigate the trends in the black sample data using statistical analysis software (Design-Expert® V8 from Stat-Ease, Inc.). The analysis of variance (ANOVA) showed a significant positive trend with both primer and topcoat thickness for the black sample data, with *p-values* of 0.0003 and 0.0017, respectively. The cracking time to failure in terms of actual factors as determined by this analysis is provided in Eq. (7.5). For this model the adjusted *R*-squared values and predicted *R*-squared values are in good agreement (0.5179 versus 0.4599) and the signal-to-noise ratio of 10.9 is well above the minimum recommended value of four. The single-factor plots are shown in Fig. 7.10. This analysis of
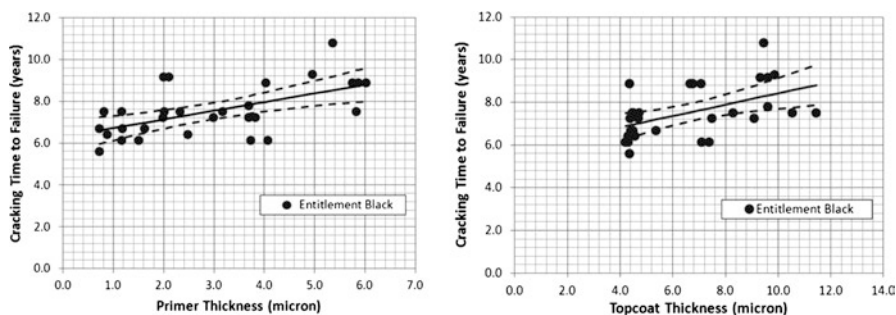
Fig. 7.10 Primer and topcoat thickness trends for the entitlement black dataset. *Solid lines* are linear fit equations and *dotted lines* are the 95 % confidence intervals. Both primer and topcoat thickness are significant factors in the cracking time to failure equation for the entitlement black dataset (Note: Test results. Actual results may vary)

the black entitlement data therefore predicts that higher primer thickness and higher topcoat thickness both lead to longer lifetimes before cracking begins.

$$\text{Cracking Time to Failure}(\text{years}) = 4.91388 + 0.36288 * A + 0.22703 * B \quad (7.5)$$

$$A = \text{primer thickness}(\text{micron})$$
$$B = \text{topcoat thickness}(\text{micron})$$

The stress (σ) a coating system experiences is driven by expansion and contraction of the coating during temperature and humidity cycles. Some initial "residual" stress is usually present in a coating, generated during the cure process through loss of solvent and mass loss on cure. As the coating weathers, additional stress can build due to further solvent and mass loss as well as additional cross-linking or densification. An equation that describes the cracking behavior of thin films in tension has been published by Beuth and is applicable to systems in which the elastic limit of the coating has not been exceeded [7]. Other researchers have used this equation to study cracking in automotive paint systems and hardcoats [8, 9]. Equation (7.6) is adapted from the Beuth paper. It describes the energy to propagate a crack in a coating system as the critical fracture energy of that system (G_c). This value is related to the material properties of the coating, including the Young's modulus (E), the Poisson ratio (ν), and the physical thickness of the coating (h). The $g(\alpha, \beta)$ term incorporates the Young's modulus and Poisson's ratio for the substrate with that of the coating. The critical fracture energy is a material property of a given coating and is essentially a constant. The equation shows that the critical fracture energy of a coating is exceeded at a lower critical strain (ε_c) for a system in which the coating is thicker. Therefore, the equation predicts the opposite behavior as seen in the entitlement experiment results on black substrates. From a fracture mechanics perspective, higher coating thickness should result in a lower critical strain to propagate a crack and, consequently, a shorter cracking time to failure.

$$G_{ss} = \frac{\pi \cdot \sigma^2 \cdot h \cdot g(\alpha, \beta)}{2 \cdot \bar{E}} \xrightarrow{\text{assumptions/constraints}} G_c = \frac{\pi \cdot E \cdot \varepsilon_c^2 \cdot h \cdot g(\alpha, \beta)}{2(1 - \nu^2)}$$

G_{ss} steady state energy release rate

critical fracture energy G_c

1. cracking occurs by channeling
2. plane strain conditions: $\sigma = \bar{E} \cdot \varepsilon$
3. strain value at critical strain ε_c
4. $\bar{E} = E / (1 - \nu^2)$

$$(7.6)$$

For a comparison with the black and clear cracking results of the entitlement experiment (Fig. 7.9), the cracking time to failure for black and clear GMOD samples is shown in Fig. 7.11. Since the GMOD cracking data was not found to be significantly affected by topcoat thickness, only the dependence on primer thickness is shown in this figure. In this data, the clear GMOD results show a similar dependence on primer thickness as do the entitlement results for the black dataset. As discussed, this behavior cannot be explained through a simple analysis of fracture mechanics of a thin elastic coating. However, Fig. 7.11 also shows that the black GMOD results have a negative dependence on primer thickness. This trend is
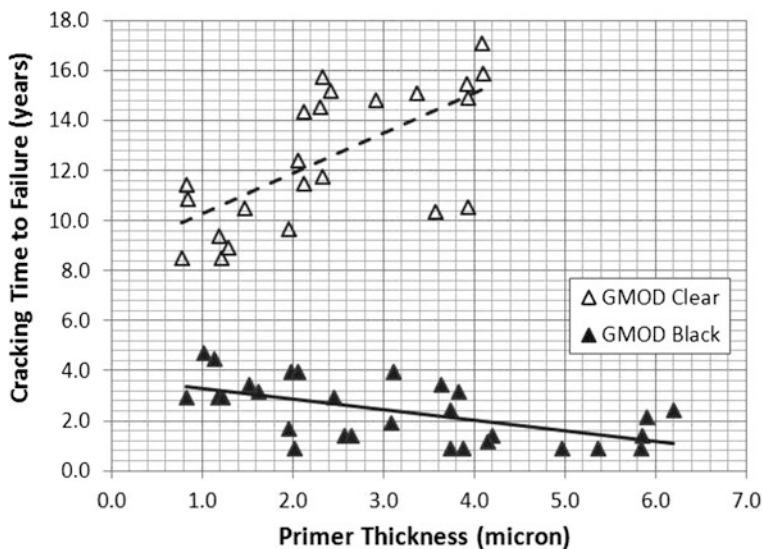
Fig. 7.11 Comparison of cracking time to failure for GMOD black and clear samples. The clear and black GMOD sample results show opposite dependencies on primer thickness. In this graph, the *lines* are drawn to guide the eye and do not represent fit equations to the data (Note: Test results. Actual results may vary)

consistent with the fracture mechanics predictions of a shorter cracking time to fail in thicker coatings.

Figure 7.12 plots the cracking time to failure data for the coatings on black substrates from the entitlement experiment alongside the cracking time to failure data for the coatings on black substrates from the GMOD experiment. The comparison in Fig. 7.12 shows that the mean cracking time to failure is longer in the entitlement experiment as compared to the GMOD experiment. This result is expected since the radiation present in the GMOD experiment is known to cause chemical degradation of UV absorbers as well as the polymer matrix over time. The graph again highlights the different dependencies of the two datasets on primer thickness. The GMOD cracking time to failure data shows the expected trend of shorter time to failure with higher primer thickness, consistent with the fracture mechanics consideration. However, the entitlement data shows the opposite trend, as discussed above.

Because the entitlement experiment has not yet yielded any adhesion failures at the point of this analysis (roughly 10 years of exposure), it is not possible to directly compare the GMOD adhesion results to those of the entitlement experiment at this time. However, a review of the GMOD adhesion data in Fig. 7.4 shows that with exposure to radiation, adhesion failures are seen in both clear and black samples well before 10 years of exposure. The indications are that the entitlement conditions have extended the times to fail for adhesion. This observation is as would be expected, since adhesion failures are known to derive largely from radiative damage at the primer and polycarbonate interface.
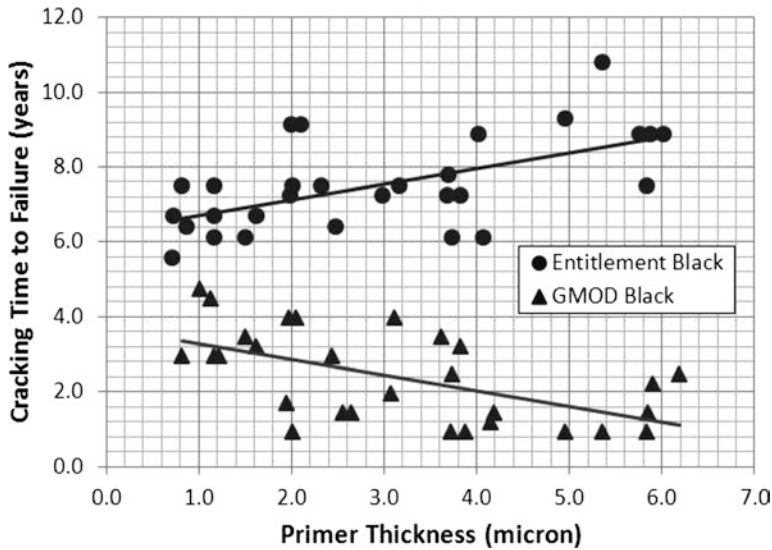
Fig. 7.12 Comparison of cracking time to failure for black samples in the GMOD and entitlement experiments. The two datasets show opposite trends with primer thickness. In this graph, the *lines* are drawn to guide the eye and do not represent fit equations to the data (Note: Test results. Actual results may vary)

Summary of GMOD and Entitlement Experiment Findings

Figure 7.13 collects the cracking time to failure data from the two experiments discussed in this paper into one graph. The harshest conditions would be expected for the GMOD black samples. These samples experience hotter temperatures than the clear GMOD samples (due to additional radiative heating), and the radiation is known to cause chemical degradation, a factor that is not present in the entitlement experiment. Accordingly, it is expected that these samples would show the shortest time to failure of all the datasets, as observed.

The entitlement datasets (clear and black) fall in the middle of the plot of Fig. 7.13 and have intermediate times to failure due to cracking. Both black and clear samples in the entitlement experiment were subjected to the same temperature and humidity conditions within the ESPEC chamber and the coated surfaces of these samples should have been exposed to the same relative humidity. It is therefore difficult to explain the higher apparent cracking time to failure results for the entitlement clear data compared with the entitlement black data. There is no obvious difference between sample conditions for the clear and the black samples in the entitlement experiment, and there is no significant difference in the coefficients of expansion for the clear and black substrates. To follow up on these observations, the assumption of equivalent temperatures for the black and clear sample sets in the entitlement experiment must be verified. This could be done using temperature probes at the surface of the samples during cycling in the environmental chamber.
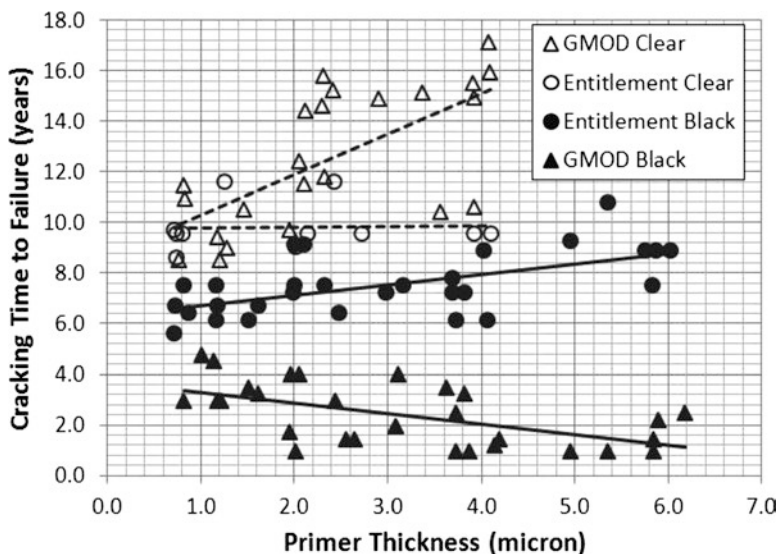
Fig. 7.13 Summary of data from GMOD and entitlement study. In this graph, the *lines* are drawn to guide the eye and do not represent fit equations to the data (Note: Test results. Actual results may vary)

Figure 7.13 shows that the black entitlement samples have shorter cracking failure times compared with the clear GMOD samples. Although the clear GMOD samples were exposed to radiation and the black entitlement samples were not, the black entitlement samples did experience more aggressive temperature and relative humidity profiles. As was shown in Fig. 7.7, the black panel temperature profile in a GMOD experiment is more aggressive than the temperature profile of the GMOD chamber. The temperature profile of the GMOD clear samples should follow that of the GMOD chamber, whereas in the entitlement experiment the GMOD black panel temperature was utilized. Accordingly, the shorter cracking times to failure observed for the black entitlement samples compared with the clear GMOD samples suggest that the temperature and humidity profile may be a more significant factor in determining cracking than the presence of radiation. At this point in the entitlement experiment, not enough cracking failures have been recorded for the clear entitlement dataset to comment on the lifetime comparison with the cracking failures of the clear GMOD samples.

At this time, the positive trends of the GMOD clear and the entitlement black data with primer thickness cannot be readily explained. They show a positive cracking time to failure dependence on primer thickness, a trend that is in the opposite direction as would be anticipated from simple fracture mechanics considerations. The positive slope of these datasets is closer in form to that predicted by adhesion time to failure models. The cracking time to failure data for the GMOD black dataset is the only dataset that follows the trend with primer thickness expected based on a simple fracture mechanics analysis.

Conclusions and Future Work

Both adhesion and cracking failures in hardcoat systems are of critical importance in automotive applications. Unfortunately, all of the models that are currently used to predict coating time to failure in these systems are built from adhesion failure studies and do not consider failure due to cracking. In this paper, analysis of adhesion and cracking data alongside these model predictions suggests that the presence of cracking in a system as a second failure mode may compromise the ability of the adhesion failure model to predict adhesion failures at higher film thicknesses. This work highlights the need for a new model that can incorporate both the cracking failures and the adhesion failures seen in hardcoat systems across the full range of coating thicknesses used in practice.

This paper presented adhesion and cracking failure data for two comparative experiments. In one experiment the samples were subjected to temperature, water spray, and radiation designed to mimic real-world exposure in Florida. In the second experiment, the same samples were subjected to equivalent temperature and humidity cycling protocols in which radiation was not a factor. The results highlighted several discrepancies that are not well understood at this time. The trend of longer cracking failure times for thicker coatings that was observed in several of the datasets does not follow the predictions of fracture mechanics models. Additionally, the longer cracking failure time for coatings on clear versus black substrates was not anticipated in an experiment where the radiative factor was excluded and the temperature and humidity profiles seen by the samples were designed to be the same.

As would be expected, both the adhesion and the cracking times to failure of black samples in the entitlement experiment (without radiation) were higher than the comparative experiment where radiation was present. But even so, it does not appear that the improvement in the cracking time to failure will substantially exceed the 10-year goal for coatings on black substrates. This finding makes the understanding of the cause of cracking in these systems even more important. In order to improve the coating performance beyond the 10-year mark for the full range of coating thicknesses, the key factors driving cracking failure must be identified. The results shown here suggest that the temperature and humidity profile seen by the samples is a key factor in determining cracking lifetimes. As such, work to better characterize the true temperatures experienced by samples in these types of experiments is of high value. Experiments that study how the mechanical properties of the coatings evolve with exposure would also be helpful to understanding the initiation and progression of cracking failures in these systems.

The entitlement study will be continued to the full failure points for both adhesion and cracking for all of the clear and black samples currently in test. Additional studies will be initiated in the meantime to look at the actual sample temperatures by affixing thermal probes to the samples tested in the two protocols discussed in this paper. This effort will provide data on the actual coating temperatures in these environments, without resorting to the assumptions currently being used to estimate sample temperatures in terms of the black panel and chamber temperatures. Material

parameters that relate to temperature, such as the coefficients of thermal expansion of the primer and topcoat, will be more thoroughly studied in these systems as well. Additionally, experiments have been initiated to track the changes in modulus and critical strain to failure in coating systems exposed to GMOD conditions.

References

1. Pickett JE (2004) UV absorber permanence and coating lifetimes. J Test Eval 32:240–245
2. Pickett JE, Sargent JR (2009) Lifetime predictions for hardcoated polycarbonate. In: Martin JW, Ryntz RA, Chin J, Dickie R (eds) Service life prediction for polymeric materials: global perspectives. Springer, New York, p 153
3. Bauer DR (1997) Predicting in-service weatherability of automotive coatings: a new approach. J Coatings Technol 69:85–95
4. Private communication with James Pickett, March 2013
5. Misovski T, Nichols ME, Hardcastle HK (2009) The influence of water on the weathering of automotive paint systems. In: Martin JW, Ryntz RA, Chin J, Dickie R (eds) Service life prediction of polymeric materials: global perspectives. Springer, New York, p 295
6. Sato K (1980) The internal stress of coating films. Prog Org Coating 8:143–160
7. Beuth JL Jr (1992) Cracking of thin bonded films in residual tension. Int J Solids Struct 29:1657–1675
8. Nichols ME (2002) Anticipating paint cracking: the application of fracture mechanics to the study of paint weathering. J Coatings Technol 74:39–46
9. Nichols ME, Peters CA (2002) The effect of weathering on the fracture energy of hardcoats over polycarbonate. Polym Degrad Stab 75:439–446

Chapter 8
Thermal Aging of Polyolefin and Effect of Pre-irradiation of γ Ray on Degradation

Masayuki Ito

Abstract The temperature dependence of the thermal aging of ethylene-propylene elastomer (EPR) pure vulcanized and linear low-density polyethylene (LLDPE) was studied using various methods. The activation energy obtained by the measurement of chemiluminescence (CL) of EPR at the constant temperature ranging from 60 to 160 °C was 82.7 kJ/mol. The rate constant of thermal molecular chain scission of EPR was calculated from the chemical relaxation curves measured at constant temperature ranging from 80 to 140 °C. The activation energy was 110 kJ/mol. The total carbonyl concentration increased logarithmically with increased thermal aging from 60 to 160 °C; the activation energy of the rate constant of the carbonyl accumulation was 95.8 kJ/mol. Pre-irradiation on EPR increased the count of CL, the rate of molecular chain scission, and the rate of accumulation of C=O, but the pre-irradiation did not change the values of these activation energies. The weight change of LLDPE resulting from thermal aging was studied at constant temperatures ranging from 90 to 170 °C. Three stages were observed including induction, the weight increase, and the weight decrease period. The activation energy for the induction period was 136 kJ/mol and was 105 kJ/mol for the weight increase. The addition of antioxidant reagent increased the induction period of LLDPE in all of the temperatures, but the activation energy of the induction period was not changed.

When LLDPE was irradiated up to 320 kGy, the induction period of weight change of the sample by thermal aging was remarkably shortened. The mechanism of this result was considered to be as follows. The irradiation of LLDPE in air accumulated hydroperoxide in the samples, which initiated autoxidation of LLDPE rapidly with applying heat.

Keywords Ethylene-propylene elastomer • Linear low density polyethylene • Thermal degradation • Gamma ray irradiation • Chemiluminescence • Chemical stress relaxation • Rate of molecular chain scission • Weight change of polymer • Carbonyl group accumulation • Index of life time prediction • Activation energy of thermal degradation

M. Ito (✉)
Advanced Research Institute for Science and Engineering, Waseda University,
245-26 Nakamachi, Kodaira, Tokyo 187-0042, Japan
e-mail: masayuki@kurenai.waseda.jp

Introduction

Polyolefin is the most widely used polymer in industry and commercial application. Thermal aging is a common in-service degradation mode in the polymer.

The temperature dependence of thermal aging of polyolefin is useful for the short time test and lifetime prediction of the polymer. The recent study pointed out the curvature on the Arrhenius plot of thermal aging of polymer [1]. This article studied the temperature dependence of thermal degradation of ethylene-propylene elastomer (EPR) and linear low-density polyethylene (LLDPE) using various methods. The oxygen uptake in the early period of thermal aging showed the very sensitive method for the evaluation of thermal degradation of polymer [2]. The oxygen uptake in the sample has to increase the weight of the sample; therefore, the weight change along with thermal aging was studied.

Polyolefin is used for an insulating material in the electric cable which is used in nuclear power plants. The electric cable is exposed to radiation and heat simultaneously during the service condition. Dose was estimated to be 500 kGy over 40 years service time [3, 4]. IEEE standards 323-1974 [3] and 323-1978 [4] have provided guides for class IE equipment and electrical type testing. The standards recommend the sequential addition of radiation and heat instead of simultaneous addition, because the sequential method is practically convenient as a test method. In this article, the effect of pre-irradiation of polyolefin on its thermal aging was also studied.

Experimental

Material

Ethylene-propylene elastomer used was commercial grade EP07P and EP11 (JSR, Japan). The molar ratio of ethylene in the copolymer is about 80 % in EP07P and 50 % in EP11. The polymer was mixed with dicumyl peroxide using a mixing roll. The sample was cured by heat press to attain a certain thickness that was different according to the method of measurement. Linear low-density polyethylene (LLDPE) was used for the measurement of weight change along with thermal aging. The different concentration of antioxidant reagent was mixed with LLDPE also using a mixing roll. The antioxidant reagent used was 4,4′-Thio bis (3-methyl-6-tert-butylphenol).

Irradiation

Co-60 γ ray was irradiated to the samples at room temperature in air. Dose rate was 3.0 kGy/h.

Chemiluminescence

Count of chemiluminescence (CL) was measured using a chemiluminescence analyzer OX-7-TC from Tohoku Electric Co. The sample was EP07P having a thickness of about 0.5 mm. The count of CL vs. time was measured at constant temperature ranging from 60 to 160 °C in air. The value of count of CL was extrapolated to time 0, and the value was defined as the initial count of CL.

Rate of Molecular Chain Scission

The rate of molecular chain scission which occurred during thermal aging was obtained by the measurement of chemical stress relaxation [5]. The stress relaxation of EP07P stimulated by heat was measured at different constant temperatures ranging from 80 to 140 °C in air. The thickness of the sample was about 0.5 mm, the width was 5.0 mm, and the distance of jowls was 80 mm. The stress decay was measured at a constant strain (10 %).

Accumulation of Carbonyl Group

The thickness of EP07P used in this experiment was about 0.1 mm. The concentration of generated carbonyl group in the sample by thermal aging was measured using infrared spectrometer type A-32 (JASCO Co.). The concentration of C=O in the film was obtained by using extinction coefficient of 300 L/mol^{-1} cm^{-1} with 1,720 cm^{-1}.

Weight Change

Each sample had a thickness of about 0.15 mm, and a diameter of about 50 mm was placed on the stainless steel pan. Heat aging was performed in an air oven controlled at constant temperature. The weight of the pan with sample was measured periodically by chemical balance at room temperature.

Result

Chemiluminescence

Figure 8.1 shows a relationship between CL count and aging time in the apparatus at 60 °C. Almost the same type of figure was obtained at all of the temperatures from 60 to 160 °C [6]. The count of luminescence is considered to represent the extent of
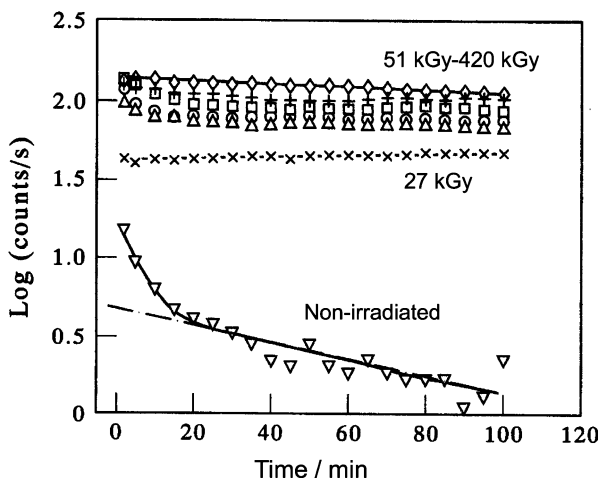
Fig. 8.1 The effect of pre-irradiation on count of chemiluminescence of EP07P at 60 °C

Fig. 8.2 Arrhenius plot of count of chemiluminescence of EP07P
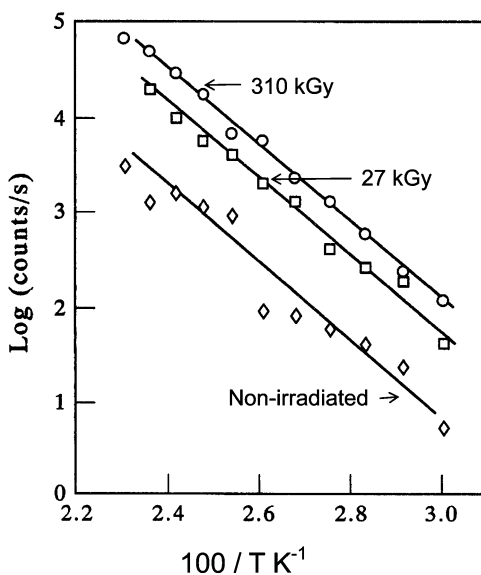
thermal oxidation of polymer [7]. The thermal degradation of polyolefin at 60 °C might be low, but CL sensitively responded to the oxidation as shown in Fig. 8.1.

The CL count increased remarkably by adding samples with a small dose which does not generally affect their mechanical properties. But the amount of emission leveled off at about 50 kGy. This dose consumed the antioxidant reagent added in the production process of EP07P by energy transfer from polymer to antioxidant reagent. The detailed mechanism was reported previously [6].

Figure 8.2 shows the Arrhenius plot of CL count of EP07P. The amount of CL increased by pre-irradiation of γ ray, but the slope was the same as that of the nonirradiated sample; activation energy was 82.7 kJ/mol.
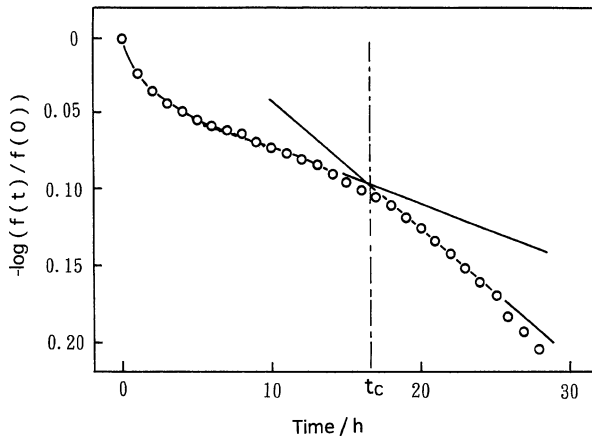
Fig. 8.3 Chemical stress relaxation of nonirradiated EP07P at 100 °C

Rate of Molecular Chain Scission

Figure 8.3 shows the stress-decay curve of EP07P at 100 °C. The rate constant of chemical stress relaxation that is proportional to the molecular chain scission is expressed by Eq. (8.1) [5]:

$$kt = -\log\big(f(t)/f(0)\big) \tag{8.1}$$

where k is the rate constant of chemical stress relaxation, $f(0)$ is the initial stress under the constant strain, and $f(t)$ is the stress at time t. The slope of the curve in Fig. 8.3 is considered to be proportionate to the rate of molecular chain scission. The very early stage of stress decay is due to the physical flow of molecular chain.

The slope of curve in Fig. 8.3 increased at time tc. This phenomena means that the effect of small amount of antioxidant reagent which was added in the production process of EP07P to prevent oxidative degradation during storage of the sample was decreased by thermal aging and the rate of molecular chain scission increased from tc.

The stress relaxation curves obtained at 110, 120, 130, and 140 °C are shown in Fig. 8.4. The value tc was observed in all of the decay curves [8]; the time associated with tc might be comparable to the lifetime of the effect of the antioxidant reagent added in the production process. The Arrhenius plot of tc is shown in Fig. 8.5; activation energy is 116 kJ/mol.

The effect of pre-irradiation on thermal aging of EP07P is shown in Fig. 8.6. This figure shows the stress-decay curves of EP07P which was irradiated up to 50 kGy. The decay curves are straight line; tc was not observed on the curves when sample was pre-irradiated. The chemical stress relaxation curves of the sample which was irradiated up to 96 kGy showed the same decay curves as that irradiated up to 50 Gy [8].
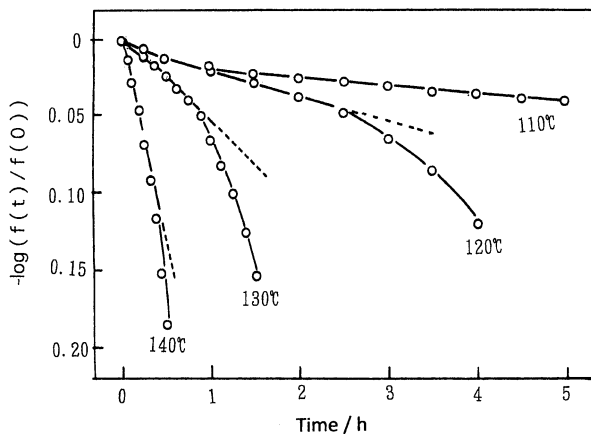
Fig. 8.4 Chemical stress relaxation of nonirradiated EP07P at various temperatures

Fig. 8.5 Arrhenius plot of tc
of nonirradiated EP07P
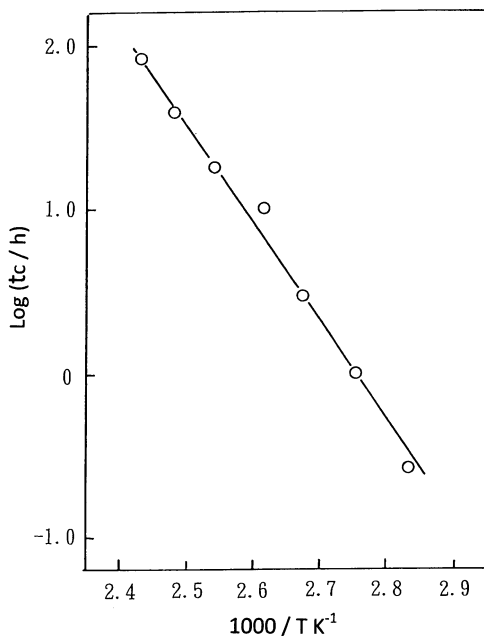
The rate of thermal chain scission Qm(*t*)/*t* is expressed by Eq. (8.2) [5]:

$$Qm(t)/t = -N(0)\ln(f(t)/f(0))/t \qquad (8.2)$$

where $N(0)$ is the initial network concentration of the elastomer, which was calculated from the initial modulus of the samples [8].

Fig. 8.6 Chemical stress relaxation of pre-irradiated EP07P at various temperatures
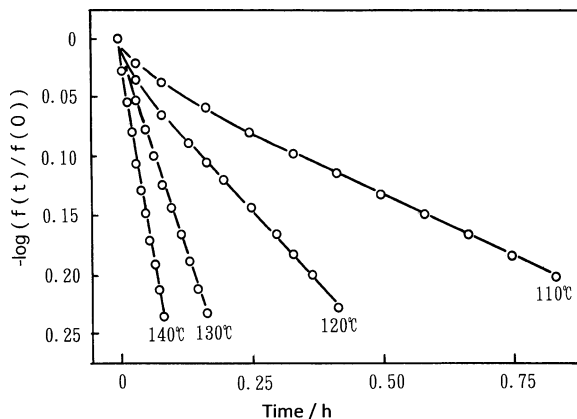
Table 8.1 Rate constant of thermal molecular chain scission of EP07P which has various thermal and irradiation histories (mol h^{-1} ml^{-1})

Temperature (°C)	Dose (kGy)			
	0 (before tc)	0 (after tc)	50	96
80	6.1×10^{-7}	6.6×10^{-7}	5.5×10^{-6}	4.3×10^{-6}
90	8.5×10^{-7}	1.5×10^{-6}	1.8×10^{-5}	1.3×10^{-5}
100	2.1×10^{-6}	4.0×10^{-6}	4.8×10^{-5}	3.8×10^{-5}
110	3.4×10^{-6}	9.9×10^{-6}	1.1×10^{-4}	9.2×10^{-5}
120	9.4×10^{-6}	2.2×10^{-5}	2.4×10^{-4}	2.3×10^{-4}
130	3.6×10^{-5}	7.4×10^{-5}	7.0×10^{-4}	5.3×10^{-4}
140	1.4×10^{-4}	2.2×10^{-4}	1.4×10^{-3}	1.4×10^{-3}

Table 8.1 shows the rate constant of thermal chain scission of EP07P before tc, after tc, and pre-irradiated up to 50 and 96 kGy. The rate of thermal chain scission after tc was about twice that before tc. Irradiation decupled the rate constant of the decay, but the rate constant did not increase even though the dose increased from 50 to 96 kGy.

Figure 8.7 shows the Arrhenius plot of the rate of thermal chain scission of EP07P which was measured before and after tc. The obtained line had the same slope, and activation energy was 110 kJ/mol.

The effect of pre-irradiation on activation energy is not observed as shown in Fig. 8.7.

Accumulation of Carbonyl Group

Oxidation of hydrocarbon produces carbonyl and carboxyl group in the material. These functional groups affect the electric properties of the sample. Therefore, the concentration of C=O produced along with aging may be an indicator of the degree of degradation of polyolefin.

Fig. 8.7 Arrhenius plot of
rate of chain scission of
EP07P
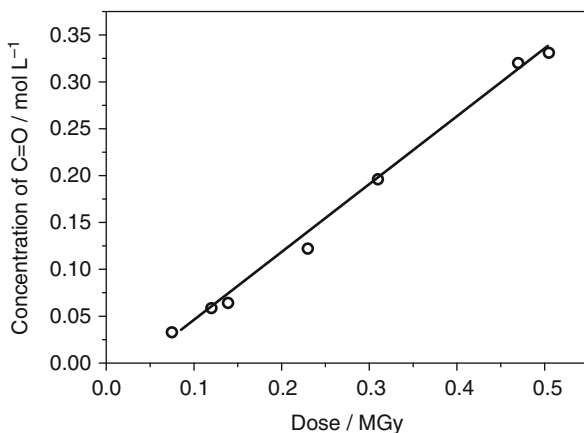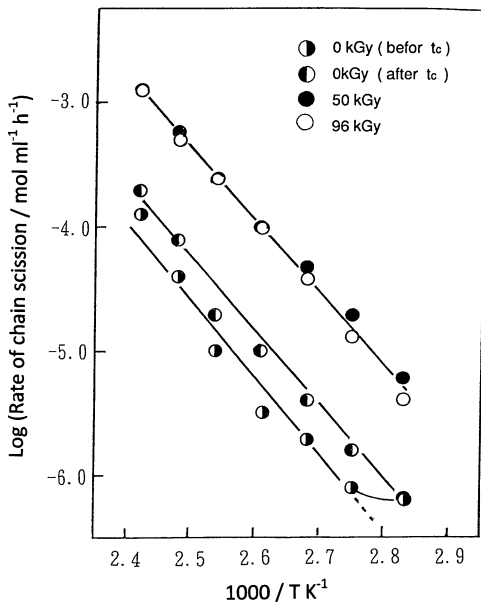
Fig. 8.8 Relationship between dose and C=O accumulated in EP07P by irradiation of γ ray

Figure 8.8 shows the relationship between dose and concentration of C=O.
The concentration of C=O linearly increased with increasing dose. The samples that
have different irradiation dose were thermally aged at 110 °C, and the result is
shown in Fig. 8.9. The concentration of C=O exponentially increased with increas-
ing thermal aging time. The point of curvature was observed when the samples
which had low pre-irradiation dose were thermally aged. When pre-irradiation
dose was more than 60 kGy, there was no curvature on the line. This suggests the
following process.

Fig. 8.9 Effect of dose on the increase in the concentration of C=O in EP07P by thermal aging at 110 °C
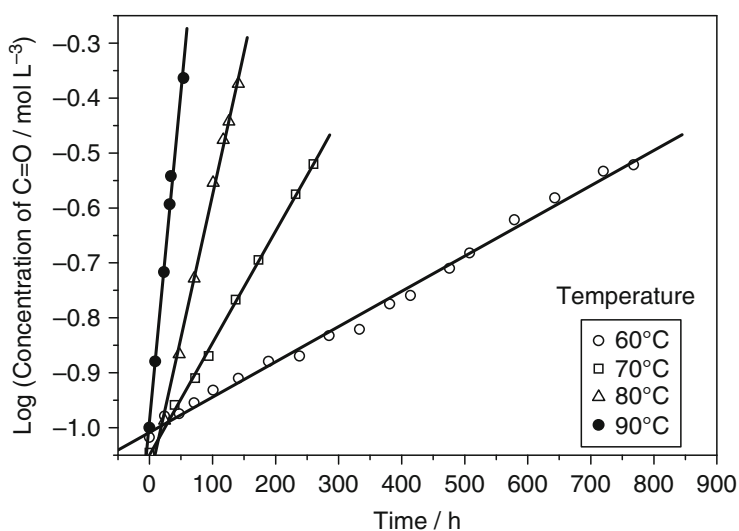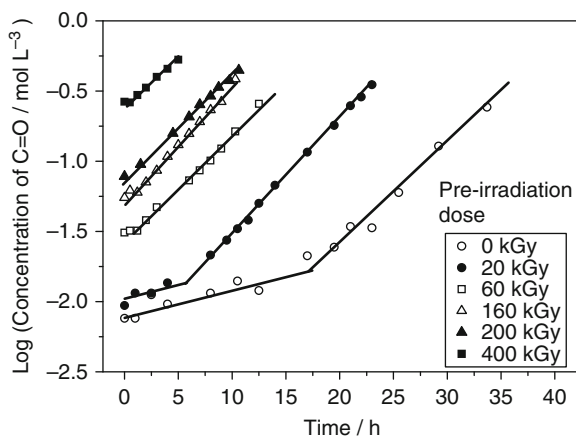
Fig. 8.10 Increase in the concentration of C=O in EP07P irradiated up to 200 kGy by thermal aging at relatively low temperatures

A small amount of antioxidant reagent added in the production process of EP07P depresses the thermal oxidation of the polymer. However, 20 h of thermal aging at 110 °C or irradiation at about 60 kGy consumed the antioxidant reagent in the sample. The rate of autoxidation at the constant temperature depends on whether the antioxidant reagent exists or not.

Figures 8.10 and 8.11 show an increase in C=O along with thermal aging at 60, 70, 80, 90, 100, 110, 120, 130, and 140 °C, respectively. All of the samples were irradiated up to 200 kGy; there might be no antioxidant reagent in those samples.
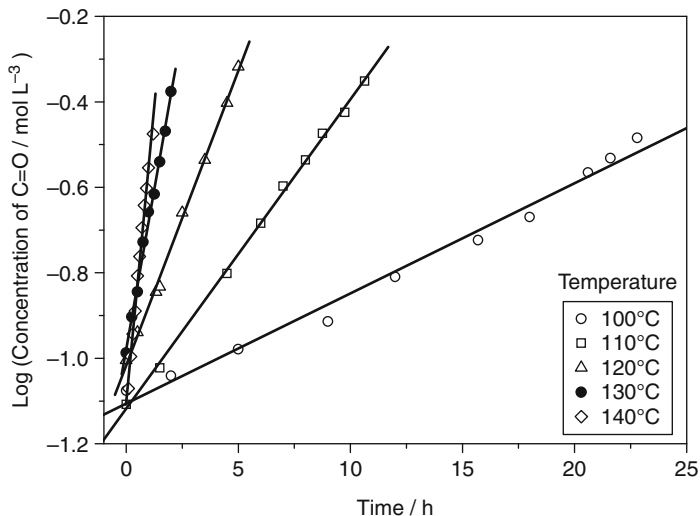
Fig. 8.11 Increase in the concentration of C=O in EP07P irradiated up to 200 kGy by thermal aging at relatively high temperatures

Fig. 8.12 Arrhenius plot of K
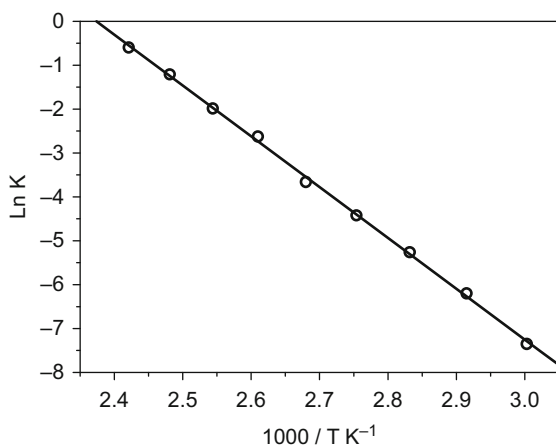
The rate constant of total carbonyl accumulation in the sample is expressed by Eq. (8.3):

$$Log C = Kt \tag{8.3}$$

In Eq. (8.3), C is the concentration of C=O observed by IR spectrometer, t is the thermal aging time, and K is the rate constant of total carbonyl accumulation in the sample.

Figure 8.12 shows the Arrhenius plot of K; the straight line was obtained from 60 to 140 °C; the activation energy is 95.8 kJ/mol.
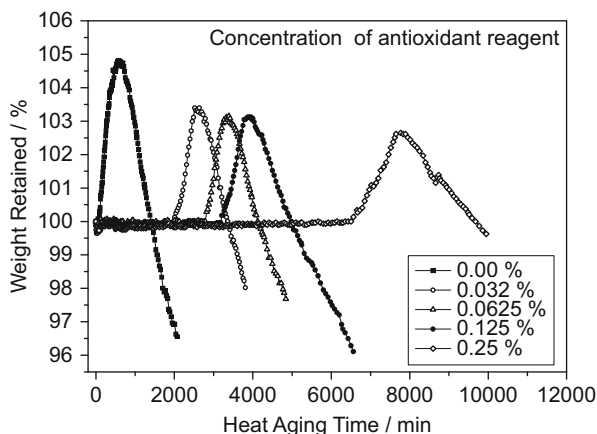
Fig. 8.13 The effect of the concentration of antioxidant reagent on weight change of LLDPE at 150 °C

Weight Change

Thermogravimetry (TG) has been widely used for evaluating the heat-resistant properties of polymers [9–15]. In this method, the weight of samples was continuously measured as the temperature of the sample was raised at a constant rate. TG method is based on the analysis of the weight decrease curve accompanying the thermal decomposition of samples during heat aging. But when thermal aging takes place in air, oxidative products accumulate in the polymer. This increases the weight of the polymer.

For a quantitative analysis of the oxidative reaction of polymer, the accurate measurement of the weight change at a constant temperature might be more useful than TG method. The previous article [16] studied the induction period, the increase in weight, and the weight decrease of EP07P along with isothermal aging; the activation energy of each stage of the thermal aging, induction period, weight increase, and weight decrease, was also investigated.

This article studied the weight change of LLDPE by thermal aging at constant temperatures. The effect of the concentration of antioxidant reagent on the weight change by thermal aging was also investigated. Figure 8.13 shows the weight change of LLDPE by thermal aging at 150 °C. The induction period where the weight of sample was kept constant in early period of thermal aging depends on the concentration of antioxidant reagent. On the other hand, the significant difference on the effect of the concentration of antioxidant reagent was not observed on the slope of weight increase curve.

The same result was obtained on the relationship between weight change and aging time at various temperatures ranging from 90 to 170 °C. The detail will be reported in the future. The effect of the concentration of antioxidant reagent on the

Fig. 8.14 Relationship between the concentration of antioxidant reagent and the induction period on the thermal aging of LLDPE at 120 °C

Fig. 8.15 Initial sage of weight change of EP07P in which antioxidant reagent was not added at various temperatures

induction period at 120 °C is shown in Fig. 8.14 as one of the examples; the induction period was proportional to the concentration of the antioxidant reagent.
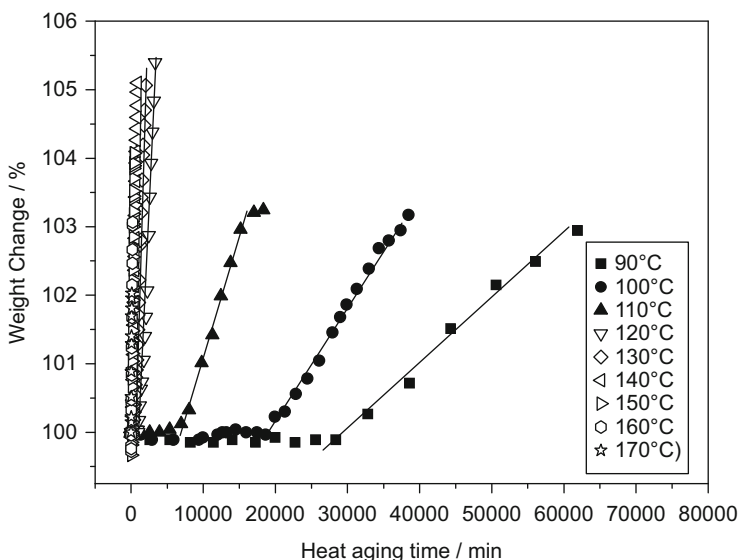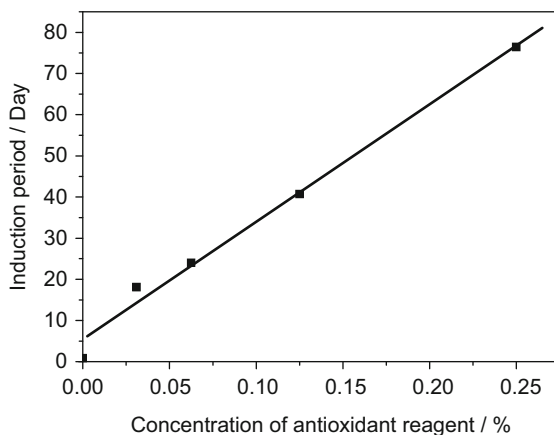
Figure 8.15 shows the initial stage of weight change of LLDPE by thermal aging at various temperatures ranging from 90 to 170 °C. The Arrhenius plot of the induction period of the samples which have different concentration of antioxidant reagent was shown in Fig. 8.16. The slope of the lines was almost the same. The apparent activation energy was 136 kJ/mol.

Figure 8.17 shows the Arrhenius plot of the rate of weight increase of the sample by thermal aging. The activation energy was 105 kJ/mol, which does not appear to depend on the concentration of antioxidant reagent.

Fig. 8.16 Arrhenius plot of thermal aging of LLDPE which contains various antioxidant concentrations
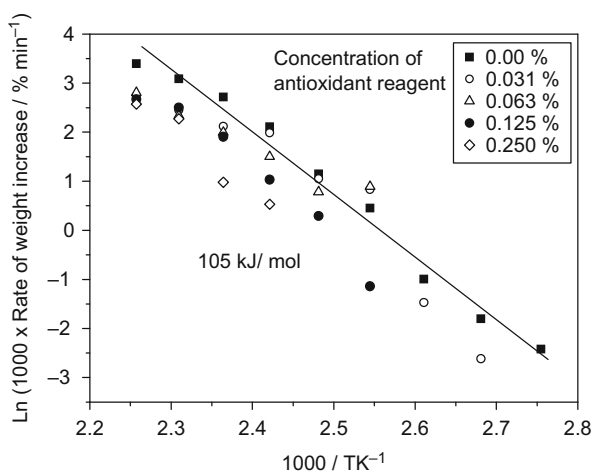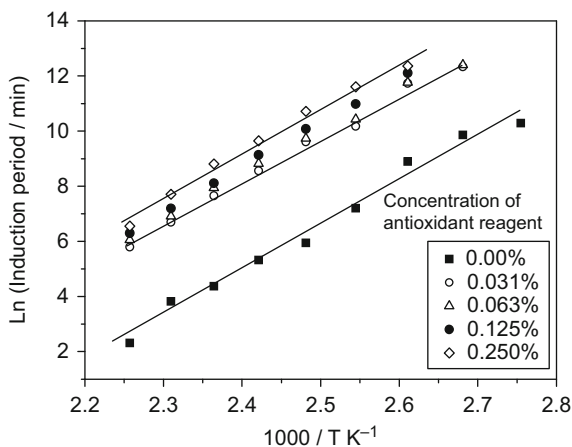
Fig. 8.17 Arrhenius plot of the weight increase of LLDPE which contains various antioxidant concentrations

Effect of Pre-irradiation of γ Ray on the Thermal Aging of LLDPE

When the polyolefin was exposed to heat after irradiation, the heat-resistant properties are affected by the irradiation. Figure 8.18 shows the effect of pre-irradiation on weight change of LLDPE by thermal aging at 150 °C. Dose of pre-irradiation was 320 kGy.

The pre-irradiation resulted in the remarkable changes on the behavior of thermal aging of LLDPE even though the thermal aging condition shown in Fig. 8.18 is the same as that shown in Fig. 8.13. The induction period of weight increase was very
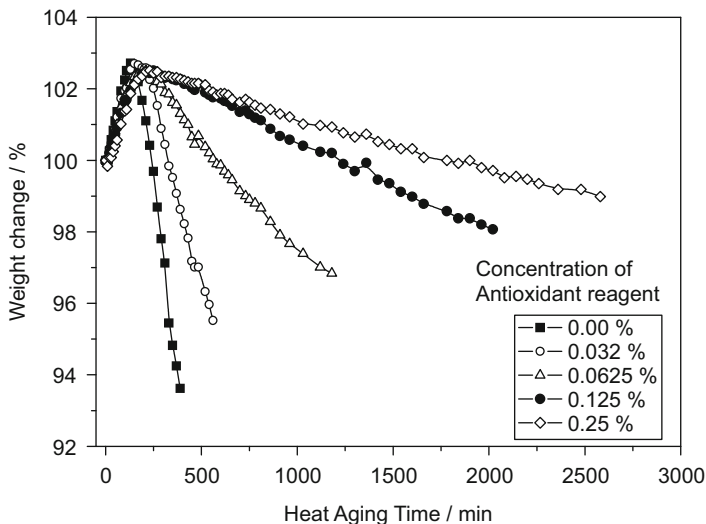
Fig. 8.18 The effect of pre-irradiation on weight change of LLDPE. The dose was 320 kGy

short, and the effect of concentration of antioxidant reagent was not observed in the induction period. The rate of weight decrease depended on the concentration of antioxidant reagent. This phenomenon was different from the result obtained for the nonirradiated samples shown in Fig. 8.13.

Discussion

Activation Energy of Thermal Aging of EP07P Obtained by Various Methods

Phenomenology as proposed by Edmund Husserl (1859–1938) can be roughly described as the sustained attempt to describe experiences without metaphysical and theoretical speculations. His idea on the relationship between an appearance and the phenomenon could be considered that the measurement by a certain method gives only an appearance of the phenomenon.

When we study the temperature dependence of the thermal aging of polymer, the obtained activation energy is considered to be an appearance of the phenomenon, i.e., the thermal aging in this study. To understand the phenomenon which occurred during thermal aging, it is useful to compare the values of activation energy obtained by various methods for one polymer.

Table 8.2 shows activation energy of thermal aging of EP07P. The value was different to the different method of measurement. The count of CL represents the

Table 8.2 Activation energy of thermal aging of EP07P obtained by various methods

Focused point	Activation energy (kJ/mol)
Induction period[a]	113
Rate of weight increase[a]	113
Slope of weight loss[a]	60.3
Chemiluminescence (oxidation)[b]	82.7
Rate of thermal chain scission[c]	110
Accumulation of C=O	95.8

[a]M. Ito, S. Inayoshi and K. Moriyama, Polymer degrad. and Stab., 93, 1935 (2008)
[b]M. Ito: Radiat. Phys. Chem. 41, 443 (1993)
[c]M. Ito, T. Sato and K. Murakami: Soc. Japan Rubber Indust. 69, 98 (1996)

Table 8.3 Activation energy of thermal aging of polyolefin obtained by the measurement of weight change

Sample	Induction period	Wight increase	Wight decrease
LLDPE	136 kJ/mol	105 kJ/mol	153 kJ/mol
EP11	110 kJ/mol	50 kJ/mol	
EP07P[a]	113 kJ/ mol	113 kJ/mol	60.3 kJ/mol

[a]Masayuki Ito, Shigekazu Inayoshi and Kentaro Moriyama Polymer degrad. and Stab., 93 (2008) 1935-1938

amount of oxidation occurred at the temperature but the count of CL dose not reflects changes in molecular structure of polymer. The increase in total carbonyl affects the electric properties of the sample, and therefore, this activation energy might be applicable in the field of electric engineering. The scission of molecular chain deteriorates the mechanical properties of polymer. The activation energy obtained by the measurement of chemical stress relaxation might be applicable to deciding the condition of short time test by heat when the mechanical properties were focused on. As seen above, it is useful to pile up the value of activation energy obtained by the measurement of various appearances.

Activation Energy of Thermal Aging of Polyolefin

Table 8.3 shows the activation energy obtained by the measurement of weight change of two kinds of EPR and LLDPE. The values in the weight increase and the weight decrease were largely different to the different sample but the induction period showed relatively near value each other.

The most likely reason might be as follows. The basic mechanisms consist of an initiation step in which hydrogen is removed from molecule leaving the free radical. This radical react with oxygen to form a peroxy radical and the autoxidation is started. The temperature dependence of these reactions is the same in the simple polyolefin.
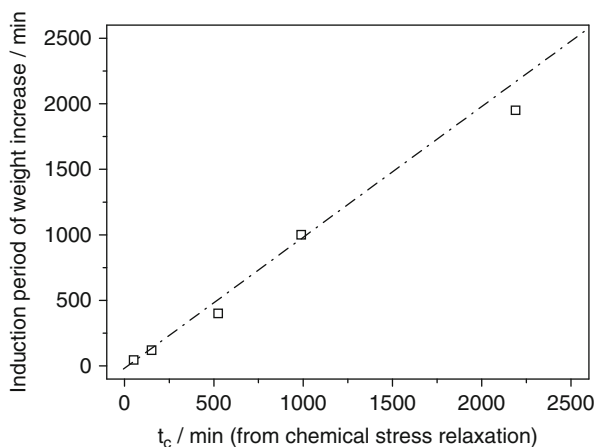
Fig. 8.19 The relationship between curvature tc from where the rate of chain scission increased and the induction period of weight increase of EP07P

The Relationship Between tc and the Induction Period

Figure 8.19 shows the relationship between the induction period of weight change of EP07P and the time tc which was obtained from chemical stress relaxation curve of the elastomer. The temperature range was between 90 to 130 °C. Both values had the same period of time as shown in this figure.

This reason is considered as follows. The small amount of antioxidant reagent was consumed by thermal aging at this period and thermal oxidation increased. This brought about the increase in the rate of chain scission and addition of carbonyl groups.

Analytical View on the Weight Change of Polyolefin by Thermal Aging

Three stages were observed on the weight change of polyolefin, i.e., the induction period, the period of weight increase, and the period of weight decrease. The mechanism of weight change of EP07P might be explained as follows.

In the initial stage, molecular chain scission was started, but the rate of scission was low before tc. The accumulation of carbonyl went on in this stage, but the concentration of C=O increased logarithmically with increasing aging time. Therefore, the reactions which occurred in the initial stage didn't have an effect on the weight of the sample.

In the second stage, the accumulation of C=O increased the weight of the sample. The scission reaction increased after tc, but the molecular chain fragment which was generated by thermal aging kept the relatively longer chain length and was not evaporated from the sample at the temperature. As a result, the weight of sample increased with increasing aging time in this stage.

In the third stage, the scission reaction generated shorter molecular chain in the sample, some of which contain C=O group in the molecule. Finally, this stage severely reduced the length of molecular chain which evaporated from sample to air at the temperature.

Effect of Pre-irradiation of Polyolefin on Thermal Aging

The relationship between weight change of LLDPE and thermal aging time is shown in Figs. 8.13 and 8.18 for the sample of nonirradiated and pre-irradiated, respectively. The irradiation shortened the induction period of the samples which contain various concentrations of antioxidant reagent. As shown in Fig. 8.18, the induction periods of all of the samples are the same.

It is solved that the difference between the result of nonirradiated samples and pre-irradiated sample might be as follows.

In the very early stage of thermal aging of PE, the radical concentration was very low. It takes a certain period of time to accumulate even low concentration of peroxide in the nonirradiated PE, which initiates autoxidation. Irradiation even at room temperature generates higher concentrations of radicals in the samples. The radicals react with oxygen in air, and hydroperoxide is produced and accumulated in PE. This hydroperoxide initiates autoxidation at the initial stage of thermal aging. The weight increase by the accumulation of carbonyl was stated from very early period of thermal aging as shown in Figs. 8.9 and 8.18.

Index of Lifetime Prediction

The activation energy is the important factor in estimating the lifetime of polyolefin along with thermal aging. The value was obtained by the measurement of rate of the weight increase and weight decrease, the rate of molecular chain scission, the accumulation of total carbonyl, and counts of CL. The point of curvature of measured value on the time scale of thermal aging is essential for predicting the lifetime of polymer.

The induction period is obtained by a simple method, i.e., the measurement of the weight of sample along with thermal aging might be one of the useful indicators for the lifetime prediction. In the future, it is expected to investigate the relationship between the induction period and the changes in practical performance of the polymer on the course of thermal aging.

References

1. Celina M, Gillen KT, Assink RA (2005) Polym Degrad Stab 90:395–404
2. Wise J, Gillen KT, Clough RL (1995) Polym Degrad Stab 49:403–418
3. IEEE Std. 323-1974 (1974) IEEE standard for qualifying class 1E equipment for nuclear power generating station. IEEE
4. IEEE Std. 323-1983 (1983) IEEE standard for qualifying class 1E equipment for nuclear power generating station. IEEE
5. Tobolsky AV (1960) Properties and structure of polymers. Willey, New York
6. Ito M (1993) Radiat Phys Chem 41:443
7. Ashby GEJ (1961) Polym Sci 50:99
8. Ito M, Sato T, Murakami K (1996) Soc Japan Rubber Indust (Japanese) 69:98
9. Kujirai T, Akahira T (1925) Sci Pap Inst Phys Chem Res 2:223
10. Doyle CD (1961) J Appl Polym Sci 5:28
11. Doyle CD (1965) Nature 207:290
12. Ozawa T (1965) Bull Chem Soc Jpn 38:1881
13. Flynn JH, Wall LA (1966) J Polym Sci B4:323
14. Friedman HL (1964) J Polym Sci C6:183
15. Ozawa T (1986) J Therm Anal 31:547
16. Ito M, Inayoshi S, Moriyama K (2008) Polym Degrad Stab 93:1935–1938

Chapter 9
Test Method Development for Outdoor Exposure and Accelerated Weathering of Vinyl Siding Specimens

Jeffrey P. Quill and Sean P. Fowler

Abstract This chapter provides an overview of extensive research conducted by the Vinyl Siding Institute (VSI) on the development of new test methods for exterior plastic building products. The purpose of the VSI study was to develop an accelerated testing protocol for use in certifying materials.

This chapter describes the development of an outdoor certification test program and subsequent efforts to create an accelerated weathering test method that could be used to predict the results of the outdoor protocol with a high degree of accuracy. Outdoor weathering tests were conducted in Florida, Arizona, and the northern temperate locations to obtain baseline data for comparison. This part of the research led to the development and subsequent publication of ASTM D6864.

Accelerated laboratory tests were performed in Fluorescent UV/condensation test apparatus and xenon arc test chambers. The process involved the examination of multiple types of equipment, multiple cycles, and multiple conditions, and comparing the various results to the outdoor exposures. Testing suggested that for this particular material, one method was more suitable than the other. The proposed method was verified with repeat testing and rugged statistical analysis. Round robin testing was conducted to determine repeatability and reproducibility.

Although the proposed accelerated method was not adopted into the VSI's certification program, its results demonstrated high rank-order correlation with outdoor test results, giving the user much greater confidence that materials passing the accelerated test will pass the outdoor test. The accelerated method, therefore, is useful during research and development because it provides a fast and reliable method for evaluating small formula changes. It is useful for selecting formulations to include in a 2-year certification test.

Keywords Service-life prediction • Real-world validation • Degradation pathways • Degradation-rate model • Accelerated life testing • Cumulative damage model • Photodegradation rate • Temperature dependence • Irradiance dependence • Reciprocity • Model robustness

J.P. Quill • S.P. Fowler (✉)
Q-Lab Corporation, 800 Canterbury Road, Cleveland, OH 44141, USA
e-mail: sfowler@q-lab.com

What Is Vinyl Siding?

Home remodeling and new construction product developers and manufactures are constantly introducing a wide range of new innovative materials and products. Cost, durability, appearance, low maintenance, and variety are the competing characteristics customers seek, with cost gaining importance in a tough economy.

Vinyl siding is industry's response to these needs in the residential cladding market, having been the most widely used material in the United States and Canada since 1995.

Vinyl siding was first introduced in the early 1960s, but didn't start becoming popular until the mid-1970s. Although home remodeling has constituted most of the vinyl siding market historically, new construction now accounts for more than one-third of vinyl siding sales.

Vinyl siding is manufactured by co-extrusion. The lower layer (substrate) is typically PVC, while the top layer (capstock) is the weatherable surface of the siding. Two common capstocks are PVC and ASAs and similar polymers.

PVC offers many advantages over other polymers in siding applications, including cost, flame retardance, and impact resistance to name a few. We will focus on one aspect of durability that tends to be very important to consumers, color retention over the life cycle of the product. Although the warranties for vinyl siding products vary considerably from one manufacturer to another, the color retention warranties typically cover decades of use. Many warranties cover 50 years and offer transfer provisions when homes are sold. Needless to say, potential warranty liabilities represent materially significant costs for manufacturers.

This chapter will focus on the work undertaken by the Vinyl Siding Institute (VSI) over a period of more than 20 years in understanding the weatherability of the wide range of colors offered by its members to the marketplace.

We will review the long-term outdoor test programs undertaken by the VSI and the extensive efforts undertaken in the development of an accelerated laboratory test protocol.

Vinyl Siding Degradation and Color Change

PVC capstock has three main failure modes:

Yellowing: The primary degradation mechanism is dehydroclorination. In this reaction, the C–Cl bond is broken by a photon of UV light, liberating chlorine which can attract hydrogen to form HCl, allowing oxidation of the polymer, cross-linking, and double-bond formation. The dehydroclorination process can be autocatalytic, resulting in polyene sequences. The absorption spectra of polyenes extend from the UV into the shorter wavelengths of visible light (blue), resulting in a yellowish appearance [1, 2].

Fade: The polymers are not photostable without the use of stabilizers. Their degradation mechanism involves the breaking of the double bond and the subsequent oxidation. This results in the formation of large quantities of species like peroxides. These species can have significantly different refractive indices than the PVC, causing scatter at the interface. If enough interferences are present, the resulting scatter will appear as a whitish haze [1, 2].

Chalking: If the yellowing and fading go on long enough, the surface integrity of the polymer can begin to fail, leading to checking, cracking, and flaking of the surface [1, 2].

What Is VSI?

The VSI is the trade association for manufacturers of vinyl and other polymeric siding and suppliers to the industry.

The VSI offers a certification that indicates a manufacturer's specific product meets or exceeds relevant ASTM standards. ASTM D3679, *Standard Specification for Rigid Poly(Vinyl Chloride) (PVC) Siding* [3], and ASTM D7254, *Standard Specification for Polypropylene (PP) Siding* [4], cover most product specifications, while ASTM D6864, *Standard Specification for Color and Appearance Retention of Solid Colored Plastic Siding Products* [5], and ASTM D7251, *Standard Specification for Color and Appearance Retention of Variegated Color Plastic Siding Products* [6], are specific to color and appearance.

An independent testing lab is used to insure that a product has been properly tested and inspected for a number of characteristics before it receives the VSI certification. Basic characteristics like length, width, and thickness are verified to insure the manufacturer is providing a product that matches the specification advertised. Other testing is more rigorous, involving testing the performance properties of the siding. Weathering exposures, for example, are conducted in three different locations over 2 years to determine if the siding will retain its color over time, in its intended service environment.

As of January 2013, 14 manufacturers representing 37 brands have products listed on the "VSI Product Certification Program's Official List of Certified Products." These manufacturers have a wide variety of colors, an average of approximately 30 each, on the certified products list [7].

VSI's Outdoor Weathering Testing Program

The outdoor weathering requirement for VSI certification requires 2-year exposures at 45° south facing in three locations: Miami Florida (subtropical), Phoenix Arizona (desert), and Cleveland, Ohio (northern industrial). Specimens are tested according

to ASTM D6864; additionally the VSI has an outdoor weathering test protocol that is used in conjunction with ASTM D6864. This protocol covers such items as number of replicates, sample size, mounting requirements, and data collection methods and procedures [8].

The VSI has determined mathematical ellipsoids for sixteen color regions, which are described in ASTM D6864. Hunter Lab, 2° Observer, specular included is used to define the parameters of the color region. These ellipsoids define the amount of acceptable color change after weathering based on visual evaluations of "initial" and "weathered" samples. They are derived by inserting the ΔL, Δa, and Δb for a weathered sample into the ellipsoid equation for the defined color region and calculating the ellipsoid value for the sample. A value less than 1.0 is "inside" the ellipsoid, and the amount of color change is acceptable. A value of 1.1 or greater is "outside" the ellipsoid, and the amount of color change is unacceptable. The concept is similar to the CMC ellipsoid equations developed by the Color Measurement Committee of the Society of Dyers and Colorists and described in AATCC Test Method 173 [9] and ASTM D2244 [10].

For a product to pass outdoor testing it must be free of any obvious mechanical failure such as peeling or cracking and uniform in appearance, and the average ellipsoid value of weathered samples must be less than or equal to 1.0.

One obvious question arises concerning the 2-year outdoor weathering certification test. How is a 2-year test sufficient for a product intended to last for decades on a house? It took decades of outdoor testing to provide VSI and its members with sufficient data to extrapolate long-term performance from shorter term exposures. Products must exhibit an ellipsoid value of less than or equal to 1.0 after 2-year exposures in all three locations in order to receive VSI certification. Large volumes of data collected over the decades show that a material passing this threshold will likely maintain acceptable color retention over the expected lifetime of the product. The following section provides an overview of some of this data.

VSI Outdoor Weathering Studies

As vinyl siding began to grow in popularity VSI determined that it needed long-term outdoor data on the types of materials commercially available at the time. In May 1984 the VSI began VS1W as a 10-year outdoor weathering study with samples on exposure in Florida, Arizona, and New Jersey. In 1994 the New Jersey portion of the test was ended. The program was extended in 1994 for 5 years, and again in 2000. There are currently 344 samples on exposure in Florida and 46 samples on exposure in Arizona. 20- and 25-year data was collected during the summers of 2005 and 2010, respectively. Subsequently VSI has undertaken a new weathering study approximately every 5 years. With VS1W and subsequent outdoor testing programs reading were to be taken at ½-, 1-, 1½-, 2-, 5-, 10-, 15-, 20-, 25-, and 30-year intervals.

VS2W was started in January 1989 as a 10-year program in Florida, Arizona, and Ohio. In 1999 the Florida and Ohio portion of the test was ended. The Arizona portion of the test was resubmitted for another 5 years in 1999 and 2004. There are currently 292 samples on exposure. Data from this study was used to develop the 2-year protocol [11].

VS3W was started in November 1994 as a 10-year program in Florida, Arizona, and Kentucky. In 2004 it was extended for another 5 years. There are currently 366 samples on exposure in Arizona, 750 samples on exposure in Kentucky, and 366 samples on exposure in Florida.

VS4W was started as a 2-year certification study but was subsequently converted to a 10-year VSI study in 2002. A set of readings was taken in 2003, 2005, and 2010, at which time the program was extended to 2015. There are currently 1,524 solid samples and 273 variegated samples on exposure in Florida, Arizona, and Ohio. This group of samples was used as the baseline for the development of an accelerated test protocol that will be discussed later in this chapter.

VS5W was started in 2005 and extended in 2010 for an additional 5 years. The samples put on exposure represent state-of-the-art product being sold at the time the test was begun.

The scope of these studies represents what actually exists on consumer's homes. Additionally, the samples continue to show change over time and the data collected is priceless when looking at warranty and product durability issues. Table 9.1 represents some of the colors on exposure in the four currently running studies. It indicated that after 10 years on exposure 90 % of the samples exposed in Florida and 80 % of the samples exposed in Arizona are still in their color ellipsoid. After 15 years the numbers fall to 80 % for Florida and 64 % for Arizona (whites only).

In 1997 VSI embarked on a 24-month outdoor weathering variability study. Four locations were selected: Louisville, KY; Cuyahoga Falls (Cleveland), OH; Chicago, IL; and LaQue, NC. 32 samples from VS2W were selected for testing, eight each from four color regions: gray, dark beige, light beige, and blue. To this sample set an additional 24 samples from VS2W and VS3W were added for a total of 56. Replicates from the original 32 samples were used in round 1 and round 2 of the accelerated weathering experiments. Additionally the ellipsoid values (EVs) obtained from this test program were used as the comparison EVs for the first two rounds of accelerated testing experimentation. Table 9.2 indicates the average ΔL value for each set of samples tested at all 4 locations, 24 replicates for each sample set.

An interesting outcome from the various outdoor test programs is that Cleveland, Ohio, consistently produces more color change than Florida or Arizona for the VSI's products. For example, during the 24-month variability study, the Cleveland location produced an average EV of >1.0, while the average EV of specimens in Florida was less than 0.20 and Arizona was approximately 0.30. Freeze-thaw conditions and industrial pollutants are the two primary conditions that exist in Cleveland and not in the other locations. For white specimens, Arizona consistently produces more color change due to yellowing of the base polymer as a result of high-UV and high-temperature conditions.

Table 9.1

Study	Color	#	0.5	1	1.5	2	4	5	10	15	20
	South Florida exposure—% in ellipsoids										
VS1W	Green	28	100	96	93	93	93	93	93	86	x
VS2W	Green	27	100	100	82	81	85	89	81	x	
VS3W	Green	30	100	100	100	100	100	93	x		
VS4W	Green	108		100	99	99					
VS1W	Yellow	44	100	98	98	95	93	90	86	80	x
VS2W	Yellow	55	100	100	100	100	95	91	85	x	
VS3W	Yellow	36	100	100	97	100	97	97	x		
VS4W	Yellow	35		100	100	100					
VS1W	White	24	100	100	96	92	100	100	100	83	x
VS2W	White	28	100	100	100	100	100	100	96	x	
VS3W	White	25	100	100	100	100	100	100	x		
VS4W	White	17		100	100	100					
VS1W	Medium beige	17	94	94	82	88	94	88	82	76	x
VS2W	Medium beige	57	100	91	75	67	61	56	42	x	
VS3W	Medium beige	63	100	98	95	98	95	98	x		
VS4W	Medium beige	60		100	98	98					
VS1W	Light beige	13	100	100	100	100	100	100	100	85	x
VS2W	Light beige	18	100	100	100	100	83	100	100	x	
VS3W	Light beige	50	96	98	98	98	98	96	x		
VS4W	Light beige	40		100	100	100					
	Arizona exposure—% in ellipsoids										
VS1W	Green										
VS2W	Green	27	96	96	93	96	93	93	78	x	
VS3W	Green	30	100	100	100	100	100	100	x		
VS4W	Green	108		100	100	100					
VS1W	Yellow										
VS2W	Yellow	55	100	100	96	96	91	91	89	x	
VS3W	Yellow	36	100	100	97	100	100	100	x		
VS4W	Yellow	35		100	100	100					
VS1W	White	22		91	95	77	82	84	86	64	x
VS2W	White	28	43	100	71	100	100	89	89	x	
VS3W	White	25	100	100	92	84	88	80	x		
VS4W	White	17		88	100	88					
VS1W	Medium beige										
VS2W	Medium beige	57	100	95	93	93	89	86	68	x	
VS3W	Medium beige	20	100	95	95	95	95	95	x		
VS4W	Medium beige	60		100	100	100					
VS1W	Light beige										
VS2W	Light beige	18	94	100	94	100	100	100	100	x	
VS3W	Light beige	50	100	100	100	98	100	100	x		
VS4W	Light beige	40		98	100	100					

"x"—pending measurement

Table 9.2 Selected VS4W data

Replicate study 24 month outdoor data			
Target	Mean ΔL	Rank	
18S	−2.60	1	
12K	3.10	2	Data
2B	4.51	3	Range
18H	5.31	4	12.16
17J	6.25	5	
13D	7.54	6	StdDev
16H	9.56	7	3.88

The importance of having this detailed knowledge of various outdoor exposures is that the key to creating an effective accelerated weathering test hinged on correlating to Cleveland results for colored specimens and Arizona for white specimens.

Accelerated Weathering for "Fast-Track" Certification

Although the 2-year outdoor weathering program represents a rapid certification cycle, industry requires faster methods of evaluating new formulations before bringing them to market. In an effort to provide a provisional fast-track approval process, the VSI formed an Accelerated Weathering Task Group (AWTG) in late 2000 whose mission was to develop an accelerated test procedure. VSI's Committee on Certification (COC) set very strict parameters for the acceptance of a fast-track approval protocol. This was a high bar that few accelerated weathering tests have ever met in any industry.

The first parameter was that an acceptable protocol must eliminate or reduce to an extremely low level the chance of a false positive result. Also known as a type I error, a false-positive result is one in which a material would achieve a positive, or "passing," result in the accelerated weathering test but subsequently fail the outdoor test. Secondly, any fast-track test must minimize "extreme false negatives." A false negative, or type II error, is a result in which a material achieves a negative, or "failing," result but subsequently passes the outdoor test. The COC defined an "extreme false negative" to be a result in which a very high performing material in the outdoor test failed in the accelerated test. The COC assumed any fast-track certification test would produce some false negatives, but the goal was to provide the best performing products with the fast-track certification option. An accelerated test that eliminated too many high performing products was of limited use to the VSI.

The task group ultimately conducted seven rounds of tests, numbered 1, 2, 3, 4, 5a, 5b, and 6. The original goal of the early rounds was to identify the best accelerated weathering test for vinyl siding products, defined as the test having the highest correlation coefficient to outdoor weathering data. As the AWTG reached this goal, the COC refined its scope in an effort to create a reliable fast-track certification process.

During the latter rounds, the specimens selected for the accelerated exposures were chosen because they exhibited relatively poor correlation with outdoor results. This meant they were more likely to show up as false positives or false negatives in the pass/fail tests conducted during the latter rounds. In other words, the sample set was intentionally biased in order to focus on improving both the exposure protocol and evaluation methodology.

The results and the evolution of the AWTG's work are described below.

Round 1

The first round of testing was conducted in both xenon and fluorescent UV accelerated weathering devices. For the xenon arc testing, two standard test methods were explored: SAE J1960 utilizing a daylight filter and ASTM G155 cycle 1, also using a daylight filter [12]. Tests were performed in the Atlas Ci65A. The xenon arc tests were to run for 2,000 h. The SAE J1960 test had to be terminated after 1,500 h due to specimen warping. This particular test cycle resulted in significantly hotter vinyl siding profile test specimens than the others, which likely accounted for the warping.

The cycle for SAE J1960, which has been replaced by SAE J2527, is as follows [13]:

- 1:00 Dark + water spray (front and back), 38 °C air temperature, 95 % relative humidity
- 0:40 Light with irradiance set to 0.55 W/m^2 at 340 nm, 70 °C black panel, 47 °C chamber air, 50 % RH
- 0:20 Light + front water spray with irradiance set to 0.55 W/m^2 at 340 nm, 70 °C black panel, 47 °C chamber air, 50 % RH
- 1:00 Light with irradiance set to 0.55 W/m^2 at 340 nm, 70 °C black panel, 47 °C chamber air, 50 % RH

    The cycle for ASTM G155 Cycle 1 is as follows:

- 1:42 Light with irradiance set to 0.35 W/m^2 at 340 nm, 63 °C black panel (chamber air and relative humidity not specified)
- 0:18 Light + front water spray with irradiance set to 0.35 W/m^2 at 340 nm, temperature and RH not specified

The fluorescent ultraviolet lamp and condensation (fluorescent UV) test utilized UVA-340 lamps as defined in ASTM G154 [14]. The cycle was 12 h of light at 0.89 W/m^2 at 50 °C, followed by 12 h of condensation at 60 °C. The devices used were the QUV with Solar Eye irradiance control.

Table 9.3 shows the xenon data for ASTM G155 cycle 1 at 2,016 h. Table 9.4 shows the xenon data for SAE J1960 at 1,500 h. 2,000 h data was unavailable due to sample warping, as discussed above. Table 9.5 shows 2,000 h data from the

Table 9.3 ASTM G155 Cycle 1

2,016 h G155 Xenon				
	Mean ΔL	StdDev	Rank	Data
2B	−0.44	0.23	2.5	Range
12K	−0.41	0.08	2.5	3.84
18S	−0.21	0.23	2.5	
17J	−0.06	0.12	2.5	StdDev
18H	0.37	0.10	5	1.36
13D	0.93	0.04	6	
16H	3.40	0.09	7	
Pearson correlation=0.67				

Table 9.4 SAE J1960 (J2527)

1,500 h J1960 Xenon				
	Mean ΔL	StdDev	Rank	Data
17J	−0.77	0.05	2	Range
2B	−0.70	0.20	2	3.37
12K	−0.67	0.13	2	
18H	−0.36	0.11	5	StdDev
18S	−0.22	0.33	5	1.19
13D	0.02	0.33	5	
16H	2.60	0.07	7	
Pearson correlation=0.51				

Table 9.5 (G154, VSI cycle 1)

2,000 h fluorescent/condensation				
	Mean ΔL	StdDev	Rank	Data
18S	0.48	0.14	1	Range
12K	2.45	1.59	2	5.97
17J	4.53	1.48	4.5	
13D	4.59	1.73	4.5	StdDev
16H	4.65	1.70	4.5	1.94
18H	4.87	0.13	4.5	
2B	6.45	0.05	7	
Pearson correlation=0.75				

fluorescent UV. The fluorescent UV test cycle had the best correlation to outdoor weathering data at 2,000 h. To determine if the correlation could be improved, the test was run a second time with an identical sample set, this time to 3,000 h. As Table 9.6 indicates greater correlation was achieved.

Table 9.6

	3,000 h Fluorescent/condensation			
	Mean DL	StdDev	Rank	Data
18S	1.03	0.12	1	Range
12K	5.18	0.15	2	7.21
18H	5.90	0.31	3.5	
17J	5.95	0.07	3.5	StdDev
2B	7.91	0.11	5	2.55
13D	8.23	0.22	6.5	
16H	8.24	0.12	6.5	
Pearson correlation = 0.92				

Table 9.7

Pearson correlation	
3,000 h vs. 24-month Ohio	0.78
2,000 h vs. 24-month Ohio	0.60
2,000 h vs. 3,000 h	0.90

Rounds 2 and 3

The fluorescent UV testing performed in round 1 was repeated in round 2, using the same sample set, with, three additional labs participating to verify the results. Round 2 also included one additional sample set. This sample set consisted of specimens that passed VS2W but displayed significant color change—i.e., they were close to failing. This round was also the first attempt to quantify the false positives and false negatives generated by the accelerated test method versus outdoor Ohio testing. Table 9.7 compares 2,000 and 3,000 h data to Ohio outdoor and 2,000 h data to 3,000 h data.

Round 3 used the same fluorescent UV test cycle as rounds 1 and 2 plus one experimental cycle using UVA-340 lamps: 20 h of light at 0.89 W/m^2 at 50 °C, followed by 4 h of condensation at 45 °C. The sample set used was from VS4W. The testing was conducted at two laboratories.

When the data was analyzed, it became apparent that using standard rank-order correlation produced too many false positives, meaning that a sample could pass the accelerated test but fail the 24-month outdoor test. Since the goal of the accelerated weathering task group was to develop a method that would allow fast-track conditional approval for new color formulations, it was deemed unacceptable to have false positives. The market effect of having false positives could potentially result in a product passing the provisional accelerated test and then losing its certification when it failed the mandatory outdoor testing. To producers of vinyl siding, this potential outcome was unacceptable.

No xenon arc exposures were performed in round 2. In round 3, some experimentation was done with xenon arc cycles in an effort to improve correlation. However, no significant improvements arose from these experiments.

The accelerated weathering task group members reevaluated their analysis method. They determined that rank-order correlation between the outdoor and accelerated tests was less important than whether the accelerated test method accurately predicted which samples would pass outdoor testing and which would fail. In an effort to determine this, threshold maximum EVs were used in subsequent testing.

Round 4

Armed with the new direction in how to analyze the data round 4 was begun. This round of testing was conducted in fluorescent UV chambers. 29 colored PVC, 3 white PVC, and 9 colored non-PVC samples from VS4W were tested. The fluorescent UV test method used was identical to the previous three rounds of testing. Four laboratories participated in these tests.

Separately, two of the laboratories conducted additional xenon arc exposures independent of the official round 4 protocol. Among the cycles tested was one designed to be similar to the fluorescent UV method: 12 h of light followed by 12 h of dark plus water spray. Multiple variations of this xenon cycle were used.

The results of round 4 indicated several interesting facts.

1. The xenon test method showed very poor correlation to VS4W outdoor data, despite significant experimentation; see Fig. 9.1. The decision was made to drop further xenon tests from the program.
2. While the fluorescent UV test method was run to 3,500 h, substantial color change took place in the first 1,500 h.
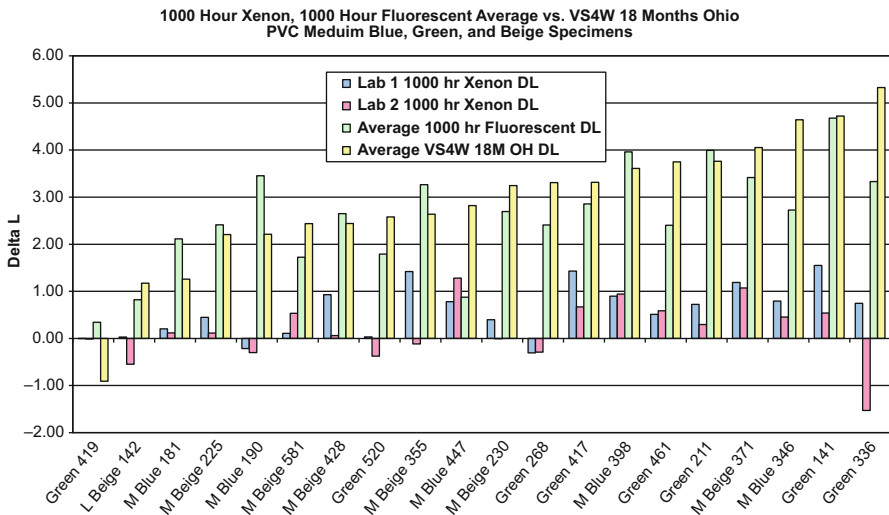
Fig. 9.1

Table 9.8 1,500 h fluorescent UV exposure ΔE Student's *t*-test results

	Accelerated and outdoor		
	Results agree	Results disagree	
Outdoor failures	93.40 %	6.60 %	
38 comparisons			(False positives)
PVC vs. PVC Ref.			
Outdoor passes	90.50 %	9.50 %	
21 comparisons			(False negatives)
Non-PVC vs. PVC Ref.			

3. The correlation to outdoor tests for non-white PVC samples was very good, but the white samples did not weather the same as they did in the Arizona outdoor testing (hot and dry).
4. Though the overall correlation was very good, over 90 % (see Table 9.8), it was determined that the number of false positives was still too high.

Round 5, A and B

To address what was learned during round 4, round 5 consisted of 2 different fluorescent UV test cycles. The first 12 h of light at 0.95 W/m² at 50 °C followed by 12 h of condensation at 60 °C, for 3,000 h. The second cycle, to simulate the hot dry climate that is harshest to white siding products, was continuous light at 0.95 W/m² at 50 °C for 1,800 h. Samples for the round 5 initially consisted of the following:

VSI accelerated weathering round 5A specimens			
	Colors	Whites	
Round 4 VS4W PVC failures	1	1	
Round 4 VS4W PVC passes	7	1	10 PVC repeats for round 4
New PVC specimens	8	5	13 new PVC specimens
New non-PVC specimens	15	2	17 new non-PVC specimens
Total	31	9	40 total specimens

After further review it was decided to add additional samples and break round 5 into two parts. Round 5A tested the above samples; round 5B would test additional samples.

Repeats from round 5A	8
Repeats from round 4	15 (not included in round 5A)
New untested colors	9 (not included in round 5A)
Total	32

Seven labs participated in round 5A. In an attempt to insure that no false positives would occur, an EV of 0.90 after 3,000 h of condensation/light and an EV of 1.50 after 1,800 h of continuous light were set. For a sample to pass the accelerated testing, all replicates from both tests must pass. As always, three replicates of each sample were run in both test cycles.

The results of round 5 indicated the following:

1. After 900 h of continuous light, significant color change had occurred. Round 5A/continuous light was terminated, and color measurements were taken.
2. It appeared that the 2,000 h data from the round 5A/light-condensation test might be as useful as the 3,000 h data allowing for a shorter test.
3. False positives were not completely eliminated. A dark red specimen that had failed in Ohio and Florida passed the accelerated test.

Round 6

A final set of adjustments was made to the fluorescent UV test cycle in an attempt to eliminate the false positive and reduce the number of extreme false negatives. Temperatures in the condensation function were decreased. Each of the following cycles was run in four laboratories:

Step 1: Condensation for 12 h at 50 °C or 55 °C
Step 2: UV for 12 h, 0.95 W/m^2 at 50 °C (UVA-340 lamps)
Step 3: Return to Step 1

A total of 43 specimens, 3 replicates each, were tested in each cycle. Most specimens were repeats from round 5. This set included all of the specimens whose accelerated testing results were considered extreme false negatives based on earlier rounds of tests. Evaluations were completed at 2016 and 3,000 h. Most change was seen by 2,016 h, as evidenced by results from a reference gray siding profile specimen (Table 9.9). Furthermore, tests run at 55 °C exhibited more color change versus those run at 50 °C.

While the cycle with the 55 °C condensation temperature did improve correlation by reducing the number of extreme false negatives, it did not eliminate the single false positive experienced in previous rounds, as seen in Table 9.10. The passing EV was set at 0.35 to achieve the best match to the outdoor results.

Table 9.9 Reference gray ΔL

	50 °C condensation	55 °C condensation
2,016 h	2.59	5.14
3,000 h	2.90	5.67

Table 9.10

Accelerated passing EV $\Longleftarrow$	0.35	
	Outdoor fail	Outdoor pass
Accelerated pass	1 (2 %)	18
Accelerated fail	16	8 (19 %)

Based on these results, the AWTG determined that the risk of producing a false positive in this accelerated test protocol was approximately 2 %. The risk of false negatives was approximately 19 %. It is important to note that each round of testing narrowed the specimen set to those considered the most problematic for the accelerated tests, creating a bias in the data away from high correlation. Round 4 showed greater pass/fail correlation than round 6 due to this bias.

Conclusions and Discussion

The use of accelerated weathering testing for product certification is a significant, even daunting, technical, and managerial challenge. The VSI overcame many of the technical challenges through a 6-year regime of accelerated weathering tests. It created a novel test cycle in a standard fluorescent UV and condensation weathering device that achieved high correlation with outdoor weathering and correctly anticipated the pass/fail results of the 2-year certification test more than 90 % of the time. Despite this technical achievement, the managerial risk to the VSI was too great and the decision was made not to include a fast-track, accelerated test in its certification program.

Although the project failed to meet VSI's objectives, this work provides many insights into accelerated weathering. Some of these lessons are discussed below.

1. Through examining different outdoor test locations, different accelerated weathering lab techniques and equipment, coupled to the development of realistic evaluation tolerances, a robust accelerated test method can be developed that will predict outdoor weathering results with a high degree of confidence. However, this study proves that significant resources, managerial attention, and patience are required to achieve this result.
2. For PVC siding products, temperature and moisture have a significant synergistic effect on photodegradation. For colored specimens, inclusion of moisture in the accelerated test was necessary to match the outdoor test results from Ohio. For white specimens, replicating the Arizona environment was critical.
3. Matching the sunlight spectrum in the long-wave UV, visible, and IR regions was NOT a significant factor in replicating outdoor test results for PVC-capped siding. If these regions of the spectrum were a significant factor in the weathering of PVC-capped siding, one might have expected xenon arc weathering chambers to have produced better correlation than these results indicate.
4. Reducing accelerated weathering test temperatures was a key breakthrough in obtaining high correlation to outdoor results. Most fluorescent UV test cycles run at 60 °C in the UV function. VSI found that reducing this to 50 °C significantly improved correlation. Even though xenon correlation was lower overall, the test cycle run at 63 °C black panel temperature outperformed the cycle run at 70 °C black panel temperature. In fact, the test at 70 °C resulted in unrealistic warping of specimens, which can occur when unstabilized PVC temperatures

rise above 70 °C. High dosages of IR radiation, which is typical of xenon arc exposures, combined with the insulating characteristics of PVC specimens, appear to result in unrealistic specimen temperatures in xenon arc tests.

5. The cycle which provided the best correlation with the 2-year outdoor results was the following:

Step 1: Condensation for 12 h at 55 °C black panel temperature.
Step 2: UV for 12 h, 0.95 W/m^2 at 50 °C black panel temperature with UVA-340 lamps.

Test time: 2,016 h

References

1. Lewis B, Frakes B (1997) Advances in weatherable plastics for the construction industry. Kent State University, Americhem
2. Summers JW, Rabinovitch EB (1997) Weathering of vinyl and other plastics. The Geon Company, New Haven, CT
3. ASTM Standard D3679 (2011) Standard Specification for Rigid Poly(Vinyl Chloride) (PVC) Siding. ASTM International, West Conshohocken, PA. doi:10.1520/D3679-11, www.astm.org
4. ASTM Standard D7254 (2007) Standard Specification for Polypropylene (PP) Siding. ASTM International, West Conshohocken, PA. doi:10.1520/D7254-07, www.astm.org
5. ASTM Standard D6864 (2011) Standard Specification for Color and Appearance Retention of Solid Colored Plastic Siding Products. ASTM International, West Conshohocken, PA. doi:10.1520/D6864-11, www.astm.org
6. ASTM Standard D7251 (2011) Standard Specification for Color and Appearance Retention of Variegated Color Plastic Siding Products. ASTM International, West Conshohocken, PA. doi:10.1520/D7251-11, www.astm.org
7. VSI Product Certification Program's Official List of Certified Products. Vinyl Siding Institute, Washington, DC, revised 25 Jan 2013
8. (2009) VSI Outdoor Weathering Practice. Vinyl Siding Institute, Washington, DC
9. AATCC TM 173 (2009) CMC: Calculation of Small Color Differences for Acceptability. American Association of Textile Chemists and Colorists, Research Triangle Park, NC, 2007
10. ASTM Standard D2244 (2011) Standard practice for calculation of color tolerances and color differences from instrumentally measured color coordinates. ASTM International, West Conshohocken, PA. doi:10.1520/D2244-11, www.astm.org
11. Technical research report for weatherability of vinyl siding products. VS2W, Vinyl Siding Institute, Washington, DC

12. ASTM Standard G155 (2005a) Standard practice for operating xenon arc light apparatus for exposure of non-metallic materials. ASTM International, West Conshohocken, PA. doi:10.1520/G0155-05A, www.astm.org
13. SAE Standard J2527 (2004) Performance based standard for accelerated exposure of automotive exterior materials using a controlled irradiance xenon-arc apparatus. SAE International, Warrendale, PA
14. ASTM Standard G154 (2012) Standard practice for operating fluorescent ultraviolet (UV) lamp apparatus for exposure of nonmetallic materials. ASTM International, West Conshohocken, PA. doi:10.1520/G0154-12

Chapter 10
Shelf Life Assessment of Poly(ethylene-co-vinyl acetate) and Polyester Polyol Resins Used as Adhesives

Mogon Patel, Laura Pilon, Peter Beavis, Paul Morrell, Niaz Khan, Anil Kumar, Julie Etheridge, Tim Cartwright, and Gregory Von White II

Abstract The thermal stability and ageing properties of Vinamul 3161 poly(ethylene-co-vinyl acetate) and AS1160 polyester polyol resins have been investigated in support of shelf life assessment and also to identify storage conditions that may extend product life. These resins are typically used in the production of adhesives for specialised applications either as binders for filler particles or to minimise the relative movement of materials in multi-material assemblies. Our studies confirm that both these resins are susceptible to moisture and hydrolysis chemistry which potentially limits shelf life. The EVA resin readily accumulates acetic acid through hydrolysis of the pendent acetate groups which increases both the acidity (pH) and volatile outgassing characteristics of the material. The temperature sensitivity of pH combined with Arrhenius kinetics was used to identify a useful shelf life for EVA in conditions representative of normal storage conditions. In a separate set of experiments, relatively short-term thermally accelerated ageing studies have been carried out on AS1160 polyester polyol to investigate sensitivity to humidity, temperature and open/close ageing conditions. This material is hygroscopic, readily accumulates moisture and is susceptible to chain scission with molecular weight changes linked to the hydrolysis-esterification equilibrium. These changes do not however adversely impact adhesive bond strength allowing the resin to be potentially used significantly beyond the manufacturer recommended shelf life limit.

Keywords Characterisation • Thermal stability • Poly(ethylene-co-vinyl acetate) • Polyol • Accelerated ageing • Bond strength • Stability • Adhesives • Hydrolysis • Chain scission • Molecular weight • Temperature sensitivity • Humidity • Shelf life • Multi-material assemblies • Esterification • Acidity • Product life

M. Patel (✉) • L. Pilon • P. Beavis • P. Morrell • N. Khan • A. Kumar
J. Etheridge • T. Cartwright
Atomic Weapons Establishment (AWE), Aldermaston, Reading RG7 4PR, UK
e-mail: mogon.patel@awe.co.uk

G. Von White II
Sandia National Laboratories, Albuquerque, NM, USA

Introduction

For many modern products, long lifetimes (up to several decades) are advantageous, particularly for high consequence applications (e.g. nuclear energy, defence, space, etc.). There is also an increasing requirement for materials (resins, ingredients) and systems to last much longer than initially envisaged (>20 years) requiring programmes to be in place to support a life extension. In most cases, it is typically the organic materials that will age relatively faster than other materials (inorganic, metals, etc.), and therefore the chemical mechanisms and rates of reactions of these materials need to be understood in order to scientifically justify a life extension.

The technical challenge in high consequence defence-related multi-material assemblies is significant as materials must withstand complex and changing environments for decades that include combinations of heat, which may accelerate chemical reactions, radiation (alpha, beta, gamma and neutron) causing material degradation, mechanical loads (with reduced stiffness and changes in damping properties through life), varying degrees of oxygen and moisture (corrosion, hydrolysis) and volatile organics (degradation and corrosion reactions) [1]. The design of accelerated material ageing experiments to replicate service is therefore fraught with potential pitfalls.

Although temperature is the most common method of ageing materials, it is inappropriate when the issue is the radioactive degradation of any material. However, in practice temperature is a key parameter affecting chemical kinetics, and its use is normally based on the application of Arrhenius kinetics. In the absence of mechanistic information, the normal practice is to use the rule of thumb (the rate of reaction doubles per 10 °C rise) to identify a simulated age. However in practice, this is rarely true for many materials and multi-material assemblies and questions the validity of accelerated ageing trials based upon this rule of thumb. Therefore great caution is required in the use of Arrhenius kinetics in life prediction [2].

Another area of interest in the defence industry is the security of supply of key ingredients and the identification and qualification of new or replacement materials. It is increasingly difficult (and in many cases impossible) to purchase the exact same materials used in the production of early assemblies/materials. The preferred option for material supply (particularly the organic materials, with volatile constituents) in the defence industry is to have greater (in-house) control over the production of constituents and formulation of materials. All programmes to develop new or replacement materials require the delivery of assessments/tests to understand the ageing and chemical compatibility issues.

Commercially, EVA is the base polymer for some athletic shoes and also used in photovoltaic (PV) cells [3, 4]. Durability is of particular concern in the solar cells industry where EVA adhesive is used as an encapsulant for photovoltaic cells [5, 6]. On exposure to UV light, the material changes colour over a number of years, with potentially significant loss in power from the cell [7, 8].

In this paper, the key organic materials under consideration are poly(ethylene-co-vinyl acetate) (denoted EVA) and polyester polyol (denoted PL) resins. These resins are employed as adhesives for a number of specific applications either as

binders for filler particles or to minimise the relative movement of materials in multi-material assemblies. A key area of interest is to understand shelf life and options for shelf life extension. Age-related changes to the adhesive could potentially impact the gas phase (resulting in corrosion of metals, sensitisation, etc.) and also influence system dynamics (e.g. de-bonding, compression set, etc.) with potential changes in system performance and/or safety [9]. We detail our initial studies on poly(ethylene-co-vinyl acetate) and AS1160 polyester polyol resins to understand thermal stability, useful shelf life and options for life extension. The general methodology, the analytical methods and the future strategy from an ageing and shelf life perspective are discussed.

Materials

Poly(ethylene-co-vinyl acetate) Resin

The poly(ethylene-co-vinyl acetate) resin used in this study (see Fig. 10.1) was adhesive grade Vinamul 3161 emulsion, batch number 2235/240211, and manufactured by Celanese in February 2011. The resin exhibits a glass transition temperature of approximately 3 °C, no melting point, and hardens on drying in air. The material was used as received and typically exhibits a pH of 5–7. The material is known to release acetic acid through hydrolysis of the acetate groups which alters the pH of the resin, and specification limits require a minimum pH of 4 (when stored at 20 °C), below which the resin cannot be used in the production of multi-material assemblies.

AS1160 Polyester Resin

Baycoll AS1160 is a highly branched polyester polyol (PL) consisting of four different constituents (see Fig. 10.2). The material typically has a low acid number, and a majority of end groups are hydroxyl that can react with a phenyl-based isocyanate to produce a polyurethane adhesive. Specification limits require the water
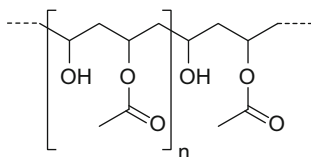
Fig. 10.1 The molecular structure of poly(ethylene-co-vinyl acetate), Vinamul 3161 resin. Water and/or hydroxyl groups in close proximity to the vinyl acetate groups are thought to promote hydrolysis chemistry leading to the production of acetic acid
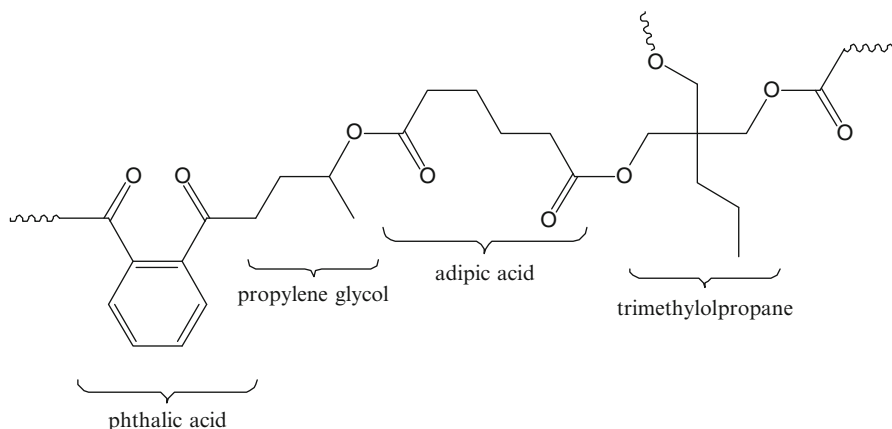
Fig. 10.2 Baycoll AS1160 resin showing the various chemical constituents, 43.5 wt% adipic acid, 43 wt% propylene glycol, 3.9 wt% phthalic acid and 9.6 wt% trimethylolpropane

content to be a maximum of 900 ppm and the hydroxyl concentration (based on ASTM D2849-69) to be 170 ± 10 mg/KOH g (expressed as KOH equivalent).

The maximum allowable manufacturer recommended shelf storage life for AS1160 is 6 years when stored at ambient conditions. It should be noted that the resin is no longer commercially available; however there is requirement to provide justification for the continued use of the available stock holding (which is beyond its manufacturer recommended 6-year shelf life) until a new replacement material is potentially sourced.

Test and Analysis

Ageing Studies on EVA Resin

The variation of resin pH as a function of time and temperatures was investigated to understand kinetics representative of the underlying chemical mechanism(s) that limits useful shelf life. Vinamul 3161 resin was aged in sealed containers and at four different temperatures (32, 45, 60, 75 °C) with the pH of the emulsion monitored at regular intervals using a Mettler Toledo SevenEasy™ pH metre. Temperature sensitivity was assessed by determining changes in pH, and the Arrhenius plot was used to predict the rate of change in pH at temperatures specific to shelf storage conditions (normally 20 °C).

Table 10.1 Experimental design and initial results from studies to assess the sensitivity of AS1160 resin to temperature, humidity and ageing in a sealed or open environment

	F1	F2	F3	F4	F5
Ageing regime	Open to air	Sealed	Sealed	Open to air (wet)	Open to air
T (°C)	90	60	75	60	75
RH (%)	–	–	–	20	–
Dew point (°C)	–	–	–	29	–
Hydroxyl concentration by titration (mg/KOH)					
Zero time (baseline)	177	177	177	177	177
7-day ageing	189	197	213	271	252
Butt tensile bond strength (MPa) by ASTM D2095					
Zero time (baseline)	42 ± 5	42 ± 5	42 ± 5	42 ± 5	42 ± 5
21 days				28 ± 7	
28 days	40 ± 3		31 ± 4	36 ± 6	39 ± 2

Ageing Studies on AS1160 Resin

The experimental test matrix for studies on AS1160 resin is detailed in Table 10.1. These studies do not advocate studies in inert gas atmospheres as AS1160 is normally stored in air. To minimise diffusion effects/gradients between the bulk and surface of the material, samples were aged as thin samples with typically 30–40 g of material aged in 250 ml conical flasks at each temperature. The flask openings were covered with aluminium foil secured with metal wire. For experiments F1, F4 and F5, the aluminium foil was punctured with three small holes to ensure ageing in a non-sealed environment, enabling the exchange of volatiles/gases with the oven atmosphere. For experiments F2 and F3, ageing in a closed environment was simulated by heating AS1160 in a sealed conical flask.

As the sensitivity of AS1160 to humidity is not well understood, the experimental matrix incorporates a controlled humidity experiment (F4). The use of 60 °C combined with 20 % RH correlates to a dew point of 29 °C and simulates relatively humid conditions. Under these conditions, the rate of moisture diffusion through the resin is accelerated with temperature potentially degrading the material either through hydrolysis, chain scission or plasticisation effects.

Trials F2 and F3 were included to assess whether AS1160 is sensitive to the retention of volatile/gaseous species. In particular, a comparison of results between F3 and F5 will provide information on whether the retention of volatiles/gaseous species is important and whether this can alter the degradation chemistry and/or rate.

Gel Permeation Chromatography

For both resins, gel permeation chromatography (GPC) was employed to measure variation in molecular weight and molecular weight distributions. For the EVA resin, samples were dissolved in tetrahydrofuran (THF) and analysed using a Viscotek TDA GPC instrument calibrated against EasiCal poly(styrene) standards. The peaks observed from the EVA samples were within the range covered by the EasiCal poly(styrene) calibration standards used within this study.

For the AS1160 resin, triple detection and conventional calibration analyses were performed on a Viscotek TDA instrument. Acetone (HPLC grade) was used as the eluent with a flow rate of 1 ml/min. Two PL gel mixed-E 300 mm columns were used with an oven temperature of 35 °C. Calibration was performed using monodisperse poly(methyl methacrylate) standards, and three runs were performed per sample (concentration ~40 mg ml^{-1}).

Moisture Content and Hydroxyl Functionality

The moisture levels in AS1160 were measured using Karl Fischer Coulometry, and the hydroxyl content was measured based on the standard ASTM D2849-69 procedure [10].

Bond Strength

When the AS1160 resin is mixed with isocyanate, and cured for up to 24 h in dry (typically less than 15 % RH), a thixotropic polyurethane adhesive is formed. The adhesive is commercially used to bond metals, organic and inorganic materials, and is particularly useful for reducing the relative movement of components in multi-material assemblies. The performance of the polyurethane adhesive requires the ultimate tensile strength (UTS) to be a minimum of 15 MPa when measured using butt tensile specimens by ASTM Test Method D2095.

Results and Discussion

Shelf Life Assessment of EVA Resin

Poly(ethylene-co-vinyl acetate) resins are known to hydrolyse to the parent carboxylic acid and an alcohol. This mechanism increases the acidity of the resin, generates pendent hydroxyl functional groups on the EVA and ultimately limits the shelf life of the resin. Water, and/or hydroxyl groups in close proximity to the vinyl

acetate groups, is thought to promote hydrolysis chemistry. The production of acetic acid is associated with an increase in acidity and a reduction in resin pH. Figure 10.3 shows pH versus time measured at a number of different temperatures. The sensitivity to temperature fits Arrhenius kinetics (see Fig. 10.4), and the resulting activation
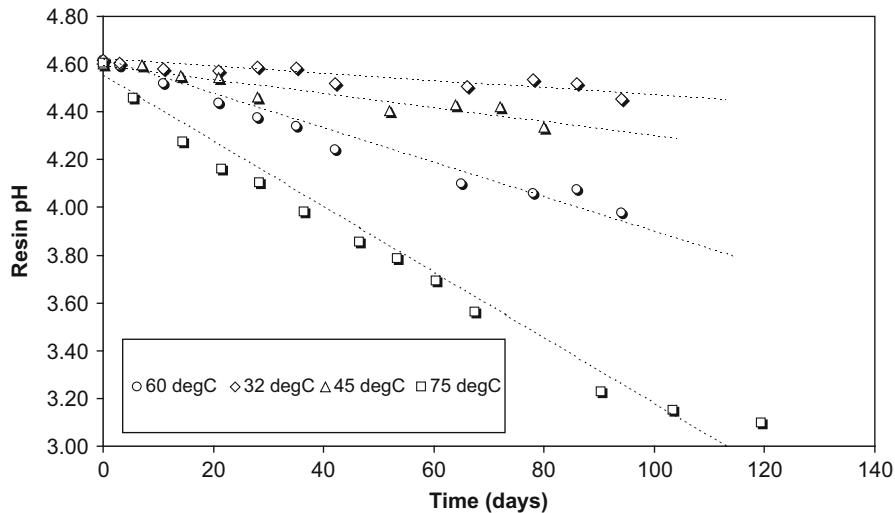
Fig. 10.3 Acidity of the uncured EVA resin (emulsion) monitored as a function of time and at a number of different temperatures. The slope of the linear regression fit to the data was used to estimate the rate of hydrolysis
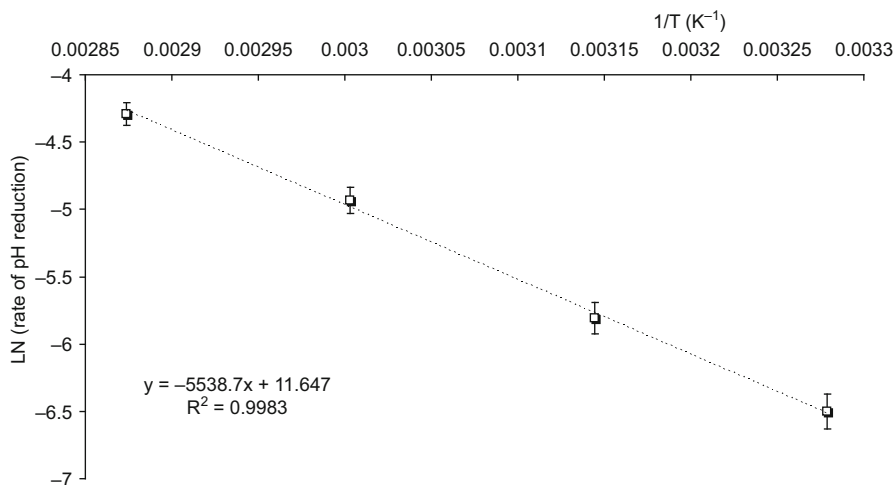
Fig. 10.4 Arrhenius plot of the rate of change in EVA resin acidity as a function of temperature. This plot allows the rate of change in acidity at temperatures representative of typical resin storage conditions (~20 °C)

energy estimated from the slope is ~46 kJ/mol. The Arrhenius plot provides a route to the determination of the rate of change in resin acidity at temperatures representative of typical shelf storage conditions (20 °C) and ultimately leads to resin shelf life prediction based on our failure criteria that a resin exhibiting a pH of below 4 is deemed not suitable for use in manufacturing operations. This methodology predicts a pH reduction rate of less than 0.5 over 6 months with a typical resin shelf life estimated within 2–3 years. This prediction is, however, highly dependent on the health or age of the material (as determined by zero time pH data) when first prepared by the manufacturer.

Figure 10.5 shows the results of GPC characterisation of the uncured EVA resin as a function of age. The chromatograms suggest a relatively broad distribution with weight average molecular weight within the range of 500,000–600,000 g/mol (relative to polystyrene standards). In particular, ageing induces an increase in the low molecular weight peak (at 12.3 mL) relative to the high molecular weight shoulder (at 11.5 mL) with a general shift to the right-hand side (towards lower molecular weight). The shift towards relatively lower molecular weights is indicative of thermally induced oxidative chain scission of the EVA and is agreed with observations reported on similar materials by Jing Jin et al. [11]. To determine whether these age-related changes influence the key properties of the material as an adhesive, a series of mechanical property studies have been carried out and reported in our previous publication [12].
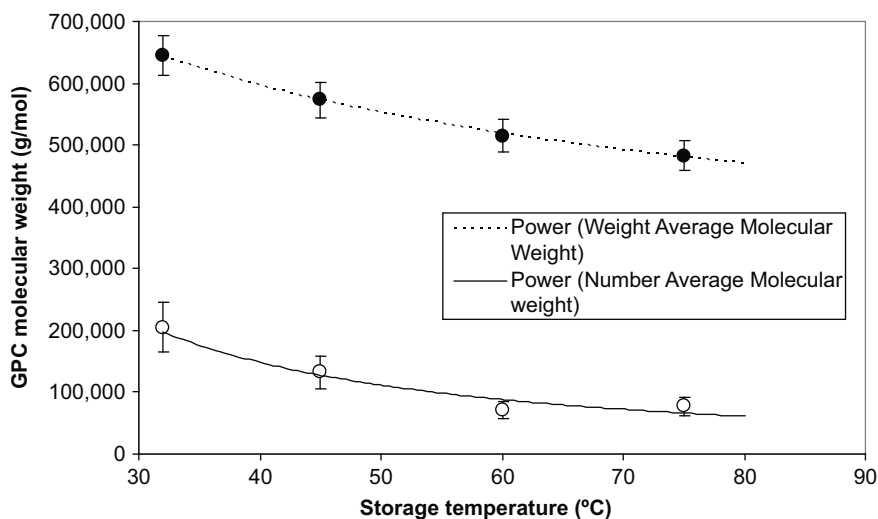
Fig. 10.5 Vinamul 3161 EVA resin molecular weight as a function of resin storage temperature (over 4 months) as measured by GPC. The weight average and number average trends fit a power law relationship with accelerated ageing, inducing a gradual reduction in molecular weight through oxidative chain scission chemistry

AS1160 Resin Ageing Studies

Our ageing studies clearly show that AS1160 resin is relatively hygroscopic and readily accumulates moisture; see Figs. 10.6 and 10.7. All aged samples show elevated moisture levels which are above specification requirements (900 ppm) compared to zero time levels. This is particularly apparent for sample F4 which has been aged in relatively humid conditions.

The results in Table 10.1 show that ageing also potentially elevates the hydroxyl concentrations which are above specification limits (170 ± 10 mg/KOH g) compared to zero time values. However, it should be noted that the absorption of moisture may provide inaccurate hydroxyl concentration measurements due to the destruction of the esterification reagent and so the hydroxyl values should be treated with caution.

In addition, complex changes in GPC molecular weight were observed that could be related to the acid/alcohol versus ester/water equilibrium shown in Fig. 10.8. In the highest temperature ageing study (see Fig. 10.9), a significant molecular weight increase was noted, while the remainder broadly decreased. As expected, the sample aged under humid conditions had the largest initial decrease in molecular weight confirming the sensitivity of the material to hydrolysis. There are also clear differences in open to air and sealed ageing regimes (see Fig. 10.10) presumably because ageing in open conditions leads to loss of low molecular weight species.

With respect to real-time ageing, a significant decrease in M_n (number average molecular weight) and a smaller decrease in M_w (weight average molecular weight) during real-time ageing over 6 years are shown in Table 10.2. It is probable that relatively small increases in the population of low molecular weight oligomers have
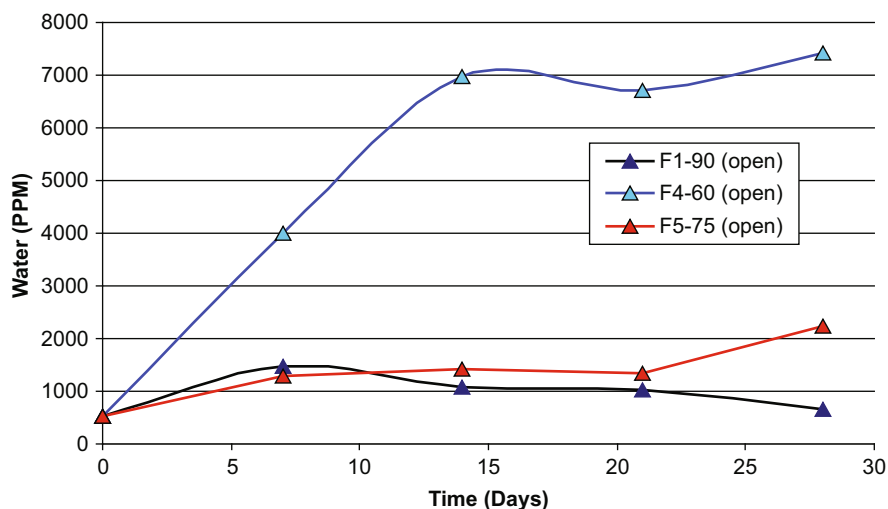
Fig. 10.6 AS1160 resin moisture content by Karl Fisher titration. All aged samples show an increase in moisture content
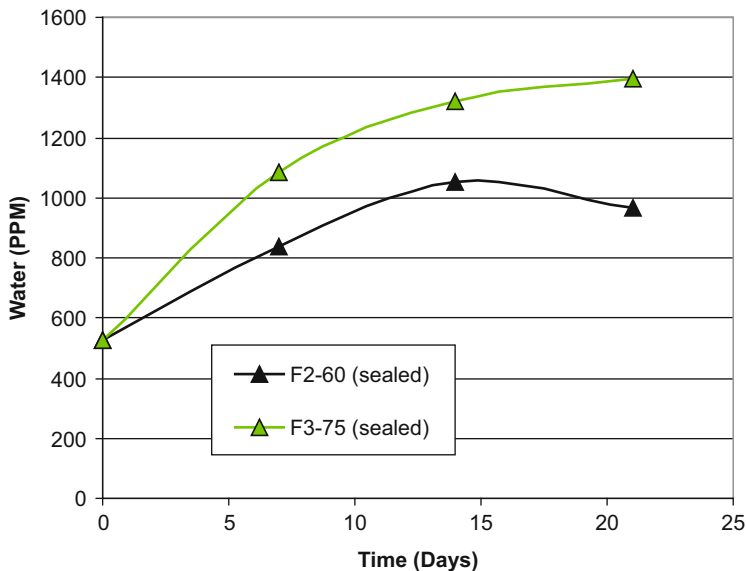
Fig. 10.7 AS1160 resin moisture content by Karl Fisher titration. All aged samples show an increase in moisture content
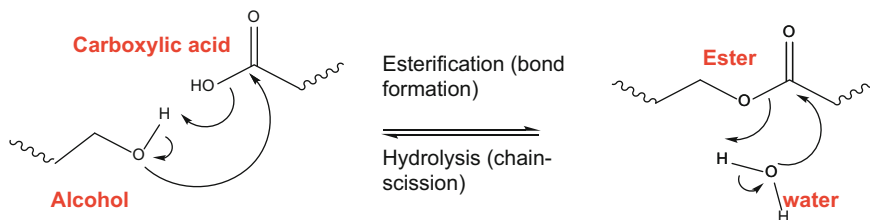
Fig. 10.8 The hydrolysis-esterification equilibrium is thought to play an important role in determining the shelf life of AS1160 polyester polyol resin. Increased humidity is likely to promote ester hydrolysis and chain scission inducing a reduction in resin molecular weight

led to this decrease, since M_n is strongly affected by low molecular weight components of the molecular weight distribution. However, overall most aged samples showed values (after 28 days) that are not too different to baseline zero time data and suggest that Baycoll AS1160 may be fairly resilient to thermal ageing although real-time ageing does appear to suggest more significant changes than that observed through accelerated ageing.

Our infrared (IR) and nuclear magnetic resonance (NMR) spectroscopy did not show significant changes in the material, either in real-time ageing over a 6-year period or in accelerated ageing.
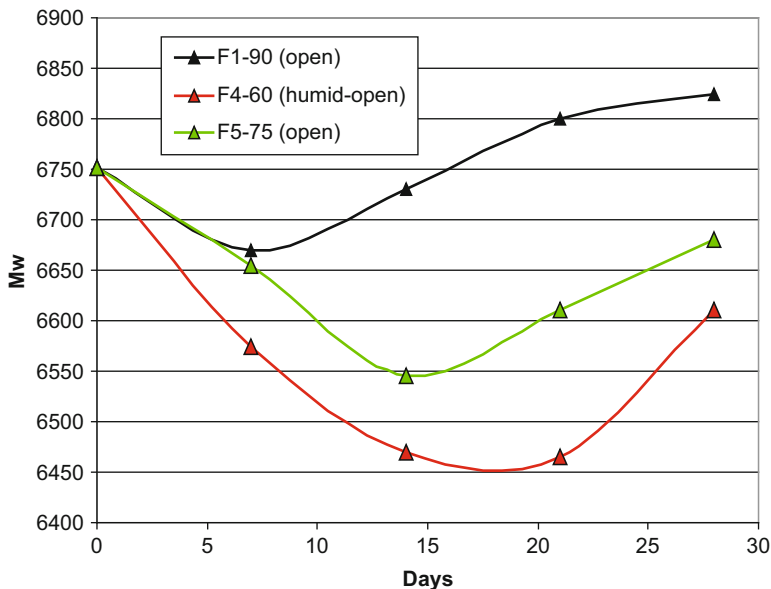
Fig. 10.9 Typical molecular weight (g/mol) changes in open to air and humid regimes
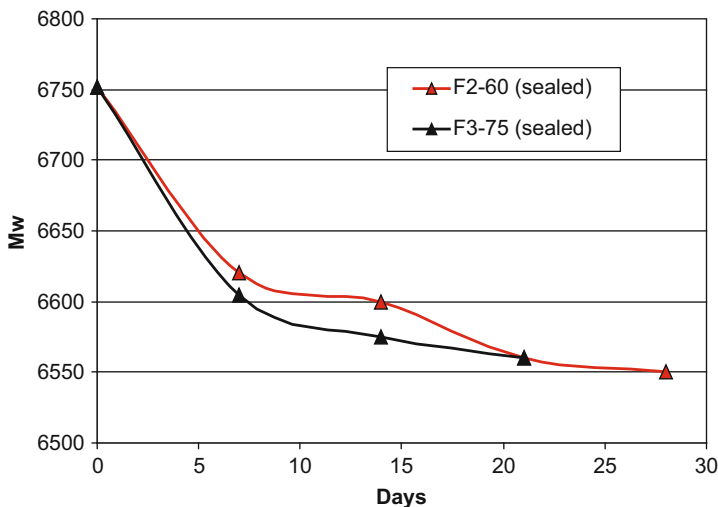
Fig. 10.10 Typical molecular weight (g/mol) changes in sealed ageing regimes

Table 10.2 Data from real-time aged Baycoll AS1160 resin showing a reduction in GPC molecular weight (units in g/mol)

Date of analysis	M_n	M_w	Polydispersity (M_w/M_n)
2005	1,950	3,800	1.95
2011	1,081	3,573	3.31

Polyurethane Adhesive Bond Strength

Although accelerated ageing suggests significant changes in resin moisture levels and complex changes in molecular weight, these changes do not appear to adversely affect adhesive bond strength which still remains well within specification limits (above 15 MPa); see Table 10.1. The bond strength remains well within specification limits even under harsh aggressive conditions, and it is unlikely that any moderate change to the polyol properties will decrease this strength to the point where it no longer satisfies the specification limits. However, a general observation is that the quality and reliability of the adhesive joints produced is found to decrease as the resin ages. This is presumably because the absorbed moisture leads to increased carbon dioxide production (through reaction with isocyanate) leading potentially to a more porous and poor-quality adhesive joint.

Overall, the accelerated ageing study did not reveal any significant changes in the mechanical properties of the adhesives even when unrealistic levels of water are present within the AS1160 resin. The resin is considered to be fairly resilient to thermal ageing, and the shelf life could be extended beyond the current manufacturer recommended 6-year limit, and storage in low humidity conditions is likely to promote shelf life.

Life Prediction Methodology and Future Direction

As demonstrated by the ageing studies reported in this paper, modern life assessment techniques often rely on the Arrhenius treatment of data collected at elevated temperatures in service representative regimes, to predict key properties at service or shelf storage temperatures. This issue arises largely because of the absence of analytical methods that can detect and track the very small changes occurring at service temperature. In addition, there is a need to better understand the failure criteria (or limits) representing the amount of age-related change that can be tolerated in order to understand the remaining service life of the material or component. The failure limits are often not known or understood at the individual material level or at the multi-material level, and engineering and/or physics assessments are often required to capture this information.

In most cases, the validation of predictions from accelerated ageing remains very difficult as real-time data from field trials remains very limited and there remains significant uncertainty on how to define the simulated age (i.e. artificially accelerated age) of multi-material assemblies.

To overcome some of these difficulties, the future research direction in the life assessment of materials is to develop and make full use (where possible) of ultrasensitive techniques (such as microcalorimetry or oxygen consumption). In the case of multi-material assemblies, a strategy to incorporate in situ diagnostic sensors (for

chemical and physical properties) to track age-related events is often adopted. This strategy should enable the rate of age-related changes to be monitored in real time, providing advance warning of potential issues and reducing the reliance on accelerated ageing and Arrhenius-type treatments.

Conclusions

The ageing properties of Vinamul 3161 poly(ethylene-co-vinyl acetate) and AS1160 polyester polyol resins have been investigated in support of shelf life assessment and to identify storage conditions that may extend product life. The temperature sensitivity of pH, combined with Arrhenius kinetics, was used to predict changes for EVA in conditions representative of normal storage conditions. In separate experiments, relatively short-term thermally accelerated sensitivity studies have been carried out on the AS1160 resin to investigate variables such as humidity, temperature and open/close ageing conditions. The AS1160 resin is highly hygroscopic and readily accumulates moisture. This is potentially associated with complex changes in molecular weight, with ageing linked to the hydrolysis-ester formation equilibrium. However, these changes do not adversely impact adhesive bond strength, allowing the resin to be potentially used significantly beyond the manufacturer recommended shelf life limit.

References

1. Patel M, Skinner AR (2001) Polym Degrad Stab 73(3):399
2. Patel M, Soames M, Skinner ARS, Stephens TS (2004) Polym Degrad Stab 83(1):111
3. Martinez-Garcia A, Sanchez-Reche A (2003) J Adhes 79:525–547
4. Zanetti M, Camino G, Thomann R, Mulhaupt R (2001) Polymer 42:4501
5. Allen NS, Edge M, Rodriguez M, Liauw CM, Fontan R (2001) Polym Degrad Stab 71:1
6. Allen NS, Edge M, Rodriguez M, Liauw CM, Fontan R (2000) Polym Degrad Stab 68:363
7. Rimez B, Rahier H, Van Assche G, Artoos T, Biesemans M, Van Mele B (2008) Polym Degrad Stab 93(4):800–810
8. Létant SE, Plant DF, Wilson T, Alviso C, Read MSD, Maxwell RS (2011) Polym Degrad Stab 96:2019

 9. Patel M, Bowditch M, Jones B, Netherton D, Khan N, Letant S, Maxwell RS, Birshall SA (2013) Polym Test 32:313
10. Standard ASTM D2849-69 replaced by ASTM D4274-05 (2005) Standard test methods for testing polyurethane raw materials: determination of hydroxyl numbers of polyols
11. Jing Jin, Shuangjun Chen, Jun Zhang (2010) Polym Degrad Stab 95:725
12. Mogon P, Simon P, Peter B, Mathew R, Paul M, Niaz K, Imran K, Nicola P, Sonia L, Von White II, Gregory LA (2013) Polym Test 32:785–793

Chapter 11
Ultra-Accelerated Weathering II: Considerations for Accelerated Data-Based Weathering Service Life Predictions

Henry K. Hardcastle

Abstract This paper discusses the effect of varying UV intensity on weathering degradation rates of materials. The effects of increasing intensities of solar UV on materials obeying strict reciprocity and materials deviating from strict reciprocity are considered. A second new high-intensity natural UV weathering device is introduced based on ASTM G90. The paper presents data from two materials degrading under different intensities of UV and compares natural weathering with data obtained at increasing levels of UV intensity with implications on SLP calculations.

Keywords Reciprocity • UV intensity • Weathering • Acceleration • Correlation • ORWET • Polystyrene • Irradiance • Temperature • Ultra-Accelerated Weathering System • UA EMMA • Exposure • Extrapolation • ASTM G90 • Color • Outdoor • Static • Dynamic • Hypervolume

Introduction

The concept of reciprocity is a foundational concept used in the weathering industry and affects interpretation of results whenever two different exposures are timed or compared by radiant energy. The concept of reciprocity, laid down by Bunsen and Roscoe in 1876 [1], is an underlying assumption of much current weathering methodology representing a simple concept: Materials react to energy and energy is the product of intensity (see y-axis of Fig. 11.1) times duration (x-axis of Fig. 11.1). For this paper, under the assumption of strict reciprocity, an exposure at twice the intensity for half of the time is the energy equivalent to the same exposure at half the intensity for twice the time. Watts (intensity) times seconds (time) equals joules (energy), and typical weathering exposures are timed in kilo- or mega-joules per meter squared (MJ/m^2) of total solar (295–2,500 nm), total ultraviolet

H.K. Hardcastle (✉)
Atlas, Ametek Measurement and Calibration Technologies, Chicago, IL, USA
e-mail: kelly.hardcastle@ametek.com
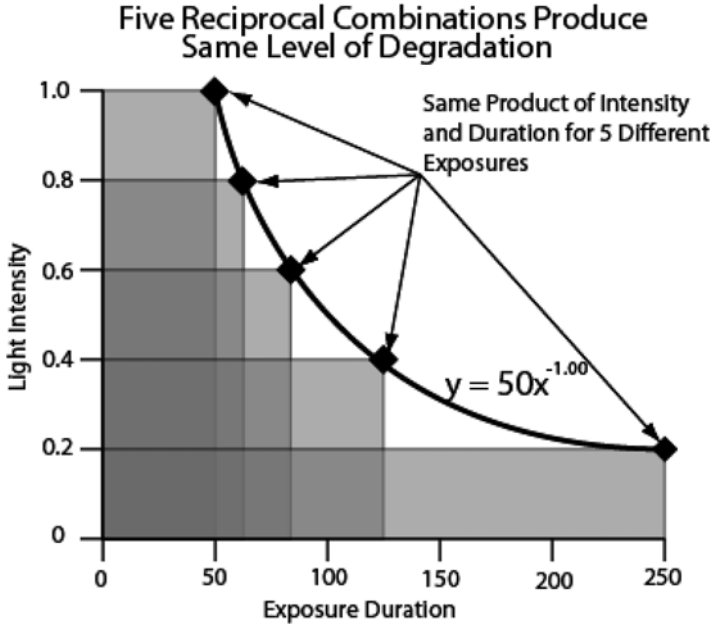
Fig. 11.1 Summarizing strict reciprocity concept—five reciprocal combinations produce same level of degradation

(UV 295–385 nm), or narrow band (e.g., 340 nm). The function has a characteristic shape with the independent variable raised to the power of −1 and will be defined as strict reciprocity for the purposes of this paper.

Background

Sedona 2004 NIST Service Life Prediction Symposium

In 2004 at the Sedona meeting of the NIST Service Life Prediction (SLP) Symposium, this author presented a simple paper checking the basic assumption of strict reciprocity in accelerated outdoor weathering and service life prediction [2]. The hypothesis tested in that paper is summarized in Fig. 11.1 and is based on the idea that equal energies of weathering exposures result in equal levels of degradation within limits (e.g., the "within limits" being that the intensity must not be so high as to cause thermal burning of the material). The key assumption tested in the Sedona paper said that within limits, two equal energy exposures with different intensities should result in the same level of property change—all other things being equal.
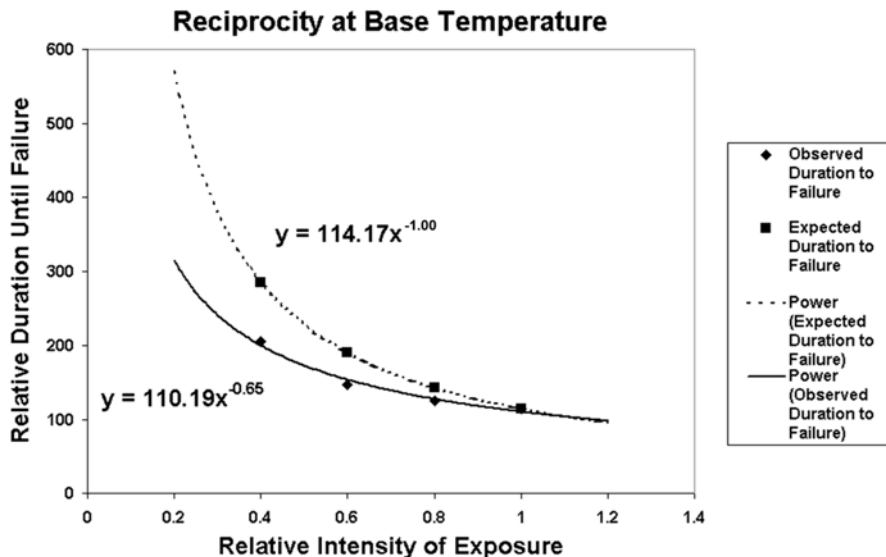
Fig. 11.2 Sedona results for polystyrene at moderate accelerations

The Sedona paper described a simple experiment exposing polystyrene standard reference materials (SRMs) to outdoor accelerated weathering conditions under concentrated solar irradiances at four different levels out to the same level of radiant energy. The exposure temperatures were held constant across different irradiance intensities via linked exposure devices. The data from the Sedona paper showed significant deviations from strict reciprocity predictions for the polystyrene SRMs in the experiment as shown in Fig. 11.2. The data indicated that the assumption of strict reciprocity was not a valid assumption for the data shown.

Additionally, the implications of these results for very high irradiance weathering testing pointed toward an interesting extrapolated prediction when the curves from Fig. 11.2 were extrapolated to irradiances achievable by weathering instrumentation under development at that time as shown in Fig. 11.3. This prediction—that if the curves for predicted and observed reciprocity were extrapolated out to very high solar irradiances, the observed degradation rate may be approximately half of what would be expected under the assumption of strict reciprocity for this material—is shown in Fig. 11.3. If correct, the implications of the prediction were clear for highly accelerated testing. For materials which did not obey strict reciprocity, for example, if weathering researchers observed failure in the real-world end use at 308 MJ/m^2 UV and then tested the material to 308 MJ/m^2 UV under high irradiance accelerated tests, the researcher may not observe failure. Under the extrapolation in Fig. 11.3, the researcher might not observe failure in the accelerated test for twice the duration than predicted by strict reciprocity. Clearly, the prediction observations represented important considerations in SLP, high irradiance testing and accelerated weathering. If the prediction was supported, it would mean strict
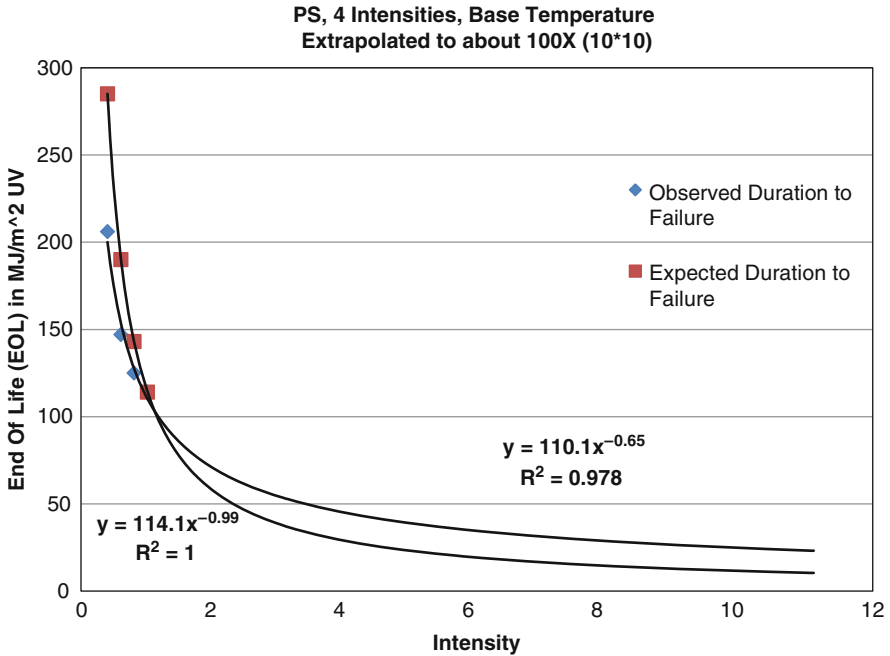
Fig. 11.3 Extrapolated predictions to test from the Sedona paper

reciprocity could be a very dangerous assumption for weathering researchers, and extrapolating the assumption of strict reciprocity can be perilous for SLP. Current ASTM and SAE accelerated weathering standards, although highly caveated, did not explicitly state possible deviations from strict reciprocity. Simultaneously, researchers regularly time accelerated weathering exposures to annual cumulative radiant energy levels observed in un-accelerated outdoor exposure reference environments. Additional research efforts were published, while instrumentation to test the extrapolated predictions was under development.

Gothenburg EWS

In 2005 at the European Weathering Symposium (EWS), a paper was presented which repeated the Sedona exposure for a different material (commercial polycarbonate) which indicated two important results [3]: First, that paper referenced a classical SLP approach. In the classical SLP approach, researchers utilize a three-step method. In step one, a model is created, typically in laboratory artificial weathering devices using DOE full factorial methods and/or multi-linear regressions varying the input factors (typically including irradiance, temperature, and moisture). In step 2, researchers then obtain time slices of environmental variables from

the environment in question and enter the time slice data into the model and solve for degradation for that particular time slice. In step 3, researchers sum up the degradation contribution from all the time slices for a prediction of accumulated degradation in that environment. Within this classical SLP methodology, a key consideration becomes evident with regard to the extrapolated prediction from the Sedona paper; the light intensity factor may be significant and important for some materials, i.e., light intensity is a significant and important factor in the degradation model as indicated by the DOE and regressions. Second, the EWS Gothenburg paper showed data from polycarbonate which differed from the polystyrene SRM data in terms of reciprocity characteristics pointing toward a material dependency of strict reciprocity and indicating strict or even consistent reciprocity was not a valid assumption across different materials.

Key Largo NIST SLP Symposium

In 2006 at the NIST SLP Symposium in Key Largo, a third paper in the series on reciprocity was presented [4]. This paper expanded the reciprocity characterization to artificial light sources (xenon) inside the laboratory. The data confirmed the outdoor results observed in the Sedona paper closely in different weathering exposure apparatus.

Budapest EWS

In due time, the development of the apparatus needed to test the extrapolated prediction from the Sedona paper was completed and fully described in a paper entitled "Ultra-Accelerated Weathering System I: Design and Functional Considerations" [5] and represented the precursor to this paper ("Ultra-Accelerated Weathering II: Considerations for Accelerated Data-Based Weathering Service Life Predictions"). A photograph of the Ultra-Accelerated Weathering System (UAWS) and the spectral reflectance of the mirror facets are shown in Fig. 11.4. "Ultra-Accelerated Weathering System I" presented results from acceleration and correlation studies of a thin film material which appeared to obey strict reciprocity; the ORWET SRM, a European SRM produced by the Swiss Federal Laboratories for Materials Testing… EMPA. (ORWET is a thin film paint of melamine resin with a CIBA pigment on aluminum substrate that has been very highly characterized for color change as a function of UV exposure.) The quantitative acceleration data indicates to researchers how fast the weathering device performs the simulation of degradation on materials with time on the x-axis (exposure in days). Figure 11.5 shows acceleration data for ORWET under four different exposure conditions at different intensities (ultraaccelerated, Florida real time, Arizona real time, and EMMA an ASTM G90 device).

Ultra-Accelerated Weathering System and Total Reflectance Spectra
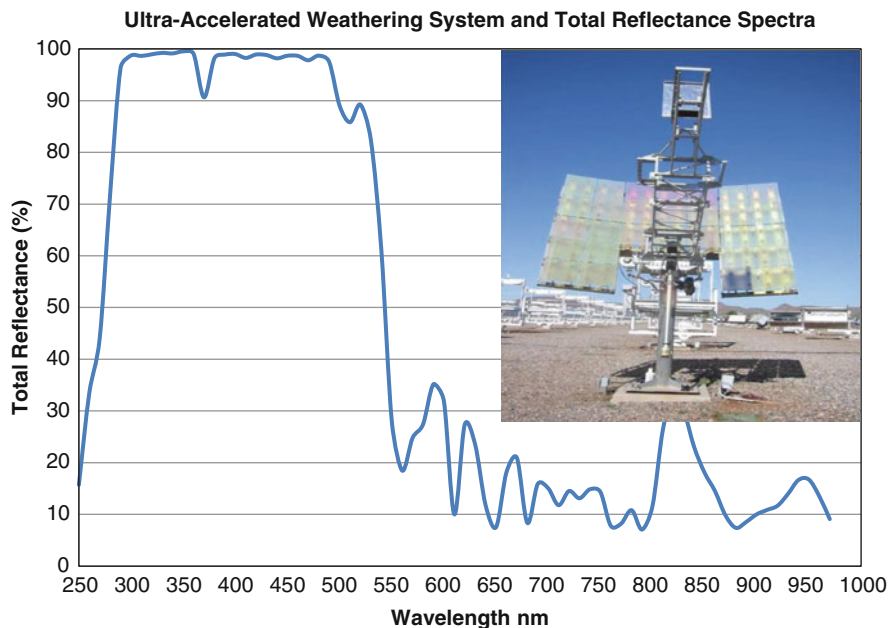
Fig. 11.4 Picture of UAWS device and reflectance spectra

Comparison of FL, AZ, EMMA and UA Exposures of ORWHET By Days
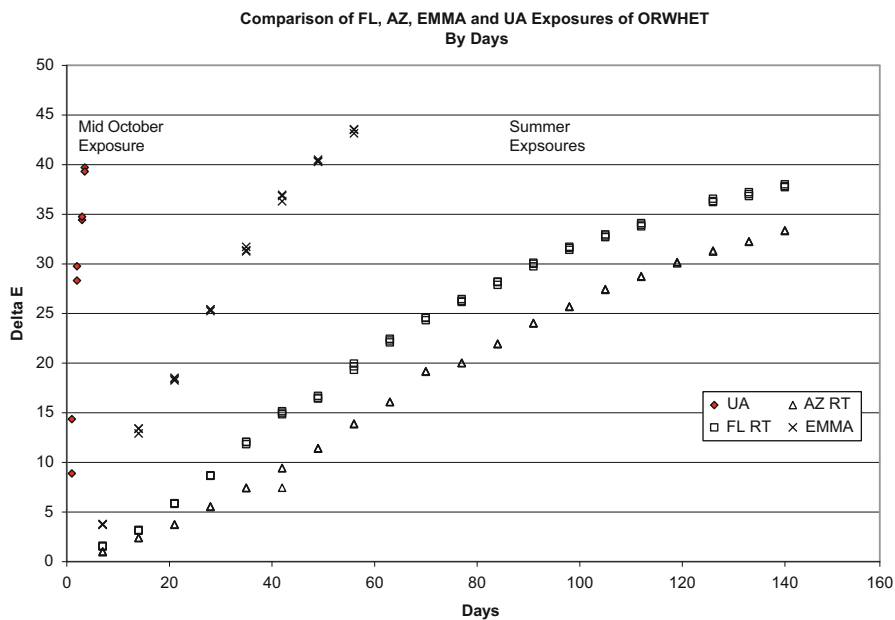
Fig. 11.5 ORWET degradation on the UAWS—by days (UA—ultra-accelerated device; FL RT—Florida real time; AZ RT—Arizona real time; EMMA—ASTM G90 device)
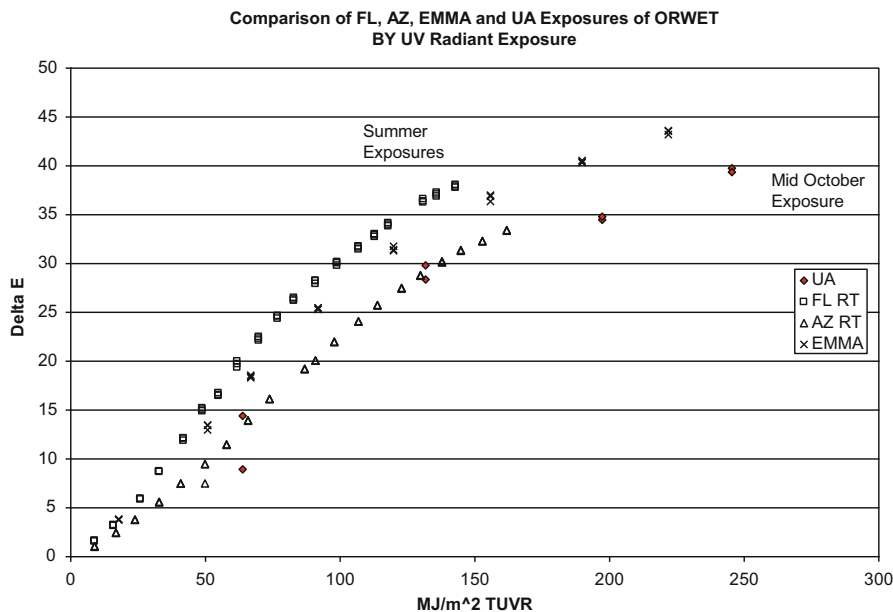
Fig. 11.6 ORWET degradation on the UAWS—by MJ/m² UV 295–385 nm

The quantitative correlation indicates to researchers how well the device simulates the natural degradation function with UV radiant energy on the *x*-axis as shown in Fig. 11.6 under the same exposure conditions as seen in Fig. 11.5. It was apparent from the Budapest data in "Ultra-Accelerated Weathering System I" that the UAWS device offered a very highly accelerated weathering method for materials having degradation behaviors like ORWET (which specifically obey strict reciprocity), and the data confirmed the radiometric characteristics of the UAWS device.

Experimental

Research Questions I

With the development of the UAWS initially completed and qualified using the acceleration and correlation data for ORWET, the capability to test the extrapolated predictions from the Sedona paper was in hand. The general research question for this work was to expose the polystyrene material, test the extrapolated predictions from the Sedona paper, and see if the significant quantitative deviations from strict reciprocity extrapolate out to the very high intensities (approximately 60 times real-time UV radiant exposure rates) and would actually be observed. Would the ultra-accelerated exposure require approximately twice the UV radiant

exposure to produce the same level of degradation as less accelerated exposures on polystyrene as indicated by the extrapolation of deviations from strict reciprocity in the Sedona paper?

Conversely, the null hypothesis tested for this effort may be stated as there is no difference observed between degradation rates for polystyrene SRMs weathered in un-accelerated exposures and ultra-accelerated exposures when compared (normalized) for UV radiant exposure on the *x*-axis of the degradation curves.

Procedure I

The previously described UAWS device was used to expose randomly selected polystyrene from the same lot previously exposed on Arizona and Florida real time 45° racks facing south as well as ASTM G90 devices [6]. The exposure procedure requires several caveats: The exposure temperatures on the UAWS were not controlled to closely simulate the un-accelerated exposure temperatures. The UAWS exposure temperatures were controlled to approximately 65 ± 10 °C, slightly higher than the normal exposure temperatures for the non-UAWS exposures. Higher exposure temperatures, however, typically result in faster degradation rates. In order to achieve these moderate exposure temperatures at the high irradiances, exposures utilized mirrors with reflectance spectra as shown in Fig. 11.4 reducing irradiance greater than 450 nm. The UAWS polystyrene exposure was identical to the UAWS ORWET exposure and utilized forced convective cooling to maintain specimens near 65 ± 10 °C (slightly warmer than the real time and G90 exposure temperatures for polystyrene). The UAWS exposure was also performed in mid-October, while the comparative real-time Arizona, Florida, and G90 exposures were performed during summer. The G90 and UAWS exposures were performed without applied moisture, while in the 45° south exposures, moisture was uncontrolled.

Observations I

For the polystyrene SRM exposure as seen in Fig. 11.7, the data appears to show very high acceleration rates. The UAWS achieved in 2 days color change requiring approximately 115 days in Arizona real time and approximately 50 days on ASTM G90 exposure. Simultaneously, the data in Fig. 11.8 appears to show significant departure from correlation between the UAWS and real time or G90 exposures when normalized for radiant exposure in MJ/m^2 UV on the *x*-axis. These results fail to support the null hypothesis of this experiment for polystyrene. The data showed significant deviation from strict reciprocity, and specifically, the observed degradation rate of polystyrene on the ultra-accelerated exposure appeared to be approximately half of what was predicted by strict reciprocity when compared with the un-accelerated exposures. These observations appear consistent with predictions of the extrapolated prediction from the Sedona paper.
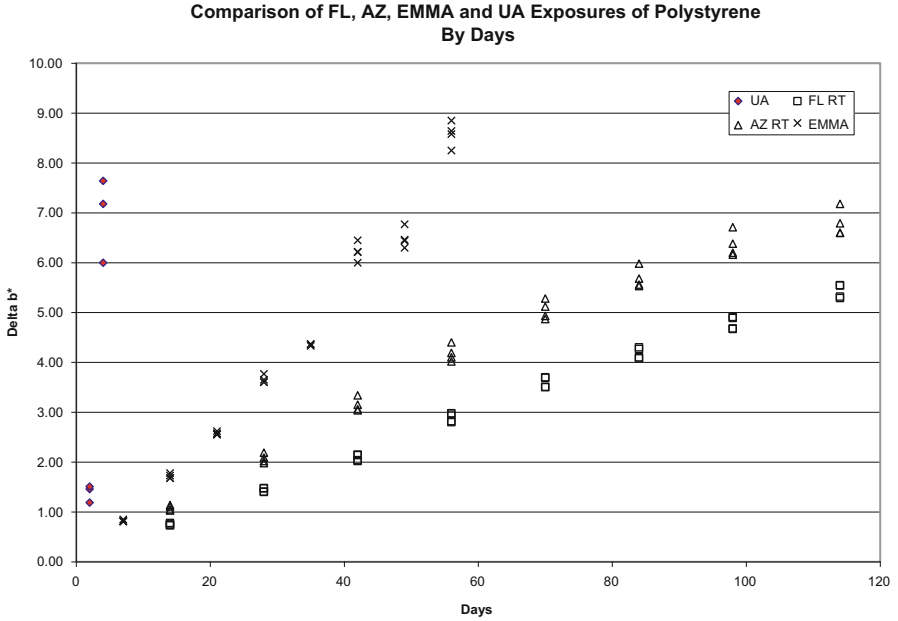
Fig. 11.7 Polystyrene degradation on the UAWS—by days
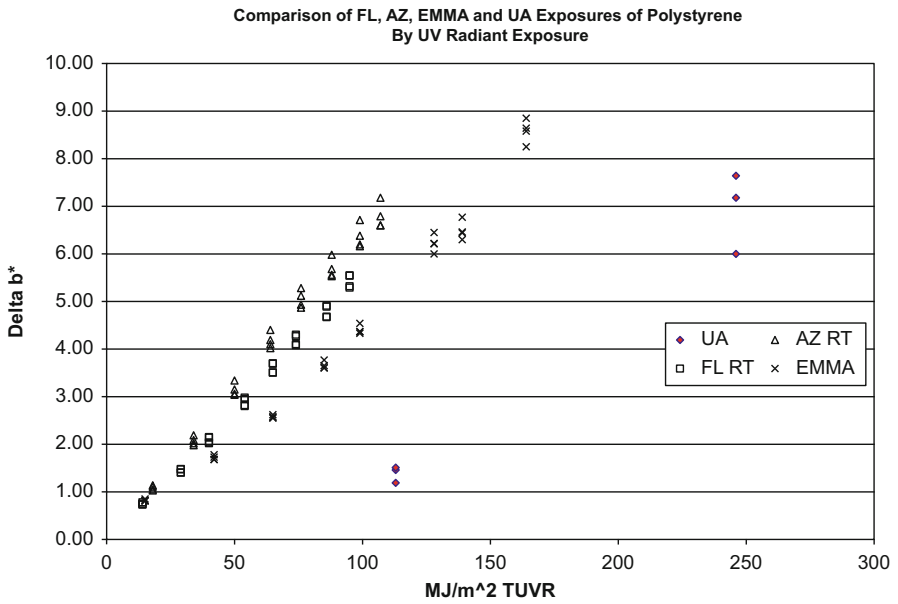
Fig. 11.8 Polystyrene degradation on the UAWS—by MJ/m² UV

Discussion I

Clearly, significant deviations from strict reciprocity represent important aspects of any weathering SLP effort. Extrapolating the assumption of strict reciprocity can be perilous to SLP efforts. Simply interchanging radiant exposure of an accelerated weathering test for real-time SLP calculations, without quantifying possible deviations from strict reciprocity, can result in considerable error as observed in the polystyrene example above. Fortunately, these characteristics are easily quantified by using DOE, multi-linear regressions, and methodologies described in this paper and elsewhere [2, 7, 8]. It is unclear if the general weathering industry addressed the reciprocity concept sufficiently in many previous SLP efforts and significant deviations from strict reciprocity might help explain previous SLP failures.

So far, this paper investigated the concept of reciprocity at extremely high acceleration rates (high irradiance) however; a possible alternative at rates between the UAWS extreme on the one hand and the current ASTM G90 acceleration rates on the other hand may yield more reasonable correlation. Might it be possible to observe less deviation from strict reciprocity at acceleration rates closer to currently used ASTM G90 weathering test methods?

Research Questions II

The general questions addressed in the previous section ask if strict reciprocity (as defined in this paper's introduction) can be assumed for very highly accelerated weathering devices. This paper's focus returns to less accelerated rates and specifically asks if increasing UV intensity reasonably predicts degradation observed at lower UV intensity for materials when exposure temperatures are comparable.

The general research question involved in this effort is to determine if strict reciprocity can be assumed for exposures closer in UV radiant intensity above current ASTM G90 methods than previously tested. If UV radiant exposure rates are approximately doubled from existing ASTM G90 Fresnel concentrators (by increasing from 10 to 20 mirrors), will similar material degradation levels be observed at the same level of UV radiant exposure as indicated by strict reciprocity? In other words, will the degradation level of materials be reached in approximately one-half the exposure time as predicted under strict reciprocity when radiant intensity is approximately doubled? Of course this effort requires temperatures be similar for both intensities.

Conversely, the null hypothesis tested for this effort may be stated as there is no difference observed between degradation rates for 10 and 20 mirrors (approximately doubled irradiance) when compensated for radiant exposure and temperature with ORWET and polystyrene SRMs weathered on G90-type Fresnel concentrator devices.

Procedure II

Two near identical G90 type Fresnel collector weathering devices were utilized for outdoor exposures. The first was maintained in a configuration with 10 standard mirrors and designated "standard EMMA" or simply "EMMA" for "Equatorial Mount with Mirrors for Acceleration." The second device utilized additional mirrors, increasing the number of mirrors to 20, and this configuration was designated as "UA EMMA" for "ultra-accelerated EMMA" as shown in Fig. 11.9. Because temperature is a co-variable of irradiance, the UA EMMA mirror facets utilized technology fully described in [5], with reflectance spectra shown in Fig. 11.9. A performance comparison of black panel temperatures (backed and unbacked) achieved simultaneously on the two devices with 10 and 20 mirrors is shown in Fig. 11.10. The final 8 standard to 20 UA mirror ratio between these devices was adjusted to achieve approximately equal exposure temperatures as demonstrated by black standard temperature sensor data shown in Fig. 11.11 and measured with Xenocal® sensing and logging devices. The approximate irradiance differences simultaneously measured on the two devices are shown in Fig. 11.12 also measured with Xenocal devices.

A series of caveats are important to note regarding this procedure: There are many variables in outdoor exposure testing that were not blocked in this experiment including moisture—moisture was not applied in the G90 exposures. The mirrors
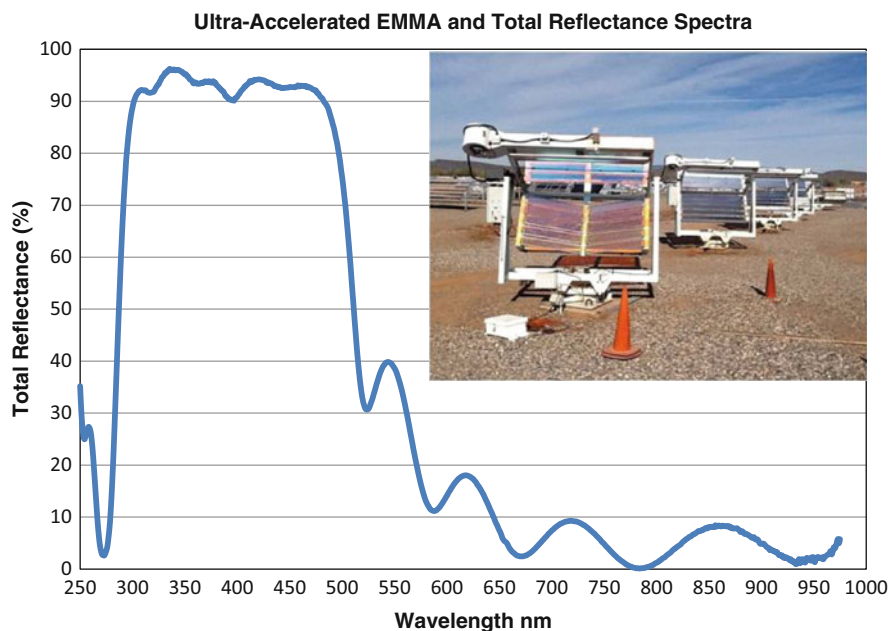
Fig. 11.9 Photograph of the UA EMMA device and reflectance spectra

UA EMMA and Standard EMMA 01/22/13 Warm Clear Day
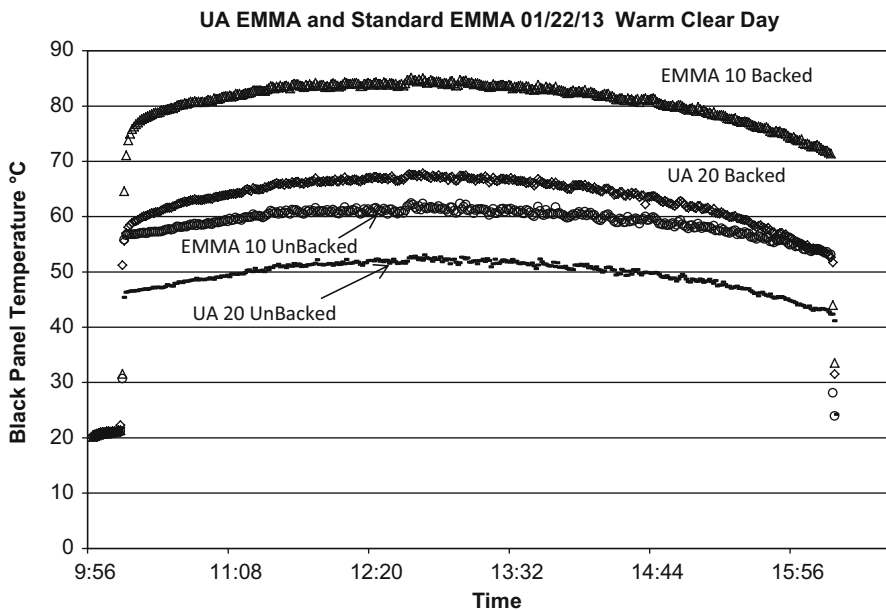
Fig. 11.10 Backed and unbacked black panel temperature performance comparison of UA EMMA (20 mirrors) to standard EMMA (10 mirrors)
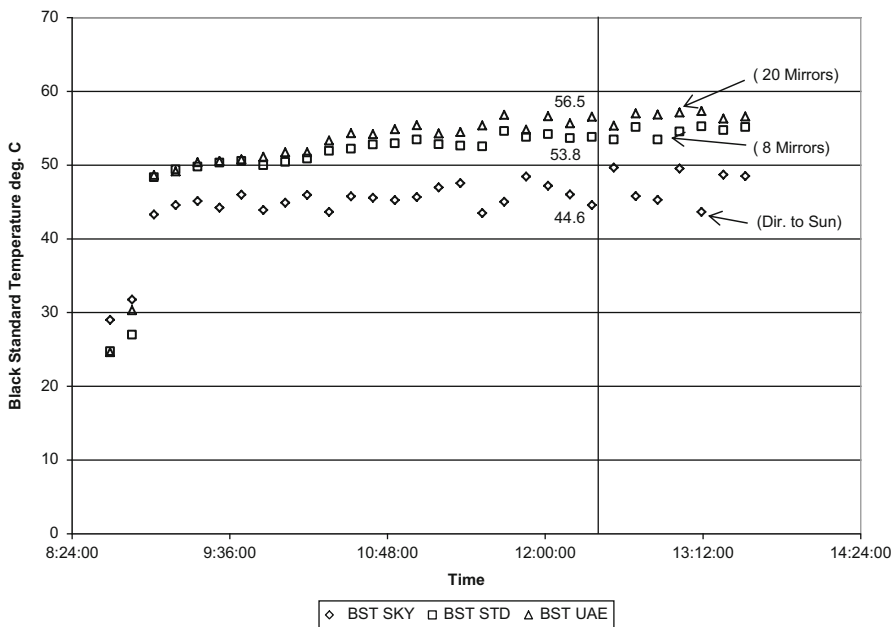
Fig. 11.11 Comparison of UA EMMA, standard EMMA, and normal incidence black standard exposure temperatures for polystyrene exposure measured with Xenocal®
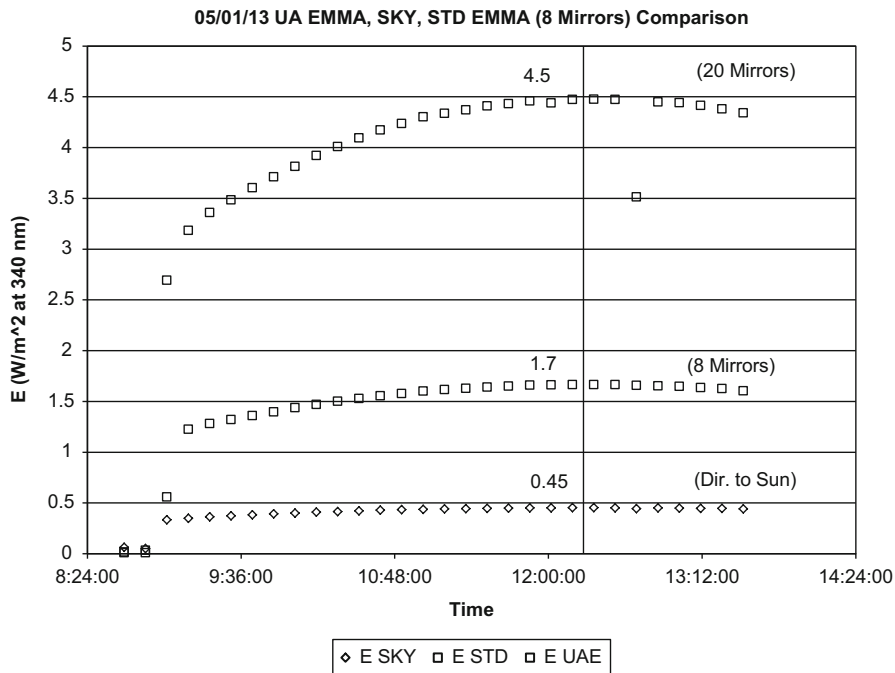
Fig. 11.12 Comparison of UA EMMA, standard EMMA, and normal incidence approximate irradiant intensities near 340 nm

on the UA EMMA device significantly reduced the irradiance above 450 nm in comparison to the standard EMMA spectral distribution. The irradiance differences were measured at 340 nm which has a high level of variability in outdoor weathering. Other unknown variables may also have affected the exposure results; however, best efforts were expended to mitigate these variables as much as possible.

Observations II

For the ORWET SRM exposures, as seen in Fig. 11.13, the data appears to show reasonable acceleration. The UA EMMA achieved in 12 days color change requiring approximately 30 days on standard EMMA. Simultaneously, the data in Fig. 11.14 appears to show reasonable correlation between UA EMMA and standard EMMA when normalized for radiant exposure with MJ/m^2 UV on the x-axis. These results appear to support the null hypothesis for ORWET. Additionally, these observations appear similar to observations reported in previous efforts [5].

For the polystyrene SRM exposure, the data appear to show some acceleration. The UA EMMA achieves color change in 12 days that requires approximately 18 days on standard EMMA as shown in Fig. 11.15. Simultaneously, for the polystyrene exposure, however, the data in Fig. 11.16 fails to show reasonable correlation

**Comparison of Standard EMMA to UA EMMA Exposure of ORWET
By Days**
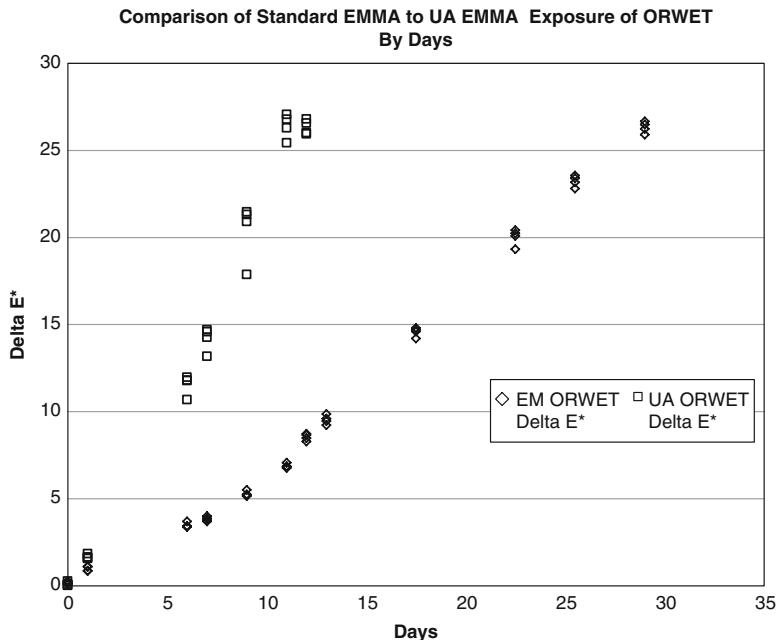
Fig. 11.13 ORWET SRM degradation comparison of UA EMMA and standard EMMA by days

**Comparison of Standard EMMA and UA EMMA Exposures of ORWET
By UV Radiant Exposure**
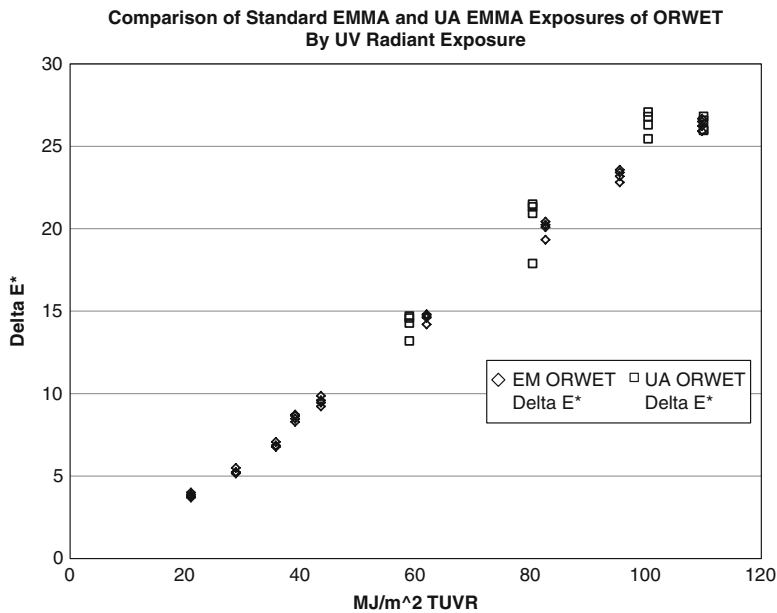
Fig. 11.14 ORWET SRM degradation comparison of UA EMMA and standard EMMA by UV radiant exposure in MJ/m^2 UV
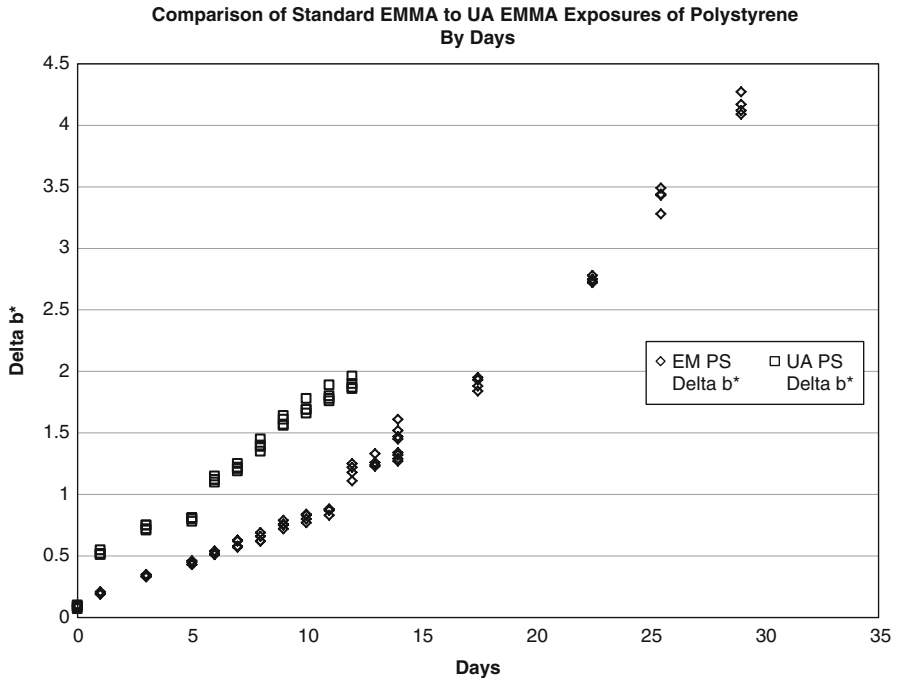
Fig. 11.15 Polystyrene SRM degradation comparison of UA EMMA and standard EMMA by days
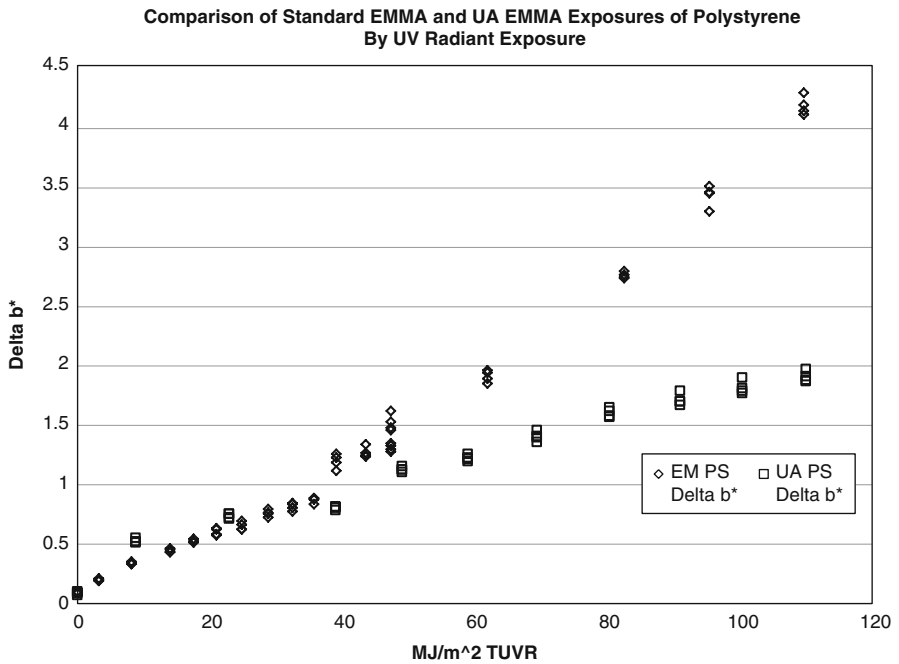
Fig. 11.16 Polystyrene SRM degradation comparison of UA EMMA and standard EMMA by UV radiant exposure in MJ/m² UV

between the UA EMMA and standard EMMA when normalized for radiant exposure on the *x*-axis. For the polystyrene SRM, the UV radiant exposure in MJ/m² UV from the less intense standard EMMA exposure had a greater effect than the UV radiant exposure from the more intense exposure on the UA EMMA at the same level of UV radiant exposure. This observation does not appear to support the null hypothesis for polystyrene. Additionally, these observations appear similar to observations in previous efforts [2, 3].

Discussion II

Clearly, the correlation graphs shown in Figs. 11.14 and 11.16 describe different behavior between the ORWET SRM (which appears to behave as predicted by strict reciprocity) and the polystyrene SRM (which does not appear to behave as predicted by strict reciprocity).

The assumption of strict reciprocity for the ORWET SRM may lead to successful service life prediction simply by accelerating the exposure's radiant intensity. The assumption of strict reciprocity for the polystyrene SRM using the same basis, however, may lead to considerable discrepancies between predicted and observed end-use color change. Thus, there appear to be limits to the assumption of strict reciprocity when extrapolated out to higher intensities as performed in these procedures.

There are several hypotheses beyond the scope of this paper as to why the polystyrene SRM deviates from strict reciprocity. One major consideration of this effort is represented by the different spectral distribution between these exposures. The reflectance facets used in the UA EMMA do not provide longer wavelengths of solar irradiance experienced on the standard EMMA target area. The effect of UVB on polystyrene interacting with the highly variable UV spectral distribution outdoors may have introduced uncertainties in the polystyrene degradation curves. Another major consideration involves the composition of the material being exposed; do normal manufacturing variations affect reciprocity characteristics of materials?

A major unanswered question, however, is represented by differences observed between variable cycles seen outdoors in end use and typical laboratory artificial test cycles. Do deviations from strict reciprocity significantly affect degradation rates for some materials at intensities observed outdoors and in artificial laboratory exposures? The self-similar nature of the strict reciprocity curve in combination with the extrapolation confirmation work above leads one to consider the effect at lower irradiance intensities. For example, the variety of irradiance intensities (approximate) for 3 days outdoors in Arizona is shown in Fig. 11.17. It is now clear from this and previous work that degradation from the maximum intensity is not equal to twice the degradation of the half maximum intensity for materials deviating from strict reciprocity in these types of variable outdoor environments. Thus, the simple intensity curves, shown in Fig. 11.17, result in complex, non-intuitive cumulative degradation functions for these types of materials. Comparing the natural outdoor intensity curves in Fig. 11.17 to a typical artificial weathering method intensity distribution as shown in Fig. 11.18 points out the highly artificial nature of

05/02/13 5°, 34°, 45° South Arizona Static Exposure Comparison
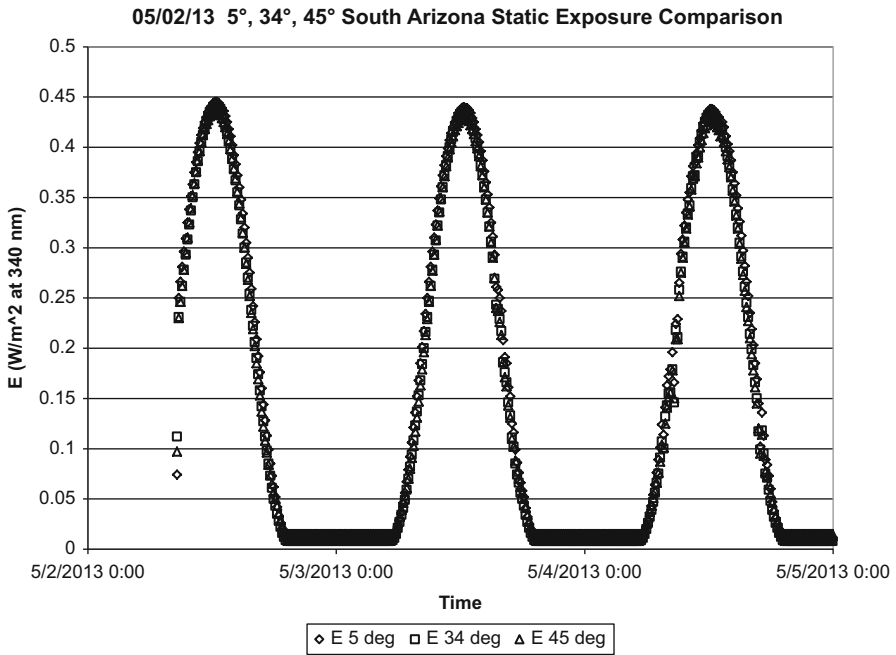
Fig. 11.17 End-use outdoor exposure approximate solar intensity at 340 nm, south direct to sun (three angles)

05/02/13 5°, 34°, 45° Arizona Static Exposure Comparison
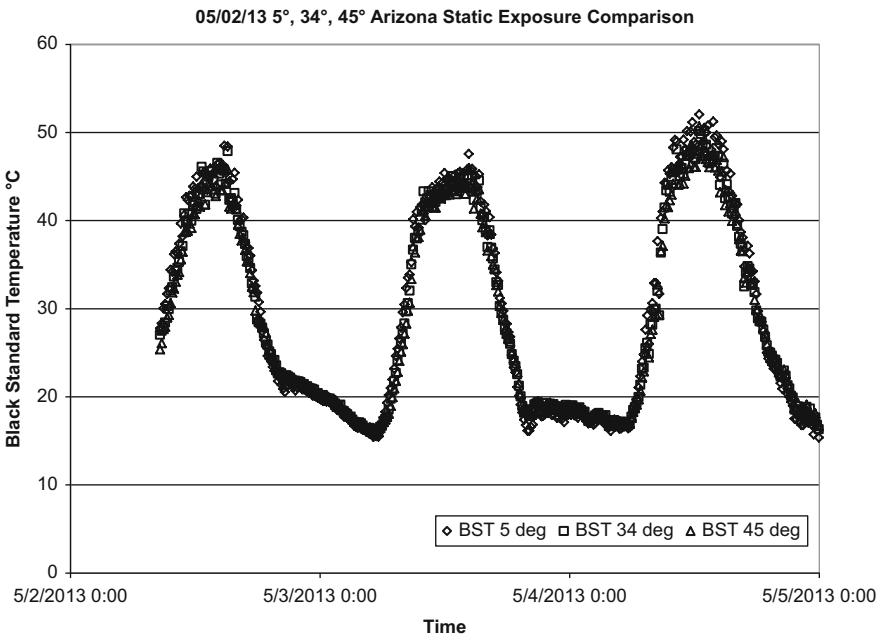
Fig. 11.18 End-use outdoor exposure approximate black standard temperature, south direct to sun (three angles)
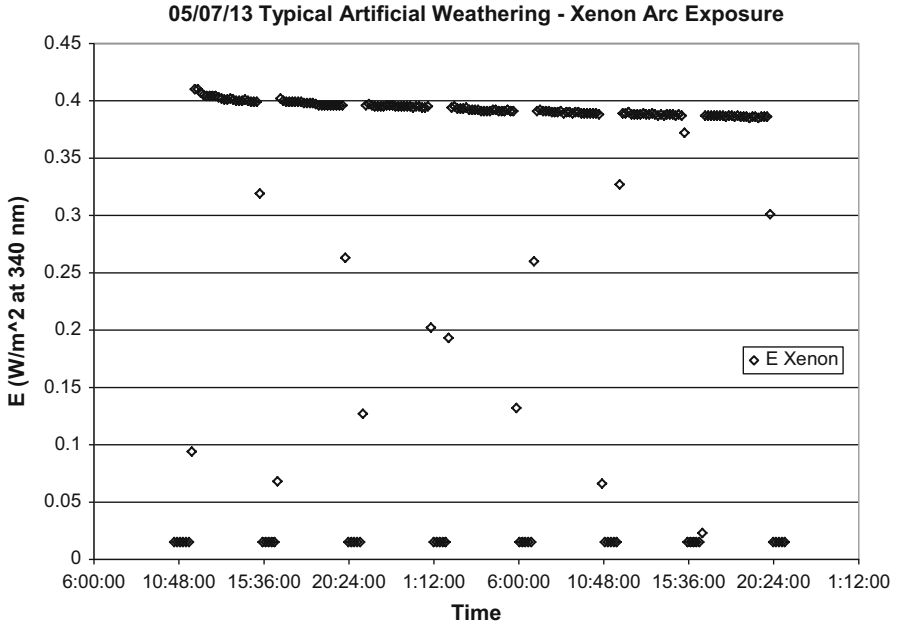
Fig. 11.19 Laboratory artificial exposure approximate xenon intensity at 340 nm

these types of steady-state test methods in light of the possible deviations from strict reciprocity as defined in the introduction of this paper. The steady-state test methods simply do not simulate the degradation effects possible with the distribution of intensities in light of possible deviations from strict reciprocity and the variability of the outdoor exposure environment.

Additionally, steady-state artificial test methods may not account for interactions with other variables such as temperature, for example. A co-variable of light intensity, temperature in outdoor exposures, as shown in Fig. 11.19, dramatically affects degradation rates by interacting with the effects of light intensity and reciprocity characteristics. However, typical artificial weathering test methods maintain static temperature levels like those shown in Fig. 11.20. The dynamic temperature changes, in combination with dynamic light intensity changes and in combination with possible deviations from strict reciprocity, appear to make it highly unlikely that steady-state artificial laboratory tests alone are suitable tools for SLP, especially for materials known to deviate from strict reciprocity. Therefore, it is highly recommended that SLP efforts include quantification of reciprocity characteristics for materials under investigation through DOE, multi-linear regression, or other suitable approaches. It is also highly recommended that SLP efforts include consideration of the highly dynamic and interactive nature of the outdoor end uses in the n-dimensional hypervolume environment [9].
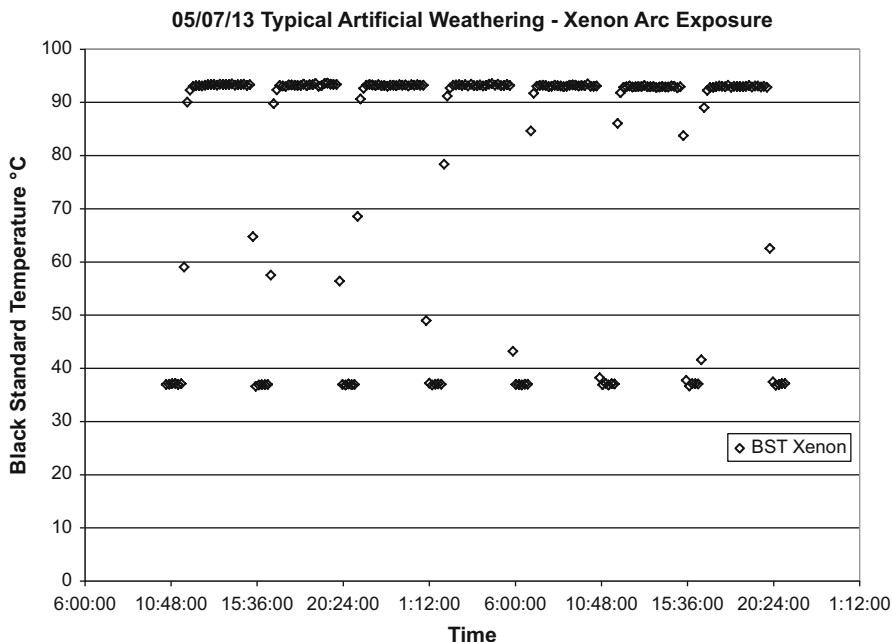
Fig. 11.20 Laboratory artificial exposure approximate black standard temperature

References

1. Hamilton JF (1966) The theory of the photographic process. Macmillan, New York, p 132
2. Hardcastle HK (2005) A new approach to characterizing reciprocity. In: Martin JW, Ryntz RA, Dickie RA (eds) Service life prediction, challenging the status quo. Federation of Societies for Coatings Technology, Blue Bell, PA
3. Hardcastle HK (2005) A characterization of the relationship between light intensity and degradation rate for weathering durability. In: Reichert T (ed) Natural and artificial ageing of polymers. 2nd European weathering symposium. Publication No. 6. Gesellschaft fur Umweltsimulation, Germany
4. Scott KP, Hardcastle HK (2009) A new approach to characterizing weathering reciprocity in xenon arc weathering devices. In: Martin JW et al (eds) Service life prediction of polymeric materials global perspectives. FSCT, Springer, New York, Chapter 6
5. Hardcastle HK, Jorgensen GJ, Bingham CE (2009) Ultra-accelerated weathering system I: design and functional considerations. In: Reichert T (ed) Natural and artificial ageing of polymers. 4th European weathering symposium, Publication No. 11, Gesellschaft fur Umweltsimulation, Germany. Subsequently re-published in CoatingsTech. American Coatings Association, Washington, DC (2010) vol 7(8), pp 28–37
6. ASTM G 90-94 (1998) Standard practice for performing accelerated outdoor weathering of nonmetallic materials using concentrated natural sunlight. 1998 Annual book of ASTM standards. American Society for Testing and Materials, Philadelphia, PA

7. Hardcastle HK (2005) United States patent application no.: 20050120811, Method and apparatus for characterizing weathering reciprocity of a material, June 2005
8. Hardcastle HK (2004) Considerations for relating artificial laboratory and natural outdoor weathering durability testing. In: Proceedings of the annual technical conference of the society of plastics engineers, Chicago, IL, May 2004
9. Hardcastle HK, Searle ND (2001) Weathering test methods. In: Ryntz R (ed) Plastics and coatings durability, stabilization, testing. Hanser, Munich, pp 189–240, Chapter 9

Chapter 12
Quantitative Mapping of Mechanisms for Photoinitiated Coating Degradation

Søren Kiil

Abstract This work concerns the mathematical modeling of photoinitiated coating degradation. Using experimental evidence available, some of the most important assumptions underlying existing models for thermoset coatings are analyzed and suggestions for further work provided. A modeling approach that can be used to implement the various effects of water on the degradation mechanisms of cross-linked coatings is also presented and experiments to test the approach are suggested. Additionally, simulations with an existing degradation model for an epoxy–amine coating are used to map the influence of model parameters on the lag time (i.e., the time passing prior to the onset of erosion) and the stable erosion rate. The simulation results can be used in the optimization of UV radiation-induced intercoat adhesion losses, which are often observed in multilayer coating systems based on top coated epoxy coatings. Finally, potential directions for future experimental research in the field are outlined.

Keywords Interlayer adhesion loss • Epoxy coatings • Weathering • Erosion mechanism • UV absorber • Humidity • Water • Crosslinking • Network degradation • Oxygen diffusion and solubility • Photoproducts • Oxidation zone • Rain • Lag time • UV radiation degradation

Introduction

Photoinitiated coating degradation, in a broad sense also termed weathering, has implications for all exterior coating uses [1]. For modern high-performance coatings, weathering is usually a slow process often taking 5 years or longer before a critical performance property has failed. In the case of an automotive clear coating, the lifetime expectancy is typically 10 years, whereas for a top coat of an industrial anticorrosive coating system, the specified service lifetime can be more than 20 years [2]. The physical and chemical processes taking place

S. Kiil (✉)
Department of Chemical and Biochemical Engineering, Technical University of Denmark, DTU, Building 229, 2800 Kongens Lyngby, Denmark
e-mail: SK@kt.dtu.dk

simultaneously during weathering are fairly complex. This has led to the development of mathematical models, which can, at least to some extent, simulate the degradation phenomena and thereby estimate service lifetimes as well as provide suggestions for product optimizations. A concise review of models developed over the years is available in Kiil [3]. However, for the models to be of any practical use, the most important assumptions underlying the different models need proper experimental verification.

Presently, the most essential assumption that needs verification appears to be the relative importance, in the degradation process, of oxygen diffusion and absorption of UV radiation by photoproducts and/or UV absorbers. In addition, there are phenomena that still need to be mapped from a mechanistic point of view and properly implemented in the mathematical models. At present, the different ways that water can affect coating degradation rates seem the most urgent. Finally, it is also of interest to explore how the mathematical models can provide quantitative information that can link photoinitiated coating degradation to important coating properties. One example in this direction is the effect of weathering on subsequent interlayer adhesion loss in a multilayer coating system. So-called epoxy–amine coatings, exposed to subsequent application of a UV radiation resistant top coat (typically a polyurethane coating), may suffer from interlayer adhesion loss due to rapid photoinitiated coating degradation of the epoxy when exposed to sunlight for just a few days prior to being top coated (e.g., Gurack et al. [4]). The aim of the work presented here is to investigate some of these issues. While the challenges pointed out are not solved, the analyses performed lead to suggestions for future experiments that are thought to help to advance the field.

Qualitative Description of Coating Degradation

The coating type selected for the investigations is epoxy–amine coatings for the heavy-duty coating sector. These thermoset materials are highly durable and tightly cross-linked coatings used for anticorrosion protection of large steel structures such as ships, wind turbines, oil rigs, and bridges. A review of anticorrosive coatings is available in Sørensen et al. [2]. To appreciate the details to be discussed in the coming paragraphs, a concise description of photoinitiated degradation of epoxy–amine coatings is required. The process that takes place when a cured epoxy–amine coating is exposed to UV radiation and humidity is schematically shown in Fig. 12.1. From the very beginning of an exposure test, photoinitiated chain scission reactions take place, which slowly degrade the top layer of the binder matrix. Simultaneously, moisture is absorbed (or desorbed depending on the relative humidity in the chamber) and starts to penetrate the coating. At the surface, an oxidation front begins to move into the coating. The rate of movement of this front can be dependent on the rates of chemical oxidations, the solubility of oxygen in the coating, the rate of diffusion of oxygen into the coating, and potential absorption of UV radiation by photoproducts (or UV absorbers if present) formed in the oxidation zone. When a critical fraction, $X_{CL, max}$, of the original network chains has been broken at the
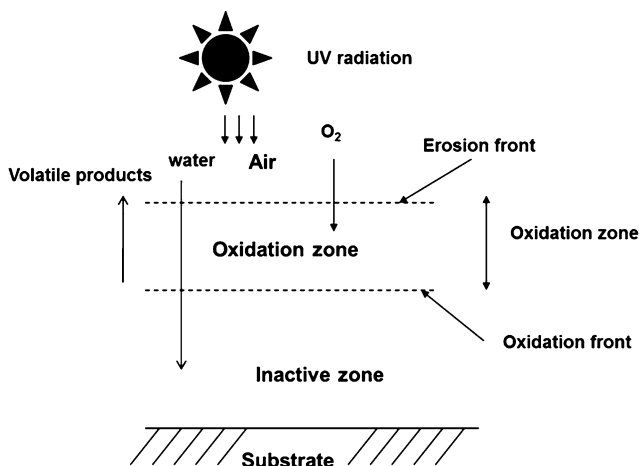
Fig. 12.1 Schematic illustration (cross-sectional view) of epoxy–amine coating during exposure to ultraviolet (UV) radiation and humidity. After Kiil [3]

coating surface, the erosion (or ablative) front (i.e., the coating surface) starts to move and the coating thickness is reduced. The time passing from initiation of UV radiation exposure to the unset of erosion is called the lag time. After some additional time, the rate of movement of the oxidation and erosion fronts can become equal, and a stable oxidation zone thickness is established. In the inactive zone, no degradation takes place. In some cases, the oxidation front moves very fast and extends the entire coating thickness within a matter of hours or days [5]. It was shown by Rezig et al. [6] that during degradation, nano-sized craters develop on the exposed surface of the coating.

Mathematical Modeling of Coating Degradation

The mathematical model, relevant for this work, was presented and verified against experimental data in an earlier work [3] and here will only be given a concise description. The closed-loop chemical mechanism used in the model is given by

$$E-CC \xrightarrow{\;h\nu\;} 2R\bullet \tag{12.1}$$

$$R\bullet + O_2 \rightarrow ROO\bullet \tag{12.2}$$

$$CH_2N + CHOH + 2ROO\bullet + O_2 \rightarrow CON(amide) + CO(carbonyl) + H_2O(1) \\ + 2ROOH \tag{12.3}$$

$$R\bullet + R\bullet \rightarrow E-CC \tag{12.4}$$

$$ROOH \xrightarrow{\;h\nu\;} volatile\ endproducts \tag{12.5}$$
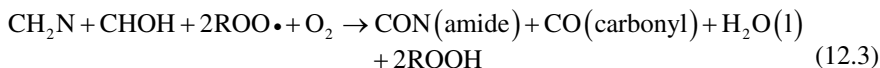
where E-CC is short for the "bridge" in the epoxy backbone and CH_2N and CHOH are the groups in the network vulnerable to hydrogen abstraction. R· and ROO· are radicals. This reduced chemical mechanism includes the main reactions responsible for the degradation of the binder matrix without considering the many intermediate species and volatile end products involved. Reaction (12.5) is shown in the mechanism, but not included in the model because the exact volatile end products formed are not known. So in the model, ROOH is accumulated, and the concentration of ROOH simply represents liquid or potentially volatile species (e.g., ketones, alcohols, phenols, and methane) that may be formed in secondary reactions. Potential residual solvent in the coating (see [7] for details on this) is not considered. The model includes photoinitiated oxidation reactions, intrafilm oxygen permeability, water absorption and diffusion, transient reduction of cross-link density, and development of a surface oxidation zone. The model was developed and solved using the front-tracking strategy provided in [8], which allows the rate of movement of the diffusion and erosion fronts to be followed. In Kiil [5], the model was extended to include the presence of a UV absorber and/or absorption of UV radiation by photoproducts formed during photodegradation. Using different sets of experimental data available in the literature, it was demonstrated that sometimes the degradation rate can be limited mainly by oxygen diffusion and sometimes by absorption of UV radiation by a UV absorber. However, a complete analysis, including all experimental evidence available in the scientific literature, was not conducted.

Results and Discussion

The analyses conducted in this paragraph will start with a thorough discussion of an important, and often debated, model assumption and look at the experimental evidence presently available to evaluate it. Then follows an analysis of how the various effects of water on thermoset coating degradation can be implemented in the mathematical models. Finally, a model-based analysis, considering parameters expected to affect interlayer adhesion loss, is performed.

Verification of Model Assumptions: Oxidation Rates Limited by Oxygen Diffusion and/or Absorption of Radiation by Photoproducts

It is an ongoing discussion in the literature (see, e.g., [3, 9, 10]) and at conferences whether the oxidation zone thickness established during photooxidation is mainly limited by oxygen diffusion or absorption of radiation by photoproducts. While this question may not be answered in the general case because it depends on the specific

system parameters, there are some experimental observations that a proposed mechanism for epoxy–amine coatings must be able to explain. These observations are presented below followed by a discussion of which of the two mechanisms that best can explain the findings.

The phenomena, termed P1–P4, that must be in agreement with a proposed mechanism of photoinitiated coating degradation of epoxy–amine systems are as follows.

P1: Transient Development in the UV–VIS Absorption Spectrum

During photooxidation, the UV–VIS absorption spectrum (in transmission mode) of epoxy coatings initially can increase dramatically. For instance, Rivaton et al. [10] in their figure 2 have shown that the UV absorbance at 300–330 nm, the spectral sensitive region for epoxies, increases from about 0.2 to 2.5 in 590 h, equivalent to a factor of 12.5. After 140 h, the UV absorption was about 2.0 and after 211 h about 2.3. In Fig. 3 in the same reference, it was shown that constant carbonyl and hydroxyl absorptions are reached after about 200 h of laboratory exposure. The absorption also increases in the visible spectrum, causing the well-known yellowing of epoxy.

P2: Variation in Oxidation Zone Thicknesses

Chemically different cross-linkers and/or differences in equivalent weights of epoxy and/or cross-linkers can result in oxidation zones of very different thicknesses. Monney et al. [9] found that for highly cross-linked epoxy–amine coatings, the stable oxidation zone, reached after 10 days, is only about 2 μm, whereas Mailhot et al. [11] observed an oxidation zone thickness of 300 μm after 4.5 days for a low-T_g epoxy–amine coating. Rivaton et al. [10] found an oxidation zone thickness of 190 μm after 6 days for phenoxy resins, which are linear macromolecules with a molecular weight of about 50,000 g/mol and repeat units identical to the epoxy part in epoxy–amine coatings.

P3: Effect of UV Absorbers on the Oxidation Zone Thickness

When a wide oxidation zone is present in a non-stabilized coating, the addition of a UV absorber to the formulation narrows the oxidation zone (e.g., from 250 to 40 μm as shown in Kiil [5]).

P4: Effect of Relative Humidity (RH) on Lag Time and Erosion Rate

Studies of photooxidation under constant and controlled conditions have shown that a lag time is evident prior to the onset of coating erosion. This lag time is independent of the relative humidity of the surrounding air (e.g., Rezig et al. [6]). The stable (constant) erosion rate, established shortly after the lag time is over, however, is indeed a function of the relative humidity. Rezig et al. [6] have shown that the stable erosion rate is reduced by more than 50 % by changing the RH from 75 to 9 %.

Analyses of Observations P1–P4

P1: The data in Fig. 2 in Rivaton et al. [10], which are valid for a film thickness of 25–50 µm (average of 37.5 µm), show that the absorbance, A, increases from 0.2 to 2.5 during photooxidation (590 h of exposure in total). Both sides of the free film were exposed to UV radiation. Prior to exposure, only phenoxy groups (and potential impurities) absorp UV radiation in the phenoxy resins. Supplementary data in Fig. 4 of Rivaton et al. show that the oxidation zone thickness for one-side-only exposure is about 100 µm in a 190 µm thick film after 145 h. Therefore, it seems reasonable to assume that the oxidation zone extends over the entire coating of 37.5 µm after 590 h and that this is the reason for the stable carbonyl signal after about 200 h (erosion will be negligible in the 590 h considered). Rivaton et al. [10] and Malajati et al. [12] have identified the main solid products of photooxidation of phenoxy resins to phenyl formate end groups, but also hydroperoxides, saturated esters, and aliphatic carboxylic acids (e.g., acetic, formic, and oxalic acids) are formed in small amounts. Using the Beer–Lambert law, an average molar absorptivity (or extinction coefficient) of a homogeneous coating can be calculated from

$$\bar{\varepsilon} = \frac{-\log\left(\dfrac{I}{I_o}\right)}{lC} = \frac{A}{lC} \tag{12.6}$$

where A is the absorbance, l the film thickness, C the concentration of absorbants, and I/I_o the transmittance of radiation. The concentration C is unknown, but the initial concentration of phenoxy groups can be calculated assuming a binder density of 1 g/ml, a binder molecular weight of 50,000 g/mol, and a repeating unit molecular weight of 288 g/mol (each containing two phenoxy groups), giving a concentration of 7,000 mol/m³. With an initial absorption, A, of 0.2, this gives a molar absorptivity of phenoxy groups of 0.76 m²/mol. If one assumes that every phenoxy group in the epoxy repeating units forms a photoproduct during exposure, then the average molar absorptivity can be calculated to 9.5 m²/mol, which is a typical order of magnitude value for carbonyl group absorption (Schulz [1] states that a typical value is 1 m²/mol). If only 10 % of the phenoxy groups are converted to photoproducts, then the average molar absorptivity is 95 m²/mol. It therefore seems reasonable to assume that there is no oxygen diffusion limitation in this particular case with thermoplastic phenoxy resins and the oxidation zone thickness is limited by UV radiation absorption of photoproducts only. The diffusion coefficient of oxygen in partly degraded phenoxy resins is expected to be much higher than in highly cross-linked epoxy–amine coatings in good agreement with this finding.

P2: Various researchers have found very different oxidation zone thicknesses for coatings exposed under similar conditions. For one epoxy–amine network, a stable oxidation zone thickness of only 2 µm was measured, whereas for another a thickness of up to 300 µm was observed after just a few days of exposure. So, even though the epoxy repeating units are identical, the rate and penetration of degradation can be very different. If limited UV radiation penetration only, as a result of

highly absorbing photoproducts being formed in the outer layers when epoxy units degrade, was controlling the stable rate of oxidation, then one should expect very similar oxidation zone thicknesses for the same epoxy repeating units. However, if oxygen permeability in the coating influences the rate of photooxidation, then different oxidation zone thicknesses would be expected as a function of differences in oxygen permeability. As discussed in Schulz [1], the glass transition temperature (T_g) of a coating has a strong influence on the oxygen diffusion rate in a given coating. Kiil [5] has compared two epoxy–amine networks with different cross-linkers, where the T_gs are −50 °C and above 100 °C, respectively, and here the oxidation zone thicknesses differ by a factor of 150. Also, the phenoxy resin results discussed under P1 show a 100 μm wide oxidation zone after 190 h, and the diffusion rate of oxygen is expected to be high in this thermoplastic (no cross-links) coating. For a cross-linked epoxy–amine coating, the oxygen solubility in the coating is about 8.5 vol.% or 3.4 mol/(m^3 coating), which can be compared to a much higher initial concentration of phenoxy groups of 4,767 mol/(m^3 coating) (data from [3]). Therefore, one should not expect much effect of dark periods, where the coating is allowed to saturate with gaseous oxygen, because the small amount of oxygen that can be dissolved in the coating is rapidly consumed when the UV radiation is initiated. Therefore, in this case, it seems that an oxygen diffusion limitation is a more plausible explanation to the observations than a limited UV radiation penetration. However, as discussed in [3, 5], it seems likely that the oxidation zone must be somewhat cracked and porous and therefore should not pose a significant barrier to oxygen diffusion, but maybe only the very top 10–20 nm are seriously damaged as investigations suggest [13, 14]. In addition, Rivaton et al. [10] actually measured an almost 40 % decrease in the rate of oxygen permeability after UV radiation exposure. More investigations are required to address this point. Summarizing, the explanation to P2 is most likely an oxygen diffusion limitation.

P3: The addition of UV absorbers to a non-stabilized coating will reduce the oxidation zone thickness, and this is the reason why these additives are used. Using data from other references, it was demonstrated how the oxidation zone thickness can be reduced from 250 to 40 μm after 30 h exposure of a nondurable epoxy–amine coating [5]. If highly absorbing photoproducts were controlling the extent of penetration of photooxidation, then one should not expect a significant effect from adding a UV absorber unless the molar absorptivity of the UV absorber is much larger than for the photoproducts. A typical molar absorptivity of a UV absorber is about 400 m^2/mol [3], and therefore, photoproducts with molar absorptivities of several thousands can be ruled out. In summary, P3 can presently be explained by both mechanisms, but an oxygen diffusion limitation seems the most likely.

P4: The effect of relative humidity on coating degradation also provides some clues to the importance of the different mechanisms. Studies of photooxidation under constant and controlled conditions have shown that a lag time is evident prior to the onset of coating erosion and that this lag time is independent of the relative humidity of the surrounding air (e.g., Rezig et al. [6]). On the other hand, the stable (constant) erosion rate, established shortly after the lag time is over, is indeed a function of the relative humidity. If oxygen diffusion is rate limiting, then this effect can be

explained. As discussed in Kiil [3], a reduction in relative humidity can cause a lowering of the glass transition temperature of the coating and thereby the oxygen diffusion coefficient in the coating. Perera and Eynde [15] have measured the T_g of an epoxy–amine network and found that it may increase from about 45 °C at RH = 75 % to about 80 °C at RH = 9 vol.%. Such an effect can actually explain why the lag time is independent of RH because a lowering of the oxygen diffusion coefficient only affects the photooxidation rate in the bulk of the coating and thereby the stable erosion rate, but not the lag time, which only depends on surface degradation (see details in [3]). Simultaneously, a reduction in the oxygen diffusion coefficient by a change in RH can also explain the change in the stable photooxidation rate. On the other hand, the observations are hard to explain based on the UV radiation absorption by photoproducts mechanism. If absorbed water in the coating should take part in the photooxidation (e.g., formation of photoinitiators) and/or form other or more photoproducts, then this should also affect the surface degradation rate, which again would affect the lag time. Summarizing, the observations of P4 are best explained by the oxygen diffusion limitation mechanism.

The above mechanistic discussion should illustrate that mapping of the governing mechanisms during photoinitiated degradation of coatings is not an easy task and more work is required to complete the understanding. Presently, none of the two rate-limiting mechanisms can fully explain the experimental observations. More experimental investigations, supported by mathematical models, are required.

Verification of Model Assumptions: Effects of Rain on Photoinitiated Coating Degradation

Another very important assumption in the modeling work is how water can affect the degradation rate and degradation mechanisms. Water, in the form of humidity, dew, or rain, can, potentially, affect the physical properties of a coating (e.g., the glass transition temperature) but also react chemically (hydrolysis) with coating ingredients or photoproducts formed during degradation. In addition, rain can wash away photoproducts and thereby initiate erosion or increase the erosion rate. Presently, from a modeling point of view [3], there are no important chemical reactions with water reported for degrading epoxy–amine coatings and the topic will not be considered further here. However, it should be stated that the topic is not covered in much detail in the literature, and for other coating types, hydrolysis can be very important (e.g., for acrylic–melamine systems).

In Kiil [3], a front-tracking approach that takes into account the erosion effect from degradation is provided. The erosion front starts to move when the local degree of conversion of elastically effective network chains (or cross-link density) has reached a critical value, termed $X_{CL, max}$. This parameter is a strong function of coating ingredients. It was illustrated how nano-pigments, in very small amounts, may raise the value of $X_{CL, max}$ and thereby increase both lag time and the stable erosion rate [3]. It would be an interesting next step to verify this approach for coatings exposed to rain. Several authors (e.g., Misovski et al. [16]; Dubois et al. [17]) have
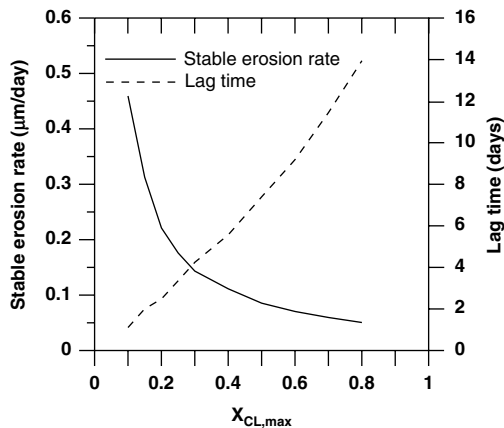
Fig. 12.2 Simulations of the effects of $X_{CL, max}$ on the stable erosion rate and lag time for a highly cross-linked epoxy–amine coating using the model of [3]. $X_{CL, max}$ is the degree of surface conversion of elastically effective network chains (cross-link density) at which erosion is initiated. The stable erosion rate is established shortly after the lag time has passed. Conditions are $T = 50$ °C, RH = 75 %, and $E_o = 480$ W/m^2 (295–400 nm). Other input and model parameters are provided in the figure caption of Fig. 3 in Kiil [3]

observed the effect of liquid water on the erosion rate, and, as a first attempt, it could therefore be assumed that the presence of rain simply decreases the value of $X_{CL, max}$, which in practice means that a smaller fraction of elastically effective network chains needs to be broken for erosion to initiate. Dubois et al. suggest (see discussion page 395 in Kiil [3]) that rain is one of the most important reasons that higher erosion rates are observed for the same epoxy coating in natural testing compared to laboratory testing when using cumulative radiation intensity (as opposed to time) as the independent variable. To illustrate the modeling approach, the effects of $X_{CL, max}$ on the stable erosion rate and lag time are shown in Fig. 12.2.

A separate simulation was required for each parameter value used in the figure. It can be seen that $X_{CL, max}$ (model input parameter) has a strong effect on both output parameters. As an example, if water (rain), hypothetically, reduces $X_{CL, max}$ from 0.4 to 0.2, then the lag time is reduced from 5.6 to 2.6 days and the stable erosion rate is doubled from 0.11 to 0.22 μm/day. Note that only $X_{CL, max}$ is varied in Fig. 12.2. In a real experiment, the presence of rain may change not only $X_{CL, max}$ but also the glass transition temperature of the coating and thereby the oxygen diffusion coefficient as discussed in a previous paragraph. The model can handle these two effects separately via the adjustable parameters $X_{CL, max}$ and the oxygen diffusion coefficient in the oxidation zone. For validation in practice, experiments, using different degrees of rainfall, need to be conducted. Initially, experiments with and without rainfall can be used for a crude test of the validity of the approach. If the model can simulate this effect, then additional experiments can be conducted with variations in the rainfall time or amount of rainfall. Two different rainfall pressures should reveal the independent effect of rain on $X_{CL, max}$ because the coating surface will be saturated

with water in both cases and the effect of water on the glass transition temperature of the coating will be the same.

It is interesting to note that the erosion front-tracking approach suggested here was used (and validated) in Kiil et al. [18] to simulate the effect of seawater velocity on the erosion rate of a chemically active underwater antifouling coating that slowly dissolves. That physical situation is somewhat similar to rain drops falling on, and affecting, a degrading coating surface. In summary, using the model of Kiil [3], it is possible to separate the effect of water on the glass transition temperature (and thereby the oxygen diffusion coefficient in the oxidation zone) and the erosion rate. However, experiments are needed to verify the approach.

Verification of Model Assumptions: Further Experimental Studies

In addition to the essential assumptions discussed above, there are other assumptions that would benefit from further investigations. These are listed in [3] and discussed for the case of epoxy–amine coatings. An example that deserves mentioning is a detailed characterization of the oxidation zone. The size and degree of penetration of cracks, the level of porosity, and the horizontal homogeneity of the surface are, in particular, issues of interest. Modern analytical tools may help to map these properties.

Effects of Model Parameters on the Lag Time and Implications for Intercoat Adhesion Issues

As mentioned in the introduction, epoxy–amine coatings, having a subsequent application of a UV radiation resistant top coat, may suffer from interlayer adhesion loss. The reason is that photoinitiated epoxy coating degradation occurs after just a few days without protection. It is desirable to extend this short time to allow more flexible application intervals. Trying to meet this challenge can be viewed in terms of the lag time. When the lag time has passed and a stable oxidation zone thickness of about 2 μm for highly cross-linked systems is established, the surface of the epoxy coating, in principle, no longer changes. This means that the adhesion of a top coat to the surface degraded epoxy coating should be the same shortly after the lag time has passed as after long time exposure (weeks or months). Additionally, the worst possible adhesion strength is most likely after the lag time is over (disregarding changes in rainfall and/or dirt/grease accumulation on the surface, which will also have an effect) because the degree of binder conversion is at its maximum. During the lag time, only little loose degraded material is expected to be present in the oxidation zone because erosion has not yet been initiated. Loose material, that is no longer part of the cross-linked structure, is expected to reduce the adhesion

Fig. 12.3 Simulations of the effects of oxygen solubility in the coating on the stable erosion rate and lag time for an epoxy–amine coating using the model of [3]. When the parameter value on the x-axis is equal to unity, it corresponds to the base case value used in [3]. Conditions are $T = 50$ °C, RH = 75 %, and $E_o = 480$ W/m^2 (295–400 nm). Other input and model parameters are provided in the figure caption of Fig. 3 in Kiil [3]
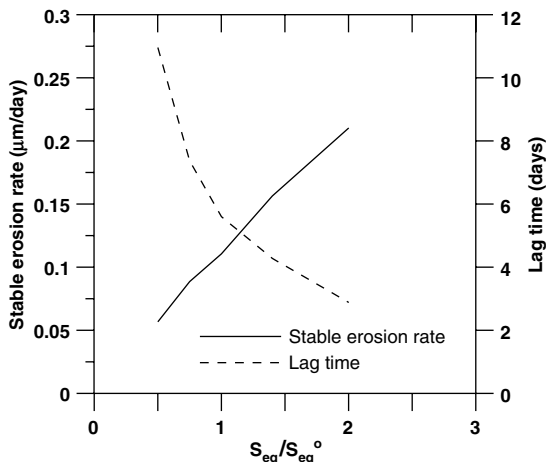
Fig. 12.4 Simulations of the effects of the rate constant of the photoinitiation reaction, k_1, on the stable erosion rate and lag time for an epoxy–amine coating using the model of [3]. When the parameter value on the x-axis is equal to unity, it corresponds to the base case value used in [3]. Conditions are: $T = 50$ °C, RH = 75 %, and $E_o = 480$ W/m^2 (295–400 nm). Other input and model parameters are provided in the figure caption of Fig. 3 in Kiil [3]
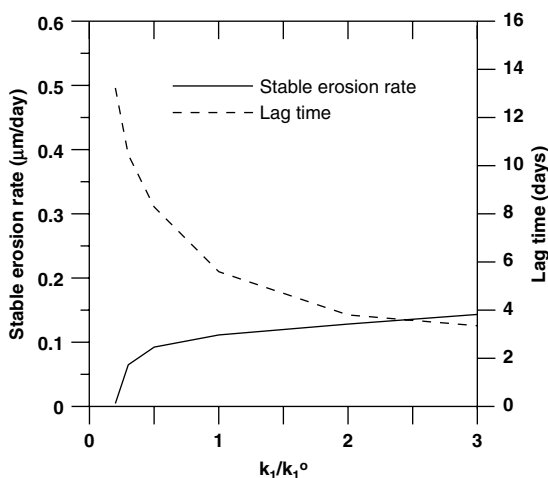
strength between the epoxy and the top coat severely. Therefore, the aim, if mechanical removal of the oxidation zone on site (so-called abrasive sweeping) is to be avoided as a means of rectifying the problem, is to extend the lag time from days to weeks. This is by no means a guarantee for good adhesion because the cross-linked structure is starting to degrade already during the lag time, but at least a practical direction for the optimization of the adhesion strength. Parameters that affect the lag time are the surface conversion at the unset of erosion ($X_{CL, max}$), oxygen solubility in the coating (S_{eq}), and the photooxidation rate constants (k_1 and k_2 as defined in [3]). The effect of $X_{CL, max}$ on the stable erosion rate and the lag time was shown in Fig. 12.2. In Figs. 12.3, 12.4, and 12.5, the influence of oxygen solubility in the coating and the photooxidation rate constants are shown. A separate simulation was required for each parameter value used in the figures.
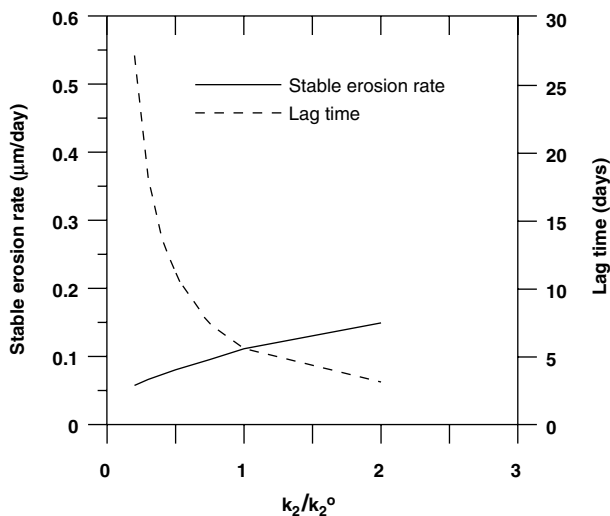
Fig. 12.5 Simulations of the effects of the rate constant of the radical oxidation reaction, k_2, on the stable erosion rate and lag time for an epoxy–amine coating using the model of Kiil [3]. When the parameter value on the *x*-axis is equal to unity, it corresponds to the base case value used in Kiil [3]. Conditions are $T = 50\ °C$, RH = 75 %, and $E_o = 480\ W/m^2$ (295–400 nm). Other input and model parameters are provided in the figure caption of Fig. 3 in Kiil [3]

It can be seen that all four parameters, at least in principle, can be used to extend the lag time and simultaneously obtain a reduction in the stable erosion rate. $X_{CL,\ max}$ may be manipulated by, e.g., a change in initial cross-link density, cross-linker stability, or addition of certain nano-pigments in very small amounts (see [3]). Photooxidation rate constants can be altered by using other cross-linkers (type and molecular weight) with better stabilities and is probably the most direct way of influencing the lag time. Absence or presence of any impurities of metal catalysts can also have an influence. Changing the oxygen solubility of the coating in a practical way is probably difficult but is, theoretically, a route to take in an attempt to increase the lag time. UV absorbers, according to the Beer–Lambert law, can only have an effect when the oxidation zone thickness extends more than a few micrometers (and UV absorbers are expensive). Exploring all these issues with relevant experimental investigations is suggested for future research.

Suggestions for Future Experiments

Based on the above analyses, it is now possible to make some concrete suggestions for future studies. First of all, it would be very useful with additional exposure studies under tightly controlled conditions and *all* relevant measurements conducted and recorded. The following data should be measured and recorded: chamber and sample temperature, UV radiation intensity and lamp distance from sample, relative

humidity of exposure and sample storage chamber air, amount and time of rainfall, transient coating weight losses and coating thickness reductions, sample size (area exposed and coating thickness), IR measurements (in reflection mode and if possible also in transmission mode), coating depth profiles including oxidation zone thicknesses at selected time intervals (using, e.g., micro-FTIR), surface appearance (e.g., cracks) and morphology, binder chemistry, and coating ingredients (molecular weights, stoichiometry, functionalities, and content of UV absorbing groups, impurities, UV absorbers, antioxidants, pigments, and additives in general). This is obviously a very demanding list, but is required for a meaningful verification of the very detailed models that are presently being developed and some studies actually come close to a fulfillment of these requirements (see, e.g., data series used in [3]). Gloss and color changes are not included here because these parameters are less important for primers or intermediate coats, but can of course be taken into account if relevant. To obtain controlled conditions (incl. the relative humidity), equipment such as the NIST sphere is required and cheaper and commercial versions of this unique apparatus would be very useful. The exposure series should cover variations in both coating formulations and exposure conditions and some should use constant conditions; others include cyclic conditions to capture dynamic effects. Exposure under natural conditions is also relevant if all conditions (incl. time of wetness and rainfalls) are continuously quantified and recorded. However, as a first step, the models should be developed to explain the rate phenomena seen in the laboratory.

With respect to verification of model assumptions, more experiments are required to characterize the oxidation zone and the effects of different rainfall pressures and coating additives on the rate of degradation. In addition, measurements of oxygen diffusion rates, as a function of degree of coating degradation and relative humidity of the exposure chamber atmosphere, would also be very useful.

Finally, it is recommended to study experimentally the model predictions of lag times and stable erosion rates presented in this work. Can lag time predictions help to optimize the intercoat adhesion loss as suggested? This should involve a quantitative mapping of the parameters that influence the lag time values.

Conclusions

Detailed mathematical modeling of photoinitiated coating degradation is becoming increasingly important as a tool to mapping of mechanisms and potential service life predictions. This, however, also put demands on researchers for proper model validation of assumptions and outputs. In the past decade or so, great progress, due to new analytical techniques and improved exposure equipment, has been made, but there are still serious obstacles to be overcome to get truly reliable predictions under a variety of exposure conditions and for different types of coatings. In the present work, the most important challenges for cross-linked (thermoset) coatings, as seen by the author, have been outlined.

References

1. Schulz U (2009) Accelerated testing. Vincentz, Hannover
2. Sørensen PA, Kiil S, Weinell CE, Dam-Johansen K (2009) Anticorrosive coatings—a review. JCT Res 6(2):135–177
3. Kiil S (2012) Model-based analysis of photoinitiated coating degradation under artificial exposure conditions. J Coat Technol Res 9(4):375–398, open access article
4. Gurack D, Krüger G, Krotzek A, Rudolf A (2011) Adhäsionsverhalten zwichen bewitterten 2K-EP. Beschichtungen und 2K-PUR-Beschichtungen-Einfluss der Bewitterung (in German), Stalbau 80, Heft 8
5. Kiil S (2013) Mathematical modeling of photoinitiated coating degradation: effects of coating glass transition temperature and light stabilizers. Prog Org Coat 76:1730–1737
6. Rezig A, Nguyen T, Martin D, Sung L, Gu X, Jasmin J, Martin J (2006) Relationship between chemical degradation and thickness loss of an amine-cured epoxy coating exposed to different UV environments. JCT Res 3(3):173–184
7. Kiil S (2010) Quantification of simultaneous solvent evaporation and chemical curing of thermoset coatings. JCT Res 7(5):569–586
8. Kiil S, Bhatia SK, Dam-Johansen K (1995) Solution of transient problems with steep gradients: novel front-tracking strategy. Chem Eng Sci 50(17):2793–2799
9. Monney L, Dubois C, Chambaudet A (1997) Ablation of organic matrix: fundamental response of a photo-aged epoxy-glass fibre composite. Polym Degrad Stab 56:357–366
10. Rivaton A, Moreau L, Gardette J (1997) Photo-oxidation of phenoxy resins at long and short wavelengths—I. Identification of the photoproducts. Polym Degrad Stab 58:321–332
11. Mailhot B, Morlat-Therias S, Ouahioune M, Gardette J (2005) Study of the degradation of an epoxy/amine resin 2: kinetics and depth-profiles. Macromol Chem Phys 206:585–591
12. Malajati Y, Therias S, Gardette J (2011) Influence of water on the photooxidation of KHJ phenoxy resins, 1. Mechanisms. Polym Degrad Stab 96:144–150
13. Nguyen T, Gu X, Vanlandingham M, Byrd E, Ryntz R, Martin JW (2013) Degradation modes of crosslinked coatings exposed to photolytic environment. JCT Res 10(1):1–14
14. Gu XH, Nguyen T, Oudina M, Martin D, Kidah B, Jasmin J, Rezig A, Sung LP, Byrd E, Martin JW (2005) Microstructure and morphology of amine-cured epoxy coatings before and after outdoor exposures—an AFM study. J Coat Technol Res 2(7):547–556
15. Perera DY, Eynde DV (1987) Moisture and temperature induced stresses (hygrothermal stresses) in organic coatings. J Coat Technol 59(748):55–63
16. Misovski T, Nichols ME, Hardcastle HK (2009) The influence of water on the weathering of automotive paint systems. In: Martin JW, Rintz RA, Chin J, Dickie RA (eds) Service life prediction of polymeric materials—global perspectives. Springer, New York, Chapter 20
17. Dubois C, Monney L, Bonnet N, Chambaudet A (1999) Degradation of an epoxy-glass-fibre under photo-oxidation/leaching complementary constraints. Compos Part A 30:361–368
18. Kiil S, Weinell CE, Pedersen MS, Dam-Johansen K (2001) Analysis of self-polishing antifouling paints using rotary experiments and mathematical modelling. Ind Eng Chem Res 40(18): 3906–3920

Chapter 13
Accelerated Service Life Testing of Photovoltaic Modules

Michael Koehl

Abstract Temperature, temperature cycling, water and UV radiation are considered as main degradation factors for PV modules by causing hydrolysis and photodegradation of polymeric components and corrosion of glass and of metallic components like grids and interconnectors.

The temperature is very important for the degradation of the PV modules, because it determines at least the reaction rate for the degradation processes caused by the other degradation factors (e.g.hydrolysis by humidity and photodegradation by UV light). Modelling of the service life of modules applied in different climatic regions requires knowledge about the transient temperature load. A model, which allows calculating the module temperature as function of the ambient temperature, the global irradiation and the wind speed, facilitates the use of any time series of climatic data for a climatic region of interest. This data could be provided by weather services, test reference years or via the Internet.

The microclimatic stress level of UV radiation and moisture on the PV modules is modelled as function of the module temperature and the important climatic parameters. Simple time transformation functions were used for the design of appropriate accelerated service life tests. The evaluated testing times differ up to an order of magnitude for different climatic locations, depending on the kinetics of the dominant degradation processes.

Outdoor Monitoring

Different test sites (see Fig. 13.1) have been equipped with instrumentation for monitoring the climate. The solar irradiance was measured by calibrated pyranometers, UV-A, UV-B with integral sensors and the wind velocity and direction with anemometers 3 m above ground. The module temperatures were measured at the

M. Koehl (✉)
Fraunhofer ISE, Freiburg, Germany
e-mail: michael.koehl@ise.fraunhofer.de

Fig. 13.1 The outdoor test facilities: City (*upper left*), Freiburg, Germany (equipped with thin-film modules and reference modules); desert (*upper right*), Sede Boqer, Israel, in cooperation with the Ben-Gurion University of the Negev and TÜV Rheinland; alps, Schneefernerhaus, Germany (*middle left*), in cooperation with TÜV Rheinland; tropics (*middle right*), Serpong, Indonesia, in cooperation with TÜV Rheinland; maritime (*lowest picture*), Gran Canaria, in cooperation with Instituto Tecnologico de Canarias

back-sheets by means of foil Pt-100 sensors except at the site in Sede Boqer, where thermocouples were used. The measurement results were stored as 5-min averages [1].

Seven module types based on crystalline solar cells were exposed. Resistive loads kept them in operation near the so-called maximum power point with the electrical power dumped to the resistor to reduce the temperature load for the modules.

Different thin-film modules were investigated within the scope of the EU-project PERFORMANCE in subproject 5 (service life assessment). Triplicates of each kind were exposed for outdoor weathering with monitoring of the module temperatures and the climatic data at the CEA/INES research station in Cadarache (France)

and at Fraunhofer ISE in Freiburg (Germany), as shown in Fig. 13.1 upper left. All modules were equipped with software-controlled electronic loads for alternating current–voltage curve monitoring and maximum power point tracking.

Data Evaluation

The frequency distributions of the average module temperatures at three different test sites show the wide variety of the climatic conditions (Fig. 13.2). The average module temperatures were 65 °C at the maximum, about 30 K above ambient air temperature.

The difference between module temperature and ambient temperature is nearly a linear function of the irradiation with a slope depending on the wind speed (see Fig. 13.3). Deviations can be observed for low and high irradiation. Radiation cooling and natural convection reduces the module temperature for a small wind speed (lower than about 4 m/s) and low solar irradiation. The higher the wind speed, the smaller the deviation caused by these cooling effects. Natural convection reduces the temperature at very high irradiation and low wind speed. Turbulent heat transfer above 7 m/s wind speed might be assumed.
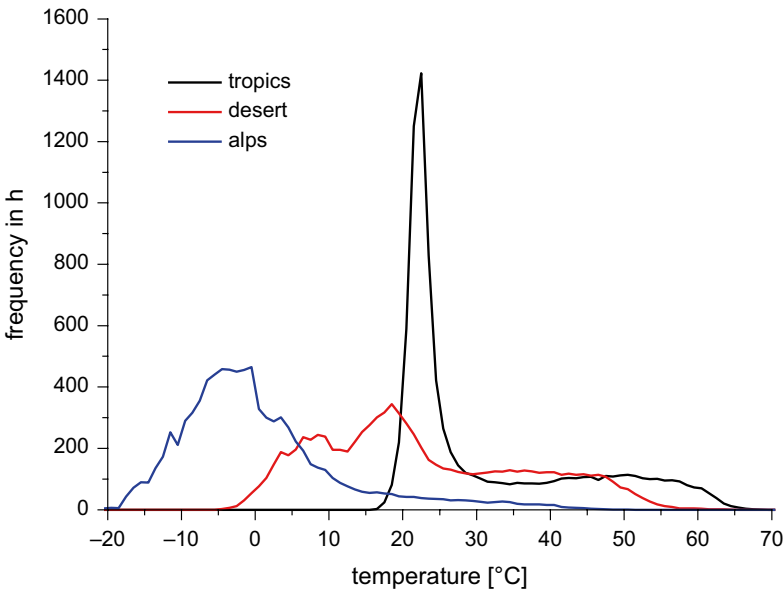
Fig. 13.2 Frequency distributions of the average temperatures of all measured modules at the different test sites for 1 year

Fig. 13.3 Difference
between the average module
temperatures and the ambient
temperatures at the desert test
site in the Negev as a
function of the global
irradiation in the plane of the
array for different wind speed
bins for 1 year. Several
dashed straight lines starting
at the origin are drawn as
guidance for the eye
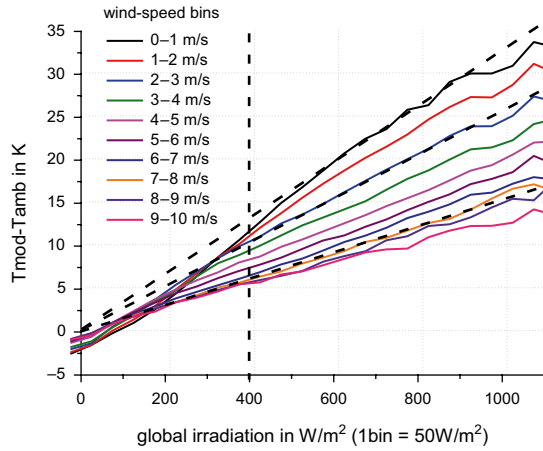
Modelling of Module Temperatures

Not only are the stresses directly caused by the operational temperatures important, but the module temperature as part of the microclimate is also a major parameter for the other microclimatic properties. The most important property is the surface humidity, but also the photodegradation by UV irradiation might be accelerated by the sample temperature. Numerous models have been proposed for the simulation of the module temperature and are discussed in a comprehensive overview [2]. One of the models was derived from the energy balance for a solar thermal collector by David Faiman [3]:

$$T_{\mathrm{mod}} = T_{\mathrm{amb}} + \frac{G}{U_0 + U_1 \cdot v} \tag{13.1}$$

T_{mod}, module temperature; T_{amb}, ambient temperature; G, global irradiation in the plane of incidence; and v, wind speed.

U_0 [W/°C m^2] is a coefficient describing the effect of the radiation on the module temperature, while U_1 describes the cooling by the wind and has the dimension W s/°C m^3.

These parameters depend on the module design and materials, but not on the location and the climatic conditions [4]. Some typical values are given in Table 13.1.

The model neglects the influence of the infrared irradiation exchange with the cold sky and the natural convection (buoyancy), which is noticeable at low wind speed and low irradiation (see Fig. 13.3). The model also neglects the back-insulation by roof mounting and building integration which would result in higher module temperatures as well and refer to literature [5, 6].

The model can be used to simulate the module temperature for operation at any location for which a time series with acceptable time resolution (hourly values or better) of the needed climatic data (solar irradiation, ambient temperature and wind speed)

Table 13.1 Parameters U_0 (W/°C m²) and U_1 (W s/°C m³) for typical PV modules

Type	Description	U_1	U_0
a-Si 1	Amorphous silicon on polymers	10.7	25.7
a-Si 3	Amorphous silicon on metal foil	5.8	25.8
a-Si 4	Amorphous silicon on glass	4.3	26.1
CIS 1	Cadmium–indium–selenide (brand 1)	3.1	23.0
CIS 2	Cadmium–indium–selenide (brand 2)	4.1	25.0
CdTe	Cadmium telluride	5.4	23.4
c-Si	Crystalline silicon	6.2	30.0
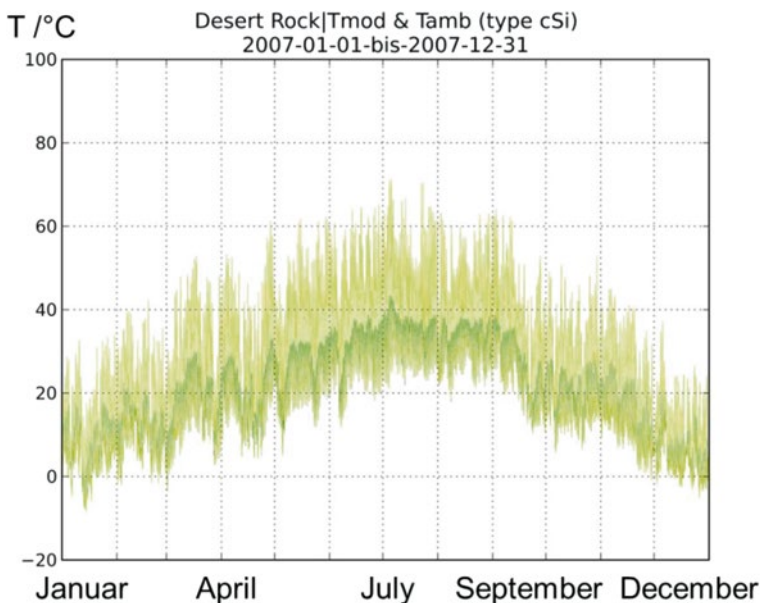
Fig. 13.4 Time series of measured ambient temperatures (*darker line*) and modelled module temperature (crystalline Silicon) for an arid location in the USA (desert rock)

is available and the module parameters U_0 and U_1 had been determined. An example is given in Fig. 13.4. Histograms of the module temperatures for different module types (see Fig. 13.5) provide a better comparison of the maximum temperature stress.

Accelerated Life Testing for Temperature Stress

The usual way of accelerating temperature stress is increasing the temperature. The kinetics of the degradation processes yield the acceleration factor. The most common model for acceleration by temperature increase is the Arrhenius relation. An increase of the absolute temperature from T_1 to T_2 will result in acceleration

$$a_{\mathrm{T}} = \exp\left[-\left(E_{\mathrm{a}} / R\right) \times \left(1 / T_2 - 1 / T_1\right)\right] \tag{13.2}$$
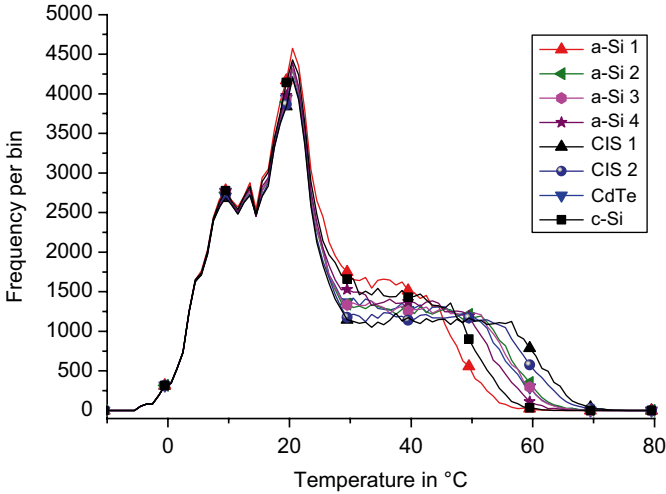
Fig. 13.5 Temperature histogram for the module temperature calculated with Faiman's model for 1 year in the Negev desert for different module types using the parameters listed in Table 13.1

where the material dependence is characterised by the activation energy E_a for the degradation process. R is the universal gas constant. Accelerating the outdoor stress conditions requires an integration of the transient temperature T_i at time intervals Δt_i for 1 year, e.g. resulting in a corresponding constant load at a reference temperature T_{ref} for a duration of

$$\Delta t_{ref} = \sum_{1}^{N} \Delta t_i \exp\left[-\left(E_a / R\right) \times \left(1 / T_{ref} - 1 / T_i\right)\right] \tag{13.3}$$

A more comparable presentation of the stress differences at different locations for unknown degradation processes can be achieved by introducing the so-called effective temperature T_{eff} [5, 6], which is defined as the constant temperature causing the same stress as the transient sample temperature during the same considered time period $N \Delta t_i$ where N is the number of integrated intervals Δt_i.

$$\Delta t_{ref} / N\Delta t_i = \exp\left[-\left(E_a / R\right) \times \left(1 / T_{ref} - 1 / T_{eff}\right)\right] \tag{13.4}$$

The monotonically increasing function of the effective temperature with growing activation energy reflects the stronger acceleration by periods of high sample temperature when the degradation processes have a high activation energy (Fig. 13.6).

The effective temperature allows an easy transformation of the stress dose to higher testing temperatures by applying Eq. (13.2) (see Fig. 13.7). The differences for life tests for the different climatic locations are obvious. They cover a range of one magnitude for activation energy of 50 kJ/mol and three times more for 100 kJ/mol.
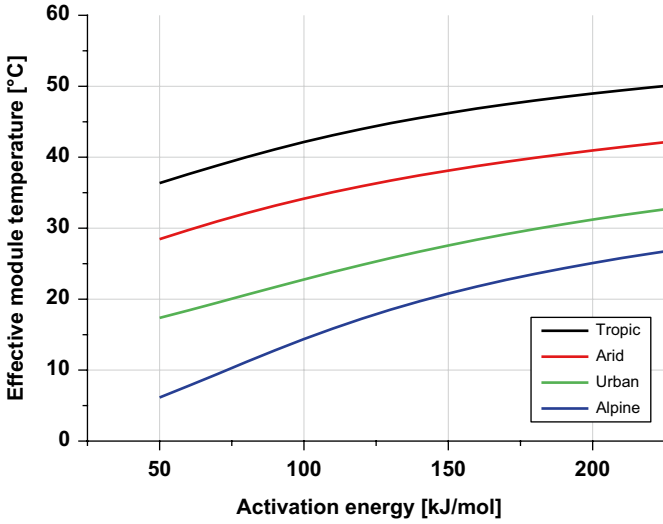
Fig. 13.6 Effective module temperatures for different locations as function of the activation energy
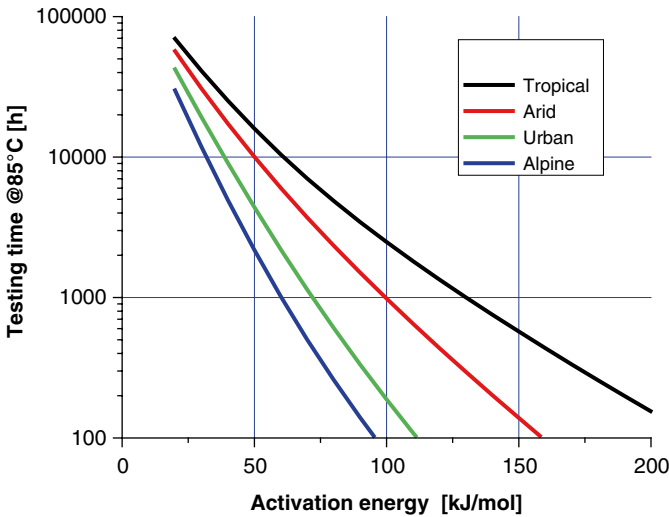
Fig. 13.7 Accelerated service life tests for a lifetime of 25 years (25a) at constant 85 °C calculated for four different locations based on module temperature measurements for 1 year as function of the activation energy of the dominating degradation process

The service life test for a desert environment requires a constant load exposure at 85 °C of 1,000 h for an activation energy of 100 kJ/mol, but ten times the testing time for 50 kJ/mol. This simple example demonstrates the importance of an estimation of the activation energies for accelerated service life testing.

Ultraviolet Irradiation

PV modules are exposed to solar irradiation. The short wavelength range is not visible but causes damages to organic (e.g. skin) and polymeric materials, since the energy of the radiation is big enough for breaking chemical bonds between carbon atoms that are found in the encapsulants or the polymeric back-sheets of the modules. The intensity and the spectral range of the relevant irradiation depend on the climatic situation on one hand and on the filtering by glazing materials or functional coatings like antireflective layers or UV screens on top of the glazing on the other hand. These intensities are not easy to measure. Most integral UV sensors suffer by differences between their individual spectral sensitivity and the sensitivity of the investigated materials, and their calibration. A simple approximation would be the assumption that the UV irradiation is about 5 % of the integral global solar irradiation G (Fig. 13.8). The errors (daily and seasonal variations of the ratio UV/G because of changes of the relevant air mass and the composition of the air) might be smaller than the measurement errors of integral UV sensors.

A suitable model for time transformation for accelerated testing takes into account the increasing irradiation I_{test} and the enhanced testing temperature T_{test}:

$$t_{test} = \left(I_o / I_{test}\right)^n \Delta t_i \cdot \exp\left[-\left(E_a / R\right)\cdot\left(1/T_{test}-1/T_o\right)\right] \quad (13.5)$$

The exponent n should be one for the so-called reciprocity resulting in a linear dose function.

A similar integration procedure as for the temperature loads resulted for the arid location in the testing times shown in Fig. 13.9. Note that the acceleration is
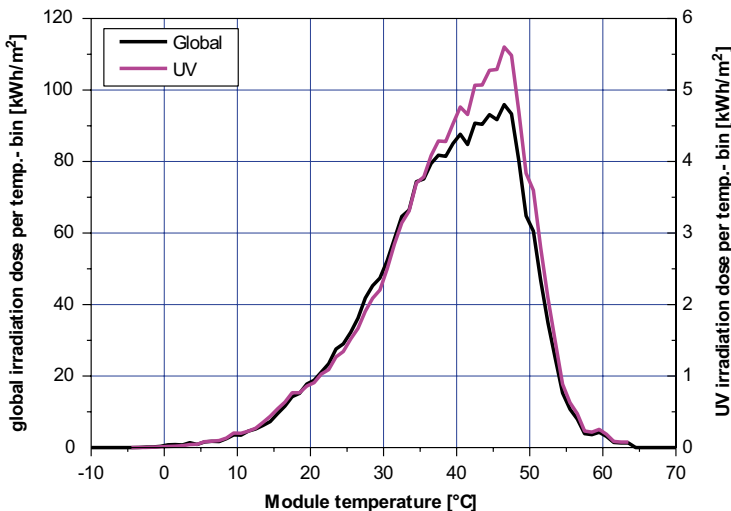
Fig. 13.8 Cumulated global solar and global UV irradiation as function of the module temperature for 1 year in the Israeli Negev desert
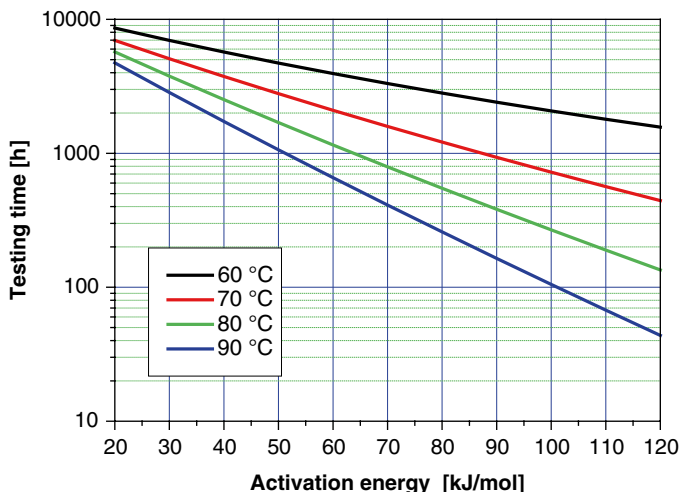
Fig. 13.9 Accelerated service life testing times at a UV radiation corresponding to 5 suns and a lifetime of 25 years (25a) for the arid test site calculated for four different accelerated testing temperatures as function of the activation energy of the dominating degradation process

very low for a test temperature of 60 °C (as applied in the type approval testing IEC 61215). A strong thermal activation of the photodegradation cannot be expected, but a slight acceleration by setting the sample temperature above 80 °C might shorten the testing times.

Humidity Impact

The water vapour absorbed in the polymeric components of a module can act as reaction partner in chemical (e.g. hydrolysis) or physical (delamination by thermomechanical stresses) degradation processes. A principal difference to energy transfer by heat conductivity (temperature) or radiation transfer (UV) is the need for mass transport of the water vapour molecules that is based on permeation, especially diffusion, processes. There are two possibilities for acceleration—increasing the moisture gradient and increasing the temperature. The second way uses the temperature dependence of the diffusion coefficient (mostly according to the Arrhenius law).

Both ways are followed by the classical damp-heat type approval testing for PV modules according to IEC 61215 and IEC 61646 [7]. Relating testing to reality has to take into account that this gradient changes during daytime. The modules are wetted by dew or high humidity in the morning at relatively low temperatures, and the surface is dried out by the absorbed solar energy increasing the module temperature during daytime. After some years, depending on the ambient climate, a kind of
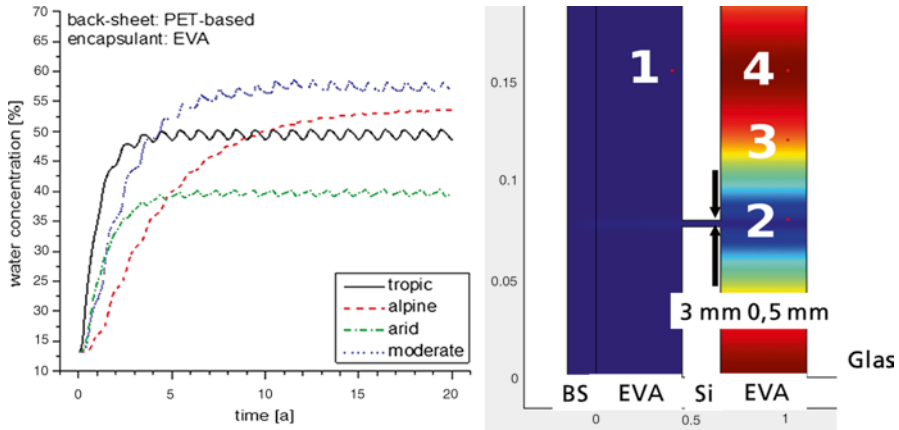
Fig. 13.10 Results of FEM simulations of the humidity in PV modules in the encapsulant. Left diagram: in front of the impermeable silicon cell (Pos 4 in the inset to the right) calculated with real monitored climatic border conditions at different locations with periodic repletion of one-year data of weathering. Right diagram: during an extended damp-heat testing for 3000 h at 85 °C and 85 % relative humidity at different places in the PV module: 1 is between the permeable back-sheet, 2 in the gap between two cells, 3 at halfway between edge and centre of a cell, 4 at the centre of the cell

equilibrium (depending on the climate conditions, too) for the water concentration in front of the silicon cells is reached [8] (Fig. 13.10), because the average path from the ambience to the centre of a silicon cell is about 70–100 mm and several years are needed for those diffusion processes (depending on the temperature).

Such studies cannot be performed for each possible material combination (esp. permeation and diffusion properties [9, 10]) and for every climatic situation. It is clear that only periods with high ambient humidity provide a humidity gradient promoting the accumulation of humidity inside the modules and that an elevated temperature promotes an enhanced humidity diffusion on one hand and a higher rate of the degradation process on the other hand. The gradient is driven by the surface humidity rh (T_{mod}) going up with increasing ambient humidity rh (T_{amb}) and down with increasing surface temperature T_{mod}:

$$rh(T_{mod}) = rh(T_{amb}) * P_{sat}(T_{mod}) / P_{sat}(T_{amb}) \qquad (13.6)$$

The stronger weighting of the higher humidity concentrations driving the permeation inwards can be modelled by the so-called effective humidity. For the PV modules, the sigmoidal function seems to fit best [11]:

$$rh_{eff} = 1 / (1 + 98 \exp(-9.4 rh(T_{mod}))) \qquad (13.7)$$

where the factor 9.4 is a free parameter fitted to the test results. It must be noticed that this strong coupling between ambient climatic conditions and the microclimatic stress conditions is more relevant for materials located in the rear part or the
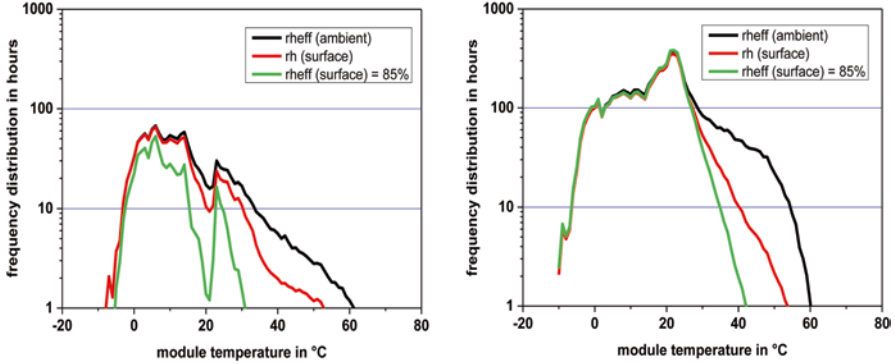
Fig. 13.11 Frequency distribution of the effective humidity at PV modules in a hot and dry arid location (*left*) and a warm, humid climate (*right*)

perimeters of the cells. The humidity at the front side of the cells is changing slower because of the relatively long diffusion path (see Fig. 13.10, spots 1 and 4).

Finally, the effective humidity levels must be transformed to the constant test condition, which is usually 0.85 for the module testing by the aid of a dose function:

$$\Delta t_{85} = \Delta t * rh_{eff} / 0.85 \qquad (13.8)$$

The histograms of the humidity as function of the module temperature are shown in Fig. 13.11 for a hot and dry and a hot and humid climate, respectively.

The integration of these loads applying the Arrhenius model for the time transformation function [Eq. (13.2)] yields functions for the life testing time at constant conditions (85 % relative humidity @ 85 °C) corresponding to 25 years service life time under operation under the monitored conditions (Fig. 13.12).

Service life tests for tropical application would not require stronger loads than the presently applied type approval damp-heat tests (1,000 h at 85 % rh @ 85 °C), if the activation energy of the dominating degradation process would be lower than 80 kJ/mol. A tenfold testing time was needed for a smaller activation energy of about 40 kJ/mol, but only 2,000 h testing for a qualification for a cold alpine climate (factor of 5 lower) would be needed in this case.

It is obvious that the activation energy is the crucial property for a service life estimation. Testing at different temperatures is needed. Figure 13.13 shows the results of such damp-heat tests for seven different modules with the same basic design using crystalline silicon cells embedded in the mostly used encapsulation material ethylene vinyl acetate (EVA) laminated with a solar glass and a polymeric back-sheet. After an initiation period, the normalised module power (the most important property) changed dramatically, and clear differences because of the different materials used by the different manufacturers can be seen. We select two modules behaving very differently for further consideration. Defining 80 % of the initial
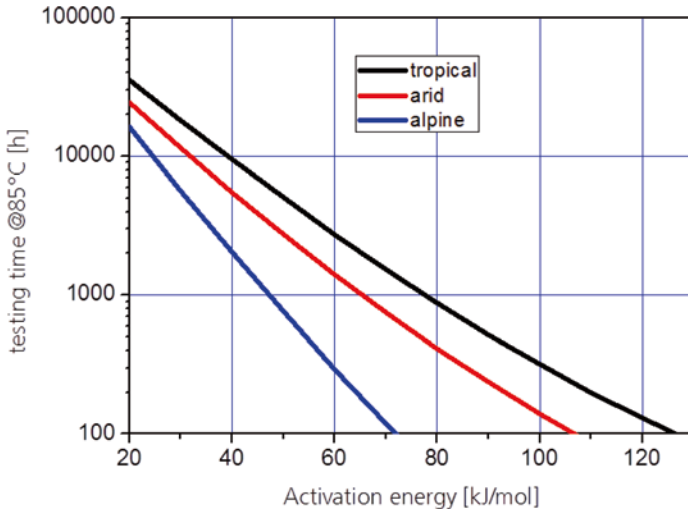
Fig. 13.12 Service life testing time at accelerated, constant conditions (85 % rel. humidity at 85 °C) corresponding to 25 years operation simulated with 1-year monitored ambient and micro-climatic stress data for three different climatic locations
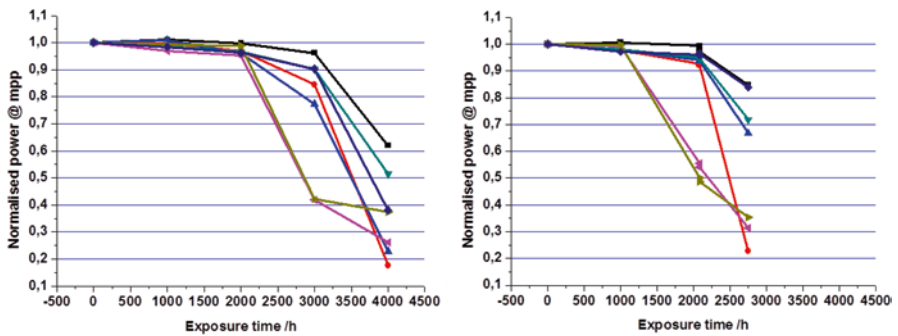
Fig. 13.13 Normalised power (standardised power output of the modules related to the virgin data before testing) over damp-heat testing time at 85 °C (*left*) and 90 °C of seven different PV modules

power as the performance criterion marking the end-of-life, or the time-to-failure, one module reached a time-to-failure of 2,400 h, the other of 3,300 h (Fig. 13.14).

The activation energies can be evaluated by transforming the testing time periods at 90 °C to 85 °C by using Eq. (13.2) in a way that they are fitting well into the degradation function at 85 °C. This results in an activation energy of 65 kJ/mol for module 1 and 35 kJ/mol for module 2 (see Fig. 13.15). This example demonstrates that the clearly longer time-to-failure might have been misleading when selecting the more durable module only on the base of a test with one single stress level. Module 1 would be the better choice in spite of shorter time-to-failure in the traditional damp-heat test, while module 2 needs dry and cold environment (Fig. 13.16).
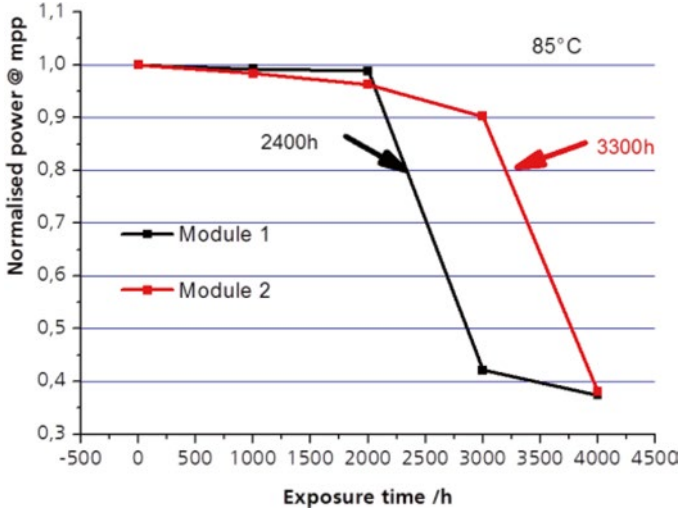
Fig. 13.14 Normalised power over testing time at 85 °C of two different PV modules
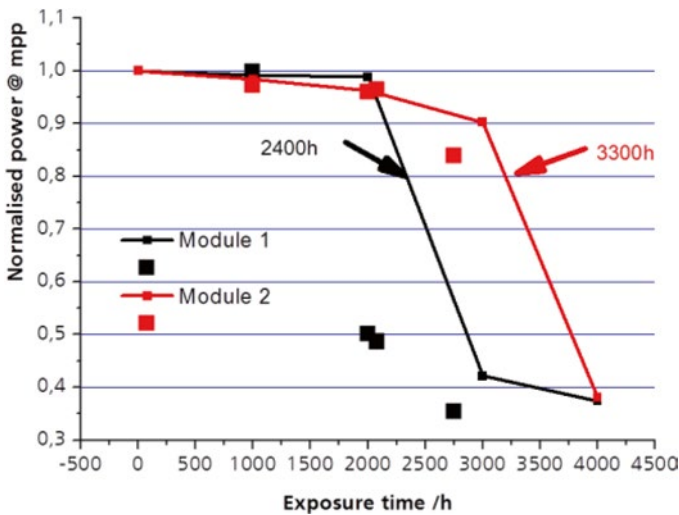
Fig. 13.15 Normalised power over testing time at 85 °C of two different PV modules and test results at 90 °C (*squares*)

Conclusions

A possible way for defining accelerated life tests for PV modules was sketched including the potential of defining stress categories for the degradation factors of temperature, humidity and UV irradiation based on monitoring the macroclimatic weathering

Testing time at 85%rh/85°C for 25 years lifetime

Time to failure 3300h

$E_a > 35$ kJ/mol

=> for alpine climates

Time to failure 2400h

$E_a > 65$ kJ/mol

=> for tropical climates
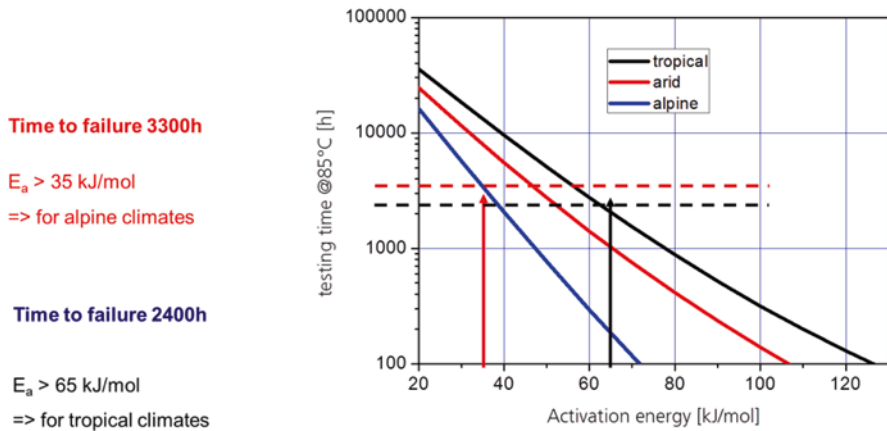
Fig. 13.16 Qualification of the moisture resistivity of two modules with different degradation processes resulting in different time-to-failure and different activation energies for three different climatic stress conditions. The longer time to failure in accelerated life testing for the module indicated in *red* does not result in better durability in operation compared to the second module because of the low activation energy

conditions and measuring and modelling some microclimatic stress conditions. Worst-case conditions have to be defined for the stress factors in the future.

The models for the microclimatic stress should allow estimating the stress conditions expected at any potential location of PV power plants provided that reliable weather data with a sufficient time resolution are available for a typical year.

The humidity impact is difficult to handle because of the long time constants of the typical diffusion processes in the used polymers.

References

1. Koehl M, Heck M, Philipp D, Weiss K-A, Ferrara C, Herrmann W (2008) Indoor and outdoor weathering of PV-modules, SPIE conference 7048, San Diego
2. Skoplaki E, Palyvos JA (2009) Operating temperature of photovoltaic modules: a survey of pertinent correlations. Renew Energy 34:23–29
3. Faiman D (2008) Assessing the outdoor operating temperature of photovoltaic modules. Prog Photovolt Res Appl 16:307–315
4. Koehl M et al (2011) Modeling of the nominal operating cell temperature based on outdoor weathering. Sol Energy Mater Sol Cells 95:1638–1646

5. Koehl M (ed) (2004) Performance and durability assessment: optical materials for solar thermal systems. ISBN 0-08-044401-6, Elsevier, p 209ff
6. Kurtz S, Whitfield K, TamizhMani G, Koehl M, Miller D, Joyce J, Wohlgemuth J, Bosco N, Kempe M, Zgonena T (2011) Evaluation of high-temperature exposure of photovoltaic modules. Prog Photovolt Res Appl 19: n/a. doi:10.1002/pip.1103
7. IEC 61215 ed. 2 (Crystalline silicon thin-film terrestrial photovoltaic (PV) modules—design qualification and type approval) and IEC 61646 ed. 2 (Thin-film terrestrial photovoltaic (PV) modules—design qualification and type approval)
8. Hülsmann JP, et al (2013) Simulation of water vapor ingress into PV-modules under different climatic conditions. J Mater 2013. doi:10.1155/2013/102691
9. Kempe MD (2006) Modeling of rates of moisture ingress into photovoltaic modules. Sol Energy Mater Sol Cells 90:2720–2738
10. Hülsmann P, Philipp D, Köhl M (2009) Measuring temperature-dependent water transport and gas permeation through high barrier films. Rev Sci Instrum 80:113901
11. Koehl M et al (2012) Modelling of conditions for accelerated lifetime testing of Humidity impact on PV-modules based on monitoring of climatic data. Sol Energy Mater Sol Cells 99:282–291

Chapter 14
Polypropylene Numerical Photoageing Simulation by Dose–Response Functions with Respect to Irradiation and Temperature: ViPQuali Project

Anja Geburtig, Volker Wachtendorf, Peter Trubiroha, Matthias Zäh, Artur Schönlein, Axel Müller, Teodora Vatahska, Gerhard Manier, and Thomas Reichert

Abstract   The aim of the joint project ViPQuali (Virtual Product Qualification) was to describe a component's ageing behaviour in a given environment, by numerical simulation.

Having chosen polypropylene (PP) as the material, which does not show sensitivity to moisture, the relevant weathering parameters of the dose–response functions could be limited to spectral irradiance and temperature.

In artificial irradiation tests, for PP plates of varied stabiliser content, spectral sensitivity as well as temperature dependence of irradiation-caused crack formation was quantified. For that purpose, samples were exposed both to artificial weathering tests at various constant temperatures and to spectrally resolved irradiation. The temperature dependence could be modelled by an Arrhenius fit. For fitting the spectral sensitivity, a plateau function was chosen. Subsequently, the stabiliser content was parameterised and extrapolated.

A. Geburtig (✉) • V. Wachtendorf
BAM Federal Institute for Materials Research and Testing, Berlin, Germany
e-mail: anja.geburtig@bam.de

P. Trubiroha
Berlin, Germany

M. Zäh
Clariant, Gersthofen, Germany

A. Schönlein
ATLAS MTT, Linsengericht-Altenhasslau, Germany

A. Müller • T. Vatahska
HTCO, Freiburg, Germany

G. Manier
Weiterstadt, Germany

T. Reichert
Fraunhofer ICT, Pfinztal, Germany

The formed dose–response functions were incorporated into a Computational Fluid Dynamics (CFD) software program, simulating the environment of a sample within a Phoenix-exposed IP/DP (Instrument Panel/Door Panel box) box, based on sun position and weather conditions, including radiation interactions. Observed local effects as well as the general ageing advance of PP hats are compared with respect to simulation and experiment.

Resulting from this project, for this most simple example of PP of varied stabiliser content, the time to failure can be estimated for each weathering exposure environment with known time-resolved irradiance and temperature conditions.

Introduction

Prediction of a product's service life, more precisely of its failure, is a long-existing challenge [1]. However, it can never be given universally, but is always dependent on the respective in use or exposure conditions.

The aim of the joint project ViPQuali[1] was to qualify plastic components for use in arbitrary but defined surroundings [2]. The relevant ageing impact parameters are simulated at the components surface, based on environment geometry and weather data. Then, ageing behaviour is computed, on the basis of empiric dose–response functions (DRF). A fundamental requirement for the concept of DRF is the existence of just one failure property, whose progress can be described quantitatively.

For plastic materials, it is well known that usually the most important weathering parameters are UV irradiance and temperature [3]. Generally, UV radiation initiates photodegradation, whereas temperature influences the kinetics of the autoxidation process ([4], p. 849ff).

For photodegradation, the spectral sensitivity generally is limited to the UV range. However, observing colour changes of pigments and also the VIS range of solar radiation may have influences. Besides, VIS and IR mainly act by radiation heating, reflecting irradiance temperature interactions.

Considering moisture, it is hard to quantify it in its incidence (as considering humidity or wetness of surface microclimates), even harder in its prediction (incorporating radiation and temperature interactions) and hardest in its action on materials ageing ([4], p. 852f). Therefore, for the ViPQuali project, materials and scenarios were chosen, for which moisture influence should not play a major role. Thus, only temperature and irradiance have to be considered, in the concept of DRF.

DRF as well as Service Life Prediction itself can be related to a specific failure criterion only. For the DRF concept, the failure property progress is to be quantitatively measurable, additionally.[2]

After all, the DRF has to be formulated as time integral of the multiplied, often coupled sensitivity terms.[3] Taking into account only sensitivity to spectral irradiance[4] and temperature, DRF for a specific material can be written as

$$w(t) = \int_0^t F\big(T(t')\big) \int_{\lambda_0}^{\lambda e} s_\lambda \cdot E_\lambda(t') \cdot d\lambda \cdot dt'$$

with $w(t)$, property change; λ, wavelength; s_λ, spectral sensitivity of the considered property; $E_\lambda(t)$, time-dependent spectral irradiance at the surface; $T(t)$, time-dependent surface temperature; and $F(T(t))$, temperature dependence term.

Separate, decoupled examination on irradiance and temperature is realised by eliminating surface heating by IR and VIS radiation. Hence, temperature dependence is investigated by irradiation at constant temperatures, in a UVA lamp weathering device. Spectral sensitivity is investigated by spectrally dispersed irradiation, at room temperature.

With additional parameter of varied stabiliser content x, universalised DRF ends in

$$w(t,x) = \int_0^t F\big(T(t'),x\big) \int_{\lambda_0}^{\lambda e} s_\lambda(x) \cdot E_\lambda(t') \cdot d\lambda \cdot dt'$$

For the uncoloured PP of different stabilisations, DRF were created and validated by direct weathering in Phoenix, Arizona [6].

Materials

Originally, four basic materials were investigated in this project. A PP homopolymer as well as a PP/PE copolymer was studied in both an uncoloured and a black type.[5]

Additionally, all four basic materials were stabilised with Hostavin N 30 and Hostanox O 10, in different amounts. Oligomeric HALS (hindered amine light stabiliser) N 30 was added in three different quantities (0.02 %, 0.06 %, 0.1 %).

---

[2] If necessary, also nonlinearities in the damage increase have to be considered (e.g. saturation in colour change).

[3] Furthermore, for bulk properties, oxygen diffusion can be a limiting factor on timescale. Diffusion can be neglected for surface-related properties only.

[4] Possible dependence of spectral sensitivity on temperature [5] is neglected here.

[5] A very low carbon black amount was added to achieve higher solar heating, but not for stabilisation increase, primarily.

Phenolic antioxidant O 10 was varied between 0 % and 0.044 %. Moreover, each stabiliser combination was prepared twice, independently, to minimise systematic errors.

Then, square plates (8 cm × 8 cm × 0.2 cm) were produced by injection moulding. After all, for each of the four basic materials, the sample plates were produced with 12 independent formulations.

From all four basic materials, components of simple geometry were produced by injection moulding. For this, a geometry of cylindrical hats was chosen. Suspecting earlier failures, these hats were higher stabilised (0.22 % N 30, 0.05 % O 10).

However, first artificial weathering tests showed high time-to-failure durations for the black materials. Due to the limited project run time, efforts were focused on the faster degrading uncoloured materials. Results shown here are only from the uncoloured sample sets.

Methods

Artificial Irradiation

To investigate spectral sensitivity, samples were exposed to spectrally dispersed irradiation [6]. Thus, sample position correlates with the irradiation wavelength. By measuring spectral irradiance as well as property change, spatially resolved, spectral sensitivity can be calculated. For uncoloured PP, the failure by crack formation was quantified as crack formation probability $w(t)$ which was correlated to near-surface carbonyl formation.[6]

For examining temperature dependency, samples were exposed to artificial irradiation at different but constant temperatures. For this, a Weiss Umwelttechnik Global UV Test 200 weathering device was equipped with UVA 340   nm lamps (Type 1A lamp according to ISO 4892-3) and run under dry conditions. By consciously excluding VIS and IR, coupling of irradiance and surface temperature was avoided. UV radiant exposure until failure H_{UV} was determined at the respective temperature, varied between 5 and 65 °C. These limits were chosen to cover the temperature range being relevant for outdoor weathering, avoiding later temperature extrapolations.

Outdoor Weathering

Aiming at later validation, hats of all four materials were exposed in an IP/DP box in Phoenix/Arizona; see Fig. 14.1. This exposure site was chosen, as it features high global solar radiation combined with relative dry climate. Besides avoiding

---

[6] Measured by FTIR/ATR

Fig. 14.1 All four basic materials (stabilised with 0.22 % N 30) had been exposed in an IP/DP box in Phoenix, for varied durations (3–36 months)

complicated moisture impact, this has the advantage of much more reproducible weather conditions. Additionally, here a wide choice of weathering data is collectable. The IP/DP box weathering scenario can be regarded as a simulation of the exposure of the dashboard behind a window screen inside a car, again roughly excluding moisture effects. By systematically replacing the hats, exposure duration was varied between 3 and 36 months. For the whole exposure time (November 2006 to October 2009), weather data had been recorded.

Numerical Fitting (for Uncoloured PP Only)

As spectral sensitivity curves for different stabilisations did not differ considerably, a common fit was pursued. For this, all data points were equally included. Additionally, an arbitrary data point ($s\lambda$ (1,000 nm) = 0) was added, to enforce the asymptotic behaviour. It can be legitimated by FTIR measurements, after prolonged conditioning and the uncertainty of carbonyl index calculation. To adapt data to the chosen function type, least squares method was used.

For temperature fit, a linear least squares fit of logarithmic radiant exposures and inverse temperatures was used, implying an Arrhenius approach. Separate fits for the respective N 30 content resulted in overlapping activation energies, within their uncertainty ranges. Therefore, a common activation energy was calculated, by

including all data points, legitimated by equal temperature positions. Using this common slope, the offsets were determined for the respective N 30 content, separately.

HALS parameterisation was necessary, as the 3D components (hats) were provided with higher HALS stabilisation than the plates for lab investigations.[7] In literature, different approaches can be found. Gugumus studied HALS efficiency [7] and suggested a linear approach for PP, whereas he found square root dependence for PE. However, both assumptions were related to bulk properties, [8] whereas here crack formation as a surface-related property is observed. Therefore, generalising, a power function fit is chosen. With its finite value at zero stabilisation, also an exponential fit could make sense. Thus, the three data points were fitted to a power function, a square root function, and an exponential function as well. Also for these fittings, least squares method was used.

Numerical Simulation of Surface Climate

For numerical simulation, first challenge is computing momentary surface climate of the hats in the IP/DP box, on the base of weather data. Meshing created geometries, attention was paid to sufficient fine structures at borders [8]. For calculating radiation actions, solar radiation had to be divided into direct and diffuse portions. For direct solar radiation, shade formation had to be calculated.

Simulating the surface climate, influence of radiation, convection, and heat flow were investigated, separately, and found that none of them can be neglected [8].

Due to calculational limitations, irradiance was not included and spectrally resolved. Instead, outside the IP/DP box, it was approximated by ASTM G 173-3 spectral irradiance. For glass transmission, angle-independent spectral transmittance was supposed, for the whole range of direct radiation incident.

Taking account of shade formation, radiation interactions, and fluid dynamics, surface climate could be modelled, based on sun position, air temperature, air velocity, and (long wave) environmental radiation data [8].

Numerical Simulation of Ageing Process

Imbedding DRF into calculated irradiance and temperature distribution chronology would give crack formation probability after examined exposure duration.

---

[7] Hats were higher stabilised, as otherwise too early failure was expected, in IP/DP box weathering.

[8] For PP, he investigated duration until a specific carbonyl absorbance was found. For PE, 50 % residual tensile strength was examined.

However, very soon it became apparent that simulating continuous sequence of surface climate is not possible, due to computational capability limitations. Instead, azimuth and altitude of sun position as well as corresponding global irradiance were considered in their frequency of occurrence. Also clouding was incorporated, on a statistic basis. For only a few relevant scenarios, full surface climate simulation was computed. Using respective histograms and a linear interpolation approach, ageing progress could be accumulated, for the examined exposure duration [8].

Results

Spectral Sensitivity

Exposure results of spectrally dispersed irradiation are shown in Fig.14.2, for uncoloured PP, and in Fig. 14.3, for the uncoloured copolymer.

For uncoloured PP, the spectral sensitivity could be described as one fit, independent of the stabilisers content [6]; see Fig. 14.2. Thus, for uncoloured PP, DRF can be written as

$$w(t,x) = \int_0^t F\left(T\left(t'\right),x\right) \int_{\lambda_0}^{\lambda e} s_\lambda \cdot E_\lambda\left(t'\right) \cdot d\lambda \cdot dt' = \int_0^t F\left(T\left(t'\right),x\right)$$

$$\int_{\lambda_0}^{\lambda e} \frac{a_1}{1 + \exp\left(\dfrac{\lambda - a_2}{a_3}\right)} \cdot E_\lambda\left(t'\right) \cdot d\lambda \cdot dt'$$
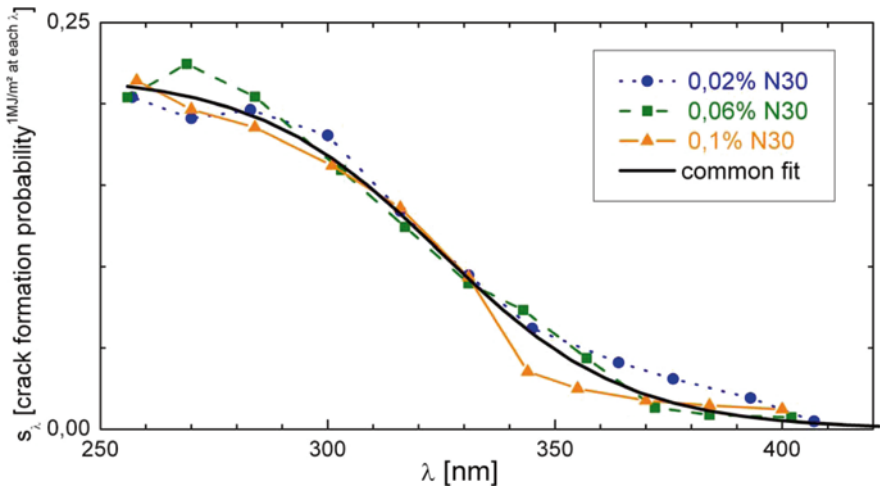
Fig. 14.2 Spectral sensitivity $s\lambda$ fit for differently stabilised uncoloured PP
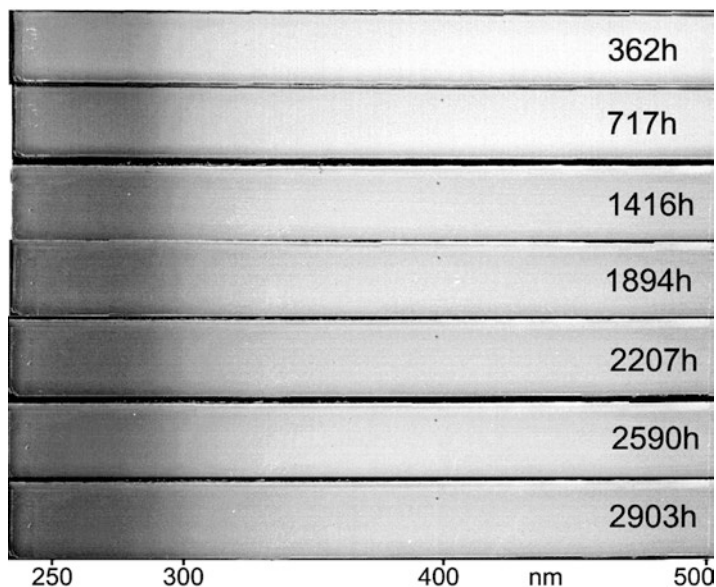
Fig. 14.3 Yellowing (*greyscaled*) after spectrally resolved irradiation, for a PP/PE copolymer of lowest HALS stabilisation

with $a_1 = 0.218 \pm 0.006$ (plateau level), $a_2 = 324.8 \pm 1.9$ (edge), and $a_3 = 20.3 \pm 1.4$ (slope).

For PP/PE copolymer, yellowing was found but limited to the spectral range below 300 nm; see Fig. 14.3. Other changes were not observed, even after about 3,000 h.

Temperature Dependence

For uncoloured PP, temperature dependence of crack formation could be fitted to Arrhenius plots[9]; see Fig. 14.4. Phenolic antioxidant O 10 did not have any effect. Samples failed according to their HALS content and could be fitted to a common (HALS-independent) activation energy. For uncoloured PP, DRF can be changed to

$$w(t, x) = \int_0^t c(x) \cdot \exp\left(\frac{-E_A / R}{T(t')}\right) \cdot \int_{\lambda_0}^{\lambda_e} \frac{a_1}{1 + \exp\left(\frac{\lambda - a_2}{a_3}\right)} \cdot E_\lambda(t') \cdot d\lambda \cdot dt'$$

[9] At 5 °C, no failures occurred after 380 MJ/m^2 UV radiant exposure.
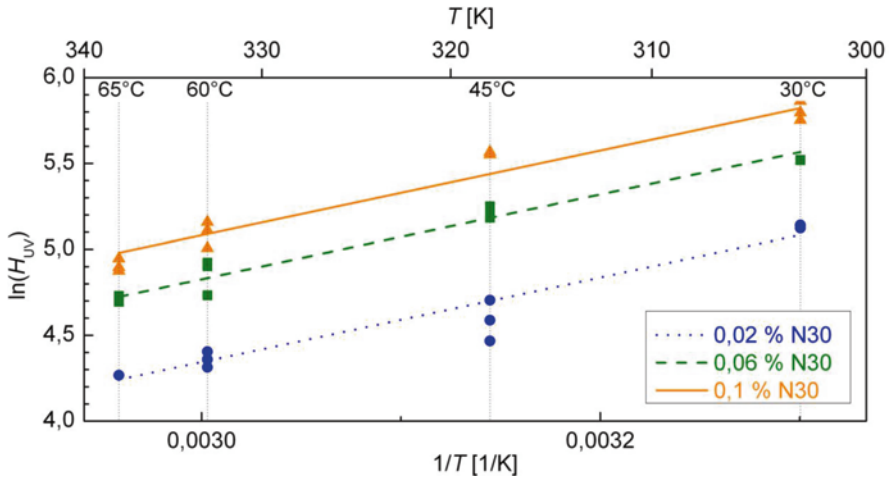
Fig. 14.4 Temperature dependence for differently stabilised uncoloured PP

with $E_A/R = (2{,}464 \pm 344)$ K (resulting in an activation energy E_A of about 20 kJ/mol) and the only stabiliser-dependent parameter $c(x)$.

After weathering device exposure, also PP/PE copolymer failed by crack formation. Yellowing was not observed. Also for PP/PE copolymer, Hostanox O 10 did not have any effect. However, temperature-dependent failure did not follow Arrhenius dependence; see Fig. 14.5.

Parameterisation of the HALS Influence

The fitting results (uncoloured PP) are shown in Fig. 14.6. Using the power function approach, the parameter $c(x)$ was fitted to $c(x) = c_1 \cdot x^{-c_2}$ with $c_1 = 957 \pm 40$ and $c_2 = 0.451 \pm 0.012$.

Dose–Response Function

For the uncoloured PP/PE copolymer, different property changes were observed. After spectrally resolved irradiation at room temperature, it showed yellowing. After irradiation at higher temperatures in a weathering device, it showed microcrack formation. With those different failure properties, both in the relevant temperature range, DRF could not be completed.
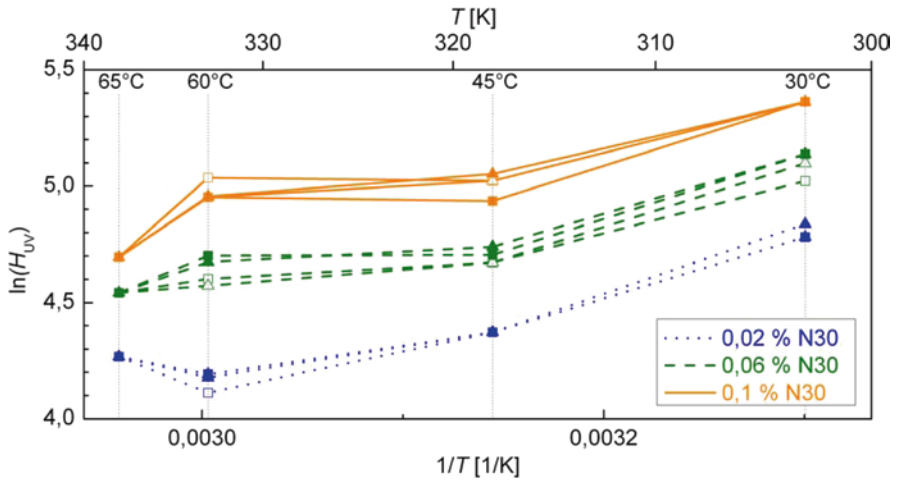
Fig. 14.5 Temperature dependence for differently stabilised uncoloured PP/PE
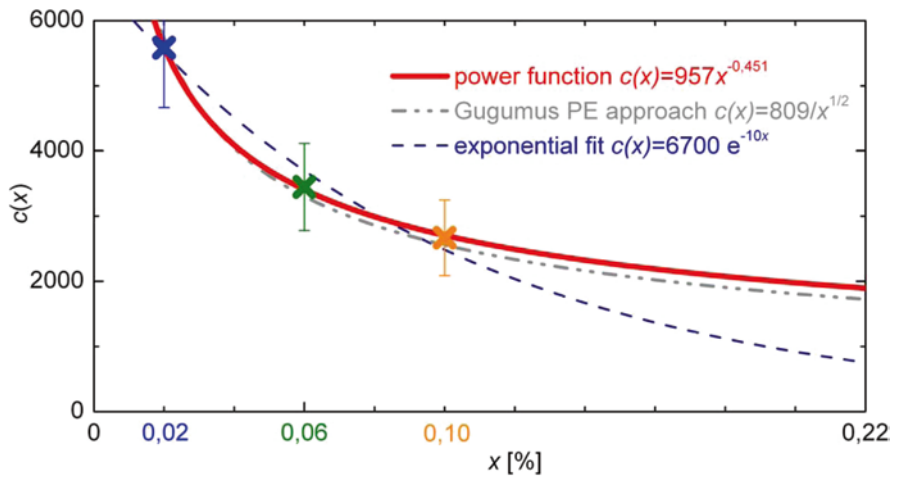
Fig. 14.6 HALS parameterisation for the uncoloured PP, for different fit approaches (three data points and extrapolation point at $x = 0.22$)

Only for uncoloured PP the DRF concept succeeded. With HALS-independent activation energy and spectral sensitivity, Arrhenius temperature dependence, and even stabiliser parameterisation, DRF can be written as

$$w(t,x) = c_1 \cdot x^{-c_2} \int_0^t \exp\left(\frac{-E_A / R}{T(t')}\right) \cdot \int_{\lambda_0}^{\lambda e} \frac{a_1}{1 + \exp\left(\dfrac{\lambda - a_2}{a_3}\right)} \cdot E_\lambda(t') \cdot d\lambda \cdot dt'$$
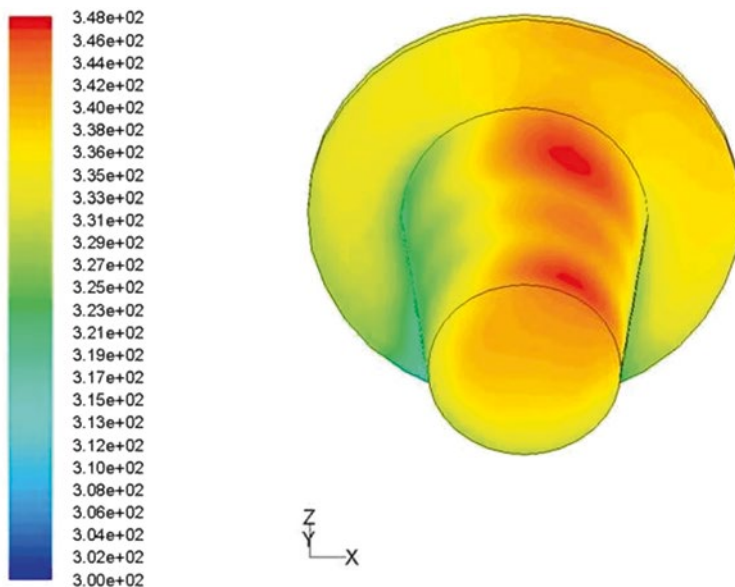
Fig. 14.7 Calculated surface temperature distribution for Phoenix, 24th June, high noon

with $c_1 = 957 \pm 40$, $c_2 = 0.451 \pm 0.012$, $E_A/R = (2{,}464 \pm 344)$ K, and $a_1 = 0.218 \pm 0.006$, $a_2 = 324.8 \pm 1.9$, and $a_3 = 20.3 \pm 1.4$.

Numerical Simulation of Surface Climate

Surface irradiance and temperature distribution were computed, on the base of weather data. Figure 14.7 shows computed surface temperature distribution, for 24th June, high noon. Circular shapes result from local fluid flow effects [8].

Numerical Simulation of Ageing Process

Knowing frequencies of all irradiance and surface temperature distributions over the specific period, the ageing evolutions can be accumulated, using DRF of uncoloured PP. Figure 14.8 shows calculated damage distribution, after 31 months' IP/DP box exposure. Crack formation occurs at values higher than 1.
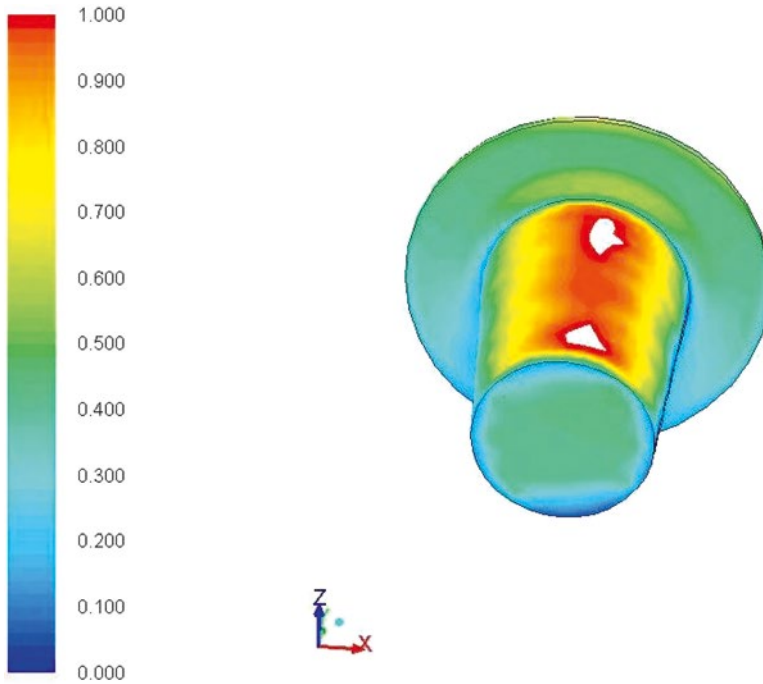
Fig. 14.8 Calculated failure probability distribution after 31 months IP/DP box irradiation

IP/DP Box Exposure Results

After IP/DP box exposure, hats were visually inspected. After 2 years, no damage was noticeable. Only the uncoloured PP hat exposed for 36 months showed intensive surface crack formation, as ring-shaped damages; see Fig. 14.9.

Discussion

Breaking down in Service Life Prediction of the uncoloured PP/PE copolymer proves the necessity of a clear failure property or a single, dominant degradation process, respectively. Geuskens [9] mentioned different effects at different wavelength irradiances. According to [10], at least hydroperoxide decomposition may proceed thermally or photochemically. However, method of spectrally dispersed irradiation is suited only for primary reactions of degradation process [11].

In contrast to uncoloured PP/PE, the missing success with both black-coloured materials is mainly owed to the limited project run time and the too high failure durations.

However, for one of the four investigated materials, a conclusive DRF was created. For spectral sensitivity, the plateau function fit, with its limited sensitivity

Fig. 14.9 Surface crack formation after 36 months IP/DP box exposure (view inside the PP hat from bottom to top)

towards smaller wavelengths, is not allowed to be extrapolated below 250 nm. Here, an explicit increase is expected, but could not be proved within the used measuring range.

For determining temperature dependency, the chosen range for laboratory tests should avoid later temperature extrapolations, which are often a source of errors. Cancelling the 5 °C irradiation after 380 MJ/m^2, this only partially succeeded. For comparison only, according to an Arrhenius fit, failure should have occurred at 5 °C, after 330, 530, and 690 MJ/m^2, respectively, with uncertainties of about 100 MJ/m^2. However, with maximum black hat surface temperature of about 75 °C (Fig. 14.7)[10] and most frequently values between 31 and 73 °C [8], the considered test range made sense.

In the end, stabiliser parameterisation was indispensable for succeeding in this project. However, it was not foreseeable that one stabiliser would show no action, at all, and that the other's action could be described independent on temperature and wavelength. Afterwards, it can be stated that phenolic antioxidant O 10 as a thermal stabiliser probably acts at higher temperatures and that activation energy does not depend on the HALS N 30 content.

However, in regard to both damage distribution and damage progress, simulation and exposure results of the uncoloured PP show good accordance.

The computed surface climate is consistent with measured surface temperatures (black standard temperature) at different IP/DP box walls [8]. Components surface

---

[10] Maximum surface temperature for uncoloured PP is about 10 K lower.

temperature distribution is strongly influenced by convective fluid flow. The observed ring-like damages result from local fluid flow effects, but not from component production problems.

For the ageing progress estimation, some approximation had to be done. A statistic approach of sun position and corresponding global irradiance was necessary, due to capability limitations. Also clouding was incorporated, on a statistic basis. Both simplifications do not relevantly influence the ageing results.

Huge uncertainties result from extrapolation of HALS parameterisation.[11] As can be seen in Fig. 14.6, all approaches would fit within uncertainty limits. However, at hat stabilisation of $x = 0.22$, the exponential fit would result in a much slower ageing (factor 2.5). The power function fit was chosen for the DRF, as it reflects current state of the art. But with its finite value at zero stabilisation, also an exponential fit could make sense. However, this demonstrates the large uncertainties of an extrapolation, over such a huge range. Depending on the respective approach, predicted ageing could be doubled.

Whereas this strategy conditioned factor 2 complicates a quantitative evaluation, damage distribution shows very impressive accordance.

Conclusions

For differently stabilised, uncoloured PP, the weathering sensitivities were quantified. Spectral sensitivity was fitted to a plateau function. Temperature dependence was described as an Arrhenius fit. The action of HALS stabiliser content (Hostavin N 30) was parameterised by a power function fit, whereas the phenolic antioxidant Hostanox O 10 did not show any influence on the ageing behaviour.

The relevant input data (irradiance and temperature direct at the surface) were calculated for a 3D component, on the basis of weather data, including shade formation, radiation interactions, and fluid dynamics.

Incorporating dose–response functions, the 3D ageing behaviour was computed, for IP/DP box exposure in Phoenix, Arizona.

The computed ageing behaviour correlated very well with both ageing processing and damage distribution.

References

1. Wypych G (2008) Handbook of material weathering, 4th edn. ChemTec Publishing, Toronto, Canada, p 211ff. ISBN 978-1-895198-38-6
2. Reichert T, Müller A, Lichtblau A, Schönlein A, Geburtig A, Fluche B, Brocke H, Köhl M, Manier G (2009) Virtual product qualification for sustainability ViPQuali. Proceedings 4th

---

[11] This could be clarified by further experiments only (e.g. IP/DP box exposure of lower stabilised PP hats). However, ViPQuali project finalised.

European weathering symposium—natural and artificial ageing of polymers, Sept 2009, Budapest, Hungary, pp 377–386, ISBN 978-3-9810472-8-8

3. Kockott D (1989) Natural and artificial weathering of polymers. Polym Degrad Stab 25:181–208

4. Czichos H, Saito T, Smith LE (eds) (2011) Springer handbook of materials measurement methods. Springer Handbooks, ISBN 978-3-642-16640-2

5. Trubiroha P, Geburtig A, Wachtendorf V (2004) Determination of the spectral response of polymers, Proceedings of the 3rd international symposium of service life prediction, Sedona, pp 241–253, ISBN 0-934010-60-9

6. Geburtig A, Wachtendorf V (2010) Determination of the spectral sensitivity and temperature dependence of polypropylene crack formation caused by UV-irradiation. Polym Degrad Stab 95:2118–2123

7. Gugumus F (1993) Current trends in mode of action of Hindered Amine Light Stabilizers. Polym Degrad Stab 40:167–215

8. Müller A, Vatahska T, Geburtig A, Manier G, Reichert T, et al. (2012) Numerische Simulation von Materialalterung: Das VipQuali-Simulationstool, Handbuch der 41. Jahrestagung der GUS, Stutensee, Germany, March 2012, pp 57–68, ISBN 978-3-9813136-4-2

9. Geuskens G, Kabamba MS (1982) Photo-oxidation of polymers—part V: a new chain scission mechanism in polyolefins. Polym Degrad Stab 4:69–76

10. Arnaud R, Lemaire J, Jevanoff A (1986) Photo-oxidation of ethylene-propylene copolymers in the solid state. Polym Degrad Stab 15:205–218

11. Trubiroha P (1989) The spectral sensitivity of polymers in the spectral range of solar radiation. In: Patsis AV (ed) Advances in the stabilization and controlled degradation of polymers, vol I. Technomic Publishing, Lancaster, pp 236–241

Chapter 15
Impact of Environmental Factors on Polymeric Films Used in Protective Glazing Systems

Kar Tean Tan, Christopher White, Donald Hunston, Aaron Forster, Deborah Stanley, Amy Langhorst, and Patrick Gaume

Abstract Accelerated and natural aging of safety films used in protective glazing systems was investigated by the use of Fourier transform infrared spectroscopy (FTIR), ultraviolet–visible spectroscopy, and tensile tests. Accelerated conditions involved simultaneous exposure of specimens to ultraviolet (UV) radiation between 295 and 450 nm and each of four temperature/relative humidity (RH) environments, i.e., (a) 30 °C at <1 % RH, (b) 30 °C at 80 % RH, (c) 55 °C at <1 % RH, and (d) 55 °C at 80 % RH. Outdoor weathering was performed in Gaithersburg, MD, in two different time periods. FTIR spectra indicate that different exposure conditions have no consequence on the nature and the proportions of the oxidation products, suggesting that similar degradation mechanisms were operative under all outdoor and indoor conditions. In the accelerated exposure, the rate of degradation is found to be influenced dominantly by UV radiation. The combination of UV radiation and temperature results in a cumulative effect, producing more rapid degradation. Analogous to the chemical changes, post-yield mechanical behaviors (such as strain hardening modulus and elongation to break) are markedly reduced, while the Young's modulus is minimally affected. Photodegradation leads finally to instability in the polymer's necking behavior and embrittlement, which is explained in terms of chain scissions of the tie molecules in the amorphous region. Samples subjected to outdoor weathering exhibit significantly slower photodegradation, but the degradation mechanism is the same so higher doses of environmental factors can be used to provide reliable acceleration in short-term aging tests.

K.T. Tan
Engineering Laboratory, National Institute of Standards and Technology,
Gaithersburg, MD 20899, USA

Department of Materials Science and Engineering, University of Maryland,
College Park, MD 20742, USA

C. White (✉) • D. Hunston • A. Forster • D. Stanley • A. Langhorst • P. Gaume
Engineering Laboratory, National Institute of Standards and Technology,
Gaithersburg, MD 20899, USA
e-mail: christopher.white@nist.gov

Introduction

Traditional annealed window glass may implode at high velocities producing jagged shards when subjected to blast pressures that resulted from natural disasters (e.g., hurricanes, tornadoes, severe wind storms, and seismic activities) or man-made destructions (e.g., burglary, vandalism, terrorist bombings, and industrial explosions). Flying glass shards pose significant risks to building occupants and can generate major damage to properties. This can be seen in a series of tornados that recently ravaged Alabama and the mid-west where destruction or damage of glazing caused serious injuries and property damage. To prevent glass shards from becoming lethal projectiles, polymeric films (known as safety films) are applied to window glass. During failure, the safety films deform to absorb energy that causes the glass to break as well as to keep broken glass shards adhered to the films. Thus, the blast load can be transferred to a building's frame and shattered glass fragments do not exit from windows at high velocities.

A variety of test methods and specifications are used to evaluate and validate the initial performance of safety films and glazing systems. These include ASTM F1642 (Standard Test Method for Glazing and Glazing Systems Subject to Air blast Loadings), ASTM F1233 (Standard Test Method for Security Glazing Materials and Systems), ISO 16933 Glass in Building—explosion-resistant security glazing—Test and Classification for Arena Air-Blast loading, and AAMA 510-06 (Voluntary Guide Specification for Blast Hazard Mitigation for Fenestration Systems). While helpful in assessing the initial material performance, these standard tests do not address an important question concerning the long-term chemical and mechanical stability of the film. It is well known that ultraviolet (UV) radiation, moisture, or extreme temperature can all contribute to the deterioration of material properties of polymer films, and this potentially shortens their useful life spans [1, 2]. Furthermore, the service life predictive capabilities for safety films are still far from being satisfactory both from the analytical and experimental points of view. A better understanding of degradation mechanics and mechanisms is key to accurately predict service life and develop products with improved long-term performance. The work here seeks to provide a fundamental understanding of the degradation mechanism for safety films exposed to various environmental factors and to clarify the effect of each environmental factor on the degradation mechanisms. Accelerated aging tests were conducted in an integrating sphere-based weathering chamber [Simulated Photodegradation via High Energy Radiant Exposure (SPHERE)] [3]. Changes in key mechanical and chemical properties as a function of exposure time at different temperatures and moisture levels during accelerated aging were measured using quasi-static tensile tests, Fourier transform infrared (FTIR) spectroscopy, and ultraviolet–visible spectroscopy. In addition, a

linkage between accelerated tests and field exposure experiments was established to provide the key that makes the accelerated testing methodology meaningful. This understanding of the degradation with various exposure factors will open new perspective for the practical long-term applications of safety films.

Experimental[1]

Materials

Two commercial safety films were investigated, both of which were obtained from their primary manufacturers. These materials are typical poly(ethylene terephthalates) (PET), but the detailed product chemistry and composition are unknown. Both are manufactured with multiple layers of optically clear films and are installed by attachment to the interior surface of the glass using a pressure-sensitive adhesive. Hereafter, they are referred to as Films A and B, respectively. The films are used as received from the manufacturers.

Accelerated and Field Exposures

Specimens were exposed to both outdoor (field) conditions and indoor experiments where the conditions were designed to accelerate the effects of exposure. For the indoor tests, the specimens were exposed to UV radiation with wavelengths ranging between 295 and 450 nm using the National Institute of Standards and Technology (NIST) integrating sphere-based weathering chamber (SPHERE) [3]). This chamber provides higher UV irradiation than normal outdoor exposure. In addition to the UV irradiation, specimens were subjected to one of four temperature/relative humidity (RH) environments: (a) 30 ± 1 °C and <1 % RH, (b) 30 ± 1 °C and 75 % RH, (c) 55 ± 1 °C and <1 % RH, and (d) 55 ± 1 °C and 75 % RH. Additionally, similar exposures were also conducted in the absence of UV radiation to examine the influence of that parameter on the material properties.

In the case of field tests, specimens were exposed on the roof of a NIST laboratory in Gaithersburg, MD. Specimens were placed in a custom-built chamber that was positioned facing south toward the equator at an angle of 5° from the horizontal plane. Solar radiation reached the specimens through a borosilicate glass plate at the top of the chamber to emulate the conditions seen in the actual applications of the films. The upper surface of the bottom side of the chamber consisted of a 3 mm

---

[1]Certain commercial products or equipment are described in this paper in order to specify adequately the experimental procedure. In no case does such identification imply recommendation or endorsement by the National Institute of Standards and Technology (NIST), nor does it imply that it is necessarily the best available for the purpose.

thick polytetrafluoroethylene sheet, which was used to minimize heating in the chamber via reflection of the solar radiation. The sides of the chamber were made with a breathable cloth that allowed transmission of water vapor but prevented dust from entering. The temperature, RH, and total irradiance in the chamber were monitored continuously during exposure using thermocouples, humidity sensors, and a radiometer, respectively.

FTIR Spectroscopy

Surface chemical properties of the specimens were measured using a Nexus 670 attenuated total-reflection Fourier transform infrared spectrometer (ATR-FTIR) equipped with a liquid nitrogen-cooled mercury cadmium telluride detector. All spectra were collected over a range of 1,000–4,000 cm^{-1} at a nominal resolution of 4 cm^{-1} and averaged over 128 scans. Band height was used as a measure of IR intensity. In this study, the carboxyl index was used as an indication for degradation in the materials. This index was determined by normalizing the absorbance of 3,255 cm^{-1} (attributable to OH stretching in carboxylic groups [4]) with a least-changed reference band. This was done to compensate for surface morphological changes during exposure that may produce inconsistent optical contact between the polymer film and the internal reflection element of the ATR cell. The reference peaks selected for Films A and B were 1,453 cm^{-1} (C–H in-plane bending of the benzene ring [5]) and 767 cm^{-1} (corresponds to a monosubstituted benzene [4]), respectively.

Tensile Tests

Mechanical properties were measured by uniaxial tensile tests performed at room temperature using an Instron testing machine. The films were cut to a dog-bone geometry conforming to the ASTM D-638. We first investigated the strain rate dependence of mechanical properties for the fresh films. This was done to establish the appropriate strain rate to be used in the subsequent measurements. It was found that elongation at break, the strain hardening modulus, and small-strain Young's modulus are statistically insensitive to crosshead speeds ranging from 1×10^{-3} mm/s to 8.33 mm/s. This indicates a range of over nearly three decades where the behavior is not sensitive to strain rate so a crosshead speed of 0.1 mm/s was used in all subsequent experimental which kept the duration of the tests within a reasonable timescale. To examine the effects of UV, temperature, and RH, mechanical properties such as strain hardening modulus, elongation at break, and Young's modulus were monitored. Strain hardening modulus was obtained by fitting a straight line to the initial plastic region of the curve, while elongation at break was taken as the value of nominal strains at ultimate failure.

Ultraviolet–Visible Spectroscopy

Ultraviolet–visible spectroscopy was utilized to monitor yellowing in the specimens during exposure. The measurements employed a Perkin-Elmer Lambda 900 Spectrometer. The surface color changes of specimens were quantified with a yellowness index (YI). YI is a measure of the visual yellowing that occurs and is based on determination of transmittances (T) near the ends of the visible wavelength region, i.e., $YI = 100 \times (T_{680} - T_{420})/T_{560}$. Here, the subscript denotes the wavelength.

Results and Discussion

Surface Chemical Property Changes upon Exposure

Surface chemistry of the films exposed to various accelerated conditions was monitored by ATR-FTIR. For simplicity, Fig. 15.1 shows typical spectra before and after exposure to 30 °C and 75 % RH in the presence of UV for various exposure times. The IR spectral properties of Films A and B show marked similarities. The assignments of bands for most PET infrared peaks have been well documented in the literature [6–9]. As compared to control specimens, FTIR analyses at various stages
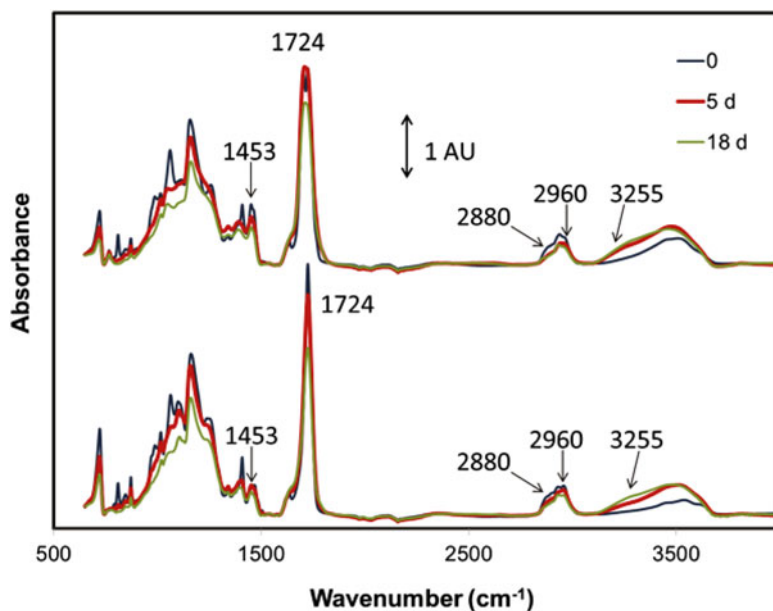
Fig. 15.1 FTIR spectra of Films A (*top*) and B (*bottom*) exposed to 30 °C and 75 % RH. Only three exposure times are shown for clarity

of degradation reveal the appearance of oxidized products on the material surfaces, reflecting structural modifications of the samples under the influence of accelerated exposure conditions. A strong band at 1,724 cm^{-1} due to C=O stretching vibration of the ester groups [6, 10] shows a reduction in intensity with increasing exposure. Similarly, the absorbance of the region around (1,250–1,000) cm^{-1} dominated by strong signals due to C–O stretching vibration [5, 6] shows significant decreases upon exposure.

Examination of the 3,800 cm^{-1} to 3,100 cm^{-1} region (assigned to hydroxyl stretching vibrations) reveals a marked increase in the absorbance of this broad band in the early stage of exposure. The complex line shape of this band suggests that more than one type of bonded OH group is formed. Hydroperoxides (3,550 cm^{-1}) are the main intermediate species present during the early events of the aging process. In later stages, a shoulder was detected at 3,255 cm^{-1}, which may be assigned to OH stretch in carboxylic groups (COOH), and the absorbance of this peak continues to increase with exposure. The absorption bands at 2,960 cm^{-1} and 2,880 cm^{-1} are due to aliphatic C–H stretch [11], while the bands peaking at 1,604, 1,584, 1,492, and 1,453 cm^{-1} stem from C–H in-plane bending of the benzene ring [5]. The intensities of these bands decrease markedly with exposure time. A band at 730 cm^{-1} due to p-substituted aromatics [6, 12] also decreases. The reduced absorbance of these bands suggests that extensive degradation has taken place in the films during the exposure. The above FTIR findings are in agreement with the photodegradation mechanisms of PET, which follows Norrish type I reaction pathways, predominantly, and lead to this formation of aldehydes and carboxylic acid [13, 14]. Although not reported here, volatile degradation products such as carbon monoxide and carbon dioxide have been found during the degradation [13, 14].

Figure 15.2 depicts the correlation between the absorbance of two characteristic FTIR bands associated with photooxidation: 1,724 vs. 1,158 cm^{-1} for Films A and B. In such a plot, all of the data for various exposure conditions collapse to a narrow band around a single curve. A direct implication of this good correlation is that the relative proportions of the photooxidation products are independent of the exposure conditions. When the peak ratios show a similar proportionality, various exposure conditions are expected to cause degradation by the same mechanisms, even though the degradation rates are quite different. Thus, the results suggest that the primary mechanism of oxidation in the films does not vary with temperature, RH, and UV.

To evaluate the effects of UV, temperature, and moisture on the kinetics of degradation, changes in carboxyl index were monitored as a function of time (Fig. 15.3). In the presence of UV, the carboxyl index progressively increases with exposure time for all four conditions. Spectra for Film B under conditions of 30 °C/0 % RH and 55 °C/0 % RH reach a plateau in the carboxyl index after ≈ 5 days while the increase in carboxyl index for all other conditions slows greatly after ≈ 30 days. This suggests saturation of chemical moieties due to the depletion of preferential reaction sites. During the early stages of exposure, various temperature/RH combinations have qualitatively the same effect on the time evolution of carboxyl index. This result indicates that the weak effect of temperature and moisture on degradation may
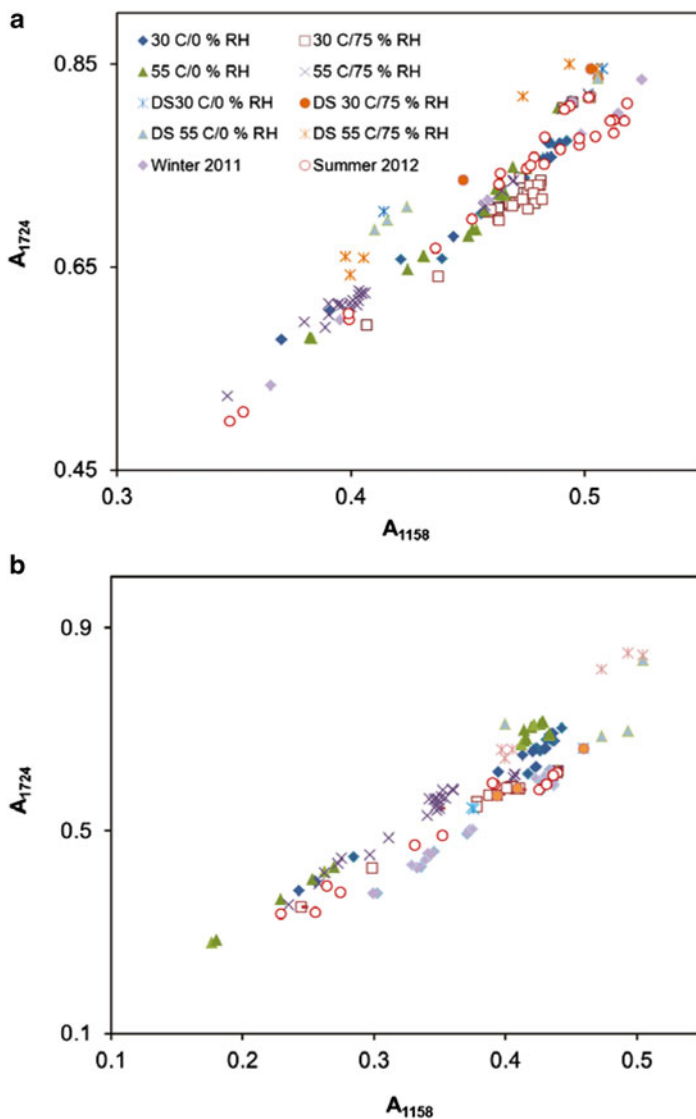
Fig. 15.2 Correlation between absorbance of 1,724 cm^{-1} and 1,158 cm^{-1} for (**a**) Films A and (**b**) B exposed to various conditions. "DS" denotes the exposure without UV radiation. Different exposure conditions have no consequence on the nature and the proportions of the photoproducts, suggesting that similar degradation mechanisms were operative under all outdoor and indoor conditions

be obscured by pronounced effect of UV and that any changes induced by these two factors are too small to be detected with the FTIR spectrometer used here.

In contrast to the early stages of exposure, temperature and moisture begin to affect the oxidation in the films after sufficiently long irradiation time. Distinct
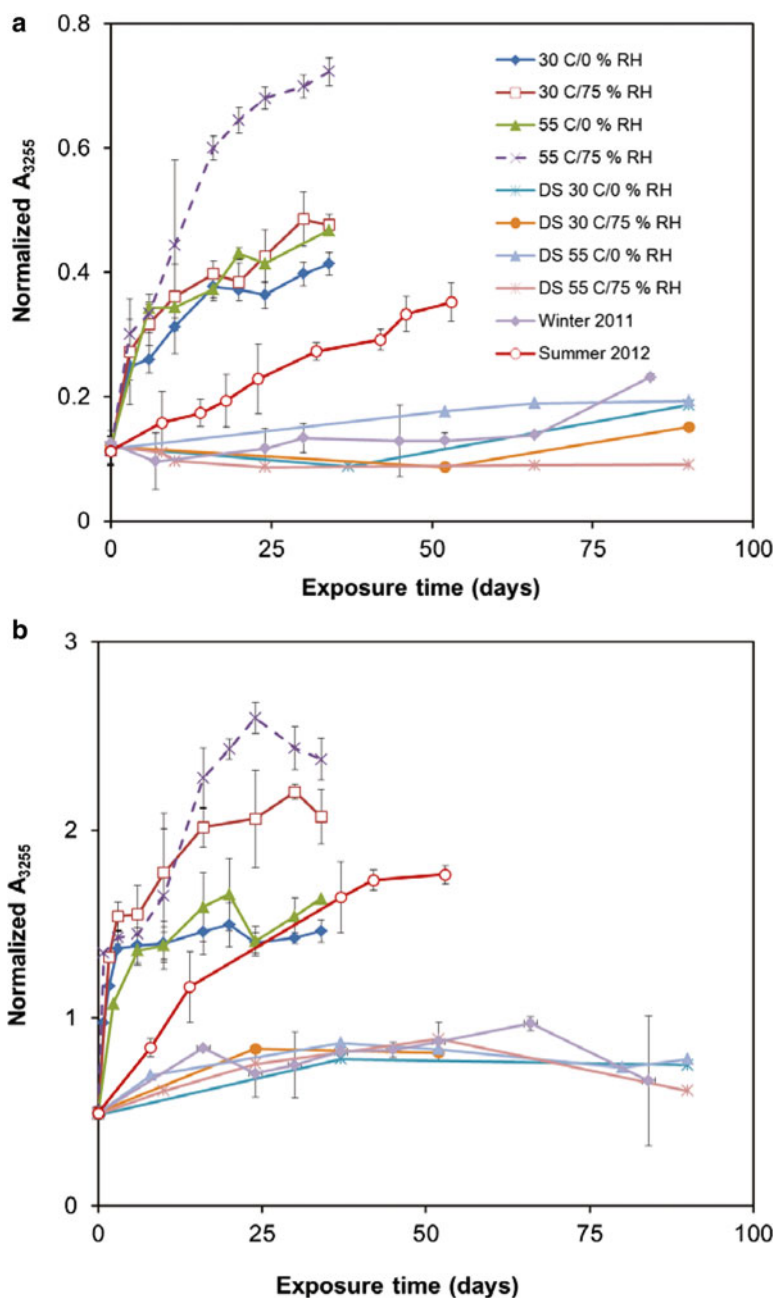
Fig. 15.3 Changes of the normalized absorbance of 3,255 cm⁻¹ in (**a**) Films A and (**b**) B as a function of exposure time for different environments. Error bars represent ±1σ from the mean values. "DS" denotes the exposure without UV radiation

dependencies on temperature and moisture were observed in Films A and B. By comparison, the extent of oxidation in Film B shows stronger moisture sensitivity than that in Film A. This is evident from higher carboxyl indexes observed in Film B exposed to a high RH level (i.e., 75 % RH), irrespectively, of temperature. In Film A, the statistically similar carboxyl indexes for 0 % RH and 75 % RH at 30 °C suggest that such a moisture dependency is absent. For exposure at 75 % RH, increasing the temperature results in more noticeable degradation which enriches the carboxyl groups on Films A and B, whereas this effect is barely detectable at the corresponding lower RH levels. Also, the combination of high temperature and RH levels is found to be deleterious for both films. For example, the carboxyl indexes for 55 °C/75 % RH for Films A and B are 70 % greater than that under 30 °C/0 % RH. It should be noted, however, that increasing the temperature from 30 to 55 °C seems insufficient, by itself, to cause any bond ruptures in commercial grade polymers where dissociation energies are 70–90 kcal/mol [15]. Hence, it is the combination of UV, temperature, and moisture that contributes to the observed chemical changes.

The fact that the polymers degrade, as observed in Fig. 15.3, indicates that quanta of light are absorbed by chromophores, which are present as impurities from manufacturing and processing. Additionally, aromatic ester groups in the main chains can readily absorb UV light and thus become a source of the initiation radicals. After absorbing UV radiation, the energy of the excited groups is dissipated via various oxidative mechanisms, leading to the formation of free radicals and various degradation products. Secondary reactions are subsequently promoted by other environmental factors, such as temperature and moisture. This explains the dominance of the UV effect in the initial stage of degradation before the effects of temperature and RH set in the later stages. Further reinforcement for this assertion is given by the largely unaltered carbonyl index measured for the specimens in the absence of UV.

In the literature, it is reported that thermo-oxidative degradation in PET does occur under sufficiently elevated temperatures [16–19]. It is thought to proceed via a scission of in-chain ester linkages, thereby yielding carboxyl and vinyl ester end groups [16–18]. In addition, the degradation process is exacerbated at temperatures above the melting point of the bulk polymer ($\approx$255 °C) [18]. Higher water contents in the polymers at temperatures above the glass transition temperature can damage the polymer directly via hydrolysis, furnishing carboxylic and alcoholic end groups [20]. Such hydrolysis reactions preferentially occur in the amorphous domains of the polymer [21, 22]. Taken together, these various findings suggest that in the absence of UV radiation, the different combinations of temperature and relative humidity utilized in this study are not damaging enough to induce significant degradation in the polymers. This may account for the observed weak dependence of degradation on temperature and RH.
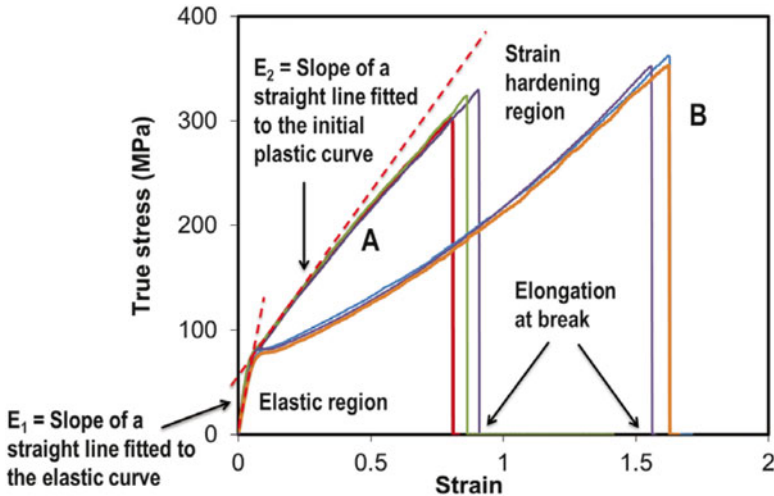
Fig. 15.4 Typical stress versus strain curves for Films A and B

Mechanical Property Changes upon Exposure

It is useful to measure a direct mechanical response of materials under the different exposure conditions. It should be noted that no attempts were made to quantitatively correlate changes in surface chemical and bulk mechanical properties. Figure 15.4 shows representative uniaxial stress–strain curves for fresh Films A and B. Three replicates are presented for each material. In a stress–strain test, Films A and B exhibit comparable features: an initial elastic region followed by yielding which produces a stable necking section that grows until failure occurs at high strains, approximately 80 % for Film A and 160 % for Film B, respectively. The necking region of the curve is characterized by a rise in stress with increasing strain which is termed strain hardening. The high values of elongation at break are indicative for intrinsic ductility of the materials, which makes them attractive for applications where toughness is desired.

Three notable differences between these materials lie at their post-yield regions. First, the previously discussed strain at break values that are 80 % for Film A and 160 % for Film B. Second, Film B shows a moderate region of strain softening (i.e., a drop in the true stress with increasing deformation) prior to the stress hardening. Such a behavior is absent in Film A. Third, the strain hardening slope at moderate deformations is larger in Film A than it is in Film B. Both films exhibit comparable strain hardening rates at large-strain levels. The presence of strain hardening effect reveals the ability of the polymers to undergo plastic flow process involving extensive molecular alignment in the direction of applied load. As a result, the propensity for strain localization is reduced by strong strain hardening. Therefore, the macroscopic response of these materials to large deformation is ductility.

Figures 15.5, 15.6, and 15.7 illustrate how the various exposure conditions impact the elongations at break, Young's moduli, and strain hardening moduli of the specimens.
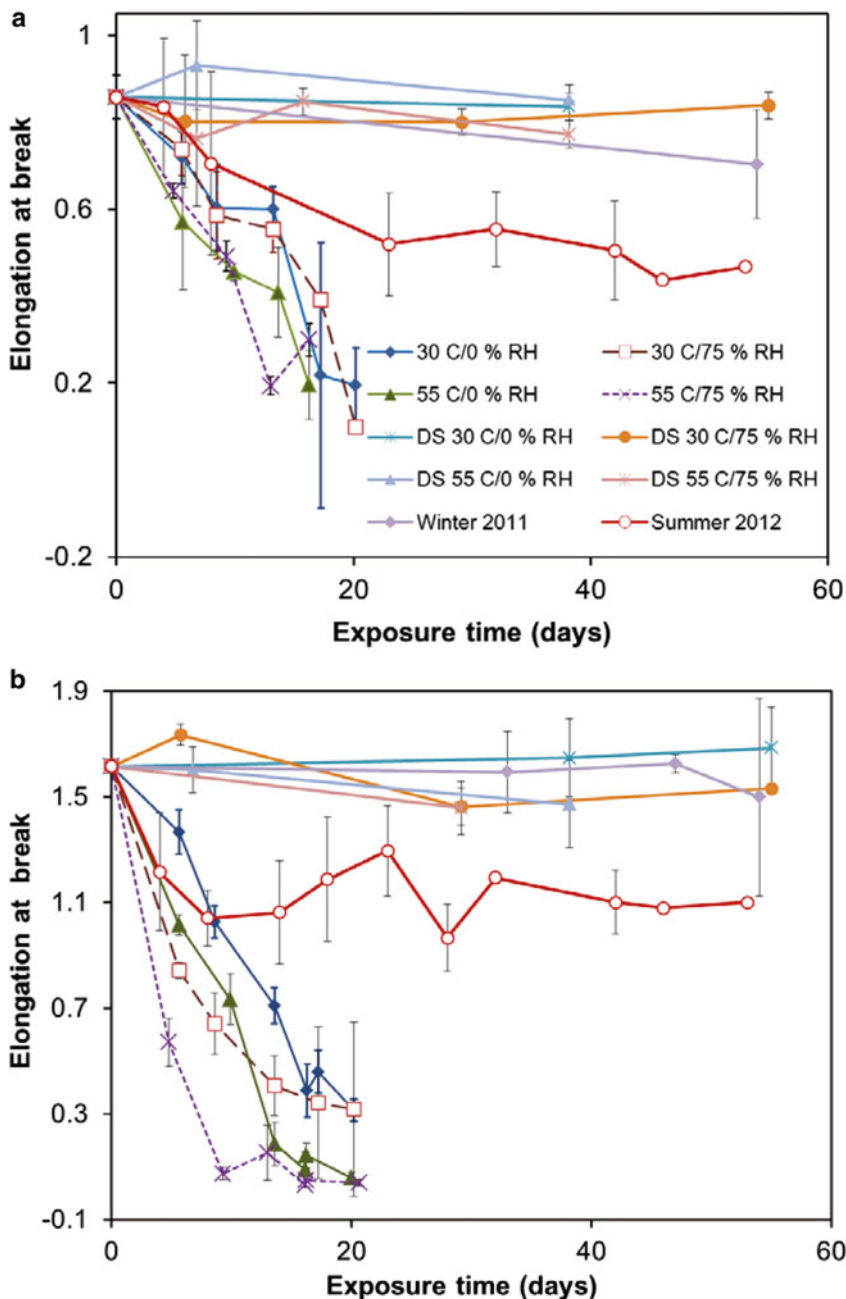
Fig. 15.5 Changes in elongation at break as a function of exposure time for various conditions for (**a**) Films A and (**b**) B. Error bars represent ±1σ from the mean values. "DS" denotes the exposure without UV radiation

Fig. 15.6 Changes in strain hardening moduli (E_2) as a function of exposure time for various conditions for (**a**) Films A and (**b**) B. Error bars represent $\pm 1\sigma$ from the mean values. "DS" denotes the exposure without UV radiation

It is evident that the exposure conditions have dramatic effects on the mechanical properties. The elongation at break precipitously declines with increasing exposure time. To put the matter into perspective, the elongation at break decreases by approximately an order of magnitude after ≈ 10 days of exposure at 55 °C/75 % RH.
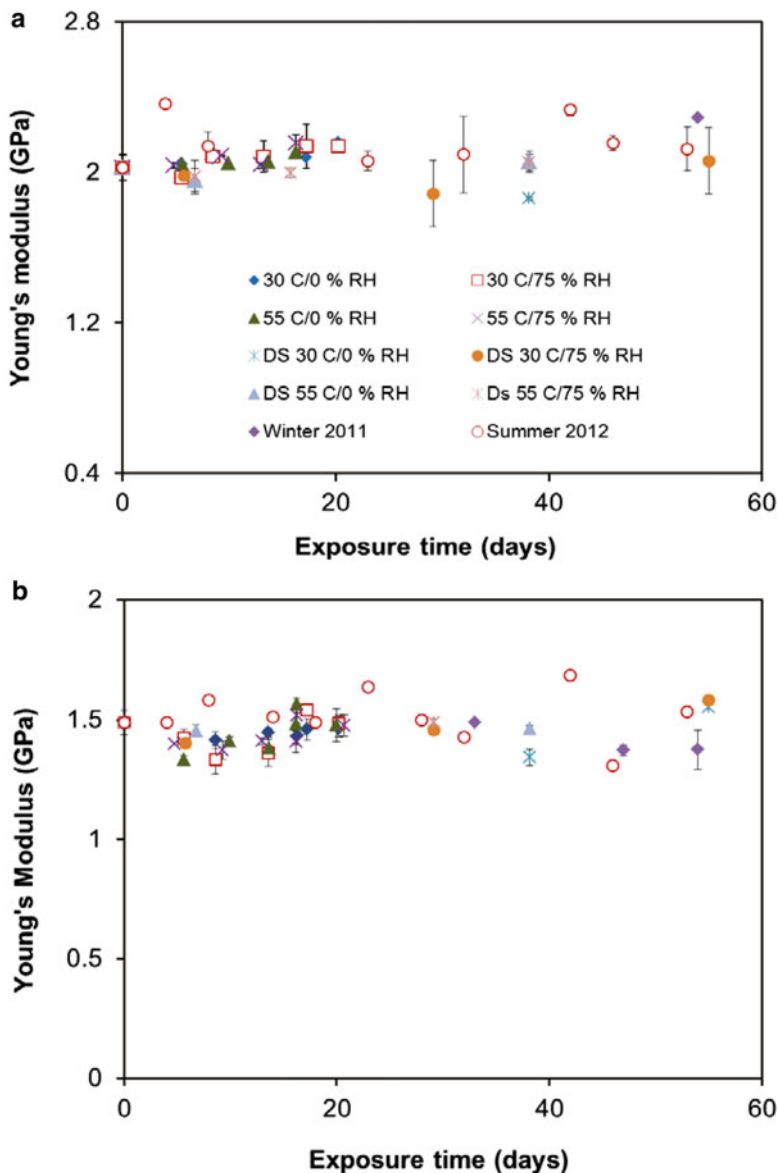
Fig. 15.7 Changes in Young's modulus as a function of exposure time for various conditions for (**a**) Films A and (**b**) B. Error bars represent ±1σ from the mean values. "DS" denotes the exposure without UV radiation

An analogous reduction in strain hardening moduli with increasing exposure times was also observed. After 20 days, the strain hardening for all exposure conditions vanishes. Contemporaneous losses in elongation at break and strain hardening capacity suggest the occurrence of severe localization of strain, which manifests

itself in brittle behavior after exposures. Indeed, this is the case because we observed that failure surfaces of exposed samples were relatively featureless compared to those unexposed samples.

Comparison of the mechanical properties at various exposure times in the absence of UV radiation reveals the weak dependence of degradation on temperature and moisture. In particular, the effect of various combinations of temperature and relative humidity on the elongation at break of Film A is not visibly notable due to large experimental scatters. The rate and the extent of decrease in strain hardening moduli, on the other hand, are found to be slightly greater at 55 °C compared to 30 °C. Unlike Film A, both strain hardening moduli and elongation at break of Film B exhibit marginally greater decreases at high relative humidity at 75 % RH for a given temperature. Also, it is apparent that both elongation at break and strain hardening modulus for Films A and B exposed to a simultaneous high temperature and RH decrease more rapidly than they did for the exposure at various RH conditions and lower temperatures.

As illustrated in Figs. 15.5, 15.6, and 15.7, the degradation of the materials in the absence of UV under the similar temperature and RH combinations is seriously retarded, as indicated by little or no changes in mechanical properties with increasing exposure time. This weak dependence is consistent with the chemical changes occurring in the films, which again underlines that this was primarily a UV-controlled phenomenon.

Interestingly, Young's moduli for all conditions are found to remain statistically unchanged within our experimental timescale, irrespective of exposure conditions (Fig. 15.7). This means that the small-strain property below the elastic limit is largely invariant by the structural changes induced by degradation. A thermo-oxidative study of polypropylene at 90 °C comes to the similar conclusion in that a detrimental effect of aging was found for the large-strain behaviors while the low strain characteristics were essentially preserved [23]. Thus, small-strain measurements may not be useful for monitoring aging behavior.

Large-strain deformation of semicrystalline polymers strongly depends on entanglement network density in the amorphous domains [24, 25]. Increasing the entanglement density leads to a tougher polymer and an increase in the corresponding strain hardening capability. Further, amorphous domains in the polymer are well known to be more labile to oxidation as compared to crystalline regions due to their higher permeability to oxygen. Thus, from the FTIR data and tensile tests, the observed losses in chemical and large-strain mechanical properties may be interpreted as a result of bond scissions occurring in tie molecules in the more oxygen-permeable amorphous domains. This gives rise to formation of low molecular weight fragments with low chain entanglement density.

Finally, photodegradation in PET is known to begin on the surface and then progresses gradually into the bulk [26–28] since that correlates with oxygen concentration. For example, early studies by Blais et al. [26] using ATR-FTIR showed that carboxyl groups formed on UV-irradiated PET films were concentrated mostly on the thin surface layer (thickness ≤ 1 μm) and the sample interior was largely unaffected. Consistent with this notion, depth profiling of 200 μm thick PET films using

a micro-FTIR spectroscopy reveals surface enrichment of carboxyl groups, which are distributed heterogeneously only on the sample outermost surface ($\leq$50 μm) after 100 h of polychromatic irradiation with wavelengths greater than 300 nm [27]. The surface-mediated degradation in our samples is confirmed by exposing the adhesive side of the safety films to the UV light source, and the chemical changes on the back face of the samples were followed with ATR-FTIR. After 1 month of exposure, degradation is observed to occur mostly on the irradiated layer of the sample and the back face is unaffected. On the basis of this observation and the foregoing considerations, it is surmised that crazes induced by this surface degradation may serve as initiation sites for failure, causing the degraded film to lose their load-bearing capacities. The proposed mechanism is in line with the literature where the surface degradation is sufficient to cause plastic instability necking and polymers embrittlement even if the bulk polymer is unaffected [29, 30].

Yellowing upon Exposure

UV–visible spectra were collected for degraded materials as well as for fresh materials prior to exposure. Films A and B were found to absorb nearly all of the UV radiation. This is due to the fact that PET is a very strong UV absorber, itself. Moreover, the safety films studied here contain commercial UV absorbers, which are commonly incorporated in the adhesives and/or impregnated in to the polyester film. The extent of yellowing during the period of exposure was evaluated using yellowness index. As shown in Fig. 15.8, changes in the yellowness index could be measured, yet neither of the PET films had any visually delectable yellowing. Typical values for a visually detectable change in yellowing are greater than 100. The values shown in Fig. 15.8 are a maximum of 35 or 14, well short of the visually detectable threshold. Figure 15.8 shows the time evolution of yellowness index for various conditions. It can be seen that Films A and B exhibit increases in yellowness indexes upon exposure. Such discoloration may be related to hydroxylation of the terephthalate ring [12, 31].

Comparison with Field Exposures

An interesting question is how the intense but short-term exposures used in this study can be translated to much less severe field exposure conditions over longer periods of time. To answer this question, correlation plots between 1,724 cm^{-1} and 1,158 cm^{-1} for the field exposures are compared with the equivalent data from the accelerated exposures. As shown in Fig. 15.2, all data points for various environments fall near a single normalized curve, indicating similar degradation mechanism operating in the field and controlled laboratory environments. Such a strong correlation between the accelerated and field exposures may be attributed to the fact that UV radiation between 295 and 400 nm in the sunlight is known to be
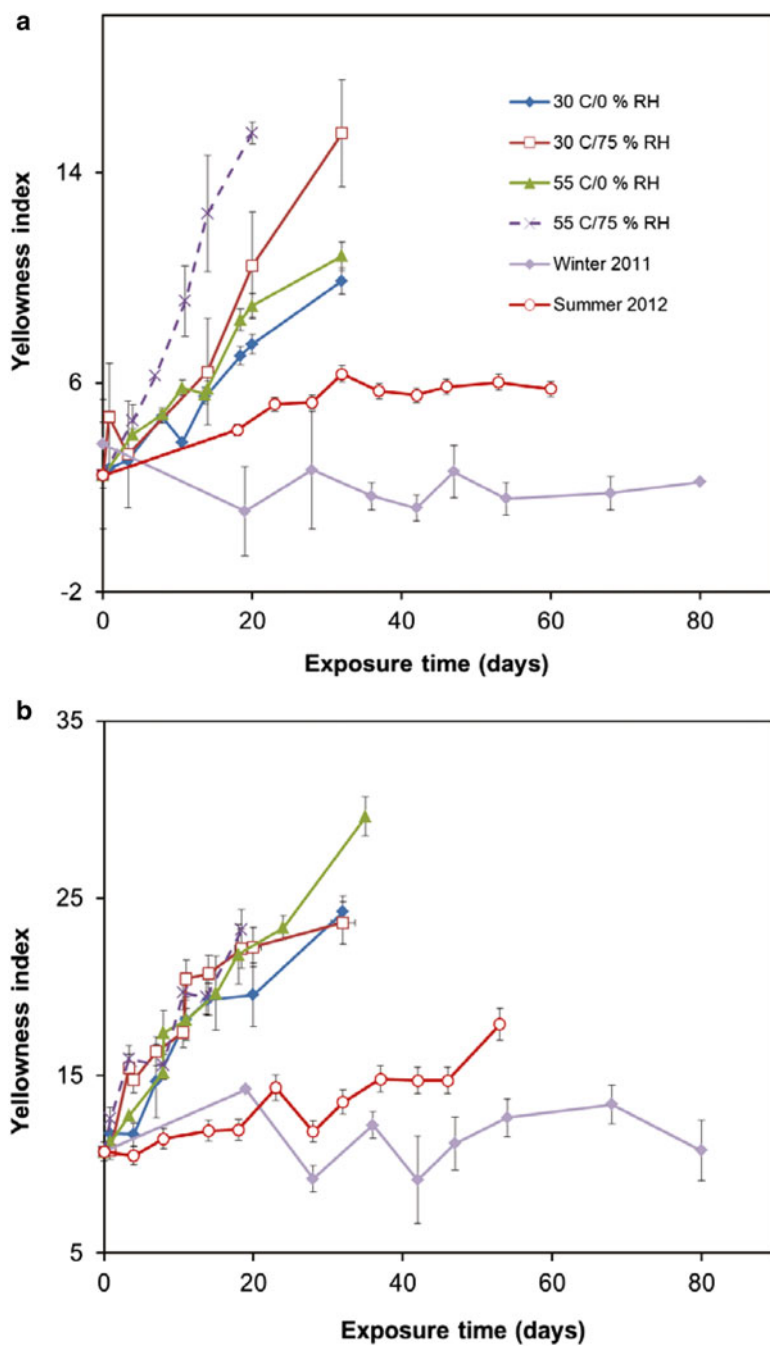
Fig. 15.8 Yellowness indexes for (**a**) Films A and (**b**) B exposed to various conditions. Error bars represent ±1σ from the mean values

photolytically active in degrading polymeric materials [32, 33], and the artificial light source used in the accelerated experiments consists of radiation that is rich in the same wavelength range. Moreover, the combinations of temperature and RH used in the accelerated tests are within the range seen in outdoor exposure conditions, thus precluding deleterious side effects from these variables. For this reason, meaningful comparisons may be made in this study using the data generated under the accelerated and field exposures. As expected a comparison between accelerated and field exposures shows that specimens aged in the field condition have much slower degradation rates both in terms of chemical and mechanical properties (see Figs. 15.3, 15.5, 15.6, and 15.7, respectively).

In the case of yellowing, the films exposed to outdoor show a very low yellowness index, indicating that the degradation is not exhibited by specimen discoloration. Visual inspection fails to reveal any significant changes after outdoor exposure. These results clearly emphasize that while a conventional descriptive methodology involving visual evaluations of physical performance of exposed specimens for defects including color change, crack size, and distribution may relate a customer-perceived failure mode, it is not sensitive to changes that resulted from degradation and provides little insight into the mechanisms leading to these macroscopic changes. This makes it difficult to develop models for accurately predicting the service life of the polymeric films based on visual observation.

In contrast, there is a significant change in the mechanical properties during both the controlled and outdoor exposures. This is especially apparent in the elongation to break data of Fig. 15.5. Developing a model for accurately predicting the service life of the polymeric films based on changing mechanical properties would be relatively straightforward.

Conclusions

Indoor accelerated and field weathering of two polymeric films used in protective glazing systems has been studied using FTIR spectroscopy, ultraviolet–visible spectroscopy, and tensile tests. Accelerated exposures led to the formation of hydroxyl and carboxyl functional groups on the surface of specimens. Substantial decreases in elongation at break and strain hardening modulus with increasing exposure time were observed while the Young's modulus remains largely unaffected within the experimental timescale. These results demonstrate the insensitivity of the small-strain properties to weathering. Prolonged exposures render specimens brittle, diminishing the mechanical integrity of the polymers through extensive chain scissions. Degradation of the polymers was found to be predominately controlled by UV radiation, while temperature and moisture contents play only a secondary role. Finally, the samples exposed to the outdoor conditions degraded in the same way as they did when subjected to the accelerated conditions, but at much slower rates.

References

1. Jacques LFE (2000) Prog Polym Sci 25:1337–1362
2. Schnabel W (1982) Polymer degradation, principle and practical applications. MacMillan, New York
3. Chin J, Byrd E, Embree N, Garver J, Dickens B, Finn T, Martin J (2004) Rev Sci Instrum 75:4951–4959
4. Colthup NB, Daly LH, Wiberley SE (1990) Introduction to infrared and Raman spectroscopy, 3rd edn. Academic, San Diego
5. Gu X, Raghavan D, Nguyen T, VanLandingham MR, Yebassa D (2001) Polym Degrad Stab 74:139–149
6. Liang CY, Krimm S (1959) J Mol Spectrosc 3:554–574
7. Boerio FJ, Bahl SK, McGraw GE (1976) J Polym Sci Polym Phys Ed 14:1029–1046
8. Bahl SK, Cornell DD, Boerio FJ, McGraw GE (1974) J Polym Sci Polym Lett Ed 12:13–19
9. Miyake A (1959) J Polym Sci 38:479–495
10. Shi W, Qu B, Ranby B (1994) Polym Degrad 44:185–191
11. Holland BJ, Hay JN (2002) Polymer 43:1835–1847
12. Edge M, Wiles R, Allen NS, McDonald WA, Mortlock SV (1996) Polym Degrad Stab 53:141–151
13. Day M, Wiles DM (1972) Can Text J 89:69
14. Rabek JF (1987) Mechanisms of photophysical processes and photochemical reactions in polymers. Wiley, New York, p 534
15. Kamal MR, Huang B (1992) In: Hamid SH, Amin MB, Maadhah AG (eds) Handbook of polymer degradation. Dekker, New York, pp 127–168
16. McNeill IC, Bounekhel M (1991) Polym Degrad Stab 34:187–204
17. Sivasamy P, Palaniandavar M, Vijayakumar CT, Lederer K (1992) Polym Degrad Stab 38:15–21
18. MacDonald WA (2002) Polym Inter 51:923–993
19. Samperi F, Puglisi C, Alicata R, Montaudo G (2004) Polym Degrad Stab 83:11–17
20. Sammon C, Yarwood J, Everall N (2000) Polym Degrad Stab 67:149–158
21. Seo KS, Cloyd JD (1991) J Appl Polym Sci 42:845
22. Ballara A, Verdu J (1989) Polym Degrad Stab 26:361–374
23. Fayolle B, Audouin L, Verdu J (2000) Polym Degrad Stab 70:333–340
24. Tervoort TA, Govaert LE (2000) J Rheol 44:1263–1277
25. van Melick HGH, Govaert LE, Meijer HEH (2003) Polymer 44:2493–2502
26. Blais P, Day M, Wiles DM (1973) J Appl Polym Sci 17:1895–1907
27. Grossetete T, Rivaton A, Gardette JL, Hoyle CE, Ziemer M, Fagerburg DR, Clauberg H (2000) Polymer 41:3541–3554
28. Hurley CR, Leggett GJ (2009) ACS Appl Mater Interfaces 1:1688–1697
29. Carlsson DJ, Wiles DM (1971) Macromolecules 4:179–184
30. So PK, Broutman LJ (1982) Polym Eng Sci 22:888–894
31. Ciolacu CFL, Choudhury NR, Dutta NK (2006) Polym Degrad Stab 91:875–885
32. Martin JW (2002) In: Martin JW, Bauer DR (eds) Service life prediction: methodology and metrologies. American Chemical Society, Washington, DC, pp 2–22
33. Pospisil J, Pilar J, Billingham NC, Marek A, Horak Z, Nespurek S (2006) Polym Degrad Stab 9:417–422

Index

A

Acceleration, 3, 7, 14, 25, 36, 38, 43, 50, 51, 54–57, 71–84, 87–93, 136, 139, 141, 142, 144, 145, 147, 148, 152, 163, 167, 169, 171, 172, 174, 175, 177, 180, 202–204, 206–207, 232–236, 245, 247

  ageing, 51, 70, 152, 158, 160, 162, 163, 232

  life testing conditions, 22, 33–35, 56, 199–212

  weathering, 25, 74, 79–82, 99, 100, 102, 135–149, 165–183

Acidity, 156–158

Activation energy, 2, 3, 12–14, 16, 26, 43, 48, 50, 51, 55, 57, 60, 88, 89, 120, 121, 123, 126–128, 130–133, 157–158, 204, 205, 207, 209, 210, 212, 219, 222–224, 227

Activation energy of thermal degradation

Additive, 23, 75, 192, 197

Adhesion, 79, 95, 97, 99–104, 107, 112, 114, 115, 151–163, 186, 188, 195–197, 233, 245

Aging, 8–10, 12–18, 47, 50, 51, 53, 54, 57, 60, 62–66, 68, 70, 89, 91–93, 119, 123, 127, 132, 133, 232, 236, 244

Arrhenius, 2, 3, 5, 7, 12–14, 16, 26, 27, 48, 55–57, 60, 87–91, 93, 118, 120–124, 126, 128, 129, 152, 154, 157, 158, 162, 163, 203, 207, 209, 219, 222–224, 227, 228

ASTM G90, 79, 80, 169, 170, 172, 174

Asynchronous degradation

μATR, 68

Automotive, 96, 97, 111, 115, 185

B

Blast resistance, 232

Bond strength, 156, 162, 163

C

Carbonyl group accumulation, 48, 65, 66, 70, 119, 123–127, 132, 191

Certification, 1–4, 8–10, 12, 15, 17, 137–139, 141–148

Chain scission, 14, 60, 66, 70, 74, 119, 121–124, 132, 155, 158, 160, 166, 247

Chalk resistance, 72–76, 83

Characterisation, 2, 3, 12–14, 63, 115, 136, 137, 149, 158, 166, 169, 171, 174, 180, 182, 195, 197, 204, 236, 240, 244

Chemical stress relaxation, 119, 121–123, 131, 132

Chemiluminescence, 119–121, 131

Climatic data, 42–45, 47, 53, 57, 200, 202

Coating, 5, 42, 71–84, 95–102, 104, 105, 107, 109–112, 115, 185–197, 206

Color, 39, 68, 79, 80, 82, 83, 99, 100, 110, 136–141, 144–148, 172, 177, 197, 235, 247

  fade, 39, 76, 77, 82–84

  retention, 72–77, 79, 80, 83, 136, 138

Compound, 2–5, 9, 10, 12–18

Correlation, 3, 5, 6, 30, 32, 43, 48, 49, 52–56, 70, 78–80, 83, 91, 99, 100, 102, 141–149, 155, 169, 171, 172, 174, 177, 180, 218, 228, 236, 237, 244, 245

Cracking, 75, 95–104, 107–115, 137, 138, 192, 195, 197, 218, 220, 222, 223, 225–227, 247